Non-linear dynamic instability analysis of uniform and thickness-tapered composite plates

Mehdi Darabi

A Thesis

in the Department of

Mechanical, Industrial, and Aerospace Engineering

Presented in Partial Fulfilment of the Requirements

for the Degree of

Doctor of Philosophy (Mechanical Engineering) at

Concordia University

Montreal, Quebec, Canada

March 2020

CONCORDIA UNIVERSITY

SCHOOL OF GRADUATE STUDIES

This is to certify that the thesis prepared

By: Mehdi Darabi

Entitled: Non-linear dynamic instability analysis of uniform and thickness-tapered composite plates

and submitted in partial fulfillment of the requirements for the degree of

Doctor of Philosophy (Mechanical Engineering)

complies with the regulations of the University and meets the accepted standards with respect to originality and quality.

Signed by the final examining committee:

_____ Chair
Dr. René Witte

_____ External Examiner
Dr. Kamran Behdinan

_____ External to Program
Dr. Lucia Tirca

_____ Examiner
Dr. Mehdi Hojjati

_____ Examiner
Dr. Mojtaba Kheiri

_____ Thesis Supervisor
Dr. Rajamohan Ganesan

Approved by _____
              Dr. Ivan Contreras, Graduate Program Director

 April 30, 2020

                    _____
                    Dr. Amir Asif, Dean
                    Faculty of Engineering and Computer Science

Abstract

Non-linear dynamic instability analysis of uniform and thickness-tapered composite plates

Mehdi Darabi, Ph.D.

Concordia University, 2020

Laminated composite plates and shells are being increasingly used in aerospace, automotive, and civil engineering as well as in many other applications of modern engineering structures. Tailoring ability of fiber-reinforced polymer composite (FRPC) materials for the stiffness and strength properties with regard to the reduction of structural weight made them superior compared with metals in such structures. In some specific applications such as aircraft wing skins composite structures need to be stiff at one location and flexible at another location. It is desirable to tailor the material and structural arrangements so as to match the localized strength and stiffness requirements by dropping the plies in laminates. Such laminates are called as tapered laminates.

In the dynamic instability that occurs in the structures subjected to harmonic in-plane loading not only the amplitude of the harmonic in-plane load but also the forcing frequencies make the structures fail at load amplitude that is much less than the static buckling load and over a range of forcing frequencies rather than at a single value. In this case, the bending deformations, the rotations and the strains are not small enough in comparison with unity, so the linear theory just provides an outline about the dynamically-unstable regions and is not capable to determine the amplitude of the steady-state vibration in these instability regions.

The main objective of this dissertation is to develop a geometric non-linear formulation and the corresponding solution method for uniform and internally-thickness-tapered laminated composite plates. This Ph.D. research work is completed by extension of this developed

geometric non-linear formulation to the uniform laminated composite cylindrical shells as well. The novel parts of this Ph.D. dissertation are the geometric non-linear formulations and corresponding displacement-based solutions obtained using approximate analytical methods, for dynamic instability analysis of internally-thickness-tapered laminated composite plates and cylindrical panels. To the best of author knowledge, there is no non-linear dynamic instability study on internally-thickness-tapered laminated composite plates and cylindrical panels in literature. There is only one study on the linear dynamic instability of internally-thickness-tapered flat plates using the FEM and Ritz method. Here the developed analytical geometric nonlinear formulation not only is capable of predicting the instability regions but also is capable of determining both stable- and unstable-solutions amplitudes of steady-state vibrations of such internally-thickness-tapered laminated composite plates and cylindrical panels in these dynamically-unstable regions. Furthermore, the effect of the influential parameters on the non-linear dynamic instability of laminated plates and cylindrical shells is extensively studied. These parametric studies were carried out on cross-ply laminated composite uniform plates, flat and cylindrical tapered plates, and uniform cylindrical shells. In this study, the non-linear von Karman strains associated with large deflections are considered. Considering the simply supported boundary condition the Navier's double Fourier series with the time-dependent coefficient is chosen to describe the out-of-plane displacement function. For the uniform laminated composite rectangular plates and uniform laminated composite cylindrical shells, a combination of displacement and a stress-based solution is considered while for the internally-thickness-tapered laminated composites plates and cylindrical panels a displacement-based solution is considered to solve the equations of motion. Then the general Galerkin method is used for the moment-equilibrium equation of motion to satisfy spatial dependence in the partial differential equation of motion to produce a set of non-linear Mathieu-Hill equations. These equations are ordinary differential equations, with time-dependency. Finally, by applying the

Bolotin's method to these non-linear Mathieu-Hill equations, the dynamically-unstable regions, stable-, and unstable-solutions amplitudes of the steady-state vibrations in these dynamically-unstable regions are obtained for both the uniform and the internally-thickness-tapered laminated composites plates and uniform cylindrical shells.

A comprehensive parametric study on the non-linear dynamic instability of these simply supported cross-ply laminated composite uniform plates, flat and cylindrical internally-thickness-tapered plates and uniform cylindrical shells are carried out to examine and compare: the effects of the orthotropy in the laminated composite uniform plates, number of layers for symmetric and antisymmetric uniform cross-ply laminated composite plates and cylindrical shells, different taper configurations and taper angles in both flat tapered plates and tapered cylindrical panels, magnitudes of both tensile and compressive axial loads in the uniform and tapered plates and uniform cylindrical shells, aspect ratios of the loaded-to-unloaded widths of the uniform plates, flat and cylindrical internally-thickness-tapered panels and length-to-radius ratio of the cylindrical shells, length-to-average-thickness ratio of the flat plates and cylindrical panels and radius-to-thickness ratio of the cylindrical shells, and curvature of the tapered cylindrical panels i.e. radius-to-loaded widths ratio on the instability regions and the parametric resonance particularly the steady-state vibrations amplitudes of cross-ply laminated composite uniform plates, flat and cylindrical internally-thickness-tapered plates and uniform cylindrical shells. The present results show good agreement with those available in the literature.

Dedication

This dissertation work is in memory of my father and

dedicated to my beloved mother

Acknowledgments

LIST OF CONTENT

LIST OF FIGURES

xiv

xvi

LIST OF TABLES

Nomenclature	
A_{ij}, B_{ij}, D_{ij}	Extensional, coupling, bending stiffnesses
(x, y, z)	Plate/cylindrical panel coordinates
(X, θ, Z)	Shell coordinates
$\epsilon_{xx}^{(0)}$, $\epsilon_{yy}^{(0)}$, $\gamma_{xy}^{(0)}$	Membrane strains in Cartesian coordinates
$\epsilon_{xx}^{(0)}$, $\epsilon_{\theta\theta}^{(0)}$, $\gamma_{x\theta}^{(0)}$	Membrane strains in Curvilinear coordinates
$\epsilon_{xx}^{(1)}$, $\epsilon_{yy}^{(1)}$, $\gamma_{xy}^{(1)}$	Flexural (bending) strains in Cartesian coordinates
$\epsilon_{xx}^{(1)}$, $\epsilon_{\theta\theta}^{(1)}$, $\gamma_{x\theta}^{(1)}$	Flexural (bending) strains in Curvilinear coordinates
E_1, E_2, G_{12}, v_{12}, v_{21}	Engineering constants of orthotropic composite ply
h_p	Ply thickness
h	Plate/Shell thickness
R	Radius of the cylindrical panel/ cylindrical shell
a	Plate/Panel length
b	Plate /Panel width
L	Shell length
ϕ	Taper angle
N_L	Number of the plies in the left (thick) side
N_R	Number of the plies in the right (thin) side
m	Longitudinal half-wave number
n	In-plane transverse half-wave number
λ_m	$m\pi/a$.
λ_n	$n\pi/b$
$F_{xx}(t)$	Pulsating longitudinal load
F_s	Static component of $F_{xx}(t)$
F_d	Harmonic component of $F_{xx}(t)$
P	Excitation frequency
p	Non-dimensionalized P
ω	Natural frequency

Nomenclature	
q_{mn}	Generalized coordinate
t	Time
u_0 , v_0 , w_0	Orthogonal components of mid-plane displacement functions
ρ	Mass density
ρ_t	Mass per unit length per unit width
$(N_{xx} , N_{yy}, N_{xy})$	The total in-plane force resultants in Cartesian coordinates
$(M_{xx} , M_{yy}, M_{xy})$	The total moment resultants in Cartesian coordinates
$(N_{xx} , N_{\theta\theta}, N_{x\theta})$	The total in-plane force resultants in Curvilinear coordinates
$(M_{xx} , M_{\theta\theta}, M_{x\theta})$	The total moment resultants in Curvilinear coordinates
α	Static load factor
β	Dynamic load factor
N_{cr}	Static buckling load
A	Amplitude of steady-state vibrations
Ω_{mn}	Frequency of the free vibration
μ_{mn}	Excitation parameter

CHAPTER 1

Introduction and scope of the dissertation

1.1   Introduction and motivation

Structures composed of composite materials are among the most important structures used in modern engineering, especially, in the aerospace industry. Due to various advantageous properties such as high strength-to-weight ratio, high stiffness-to-weight ratio, and flexibility in design, laminated composite structures have been increasingly used in various engineering disciplines such as automotive industries, transportation, and civil infrastructure. Tailoring ability of the stiffness and strength properties and substantial reduction in part count offered by such material systems are other advantages that made them superior compared with metals in aerospace applications. Fiber-reinforced-polymer composites can also be manufactured in complex geometric shapes resulting in both higher product performance and manufacturability.

In some specific applications, the composite structure needs to be stiff at one location and flexible at another location. It is desirable to tailor the material and structural arrangements so as to match the localized strength and stiffness requirements by dropping the plies. Such a laminate is referred to as a tapered laminate. Aircraft wing skins, helicopter yoke and near field joints in solid rocket boosters are some applications of the tapered structures in aerospace industries. In the uniform thickness laminates, the material properties only change in the out-of-plane direction by changing the fiber directions in the layers so the strength and stiffness of those structures are constant along the length. In the tapered composite structures, the material properties not only change in the out-of-plane direction by changing the fiber directions in the layers but also change along the length of the structures by dropping the plies so this dropping the plies makes the strength and stiffness of the tapered composite structures to be functions of

the lengthwise coordinate. The behavior of structures composed of advanced composite materials is more complicated than isotropic structures and the tapered composite structures bring more complexity into the analysis than the uniform composite structures.

The light-weight structures that are composed of slender columns and thin-walled plates and shells that have been developed with the advent of aircraft are stiff in axial or in-plane deformations but flexible in bending deformations. Since these structural members within the range of small strains can be easily deformed into states with the finite rotation they are oversensitive to various instability phenomena. In fact, when they are subjected to axial or in-plane forces they often lose stability at fairly low-stress levels that results in large bending deformations.

If composite plates or shells are subjected to the static longitudinal load, gradually increasing this static longitudinal load when the load reaches a critical level, by a very small out-of-plane transverse disturbance, the composite plates or shells may suddenly change shape and undergo a large out-of-plane deflection (bending), so that the composite plate or shell structures are said to have buckled. When composite plates and shells are subjected to the dynamic longitudinal load, they may fail in dynamic buckling or dynamic instability. If the dynamic load is suddenly applied, or it is changing instantaneously, such as impulsive loading then dynamic buckling will happen for the plates or shells. If a composite plate is subjected to a longitudinal periodically pulsating load as shown in Fig. 1.1 and described in Eq. (1.1), for certain relationships between the amplitude of both static and harmonic components of the longitudinal periodically pulsating load, frequency of the harmonic component of the longitudinal periodically pulsating load, and the natural frequency of the composite plate for out-of-plane transverse vibrations which are explained in more detail in the next few sentences, the composite plate becomes dynamically unstable and the out-of-plane transverse vibrations occur. Because this longitudinal periodically pulsating load is parametric load compared to

2
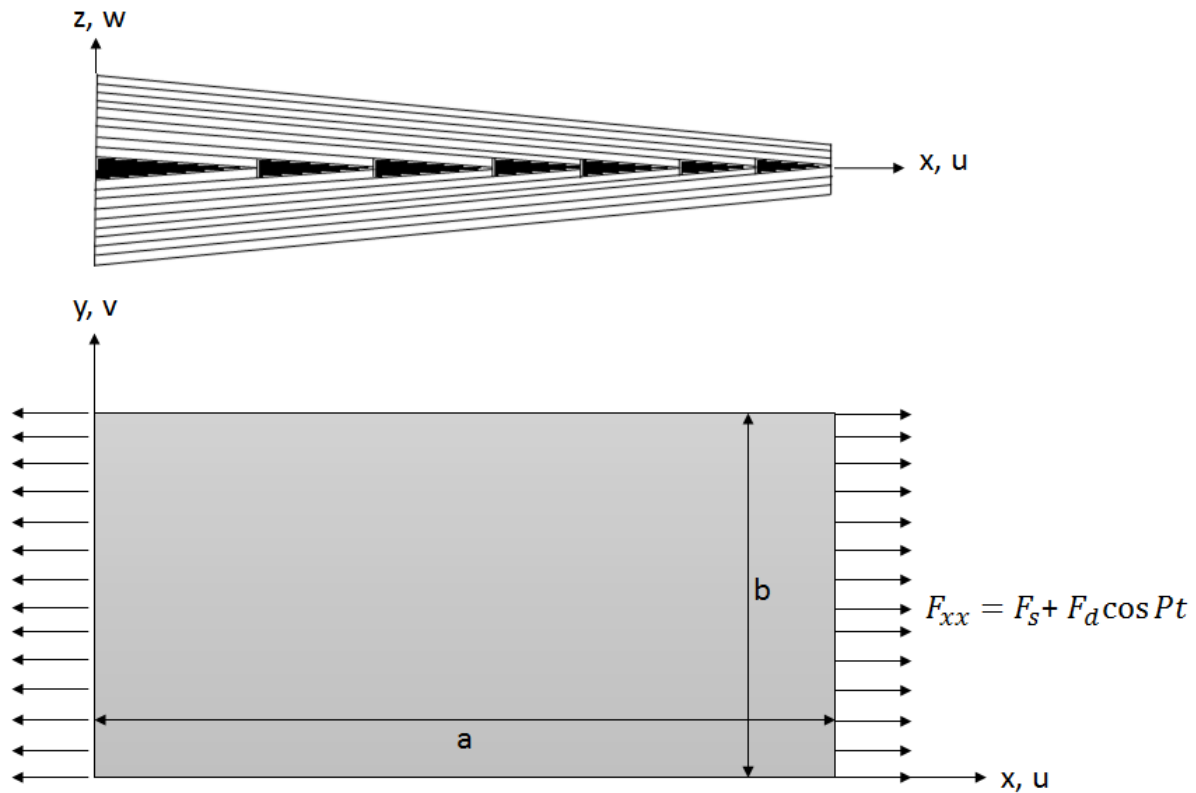
Figure 1.1 The geometry and loading condition of a laminated composite rectangular thickness-tapered plate

the out-of-plane transverse deflections (out-of-plane transverse vibrations) but not compared to (respected with) the longitudinal deformations (longitudinal vibrations) this phenomenon is called the "dynamic instability of elastic systems" (here dynamic instability of composite plate) as the study of vibrations induced by the parametric pulsating loading [1]. The mechanism of dynamic buckling is similar to that of the static buckling and the only difference is that in dynamic buckling the inertia forces are taken into account so the dynamic buckling load is lower than the static buckling load for the same structure. But when such plates are subjected to the longitudinal periodically pulsating load as shown in Fig. 1.1 they may fail in dynamic instability which is more complicated than either dynamic buckling or static buckling. Figure 1.1 shows the geometry and loading condition of a typical laminated composite rectangular thickness-tapered plate, having length a and width b with respect to the Cartesian coordinates

(x, y, z) which are assigned in the mid-plane of the plate. Here, u, v and w are the displacement components of the plate regarding this coordinate system in the $x, y, and\ z$ directions, respectively. The rectangular plate as shown in Fig.1.1 is subjected to a longitudinal periodically pulsating load per unit width as follow:

$$F_{xx}(t) = F_s + F_d cosPt \qquad (1.1)$$

where F_s is a time-invariant component, $F_d cosPt$ is the harmonically-pulsating component, and P denotes the frequency of excitation in radians per unit time.

When a composite plate is subjected to the longitudinal periodically pulsating load as shown in Fig. 1.1, if the amplitude of both static and harmonic components of the load together is less than that of the static buckling value, then in general, the plate experiences only longitudinal vibrations. However, for certain relationships between the frequency of harmonic component of the load (P) and the natural frequency of the composite plate for out-of-plane transverse vibrations (ω), the plate becomes dynamically unstable i.e. out-of-plane transverse vibrations occur. The amplitude of these out-of-plane transverse vibrations rapidly increases to large values. This large value is not infinite, it means that it is limited but also large compared to the plate thickness which will be explained in more detail later. For sufficiently small values of harmonic component of the longitudinal periodic load, when the frequency of harmonic component of the longitudinal periodic load (P) is equal to double the natural frequency of plate for out-of-plane transverse vibrations (ω) then parametric resonance occurs. This parametric resonance caused by the parametric pulsating loading (explained above) differs from the ordinary resonance of forced vibrations in which vibrations of the system caused by the applied periodic load in the same direction of the vibrations of the system. The ordinary resonance of forced vibrations occurs when the natural frequency of the system and exciting frequency (frequency of the periodic load) are equal. Whenever longitudinal static loading causes static instability (static buckling), the longitudinal periodically pulsating load which is

4

a combination of both static and harmonic components will cause dynamic instability as explained above. In both the static and dynamic buckling, the main factor is only the critical load, but in dynamic instability, not only the amplitude of both static and harmonic components of the longitudinal periodically pulsating load (F_s and F_d) but also the natural frequency of out-of-plane transverse vibrations (ω) together with the frequency of the harmonic component of the longitudinal periodically pulsating load (P) will play important roles. When the frequency of the harmonic component of longitudinal periodically pulsating load and the natural frequency of out-of-plane transverse vibrations of the plate structure satisfies some specific conditions, parametric resonance will happen in the plate structure, which makes the plate to fall into a state of dynamic instability. This instability is of concern because it can occur at load amplitudes that are much less than the static buckling load (N_{cr}), so a structural component designed to withstand static buckling may fail in a periodic loading environment. Further, the dynamic instability occurs over a range of forcing frequencies rather than at a single value [2, 3] as shown in Fig. 1.2. Those dynamic instability regions are separated by two lines with a common point of origin in the load amplitude vs forcing frequencies as shown in the sample graph in Fig. 1.2. The aforementioned two lines are not perfectly straight and they curve slightly outwards. In this sample graph in Fig. 1.2 The static and harmonic components of the longitudinal periodically pulsating load are considered as $F_s = \alpha N_{cr}$ and $F_d = \beta N_{cr}$, respectively. In this figure, the static load factor is 20% and the dynamic load factor is varied from zero to 80%. It means that 20% of the critical buckling load of the plate is applied to the static component (F_s) of the longitudinal periodically pulsating load (F_{xx}) in Eq. 1.1, and the harmonic component (F_d) of the pulsating longitudinal load (F_{xx}) is varied from 0 to 80% of the critical buckling load of that plate.
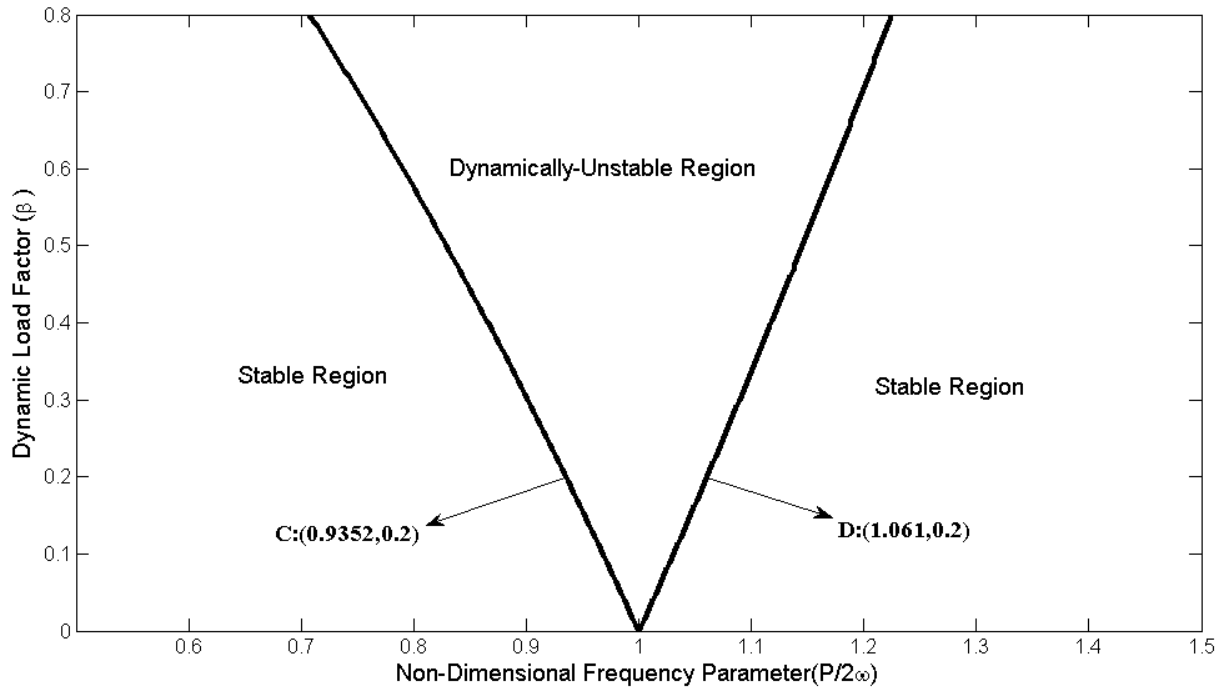
Figure 1.2 A sample dynamically-unstable region of a thickness-tapered plate subjected to longitudinal periodically pulsating load having static load factor of $\alpha = 0.2$

Stability analysis based on classical linear theories provided only an outline of the instability regions. The majority of the research works available in the literature on dynamic instability of plates, shells and all other engineering structures are limited to the linear analysis. According to linear theory, one expects the vibration amplitudes in the regions of dynamic instability to increase unboundedly with time indeed very rapidly so as to increase exponentially. But studies [1, 2] show that there is vibration with steady-state amplitudes in dynamically-unstable regions. Figure 1.3 shows the amplitudes of steady-state out-of-plane transverse vibrations of the internally-thickness-tapered laminated composite plate in the dynamically-unstable region of the plate shown in Fig.1.2. The graphs in Fig. 1.3 are plotted for both the static and dynamic load factor of 20%. As shown in Fig. 1.3 in addition to zero solution correspond to the case where out-of-plane transverse vibrations of the plate are absent, there exists simultaneously both the stable (solid curve) and unstable (dashed curve) non-zero solutions correspond to the stable- and unstable-amplitudes of steady-state vibrations of the laminated composite plate in a state of dynamic instability. When the frequency of the harmonic component of the

6
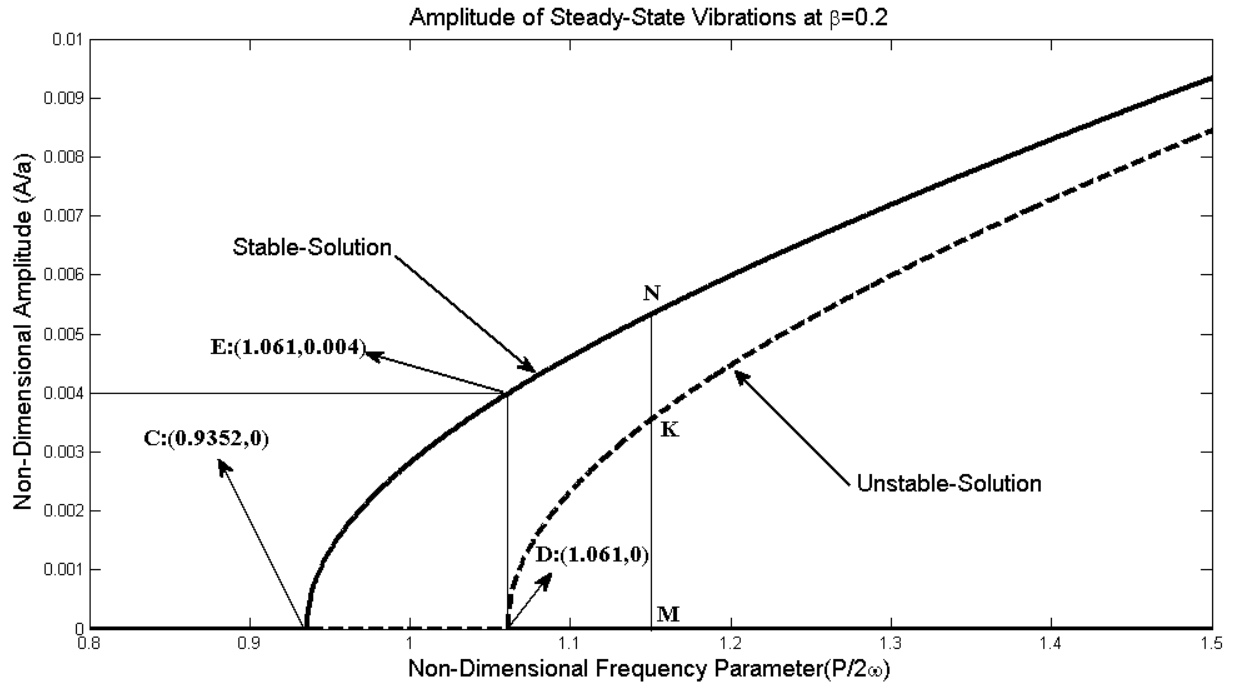
Figure 1.3 Sample graphs of both the stable- and unstable-solution amplitudes of steady-state vibrations of a thickness-tapered plate subjected to longitudinal periodically pulsating load having the static load factor of $\alpha = 0.2$ and the dynamic load factor of $\beta = 0.2$

longitudinal periodically pulsating load is lower than the corresponding frequency of point C in this figure there are not any out-of-plane transverse vibrations of the plate subjected to the longitudinal periodically pulsating load. But for the frequencies higher than the frequency of point C and lower than the frequency of point D, with very small out-of-plane transverse disturbance the longitudinal periodically pulsating load causes the plate to fall into the dynamically-unstable region i.e. the out-of-plane transverse steady-state vibrations occur in the plate that its amplitude increases on the stable-amplitude curve of CE. As one can see from Fig. 1.3 the frequencies of points C and D are the same frequencies of the lower and upper boundaries of the corresponding dynamically-unstable region shown in Fig.1.2 having a harmonic component load factor of 20%, respectively, and for the range of frequencies being in this domain i.e. CD region the plate is dynamically-unstable subjected to the longitudinal periodic pulsating load. So when both stable- and unstable-amplitude of steady-state vibrations

are zero, the range of frequencies between these two zero-amplitude i.e region bounded by the line CD, predicate also the dynamically-unstable region at this certain value of harmonic component load factor of 20%. As shown in a sample graph in Fig. 1.3, initially stable-amplitude on branch CE curve increases approximately exponentially in this dynamically-unstable region but while the frequency of harmonic component of the longitudinal periodically pulsating load is increased in this region (from point C to D) the speed of the growth of amplitudes decreases gradually.

Let us assume that the harmonic component of the longitudinal periodically pulsating load has a frequency as point M which is greater than the frequency of point D at the upper boundary of the dynamically-unstable region. In this case, the zero solution is stable so out-of-plane transverse vibrations will not occur. However, at the same frequency still, another stable solution is possible, corresponding to the steady-state out-of-plane transverse vibrations with amplitude MN. These vibrations can be realized by selecting a frequency value from the dynamically-unstable region CD and through this stable-amplitude of out-of-plane transverse vibrations of the plate on curve CN by a stepwise increasing the frequency of the harmonic component of the longitudinal periodically pulsating load. These same out-of-plane transverse vibrations at the frequency of point M having stable-amplitude as MN can be developed differently; if one enforces a sufficiently strong out-of-plane disturbance to the plate, the out-of-plane vibrations of the plate can occur and its amplitude grows on the branch CN of the non-zero stable-amplitude curve. The unstable-amplitude branch DK plays an important role in the determination of the magnitude of the initial out-of-plane transverse disturbance to cause this steady-state out-of-plane transverse vibrations at such frequency as M of the harmonic component of the longitudinal periodically pulsating load. This branch separates the region of zero solutions (zero stable-amplitude) from the region of non-zero solutions which corresponds to the non-zero stable-amplitude of out-of-plane transverse vibrations located on the branch

8

CN curve. As long as the initial out-of-plane transverse disturbance on the plate is smaller than MK, the plate returns to the original state of equilibrium. If the disturbance is larger than MK, steady-state out-of-plane transverse vibrations arise with a non-zero stable-amplitude MN. This out-of-plane transverse vibration of the plate subjected to longitudinal periodically pulsating load is limited and determined by the "Stability in large" [1]. If one uses the theory of small disturbances, the steady-state out-of-plane transverse vibrations having non-zero stable-amplitude as on the branch CN can occur only for the frequencies of the harmonic component of the longitudinal periodically pulsating load that its range belongs to the frequencies in dynamically-unstable region CD. However, experiments show that frequencies lying only slightly at the higher frequencies than the dynamically-unstable region CD cause a "break" [1] of out-of-plane transverse vibrations. The existence of two stable amplitudes at frequencies higher than the frequencies of dynamically-unstable region CD leads to a phenomenon which is called the "overhang" [1]. By a gradual increase in the frequency of harmonic component of the longitudinal periodically pulsating load, we can bring the steady-state out-of-plane vibrations of the plate into this region where these two stable solutions (stable-amplitudes) exist. The growth of amplitude will continue initially with the non-zero stable curve CE until a jump of out-of-plane transverse vibrations occurs at a certain point of curve EN. The amplitude of steady-state out-of-plane vibrations of the plate decreases suddenly to the magnitude of the other stable-amplitude at this frequency which is zero and continues along the zero-stable-amplitude curve (line). Steady-state out-of-plane transverse vibrations are stable until the vibrations of the plate are transferred to the unstable branch DK by the disturbances that are not eliminated in practice [1]. Therefore for small out-of-plane initial disturbance for the frequencies of the harmonic component of the longitudinal periodically pulsating load that their ranges are outside the dynamically-unstable regions, the out-of-plane

transverse vibrations do not occur in the plate and those regions as shown in Fig. 1.2 are called dynamically-stable regions.

When the plates fall into the dynamically-unstable regions the dynamic instability problem should be considered as per the non-linear large deflection theory i.e. it should be modeled based on the geometrical non-linearity. The graphs in Fig. 1.2 and Fig.1.3 are the results of a square internally-thickness-tapered plate with 12 and 6 plies at its thick and thin sections, respectively that its length-to-average-thickness ratio is equal to 193.24. As we can see in Fig. 1.3 at the end of the dynamically-unstable region, at point E on the stable-amplitude curve CEN of the steady-state out-of-plane transverse vibrations of the plate, the stable-amplitude is equal to 0.004 of the length of the tapered plate. So if we multiply the 0.004 (amplitude-to-length ratio) to 193.24 (length-to-average- thickness ratio), the stable-amplitude of steady-state out-of-plane transverse vibrations of the tapered plate subjected to the longitudinal periodically pulsating load having both the static and harmonic components are 20% of its critical buckling load, will become 0.772 of its average-thickness. Since the plate undergoes large deflections compared to the thickness of the plate that is to say that the out-of-plane transverse deflection is of the same order as the thickness of the plate due to the out-of-plane transverse vibrations, we thus have a geometrical non-linearity in the plate at this stage (dynamically-unstable region) and the strains-displacements relations are non-linear as follows:

$$\epsilon_{xx} = \frac{\partial u}{\partial x} + \frac{1}{2}[(\frac{\partial u}{\partial x})^2 + (\frac{\partial v}{\partial x})^2 + (\frac{\partial w}{\partial x})^2] \tag{1.2a}$$

$$\epsilon_{yy} = \frac{\partial v}{\partial y} + \frac{1}{2}[(\frac{\partial u}{\partial y})^2 + (\frac{\partial v}{\partial y})^2 + (\frac{\partial w}{\partial y})^2] \tag{1.2b}$$

$$\epsilon_{zz} = \frac{\partial w}{\partial z} + \frac{1}{2}[(\frac{\partial u}{\partial z})^2 + (\frac{\partial v}{\partial z})^2 + (\frac{\partial w}{\partial z})^2] \tag{1.2c}$$

$$\gamma_{xy} = \frac{\partial u}{\partial y} + \frac{\partial v}{\partial x} + [\frac{\partial u}{\partial x}\frac{\partial u}{\partial y} + \frac{\partial v}{\partial x}\frac{\partial v}{\partial y} + \frac{\partial w}{\partial x}\frac{\partial w}{\partial y}] \tag{1.2d}$$

$$\gamma_{xz} = \frac{\partial u}{\partial z} + \frac{\partial w}{\partial x} + [\frac{\partial u}{\partial x}\frac{\partial u}{\partial z} + \frac{\partial v}{\partial x}\frac{\partial v}{\partial z} + \frac{\partial w}{\partial x}\frac{\partial w}{\partial z}] \tag{1.2e}$$

$$\gamma_{yz} = \frac{\partial v}{\partial z} + \frac{\partial w}{\partial y} + \left[\frac{\partial u}{\partial y}\frac{\partial u}{\partial z} + \frac{\partial v}{\partial y}\frac{\partial v}{\partial z} + \frac{\partial w}{\partial y}\frac{\partial w}{\partial z}\right] \tag{1.2f}$$

where u, v and w are displacements of a generic point of the plate at the distance z from the mid-plane of the plate in the $x, y, and\ z$ directions, respectively. And ϵ_{xx}, ϵ_{yy}, ϵ_{zz}, γ_{xy}, γ_{xz} and γ_{yz} are 3D strains components of an element of the plate at this generic point with regard to the Cartesian coordinates (x, y, z) based on the Green-Lagrange strain components.

If we assume that the plate is sufficiently thin, based on Kirchhoff's hypotheses, we can define the displacement of this generic point of the plate at the distance z from the mid-plane in terms of the displacements of a generic point of the mid-plane of the plate as follows:

$$u = u_0(x, y, t) - z\frac{\partial w_0(x,y,t)}{\partial x} \tag{1.3}$$

$$v = v_0(x, y, t) - z\frac{\partial w_0(x,y,t)}{\partial y} \tag{1.4}$$

$$w = w_0(x, y, t) \tag{1.5}$$

Where u_0, v_0 and w_0 are displacements of a generic point of the mid-plane of the plate in the $x, y, and\ z$ directions, respectively. Therefore, the strain components ϵ_{xx}, ϵ_{yy} and γ_{xy} at an arbitrary point of the plate are related to the membrane strains (mid-plane strains) $\epsilon_{xx}^{(0)}$, $\epsilon_{yy}^{(0)}$ and $\gamma_{xy}^{(0)}$, and to the bending curvatures in the x and y directions and twisting curvature of the mid-plane which are denoted as $\epsilon_{xx}^{(1)}$, $\epsilon_{yy}^{(1)}$ and $\gamma_{xy}^{(1)}$, as follows:

$$\begin{Bmatrix}\epsilon_{xx}\\\epsilon_{yy}\\\gamma_{xy}\end{Bmatrix} = \begin{Bmatrix}\epsilon_{xx}^{(0)}\\\epsilon_{yy}^{(0)}\\\gamma_{xy}^{(0)}\end{Bmatrix} + z\begin{Bmatrix}\epsilon_{xx}^{(1)}\\\epsilon_{yy}^{(1)}\\\gamma_{xy}^{(1)}\end{Bmatrix} \tag{1.6}$$

For von Karman hypothesis, the in-plane displacements u_0 and v_0 are infinitesimal, and in the strain-displacement relations, only those non-linear terms which depend on w_0 are preserved and all other non-linear terms of u_0 and v_0 were neglected. Hence the following membrane strains and the flexural (bending) strains are given by:

$$\{\epsilon^0\} = \begin{Bmatrix} \epsilon_{xx}^{(0)} \\ \epsilon_{yy}^{(0)} \\ \gamma_{xy}^{(0)} \end{Bmatrix} = \begin{Bmatrix} \frac{\partial u_0}{\partial x} + \frac{1}{2}(\frac{\partial w_0}{\partial x})^2 \\ \frac{\partial v_0}{\partial y} + \frac{1}{2}(\frac{\partial w_0}{\partial y})^2 \\ \frac{\partial u_0}{\partial y} + \frac{\partial v_0}{\partial x} + (\frac{\partial w_0}{\partial x} \frac{\partial w_0}{\partial y}) \end{Bmatrix} \tag{1.7}$$

$$\{\epsilon^1\} = \begin{Bmatrix} \epsilon_{xx}^{(1)} \\ \epsilon_{yy}^{(1)} \\ \gamma_{xy}^{(1)} \end{Bmatrix} = \begin{Bmatrix} -\frac{\partial^2 w_0}{\partial x^2} \\ -\frac{\partial^2 w_0}{\partial y^2} \\ -2\frac{\partial^2 w_0}{\partial x \partial y} \end{Bmatrix} \tag{1.8}$$

As mentioned above dynamic instability can occur in much lower loads than critical buckling load and we consider a percentage of critical buckling load. In Fig.1.2 the static component of the longitudinal periodically pulsating load is 20% of the critical buckling load of the plate and the harmonic component of the longitudinal periodically pulsating load is varied from 0 to 80% of the critical buckling load of that plate. By increasing the harmonic component of the longitudinal periodically pulsating load from 0 to 80% the width of the dynamically-unstable region is increased. This means that a longer frequencies range of the harmonic component of the longitudinal periodically pulsating load causes the plate to become dynamically-unstable. In Fig. 1.3 the graphs of amplitudes of the steady-state out-of-plane transverse vibrations of the plate subjected to longitudinal periodically pulsating load are plotted for both the static and harmonic component of 20% of its critical buckling load. In this case, as mentioned above the stable-amplitude of steady-state out-of-plane transverse vibrations of the tapered plate is 0.772 of its average-thickness at the highest point inside the dynamically-unstable region which is of the same order as plate thickness. We suppose at this level of loading that the static and harmonic component of the longitudinal periodically pulsating load together includes 40% of its critical buckling load and corresponding out-of-plane transverse deflection of the plate is almost as large as the plate thickness in the dynamically-unstable region, the stress-strain relations to remain linear. In this thesis also for the parametric studies of the amplitude of the out-of-plane transverse vibrations of the studied

12

composite plates and shells, the composite plates and shells subjected to the lower level of longitudinal periodically pulsating loadings that the amplitudes in the dynamically-unstable regions do not exceed to a much higher level of the out-of-plane deflections in which, the stresses-strains relations become non-linear. However, for the out-of-plane deflections caused by the out-of-plane vibrations in the dynamically-unstable region, it needs strain analysis for the chosen composite materials in this thesis to know whether the stresses-strains relations are linear or not. In this thesis, the linear stress-strain relations considered in the formulations of the dynamic instability problem, and the effect of material non-linearity doesn't take into account. So here in this thesis anywhere we say non-linear or non-linear terms it refers to geometrical non-linearity.

The influence of the non-linear terms is therefore very important and essential, which shows that steady-state out-of-plane transverse vibrations exist in the dynamically-unstable regions. With increasing amplitudes, the influence of non-linear terms becomes more and more apparent, i.e, these terms limit the infinite increase in amplitudes predicted by linear theory. Initially, amplitudes of the out-of-plane vibrations increase approximately exponentially. As the amplitudes increase, the character of the vibrations changes i.e. the speed of amplitudes growth decreases gradually.

In this research work which is on the non-linear dynamic instability analysis of uniform and tapered composite plates and uniform composite cylindrical shells, the following assumptions are considered in the formulations:

- The boundary condition for all the studied composite plates and shells in this research is simply supported.

- The in-plane inertia forces in the equation of motions are neglected.

- The damping effects are not considered in the formulations.

- The formulations of the dynamic instability problems of all the studied composite plates and shells in this research are limited to the cross-ply laminated composites.

- For the laminated composite internally-thickness-tapered flat plates and cylindrical panels, the extensional stiffness terms are replaced by their average values in the formulation. Without this assumption, it is mathematically impossible to solve the two in-plane force-equilibrium equations of motion. This simplification is therefore taken into account in the solution method of this study.

In this research work, the von Karman-type of plate equation is used to develop the equations of motion of the plate, including geometrical non-linearity. The first two equations of motion of the plate are the force-equilibrium equations. From these two in-plane force-equilibrium equations of motion, the two in-plane displacements are determined in terms of the out-of-plane transverse displacement function of the mid-plane of the plate. Consequently, the in-plane force-resultants are obtained from the in-plane displacements and further by applying the boundary conditions. Then, we substitute these in-plane force-resultants in the third equation of motion which is the moment-equilibrium equation of motion. The general Galerkin method is applied to the third equation of motion which is the moment-equilibrium equation of motion, to obtain a set of non-linear Mathieu-Hill equations as follows:

$$M_{mn}\ddot{q}_{mn}(t) + K_{mn}q_{mn}(t) - (F_s + F_d \cos Pt)Q_{mn}q_{mn}(t) + \eta_{mn}q_{mn}^3(t) = 0 \qquad (1.9)$$

Where the coefficients M_{mn}, K_{mn}, Q_{mn} and η_{mn} are functions of mass density, extensional stiffnesses, bending stiffnesses, plate geometries, and the number of longitudinal (m) and transverse (n) half-waves in the corresponding standing wave pattern of the out-of-plane displacement function. And $q_{mn}(t)$ is the time-dependent coefficient (amplitude) of the out-of-plane displacement function. The subscripts m and n have the following ranges:

$$m, n = 1,2,3,4,..,N. \qquad (1.10)$$

This differential equation describes the parametric out-of-plane transverse vibrations of the internally-thickness-tapered plate shown in Fig. 1.1, include the effects of geometrically non-linear terms. As mentioned above, the dynamically-unstable regions are determined by the linear parts of the Eq. (1.9) [1], it is, therefore, more convenient (practical) to write the non-linear Mathieu-Hill equation (1.9) in the following form which only includes the linear parts:

$$M_{mn}\ddot{q}_{mn}(t) + (K_{mn}^* - Q_{mn}^* \cos Pt)q_{mn}(t) = 0 \tag{1.11}$$

where

$$K_{mn}^* = K_{mn} - F_s Q_{mn} \tag{1.12}$$

and

$$Q_{mn}^* = F_d Q_{mn} \tag{1.13}$$

The basic solutions of Mathieu-Hill equation include two periodic solutions: that is to say periodic solutions of periods T and $2T$ with $T = 2\pi/P$. The solutions with the period $2T$ are of greater practical importance because the widths of these unstable regions are generally larger than those associated with solutions having the period T. By using Bolotin's method [1] for the parametric out-of-plane transverse vibrations, the solution of period $2T$ is given by the following equation:

$$q(t) = \sum_{k=1,3,5,\ldots}^{\infty} f_k \sin\frac{kPt}{2} + g_k \cos\frac{kPt}{2} \tag{1.14}$$

where f_k and g_k are arbitrary vectors. If one investigates the instability at the principal dynamically-unstable region, one can neglect the influence of higher harmonics in the expansion of the above equation and can assume

$$q(t) = f \sin\frac{Pt}{2} + g \cos\frac{Pt}{2} \tag{1.15}$$

The principal region of dynamic instability, which corresponds to the solution of the period, $2T$ is determined by substituting Eq. (1.15) in Eq. (1.11) and equating the determinant of the coefficient matrix of the linear part of the governing equation to zero as follows:

$$\begin{vmatrix} K_{mn}^* - \frac{Q_{mn}^*}{2} - \frac{M_{mn}}{4}P^2 & 0 \\ 0 & K_{mn}^* + \frac{Q_{mn}^*}{2} - \frac{M_{mn}}{4}P^2 \end{vmatrix} = 0 \qquad (1.16)$$

Equation (1.16) can be reorganized in the most simplified form of an eigenvalue problem as follow:

$$\begin{vmatrix} K_{mn}^* - \frac{Q_{mn}^*}{2} & 0 \\ 0 & K_{mn}^* + \frac{Q_{mn}^*}{2} \end{vmatrix} - P^2 \begin{vmatrix} \frac{M_{mn}}{4} & 0 \\ 0 & \frac{M_{mn}}{4} \end{vmatrix} = 0 \qquad (1.17)$$

In this eigenvalue equation K_{mn}^* and Q_{mn}^* are functions of the static component F_s and of the harmonic component of the longitudinal periodically pulsating load, respectively. Solving this equation gives two roots for frequency P which are functions of the harmonic component of the longitudinal periodic pulsating load corresponding to the lower and the upper boundaries of the dynamically-unstable region. By setting $F_s = 0.2N_{cr}$ and by defining $F_d = \beta N_{cr}$, these two frequency functions P are plotted in terms of the dynamic load factor β which varies from zero to 80% as shown in Fig. 1.2. The critical buckling load N_{cr} of the studied thickness-tapered composite plate is obtained as follows:

$$|K_{mn} - N_{cr}Q_{mn}| = 0 \qquad (1.18)$$

The fundamental frequency of the studied thickness-tapered plate is also calculated as follow:

$$|K_{mn}^* - \omega^2 M_{mn}| = 0 \qquad (1.19)$$

Now we introduce the following notations:

$$\omega_{mn} = \sqrt{\frac{K_{mn}}{M_{mn}}} \qquad (1.20)$$

$$\gamma_{mn} = \frac{\eta_{mn}}{M_{mn}} \qquad (1.21)$$

$$N_* = \frac{K_{mn}}{Q_{mn}} \qquad (1.22)$$

Then rewrite the Eq. (1.9) in the most common form of the non-linear Mathieu-Hill equation as follows:

$$\ddot{q}_{mn}(t) + \Omega_{mn}^2 (1 - 2\mu_{mn} \cos pt)q_{mn}(t) + \gamma_{mn}q_{mn}^3 (t) = 0 \qquad (1.23)$$

where Ω_{mn} is the frequency of the free vibration of the plate loaded by a constant longitudinal force F_s,

$$\Omega_{mn} = \omega_{mn}\sqrt{1 - \frac{F_s}{N_*}} \qquad (1.24)$$

and μ_{mn} is a quantity that is called the excitation parameter,

$$\mu_{mn} = \frac{F_d}{2(N_* - F_s)} \qquad (1.25)$$

Using again the first Bolotin's approximation, considering the case of the out-of-plane transverse vibrations at the principal dynamically-unstable region, substituting Eq. (1.15) in Eq. (1.23) then by equalizing the coefficients of the terms $\sin(Pt/2)$ and $\cos(Pt/2)$, and neglecting the terms containing higher harmonics, the following system of equations for the coefficients f and g remains:

$$\left[\Omega_{mn}^2(1 + \mu_{mn}) - \frac{P^2}{4}\right] f + \Gamma(f, g) = 0, \qquad (1.26a)$$

$$\left[\Omega_{mn}^2(1 - \mu_{mn}) - \frac{P^2}{4}\right] g + \Psi(f, g) = 0, \qquad (1.26b)$$

where $\Gamma(f, g)$ and $\Psi(f, g)$ are defined as:

$$\Gamma(f, g) = \frac{3\gamma_{mn}}{4} A^2 f \qquad (1.27a)$$

$$\Psi(f, g) = \frac{3\gamma_{mn}}{4} A^2 g \qquad (1.27b)$$

and A is the amplitude of steady-state out-of-plane transverse vibrations of the plate which is given by:

$$A = \sqrt{f^2 + g^2} \qquad (1.28)$$

By substitution of Eqs. (1.27a, b) in Eqs. (1.26a, b) a system of two homogeneous linear equations with respect to f and g can be obtained. It is obvious that this system of two homogeneous linear equations will be satisfied for $f = g = A = 0$. This solution corresponds to the case where the out-of-plane transverse vibrations of the plate are absent. However, this

system of two homogeneous linear equations (Eqs. (1.26a,b)) still has solutions that differ from

zero only in the case where the determinant composed of the coefficients vanishes:

$$\begin{vmatrix} 1 + \mu_{mn} - n_{mn}^2 + \frac{3\gamma_{mn}}{4\Omega_{mn}^2}A^2 & 0 \\ 0 & 1 - \mu_{mn} - n_{mn}^2 + \frac{3\gamma_{mn}}{4\Omega_{mn}^2}A^2 \end{vmatrix} = 0 \qquad (1.29)$$

where

$$n_{mn} = \frac{P}{2\Omega_{mn}} \qquad (1.30)$$

By expanding the determinant, and then by solving the resulting equation with respect to the

amplitude, A, of the steady-state out-of-plane transverse vibrations of the plate, the following

equation is obtained:

$$A = \frac{2\Omega_{mn}}{\sqrt{3\gamma_{mn}}}\sqrt{n_{mn}^2 - 1 \pm \mu_{mn}} \qquad (1.31)$$

In the above equation, only the term $+\mu_{mn}$ yields a stable solution, and the term $-\mu_{mn}$

yields an unstable solution [1]. The amplitudes of the steady-state out-of-plane transverse

vibrations of the plate as obtained in the Eq. (1.31) are in terms of Ω_{mn}, μ_{mn}, and n_{mn} which

include the static component, the static and harmonic components, and the frequency of the

harmonic component of the longitudinal periodically pulsating load, respectively. By setting

respectively $F_s = 0.2N_{cr}$ and $F_d = 0.2N_{cr}$, these amplitudes of steady-state out-of-plane

vibrations of the plate are plotted as a function of the frequency of the harmonic component of

the longitudinal periodically pulsating load P as shown in Fig. 1.3.

Comparison of Eq. (1.29) with Eq. (1.16) by replacing μ_{mn}, n_{mn} , γ_{mn} and Ω_{mn} in terms of

K_{mn}^*, Q_{mn}^* and M_{mn} reveals that dynamically-unstable regions can also be determined by

setting $A = 0$ in Eq. (1.29). This is also discussed earlier by comparing Fig. 1.2 and Fig. 1.3.

In Fig. 1.3, when at the same time the stable-amplitude and unstable-amplitude of the steady-

state out-of-plane transverse vibrations of the plate are null, i.e. points C and D of Fig. 1.3,

these points exactly coincide with the corresponding points on the lower boundary and upper boundary of the dynamically-unstable region of Fig.1.2.

1.2 Research objectives and organization of the Manuscript-Based Dissertation

Based on the aforementioned discussion on the importance of the non-linear analysis of dynamic instability for composite plates and shells, the main objective of this dissertation is to develop a geometric non-linear formulation and corresponding solution method for uniform and internally-thickness-tapered laminated composite plates and uniform cylindrical shells. The contributions of this research work include four journal articles, which are presented in chapters 2 to 5 in this dissertation. The articles in Chapters 2, 3, and 5 have been published in international high-impact peer-reviewed journals, and the article in Chapter 4 is ready to be submitted to another international high-impact peer-reviewed journals. These articles are briefly explained and described in the following paragraphs. The articles that are presented in Chapters 2 and 5 are an extension from previous research work of the author of this Ph.D. thesis on the non-linear dynamic instability analysis of functionally graded cylindrical shells [2] to the non-linear dynamic instability analysis of uniform-thickness laminated composite plates and cylindrical shells, respectively. However, those articles in Chapters 3 and 4 contain newly developed displacement-based approximate analytical solutions for non-linear dynamic instability analysis of internally-thickness-tapered laminated composite plates and cylindrical panels, respectively. All these analytical geometric nonlinear formulations and corresponding approximate solutions that are presented in these chapters of the dissertation not only are capable of predicting the instability regions but also are capable of determining both stable- and unstable-solutions amplitudes of steady-state vibrations of uniform-thickness laminated composite plates, internally-thickness-tapered laminated composite plates, internally-thickness-tapered laminated composite cylindrical panels, and uniform-thickness laminated

composite cylindrical shells in these dynamically-unstable regions. The importance of these solutions is that they give engineers and designers of composite plates and shells an overview of the vibrational state of these composite structures in these dynamically-unstable regions. The solutions reveal that vibrations with steady-state amplitudes exist in these dynamically-unstable regions. Moreover, they can know about the magnitude and the trend of growth of the amplitudes of steady-state vibrations of these composite structures in these dynamically-unstable regions. The parametric studies carried out in this thesis, give a design criterion to engineers and designers of composite plates and shells, to design more efficient composite plates/shells which, for some reason, if these structures fall into dynamically-unstable regions, to have lower amplitudes of steady-state vibrations in these dynamically-unstable regions. Furthermore, the effect of the influential parameters on the non-linear dynamic instability of laminated plates and cylindrical shells is extensively studied. These parametric studies were carried out on cross-ply laminated composite uniform plates, flat and cylindrical tapered plates, and uniform cylindrical shells. To the best of author knowledge, there is no non-linear dynamic instability study on internally-thickness-tapered laminated composite plates and cylindrical panels in literature. There is only one study on the linear dynamic instability of internally-thickness-tapered flat composite plates using the FEM and Ritz method conducted at Concordia University by the supervisor of the present thesis. The non-linear dynamic instability formulations and corresponding displacement-based solutions for internally-thickness-tapered laminated composite plates and cylindrical panels using approximate analytical methods are presented in chapters 3 and 4 of this Ph.D. thesis, respectively, are the novel parts of this dissertation. This manuscript based dissertation has been compiled based on requirements described in the "Thesis Preparation and Thesis Examination Regulation" booklet of the School of Graduate Studies at Concordia University. The dissertation includes six chapters addressing the objectives illustrated in the previous paragraph. Chapter 1 presents an introduction and

objective of this Ph.D. research work. In Chapter 2 the non-linear dynamic instability of laminated composite uniform thin plates subjected to periodic in-plane loads is studied. The non-linear dynamic instability of internally-thickness-tapered composite plates and internally-thickness-tapered composite cylindrical panels are presented in Chapters 3 and 4, respectively. In Chapter 5 the non-linear dynamic instability analysis of laminated composite uniform cylindrical shells subjected to periodic axial loads is investigated. All these chapters from Chapter 2 to Chapter 5 include the state of the art review, modeling and formulation, solution of the problem, and finally the results that address comprehensive parametric studies for the mentioned corresponding composite structures of each chapter. Finally, the main conclusions of the dissertation research are highlighted with recommendations for future work in Chapter 6. The articles in Chapters 2-5 are briefly described as follow:

Chapter 2 presents the following article:

M. Darabi, R. Ganesan.; "Non-linear dynamic instability analysis of laminated composite thin plates subjected to periodic in-plane loads". International Journal of Non-linear Dynamics, Volume 91, Issue 1, January 2018, Pages 187-215.

https://doi.org/10.1007/s11071-017-3863-9

In this chapter, the dynamic instability of thin laminated composite plates subjected to harmonic in-plane loading is studied based on the non-linear analysis. The equations of motion of the plate are developed using von Karman-type of plate equation including geometric non-linearity. The non-linear large deflection plate equations of motion are solved by using Galerkin's technique that leads to a system of non-linear Mathieu-Hill equations. Dynamically unstable regions and both stable- and unstable-solution amplitudes of the steady-state vibrations are obtained by applying the Bolotin's method. The non-linear dynamic stability characteristics of both antisymmetric and symmetric cross-ply laminates with different lamination schemes are examined. A detailed parametric study is conducted to examine and

compare the effects of the orthotropy, the magnitude of both tensile and compressive longitudinal loads, aspect ratios of the plate including length-to-width and length-to-thickness ratios, and in-plane transverse wave number on the parametric resonance particularly the amplitude of the steady-state vibration. The present results show good agreement with that available in the literature.

Chapter 3 presents the following article:

M. Darabi, R. Ganesan.; "Non-linear vibration and dynamic instability of internally-thickness-tapered composite plates under parametric excitation". International Journal of Composite Structures, Volume 176, September 2017, Pages 82-104.

https://doi.org/10.1016/j.compstruct.2017.04.059

Internally-tapered composite plates are formed by terminating or dropping-off some of the plies in the laminates at pre-determined locations, which is an important method for stiffness tailoring and weight saving in these structures. In the present work, the dynamic instability of internally-thickness-tapered laminated composite plates subjected to harmonic in-plane loading is studied based on non-linear vibration analysis. The non-linear von Karman strains associated with large deflections and curvatures are considered. The in-plane displacements are determined from the two in-plane force-equilibrium equations of motion of non-linear large deflection tapered plate. Consequently, the in-plane force-resultants can be obtained from the in-plane displacements and further applying the boundary conditions. Then the general Galerkin method is used for the moment-equilibrium equation of motion to satisfy spatial dependence in the partial differential equation of motion to produce a set of non-linear Mathieu-Hill equations. These equations are ordinary differential equations, with time-dependency. By applying the Bolotin's method to these equations, the dynamically-unstable regions, stable-, and unstable-solutions amplitudes of the steady-state vibrations are obtained. The non-linear dynamic stability characteristics of symmetric cross-ply laminates with different taper

configurations are examined. A comprehensive parametric study is carried out to examine and compare the effects of the taper angles, magnitudes of both tensile and compressive in-plane loads, aspect ratios of the tapered plate including length-to-width and length-to-average-thickness ratios on the instability regions and the parametric resonance particularly the amplitude of the steady-state vibration. For linear vibrations, the present results show good agreement with those available in the literature which were obtained based on linear analysis.

Chapter 4 presents the following article:

M. Darabi, R. Ganesan.; "Non-linear analysis of parametric instability of internally-thickness-tapered composite cylindrical panels". Will be submitted to International Journal of Thin-Walled Structures, 2020

In the present work, the dynamic instability of internally-thickness-tapered laminated composite cylindrical panels subjected to harmonic in-plane loading is studied based on the large deflection shell theory. Internally-tapered laminated curved panels provide a considerable weight saving and stiffness tailoring by terminating or dropping-off some of the plies in the laminates at the pre-determined locations in the engineering applications. The non-linear von Karman strains associated with large deflections and curvatures are considered in the present work. Considering the simply supported boundary condition for the laminated orthotropic thickness-tapered cylindrical panel, the Navier's double Fourier series with the time-dependent coefficient is chosen to describe the out-of-plane displacement function. Then the in-plane displacements are determined from the two in-plane force-equilibrium equations of motion of non-linear large deflection of tapered cylindrical panels. Consequently, the in-plane force-resultants can be obtained from the in-plane displacements and further by applying the boundary conditions. Then the general Galerkin method is used for the moment-equilibrium equation of motion to satisfy spatial dependence in the partial differential equation of motion to produce a set of non-linear Mathieu-Hill equations. These equations are ordinary differential

equations, with time-dependency. By applying the Bolotin's method to these equations, the dynamically-unstable regions, stable-, and unstable-solutions amplitudes of the steady-state vibrations are obtained. The non-linear dynamic stability characteristics of cylindrical symmetric cross-ply laminates with different taper configurations are examined. A comprehensive parametric study is carried out to examine and compare the effects of the taper angles, magnitudes of both tensile and compressive axial loads, curvature of the panel i.e. radius-to-side ratio, aspect ratios of the cylindrical tapered panel including the loaded-to-unloaded width and length-to-average-thickness ratios on the instability regions and the parametric resonance particularly the steady-state vibrations amplitude. The present results show good agreement with those available in the literature.

Chapter 5 presents the following article:

M. Darabi, R. Ganesan.; "Non-linear dynamic instability analysis of laminated composite cylindrical shells subjected to periodic axial loads". International Journal of Composite Structures, Volume 147, July 2016, Pages 168-184.

The dynamic instability of thin laminated composite cylindrical shells subjected to harmonic axial loading is investigated in the present work based on the non-linear analysis. The equations of motion are developed using Donnell's shallow-shell theory and with von Karman-type of non-linearity. The non-linear large deflection shallow-shell equation of motion is solved by using Galerkin's technique that leads to a system of non-linear Mathieu-Hill equations. Both stable and unstable solutions amplitude of the steady-state vibrations is obtained by applying the Bolotin's method. The non-linear dynamic stability characteristics of both symmetric and antisymmetric cross-ply laminates with different lamination schemes are examined. A detailed parametric study is conducted to examine and compare the effects of the magnitude of both tensile and compressive axial loads, aspect ratios of the shell including length-to-radius and

thickness-to-radius ratios, and different circumferential wave numbers as well on the parametric resonance particularly the amplitude of the steady-state vibration. The present results show good agreement with that available in the literature.

CHAPTER 2

Non-linear dynamic instability analysis of laminated composite thin plates subjected to periodic in-plane loads

2.1 Introduction

Laminated composite plates are being increasingly used in aerospace, automotive, and civil engineering as well as in many other applications of modern engineering structures. Tailoring ability of fiber-reinforced polymer composite (FRPC) materials for the stiffness and strength properties with regard to reduction of structural weight made them superior compared with metals in such structures. To use them efficiently as a structural component it is required to have a good knowledge and understanding of their mechanical behavior such as deformations, stress distributions, natural frequencies, and static and dynamic instabilities under various loading and boundary conditions. Many scholars and researchers from different disciplines have been conducting their research works to study and investigate those mentioned structural behavior of composite structures. One of the most interesting fields of study of laminated composite plates is the dynamic instability under periodic in-plane loads.

When the lightweight structural components are subjected to dynamic loading particularly periodic in-plane loads, when the frequency of in-plane dynamic load and the frequency of vibration satisfy certain specific conditions, parametric resonance will occur in the structure, which makes the plate enter into a state of dynamic instability [2]. This instability is of concern because it can occur at load magnitudes that are much less than the static buckling load, so a component designed to withstand static buckling may fail in a periodic loading environment. Further, the dynamic instability occurs over a range of forcing frequencies rather than at a single value [2, 3].

The interest to study the dynamic stability behavior of engineering structures dates back to the text by Bolotin [1] which addresses numerous problems on the stability of structures under pulsating loads. According to the general theory of dynamic stability of elastic systems by using Bolotin's method a set of differential equations of the Mathieu-Hill type are derived, and by seeking periodic solutions using Fourier series expansion the boundaries of unstable regions are determined. An extensive bibliography of the earlier works on parametric response of structures was presented by Evan-Iwanowsky [4].

A detailed research survey on the dynamic stability behavior of plates and shells in which the literature from 1987 to 2005 has been reviewed can be found in the review paper by Sahu and Datta [5].

Srinivasan and Chellapandi [6] studied the dynamic instability of rectangular laminated composite plates under longitudinal periodic loads. They used finite strip method and using Bolotin's procedure to obtain the parametric instability regions. Although the numerical results have been limited only for the clamped plates but their method is applicable for any boundary conditions. They investigated three different configurations including symmetric, antisymmetric and asymmetric plates and the effects of aspect ratios of the plate on unstable regions.

Influence of out-of-plane transverse shear deformation on dynamic instability also has been addressed in literature [7, 8]. Moorthy and Reddy et al [9] used first order shear deformation plate theory to study the effects of damping, length-thickness ratio, boundary conditions, number of layers and lamination angles on instability regions.

Dynamic instability of laminated composite plates supported on elastic foundation, subjected to periodic in-plane loads was investigated by Patel et al [10]. They used C^1 eight-nodded shear-flexible plate element which allows both displacement and stress continuity at the interfaces between the layers. The influences of various parameters such as ply-angle, static

27

load factor, thickness and aspect ratios, and elastic foundation stiffness on dynamic instability regions were examined.

Ramachandra and Panda [11] investigated the dynamic instability problem of composite plates subjected to periodic non-uniform in-plane loads. Both the static and dynamic components of the applied load were assumed to vary according to either parabolic or linear distributions. They used Ritz method to estimate the in-plane stress distribution within the pre-buckling range due to the applied non-uniform load. Galerkin's method was implemented to derive the Mathieu type of equations. The effects of span-thickness and aspect ratios, boundary conditions and static load factor on dynamic instability regions were investigated.

All these mentioned works are based on linear analysis and so lead to the determination of dynamic instability regions. Stability analysis based on classical linear theories provided only an outline of the parameter regimes where non-linear effects are of importance. According to Popov [12] without adequate non-linear analysis the results in some cases can be inaccurate. According to linear theory, one expects the vibration amplitudes in the regions of dynamic instability to increase unboundedly with time indeed very rapidly so as to increase exponentially. However, this conclusion contradicts experimental results which reveal that vibrations with steady-state amplitudes exist in the instability regions. As the amplitude increases, the character of the vibrations changes; the speed of the growth gradually decreases until vibrations of constant (or almost constant) amplitude are finally established [1].

Some non-linear vibrations of composite panels have been addressed by Alijani and Amabili [13] from 2003 to 2013. But a few works have been conducted considering the non-linear plate theories for dynamic stability problems. A higher-order geometrically non-linear theory was used by Librescu and Thangjitham [14] to investigate the parametric instability of symmetrically laminated plates. The geometrically non-linear parametric instability characteristics of composite plates based on finite element formulation using C^1 eight-noded

shear-flexible plate element have been studied by Ganapathi et al [15]. They used Newmark integration scheme coupled with a modified Newton-Raphson iteration procedure to solve the non-linear governing equations.

To the best of authors' knowledge there is no comprehensive work on non-linear dynamic instability of thin laminated composite plates which considers the effects of stacking sequence, aspect ratios, lamination symmetry and so on. In the present work, von Karman-type of plate equation is used to develop the equation of motion of plate including geometric non-linearity for thin laminated composite flat plate subjected to harmonic in-plane loading. Galerkin's technique is then employed to solve the non-linear large deflection plate equations of motion and a system of non-linear Mathieu-Hill equations are derived. The dynamically-unstable regions, and both stable and unstable solutions amplitudes of steady-state vibrations are determined by applying the Bolotin's method. The parametric studies are performed to investigate and compare the effects of lamination schemes including stacking sequence and number of plies of symmetric and antisymmetric cross-ply laminated plates, the magnitude of in-plane loads both tensile and compressive loads, aspect ratios of the plate including length-to-width and length-to-thickness ratios, and n-plane transverse wave number on the parametric resonance particularly of the steady-state vibrations. The present results show good agreement when compared with that available in the literature and hence can be used as bench mark results for future studies.

2.2   Formulation

A thin simply supported laminated composite rectangular plate, having length a and width b with respect to the Cartesian coordinates (X, Y, Z) which are assigned in the mid-plane of the plate is considered as shown in Fig. 2.1.
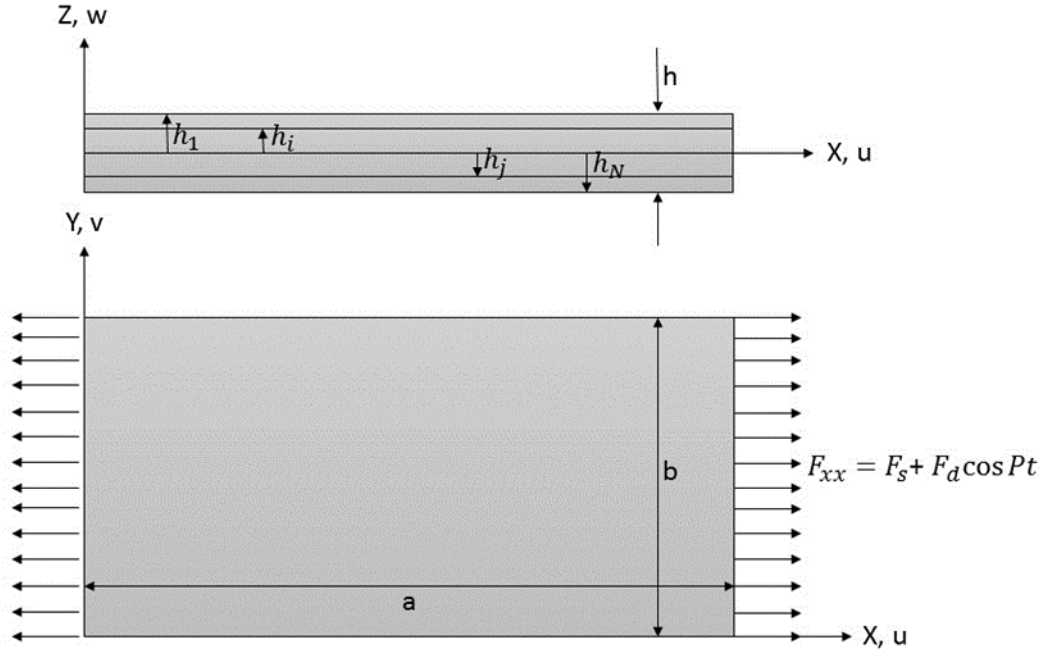
Figure 2.1 The geometry and loading condition of a laminated composite rectangular plate

Here, u, v and w are the displacement components of the plate with reference to this coordinate system in the $X, Y, and\ Z$ directions, respectively.

The plate as shown in Fig.1 is subjected to a periodically pulsating load in the length direction with the longitudinal loading per unit length as follow:

$$F_{xx}(t) = F_s + F_d cosPt \tag{2.1}$$

where F_s is a time invariant component, $F_d cosPt$ is the harmonically pulsating component, and P denotes the frequency of excitation in radians per unit time.

Since $u_0 \ll w_0$ and $v_0 \ll w_0$ we can consider that $\rho_t\ {\partial^2 u_0}/{\partial t^2} \to 0$ and $\rho_t\ {\partial^2 v_0}/{\partial t^2} \to 0$. Therefore by neglecting the in-plane inertia forces the equations of motion in the form of that originally presented by von Karman [16] and used in further development in Lagrangian coordinates by Fung [16, 17], under the longitudinal pulsating load are given by

$$\frac{\partial N_{xx}}{\partial x} + \frac{\partial N_{xy}}{\partial y} = 0 \tag{2.2}$$

$$\frac{\partial N_{xy}}{\partial x} + \frac{\partial N_{yy}}{\partial y} = 0 \tag{2.3}$$

30

$$\frac{\partial^2 M_{xx}}{\partial x^2} + 2\frac{\partial^2 M_{xy}}{\partial x \partial y} + \frac{\partial^2 M_{yy}}{\partial y^2} + N_{xx}\frac{\partial^2 w_0}{\partial x^2} + 2N_{xy}\frac{\partial^2 w_0}{\partial x \partial y} + N_{yy}\frac{\partial^2 w_0}{\partial y^2} = \rho_t \frac{\partial^2 w_0}{\partial t^2} \qquad (2.4)$$

where

$$\rho_t = \int_{-\frac{h}{2}}^{\frac{h}{2}} \rho \, dz \qquad (2.5)$$

and (N_{xx}, N_{yy}, N_{xy}) are the total in-plane force resultants and (M_{xx}, M_{yy}, M_{xy}) are the total moment resultants that are defined by

$$\begin{Bmatrix} N_{xx} \\ N_{yy} \\ N_{xy} \end{Bmatrix} = \int_{\frac{-h}{2}}^{\frac{h}{2}} \begin{Bmatrix} \sigma_{xx} \\ \sigma_{yy} \\ \sigma_{xy} \end{Bmatrix} dz \qquad (2.6)$$

$$\begin{Bmatrix} M_{xx} \\ M_{yy} \\ M_{xy} \end{Bmatrix} = \int_{\frac{-h}{2}}^{\frac{h}{2}} \begin{Bmatrix} \sigma_{xx} \\ \sigma_{yy} \\ \sigma_{xy} \end{Bmatrix} Z \, dz \qquad (2.7)$$

The nonzero von Karman strains associated with non-linear large deflections and curvatures are given by

$$\begin{Bmatrix} \epsilon_{xx} \\ \epsilon_{yy} \\ \gamma_{xy} \end{Bmatrix} = \begin{Bmatrix} \epsilon_{xx}^{(0)} \\ \epsilon_{yy}^{(0)} \\ \gamma_{xy}^{(0)} \end{Bmatrix} + z \begin{Bmatrix} \epsilon_{xx}^{(1)} \\ \epsilon_{yy}^{(1)} \\ \gamma_{xy}^{(1)} \end{Bmatrix} \qquad (2.8)$$

$$\{\epsilon^0\} = \begin{Bmatrix} \epsilon_{xx}^{(0)} \\ \epsilon_{yy}^{(0)} \\ \gamma_{xy}^{(0)} \end{Bmatrix} = \begin{Bmatrix} \frac{\partial u_0}{\partial x} + \frac{1}{2}\left(\frac{\partial w_0}{\partial x}\right)^2 \\ \frac{\partial v_0}{\partial y} + \frac{1}{2}\left(\frac{\partial w_0}{\partial y}\right)^2 \\ \frac{\partial u_0}{\partial y} + \frac{\partial v_0}{\partial x} + \frac{\partial w_0}{\partial x}\frac{\partial w_0}{\partial y} \end{Bmatrix} \qquad (2.9)$$

$$\{\epsilon^1\} = \begin{Bmatrix} \epsilon_{xx}^{(1)} \\ \epsilon_{yy}^{(1)} \\ \gamma_{xy}^{(1)} \end{Bmatrix} = \begin{Bmatrix} -\frac{\partial^2 w_0}{\partial x^2} \\ -\frac{\partial^2 w_0}{\partial y^2} \\ -2\frac{\partial^2 w_0}{\partial x \partial y} \end{Bmatrix} \qquad (2.10)$$

where $(\epsilon_{xx}^{(0)}, \epsilon_{yy}^{(0)}, \gamma_{xy}^{(0)})$ are the membrane strains, $(\epsilon_{xx}^{(1)}, \epsilon_{yy}^{(1)}, \gamma_{xy}^{(1)})$ are the flexural (bending) strains and (u_0, v_0, w_0) are mid-plane displacements.

The thin rectangular plate is constructed by a cross-ply laminated composite material having density ρ. Hence the state of stress is governed by the generalized Hooke's law. The linear

constitutive relations for the kth orthotropic lamina in the principal material coordinates of a lamina are

$$
\begin{Bmatrix} \sigma_1 \\ \sigma_2 \\ \sigma_6 \end{Bmatrix}^{(k)} = \begin{bmatrix} Q_{11} & Q_{12} & 0 \\ Q_{12} & Q_{22} & 0 \\ 0 & 0 & Q_{66} \end{bmatrix}^{(k)} \begin{Bmatrix} \epsilon_1 \\ \epsilon_2 \\ \epsilon_6 \end{Bmatrix}
\tag{2.11}
$$

where $[Q]^{(k)}$ is the reduced stiffness matrix of the kth lamina and its components $Q_{ij}^{(k)}$ are known in terms of the engineering constants of the kth layer, as

$$
Q_{11} = \frac{E_{11}}{1-v_{12}v_{21}}
\tag{2.12a}
$$

$$
Q_{12} = \frac{v_{12}E_{22}}{1-v_{12}v_{21}}
\tag{2.12b}
$$

$$
Q_{22} = \frac{E_{22}}{1-v_{12}v_{21}}
\tag{2.12c}
$$

$$
Q_{66} = G_{12}
\tag{2.12d}
$$

where E_{11} and E_{22} are the elastic moduli in the principal material coordinates, G_{12} is the shear modulus and v_{12} and v_{21} are the Poisson's ratios.

The constitutive equation of the laminate which is made of several orthotropic layers, with the arbitrarily oriented material axes to the laminate coordinate, can be obtained by transformation of the stress-strain relations in the laminate coordinates as follow:

$$
\begin{Bmatrix} \epsilon_{xx} \\ \epsilon_{yy} \\ \gamma_{xy} \end{Bmatrix}^{(k)} = \begin{bmatrix} \bar{Q}_{11} & \bar{Q}_{12} & \bar{Q}_{16} \\ \bar{Q}_{12} & \bar{Q}_{22} & \bar{Q}_{26} \\ \bar{Q}_{16} & \bar{Q}_{26} & \bar{Q}_{66} \end{bmatrix}^{(k)} \begin{Bmatrix} \epsilon_{xx} \\ \epsilon_{yy} \\ \gamma_{xy} \end{Bmatrix}
\tag{2.13}
$$

where $[\bar{Q}]^{(k)}$ is the transformed reduced stiffness matrix defined as follow:

$$
[\bar{Q}] = [T]^{-1}[Q][T]^{-T}
\tag{2.14}
$$

where $[T]$ is the transformation matrix between the principal material coordinates and the plate's coordinates given by

$$
[T] = \begin{bmatrix} \cos^2 \vartheta & \sin^2 \vartheta & 2\cos\vartheta\sin\vartheta \\ \sin^2 \vartheta & \cos^2 \vartheta & -2\cos\vartheta\sin\vartheta \\ -\cos\vartheta\sin\vartheta & 2\cos\vartheta\sin\vartheta & \cos^2 \vartheta - \sin^2 \vartheta \end{bmatrix}
\tag{2.15}
$$

and ϑ is the angular orientation of the fibers. By following the equations (2.6)-(2.15) the force

and moment resultants are defined as

$$
\begin{Bmatrix} N_{xx} \\ N_{yy} \\ N_{xy} \\ M_{xx} \\ M_{yy} \\ M_{xy} \end{Bmatrix} = \begin{bmatrix} A_{11} & A_{12} & A_{16} & B_{11} & B_{12} & B_{16} \\ A_{12} & A_{22} & A_{26} & B_{12} & B_{22} & B_{26} \\ A_{16} & A_{26} & A_{66} & B_{16} & B_{26} & B_{66} \\ B_{11} & B_{12} & B_{16} & D_{11} & D_{12} & D_{16} \\ B_{12} & B_{22} & B_{26} & D_{12} & D_{22} & D_{26} \\ B_{16} & B_{26} & B_{66} & D_{16} & D_{26} & D_{66} \end{bmatrix} \begin{Bmatrix} \epsilon_{xx}^{(0)} \\ \epsilon_{yy}^{(0)} \\ \gamma_{xy}^{(0)} \\ \epsilon_{xx}^{(1)} \\ \epsilon_{yy}^{(1)} \\ \gamma_{xy}^{(1)} \end{Bmatrix} \qquad (2.16)
$$

where A_{ij} denote the extensional stiffnesses, D_{ij} the bending stiffnesses, and B_{ij} the bending-

extensional coupling stiffnesses

$$
A_{ij} = \sum_{k=1}^{N} \bar{Q}_{ij}^{(k)}(h_k - h_{k+1}) \qquad , (i,j = 1,2,6) \qquad (2.17a)
$$

$$
B_{ij} = \frac{1}{2} \sum_{k=1}^{N} \bar{Q}_{ij}^{(k)}(h_k^2 - h_{k+1}^2) \qquad (2.17b)
$$

$$
D_{ij} = \frac{1}{3} \sum_{k=1}^{N} \bar{Q}_{ij}^{(k)}(h_k^3 - h_{k+1}^3) \qquad (2.17c)
$$

where h_k and h_{k+1} are measured from the plate reference surface to the outer and inner

surfaces of the kth layer, respectively, as shown in Fig. 1. From Eq.(2.16) the strains can be

written as

$$
\begin{Bmatrix} \epsilon_{xx}^{(0)} \\ \epsilon_{yy}^{(0)} \\ \gamma_{xy}^{(0)} \end{Bmatrix} = [A_{ij}]^{-1} \begin{Bmatrix} N_{xx} \\ N_{yy} \\ N_{xy} \end{Bmatrix} - [A_{ij}]^{-1}[B_{ij}] \begin{Bmatrix} \epsilon_{xx}^{(1)} \\ \epsilon_{yy}^{(1)} \\ \gamma_{xy}^{(1)} \end{Bmatrix} =
$$

$$
\begin{Bmatrix} a_{11}N_{xx} + a_{12}N_{yy} - b_{11}\epsilon_{xx}^{(1)} - b_{12}\epsilon_{yy}^{(1)} \\ a_{12}N_{xx} + a_{22}N_{yy} - b_{21}\epsilon_{xx}^{(1)} - b_{22}\epsilon_{yy}^{(1)} \\ a_{66}N_{xy} - b_{66}\gamma_{xy}^{(1)} \end{Bmatrix} \qquad (2.18)
$$

where

$$
a_{11} = \Delta A_{22} \,, a_{12} = -\Delta A_{12} \,, a_{22} = \Delta A_{11}, a_{66} = \frac{1}{A_{66}} \,,
$$

$$
b_{11} = \Delta(A_{22}B_{11} - A_{12}B_{12}) \,, b_{12} = \Delta(A_{22}B_{12} - A_{12}B_{22}) \,,
$$

$$
b_{21} = \Delta(A_{11}B_{12} - A_{12}B_{11}), \; b_{22} = \Delta(A_{11}B_{22} - A_{12}B_{12}) \,,
$$

$$b_{66} = \frac{B_{66}}{A_{66}}, \Delta = \frac{1}{(A_{11}A_{22} - A_{12}^2)} \tag{2.19}$$

The moment resultants also can be written from Eq.(2.16) as

$$\begin{Bmatrix} M_{xx} \\ M_{yy} \\ M_{xy} \end{Bmatrix} = [b_{ij}]^T \begin{Bmatrix} N_{xx} \\ N_{yy} \\ N_{xy} \end{Bmatrix} + [d_{ij}] \begin{Bmatrix} \epsilon_{xx}^{(1)} \\ \epsilon_{yy}^{(1)} \\ \gamma_{xy}^{(1)} \end{Bmatrix} = \begin{Bmatrix} b_{11}N_{xx} + b_{21}N_{yy} + d_{11}\epsilon_{xx}^{(1)} + d_{12}\epsilon_{yy}^{(1)} \\ b_{12}N_{xx} + b_{22}N_{yy} + d_{12}\epsilon_{xx}^{(1)} + d_{22}\epsilon_{yy}^{(1)} \\ b_{66}N_{xy} + d_{66}\gamma_{xy}^{(1)} \end{Bmatrix}$$

$$\tag{2.20}$$

where

$$[b_{ij}] = [A_{ij}]^{-1}[B_{ij}] \tag{2.21a}$$

$$[d_{ij}] = -[B_{ij}][b_{ij}] + [D_{ij}] \tag{2.21b}$$

$$d_{11} = \Delta(A_{11}A_{22}D_{11} - A_{11}B_{12}^2 - A_{12}^2 D_{11} + 2A_{12}B_{11}B_{12} - A_{22}B_{11}^2)$$

$$d_{12} = \Delta(A_{11}A_{22}D_{12} - A_{11}B_{12}B_{22} - A_{12}^2 D_{12} + A_{12}B_{11}B_{22} + A_{12}B_{12}^2 - A_{22}B_{11}B_{12})$$

$$d_{21} = \Delta(A_{11}A_{22}D_{12} - A_{11}B_{12}B_{22} - A_{12}^2 D_{12} + A_{12}B_{11}B_{22} + A_{12}B_{12}^2 - A_{22}B_{11}B_{12})$$

$$d_{22} = \Delta(A_{11}A_{22}D_{22} - A_{11}B_{22}^2 - A_{12}^2 D_{22} + 2A_{12}B_{12}B_{22} - A_{22}B_{12}^2)$$

$$d_{66} = \frac{A_{66}D_{66} - B_{66}^2}{A_{66}} \tag{2.21c}$$

Here we define the membrane forces in terms of Airy's stress function φ as

$$N_{xx} = \frac{\partial^2 \phi}{\partial y^2} \tag{2.22a}$$

$$N_{yy} = \frac{\partial^2 \phi}{\partial x^2} \tag{2.22b}$$

$$N_{xy} = -\frac{\partial^2 \phi}{\partial x \partial y} \tag{2.22c}$$

Substituting Equations (2.10) and (2.22 a-c) into equations (2.18) and (2.20) the strains and moment resultants are given in terms of the Airy's stress function ϕ and w_0. By combining the mid-plane strains, the compatibility equation can be expressed as

$$\frac{\partial^2 \epsilon_{yy}^{(0)}}{\partial x^2} + \frac{\partial^2 \epsilon_{xx}^{(0)}}{\partial y^2} - \frac{\partial^2 \gamma_{xy}^{(0)}}{\partial x \partial y} = (\frac{\partial^2 w_0}{\partial x \partial y})^2 - \frac{\partial^2 w_0}{\partial x^2}\frac{\partial^2 w_0}{\partial y^2} \tag{2.23}$$

Replacing the strains in terms of the Airy's stress function ϕ from Eq. (2.18) and w_0 into Eq.(2.23) the non-linear equation of compatibility can be derived as:

$$a_{22}\frac{\partial^4\phi}{\partial x^4} + a_{11}\frac{\partial^4\phi}{\partial y^4} + (2a_{12} + a_{66})\frac{\partial^4\phi}{\partial x^2\partial y^2} + b_{21}\frac{\partial^4 w_0}{\partial x^4} + b_{12}\frac{\partial^4 w_0}{\partial y^4} + (b_{11}+b_{22} -$$

$$2b_{66})\frac{\partial^4 w_0}{\partial x^2\partial y^2} = (\frac{\partial^2 w_0}{\partial x\partial y})^2 - \frac{\partial^2 w_0}{\partial x^2}\frac{\partial^2 w_0}{\partial y^2} \tag{2.24}$$

2.3   Solution for laminated orthotropic plates

Considering the simply supported boundary condition for the laminated orthotropic plate, the Navier's double Fourier series with the time dependent coefficient $q_{mn}(t)$ is chosen to describe the out-of-plane displacement function $w_0(x, y, t)$:

$$w_0 = \sum_{m=1}^{\infty}\sum_{n=1}^{\infty} q_{mn}(t)\sin\frac{m\pi}{a}x \sin\frac{n\pi}{b}y \tag{2.25}$$

where m and n represent the number of longitudinal and transverse half waves in corresponding standing wave pattern, respectively.

F_{xx} is the average longitudinal force at the edge, thus the stress function has to satisfy the following condition

$$\frac{1}{b}\int_0^b \frac{\partial^2\phi}{\partial y^2} dy = F_{xx} \quad at\ x = 0, a \tag{2.26}$$

Airy's stress function can be governed by substituting Eq. (2.25) into Eq. (2.24) and applying different trigonometric relations, as:

$$\phi = \frac{1}{2}F_{xx}y^2 + \sum_{m=1}^{\infty}\sum_{n=1}^{\infty}\left\{-\frac{1}{2}A_{mn}q_{mn}(t)\xi_1[\sin(\lambda_m x - \lambda_n y) + \sin(\lambda_m x + \lambda_n y)] + \right.$$

$$\left.\frac{1}{32}B_{mn}q_{mn}^2(t)[\xi_2 \cos(2\lambda_m x) - \xi_3 \cos(2\lambda_n y)]\right\} \tag{2.27}$$

where $\lambda_m = m\pi/a$, $\lambda_n = n\pi/b$ and

$$A_{mn} = b_{21}\lambda_m^4 + b_{12}\lambda_n^4 + (b_{11}+b_{22} - 2b_{66})\lambda_m^2\lambda_n^2 \tag{2.28a}$$

$$B_{mn} = \lambda_m^2\lambda_n^2 \tag{2.28b}$$

$$\xi_1 = 1\Big/\left(a_{22}\lambda_m^4 + a_{11}\lambda_n^4 + (2a_{12} + a_{66})\lambda_m^2\lambda_n^2\right) \tag{2.28c}$$

$$\xi_2 = \frac{1}{(a_{22}\lambda_m{}^4)} \tag{2.28d}$$

$$\xi_3 = \frac{1}{(a_{11}\lambda_n{}^4)} \tag{2.28e}$$

Substituting the relations (2.22a-c) in Eqs. (2.2) and (2.3), these equations are satisfied automatically. With the definitions (2.22a-c), the membrane forces N_{xx} , N_{yy} and N_{xy} are computable by this solution and the boundary condition (2.26) is satisfied. As mentioned before by substituting Eqs. (2.10) and (2.22a-c) into equations (2.20) the moments are given in terms of the Airy's stress function ϕ and w_0 so by inserting these functions the moment resultants M_{xx} , M_{yy} and M_{xy} are also computable. By substituting these stress and moment resultants and the out-of-plane displacement as defined in Eq.(2.25) into the third equation of motion, Eq. (2.4) and after multiplying the governing equation by $\sin \lambda_m x \cos \lambda_n y$ and integrating over the plate area, a system of $m \times n$ second-order ordinary differential equations is obtained:

$$M_{mn}\ddot{q}_{mn}(t) + K_{mn}q_{mn}(t) - (F_s + F_d \cos pt)Q_{mn}q_{mn}(t) + \eta_{mn}q_{mn}^3(t) = 0 \tag{2.29}$$

where M_{mn}, K_{mn} , Q_{mn} and η_{mn} are matrices that are defined in the Appendix (Eqs.(A.1)-(A.4)) and $\ddot{q}_{mn}(t)$, $q_{mn}(t)$ and $q_{mn}^3(t)$ are column vectors consisting of the $\ddot{q}_{mn}(t)$'s, $q_{mn}(t)$'s and $q_{mn}^3(t)$'s respectively. The subscripts m and n have the following ranges:

$$m, n = 1,2,3,4,..,N. \tag{2.30}$$

Introducing following notation:

$$\omega_{mn} = \sqrt{\frac{K_{mn}}{M_{mn}}} \tag{2.31a}$$

$$\gamma_{mn} = \frac{\eta_{mn}}{M_{mn}} \tag{2.31b}$$

$$N_* = \frac{K_{mn}}{Q_{mn}} \tag{2.31c}$$

Eq. (2.29) can be written in the form of the non-linear Mathieu equation as follow:

$$\ddot{q}_{mn}(t) + \Omega_{mn}^2 (1 - 2\mu_{mn} \cos pt)q_{mn}(t) + \gamma_{mn}q_{mn}^3 (t) = 0 \tag{2.32}$$

where Ω_{mn} is the frequency of the free vibration of the plate loaded by a constant longitudinal force F_s,

$$\Omega_{mn} = \omega_{mn}\sqrt{1 - \frac{F_s}{N_*}} \tag{2.33}$$

and μ_{mn} is a quantity that is called the excitation parameter,

$$\mu_{mn} = \frac{F_d}{2(N_* - F_s)} \tag{2.34}$$

2.4 Amplitude of vibrations at the principal parametric resonance

As mentioned above Eq. (2.32) is a non-linear Mathieu equation where the non-linear term $\gamma q_{mn}^3(t)$ represents the effect of large deflection. According to Liapunov Principle, dynamically-unstable region is determined by the linear parts of the Eq. (2.32) [1] which will be discussed in the next section. Here the focus is set on the parametric resonance of the system. The basic solutions of Mathieu equation include two periodic solutions: i.e. periodic solutions of periods T and $2T$ with $T = 2\pi/P$. The solutions with period $2T$ are of greater practical importance as the widths of these unstable regions are usually larger than those associated with solutions having period T. Using Bolotin's [1] method for parametric vibration, the solution of period $2T$ is given by the following equation:

$$q(t) = \sum_{k=1,3,5,\ldots}^{\infty} f_k \sin\frac{kPt}{2} + g_k \cos\frac{kPt}{2} \tag{2.35}$$

where f_k and g_k are arbitrary vectors. If we investigate the vibration at the principal resonance at frequency $\approx 2\Omega$, we can neglect the influence of higher harmonics in the expansion of above equation and can assume

$$q(t) = f \sin\frac{Pt}{2} + g \cos\frac{Pt}{2} \tag{2.36}$$

as an approximation. By substituting this function into Eq. (2.32) and equating the coefficients of $\sin(Pt/2)$ and $\cos(Pt/2)$ terms and neglecting terms containing higher harmonics, the following system of equations for the coefficients a and b remains:

$$\left[\Omega_{mn}^2(1 + \mu_{mn}) - \frac{P^2}{4}\right]f + \Gamma(f, g) = 0, \tag{2.37a}$$

$$\left[\Omega_{mn}^2(1 - \mu_{mn}) - \frac{P^2}{4}\right]g + \Psi(f, g) = 0, \tag{2.37b}$$

where $\Gamma(f, g)$ and $\Psi(f, g)$ are defined as coefficients of the terms including $\sin(Pt/2)$ and $\cos(Pt/2)$ which were obtained from the first approximation of expansion in a Fourier series as:

$$\Gamma(f, g) = \frac{3\gamma_{mn}}{4}A^2 f \tag{2.38a}$$

$$\Psi(f, g) = \frac{3\gamma_{mn}}{4}A^2 g \tag{2.38b}$$

where A is the amplitude of steady-state vibrations and is given by:

$$A = \sqrt{f^2 + g^2} \tag{2.39}$$

By substitution of Eqs. (2.38a, b) into Eqs. (2.37a, b) a system of two homogeneous linear equations with respect to f and g can be obtained. This system has solutions that differ from zero only in the case where the determinant composed of the coefficients disappears:

$$\begin{vmatrix} 1 + \mu_{mn} - n_{mn}^2 + \frac{3\gamma_{mn}}{4\Omega_{mn}^2}A^2 & 0 \\ 0 & 1 - \mu_{mn} - n_{mn}^2 + \frac{3\gamma_{mn}}{4\Omega_{mn}^2}A^2 \end{vmatrix} = 0 \tag{2.40}$$

where

$$n_{mn} = \frac{P}{2\Omega_{mn}} \tag{2.41}$$

Expanding the determinant and solving the resulting equation with respect to the amplitude, A, of the steady-state vibrations the following equation is obtained:

$$A = \frac{2\Omega_{mn}}{\sqrt{3\gamma_{mn}}}\sqrt{n_{mn}^2 - 1 \pm \mu_{mn}} \tag{2.42}$$

It can be proved that in the $\pm\mu_{mn}$ term of the above equation, only $+\mu_{mn}$ term yields the stable solution, and all the other terms yield unstable solutions.

2.5 Dynamic instability regions

The resonance curve is not influenced by non-linearity of Eq. (2.29) and as mentioned in the previous section the dynamic instability regions are determined by linear part of Mathieu-Hill equation, and so the equation (2.29) can be rewritten as follow:

$$M_{mn}\ddot{q}_{mn}(t) + (K_{mn}^* - Q_{mn}^* \cos Pt)q_{mn}(t) + \eta_{mn}q_{mn}^3(t) = 0 \qquad (2.43)$$

where

$$K_{mn}^* = K_{mn} - F_s Q_{mn} \qquad (2.44)$$

and

$$Q_{mn}^* = F_d Q_{mn} \qquad (2.45)$$

The principal region of dynamic instability which corresponds to solution of period $2T$ is determined by substituting Eq. (2.37) into Eq. (2.43) and equating the determinant of the coefficient matrix of linear part of the governing equation to zero as follow:

$$\begin{vmatrix} K_{mn}^* - \dfrac{Q_{mn}^*}{2} - \dfrac{M_{mn}}{4}P^2 & 0 \\ 0 & K_{mn}^* + \dfrac{Q_{mn}^*}{2} - \dfrac{M_{mn}}{4}P^2 \end{vmatrix} = 0 \qquad (2.46)$$

Comparing equations (2.46) and (2.40) by replacing μ_{mn}, n_{mn}, γ_{mn} and Ω_{mn} in terms of K_{mn}^*, Q_{mn}^* and M_{mn} reveals that the dynamic instability regions are determined by setting $A = 0$ in equation (2.40).

Equation (2.46) can be rearranged to the more simplified form of an eigenvalue problem as follow:

$$\begin{vmatrix} K_{mn}^* - \dfrac{Q_{mn}^*}{2} & 0 \\ 0 & K_{mn}^* + \dfrac{Q_{mn}^*}{2} \end{vmatrix} - P^2 \begin{vmatrix} \dfrac{M_{mn}}{4} & 0 \\ 0 & \dfrac{M_{mn}}{4} \end{vmatrix} = 0 \qquad (2.47)$$

2.6 Numerical results and discussions

Non-linear dynamic stability characteristics of cross-ply laminated composite rectangular plates subjected to combined static and periodic longitudinal loads are studied here. The

material properties used in the present analysis are chosen in accordance with Ramachandra. et al [11] as $E_1/E_2 = 40$, $G_{12}/E_2 = 0.5$ and $v_{12} = 0.25$.

As mentioned before the main objective of this work is to study the influence of geometric non-linearity on the dynamic instability of laminated composite rectangular plates which are characterized by the non-linear Mathieu-Hill equation as given by Eqs. (2.29) and (2.32). In section 5 it was observed that the dynimaic instability regions based on the large deflection formulation are achieved by either linear part of the non-linear Mathieu-Hill equation or by setting $A = 0$ in equation (2.40).

2.6.1   Validation

In order to validate the present formulation which is based on the non-linear analysis we also obtain the numerical results that correspond to the dynamically-unstable regions to compare them with those available in the literature [9, 11], for cross-ply laminated composite plates.

Figure 2 displays the boundaries of the first (from left to the right of the frequency axis) dynamically-unstable region of a four-layered symmetric $[(0°, 90°)_1]_S$ cross-ply laminated square plate having thickness ratio of $a/h = 25$. Here to compare the results with Moorthy et al [9] and Ramachandra et al [11] the static and periodic components of the longitudinal load are considered as $F_s = \alpha N_{cr}$ and $F_d = \beta N_{cr}$ where α and β are static and periodic load factors, respectively. In this figure α is zero and the critical buckling load N_{cr} of the studied plate has been calculated as follow:

$$|K_{mn} - N_{cr}Q_{mn}| = 0 \tag{2.48}$$
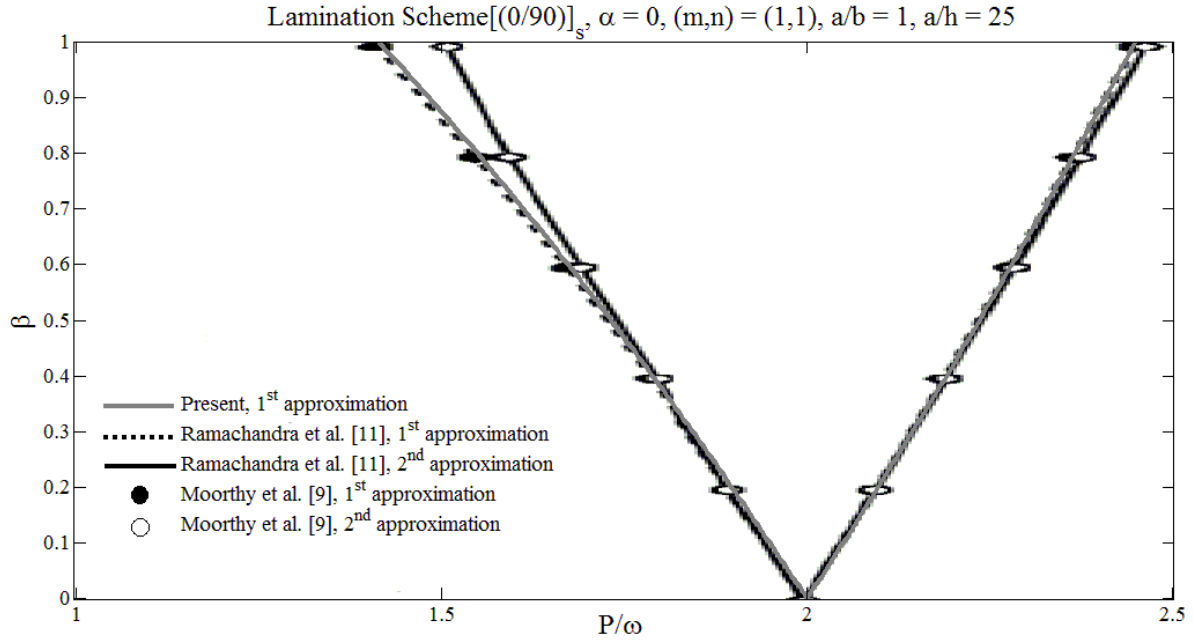
Figure 2.2 The first unstable region of a four-layered symmetric $[(0^\circ, 90^\circ)_1]_S$ cross-ply laminated square plate with thickness ratio of $a/h = 25$ subjected to periodic longitudinal load having static load factor of $\alpha = 0$

The free vibration frequencies of the studied plate are also calculated as follow:

$$|K_{mn} - \omega^2 M_{mn}| = 0 \tag{2.49}$$

As it can be observed from this figure each unstable region is separated by two lines with a common point of origin. Actually these two lines are not completely straight and they curved slightly outward. In this figure the "1st approximation" predicate to the smallest possible truncation which corresponds to $k = 1$ in Eq. (2.35) and the next smallest truncation, called the "2nd approximation" corresponds to $k = 3$ in Eq. (2.35). As it has been mentioned in section 4, in the present work the influence of higher harmonics in the expansion of Eq. (2.35) has been neglected and led to Eq. (2.36) which is the "1st approximation". It is observed from this figure that there is an excellent agreement between the present results with those obtained by Moorthy et al [9] and Ramachandra et al [11] and as one can see all the corresponding three plots almost completely coincide with each other.

As an another comparison of the present results with Moorthy et al [9] and also to investigate the effects of orthotropy on the first unstable region,$(m, n) = (1,1)$, the results are plotted in
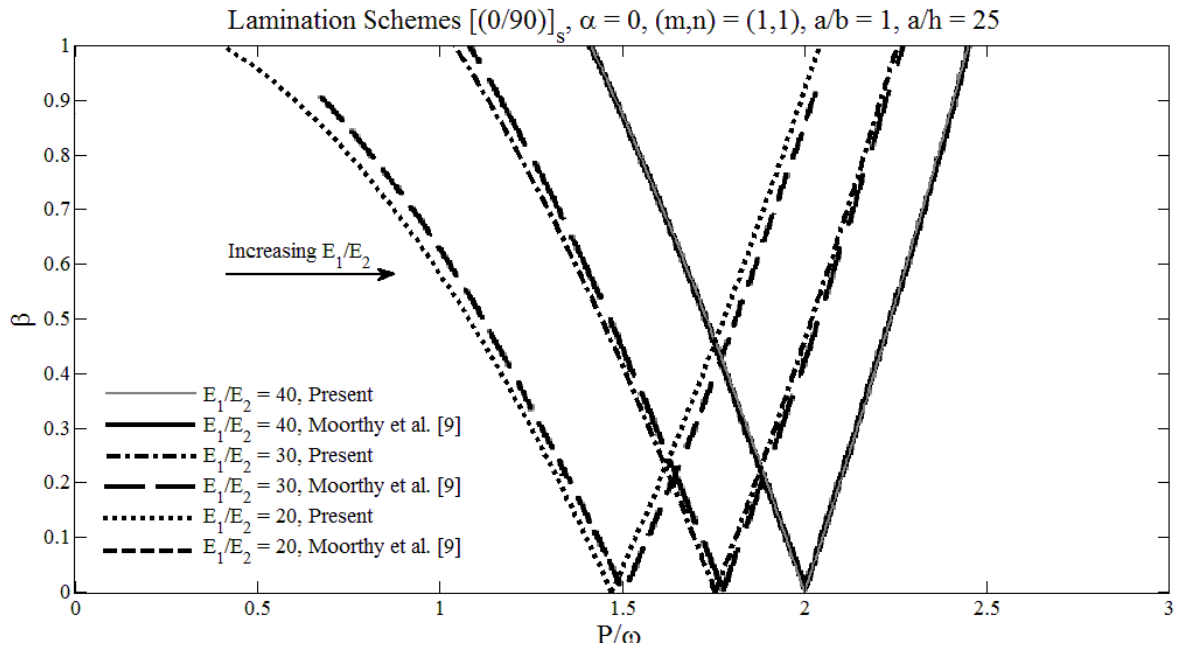
Figure 2.3 Effect of orthotropy on the first unstable region, $(m, n) = (1, 1)$, of a four-layered symmetric $[(0°, 90°)_1]_S$ cross-ply laminated square plate with thickness ratio of $a/h = 25$ subjected to periodic longitudinal load having static load factor of $\alpha = 0$

Fig. 2.3. The figure represents the plots for four-layered symmetric $[(0°, 90°)_1]_S$ cross-ply laminated square plate with thickness ratio of $a/h = 25$ subjected to periodic longitudinal load having again static load factor of $\alpha = 0$. For a better comparison of the results here the plots are depicted based on the critical buckling load and fundamental frequency of the plate having orthotropic ratio of $\frac{E_1}{E_2} = 40$ for all the three cases i.e. for $\frac{E_1}{E_2} = 40, \frac{E_1}{E_2} = 30$ and $\frac{E_1}{E_2} = 20$. As it can be observed from this figure that for the case $\frac{E_1}{E_2} = 40$ the present plot and the corresponding one by Moorthy et al [9] almost completely coincide with each other and there is a very small difference between present plots and that of Moorthy et al [9] for the orthotropic ratios of 30 and 20. This figure illustrates that at any certain value of load factor β, that is, at any certain longitudinal periodic load, once the ratio of $\frac{E_1}{E_2}$ is decreased, the values of excitation frequency for instability tend to decrease and the range of values (or in other words the width of instability region) increases. Here again there is an excellent agreement between these two studies.

In the analysis of dynamic stability of plates and shells, there exists simultaneously the stable and unstable solutions. Figure 2.4 presents the effect of orthotropy on both the stable- and unstable-solution amplitudes of steady-state vibrations of the first mode, $(m, n) = (1,1)$, for the four-layered symmetric $[(0^{°}, 90^{°})_1]_S$ cross-ply laminated square plate. The plates have thickness ratio of $a/h = 25$ and subjected to periodic longitudinal load with static load factor of $\alpha = 0$ and dynamicload factor of $\beta = 0.3$. The critical buckling load and fundamental frequency of the plate for all these three cases of $\frac{E_1}{E_2}$ are the same as the case which has been explained in Fig. 2.3. It is a characteristic of the non-linear response that the resonance curves are bent toward the axis of increasing frequencies [1]. The difference between these two solutions refers to the required magnitudes of frequency and amplitude to stimulate a parametric resonance. If this difference between them is small, then there might be the possibility of occurring parametric resonance. If the difference is large, it means high values of vibration frequency and amplitude are needed to stimulate a possible parametric resonance. The dynamic stability of such a plate or shell system is said to be good [2, 18]. As it is observed from this figure both the stable and unstable amplitudes of steady-state vibrations shift to the right having lower frequencies of excitation; Or in other words, at any certain excitation frequency both stable and unstable amplitudes of steady state vibrations increase as the ratio of $\frac{E_1}{E_2}$ is decreased. Also it is evident from this figure that once the amplitude is zero the corresponding excitation frequency coincides with the boundaries of dynamically-unstable regions, having dynamic load factor of $\beta = 0.3$. The zero stable- and unstable-solution amplitudes of this figure exactly coincide with the left and right curves of corresponding unstable

Lamination Schemes $[(0/90)]_s$, $\alpha = 0$, $\beta = 0.3$, $(m,n) = (1,1)$, a/b = 1, a/h = 25
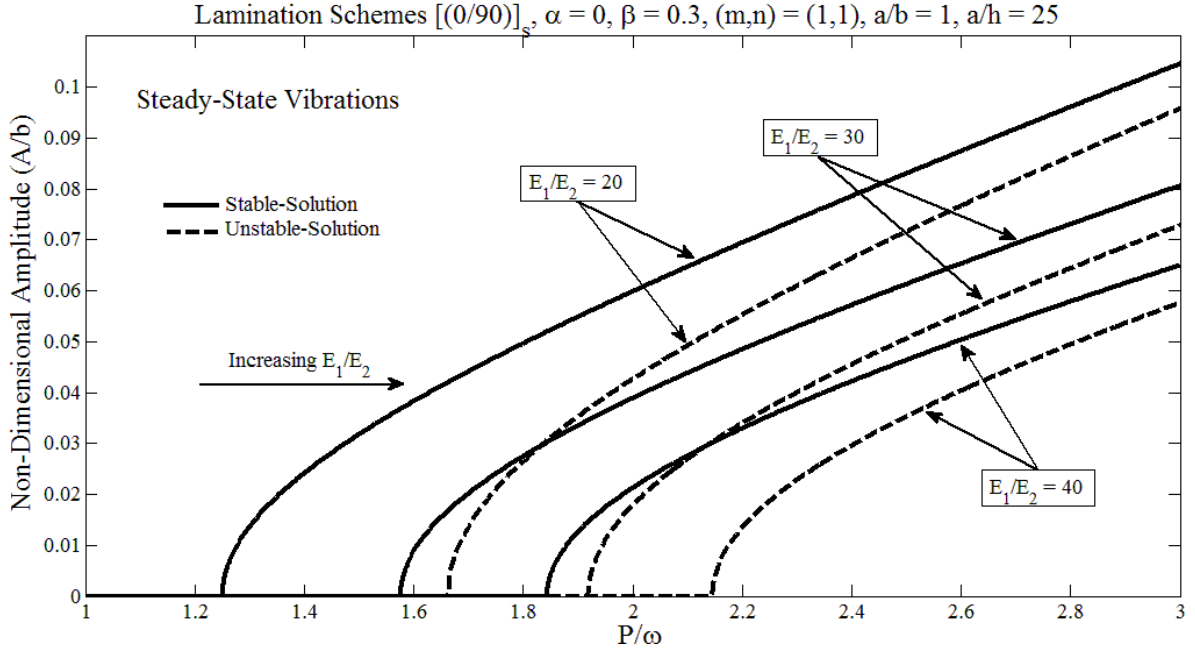
Figure 2.4 Effect of orthotropy on both the stable- and unstable-solution amplitudes of steady-state vibrations of the first mode, $(\boldsymbol{m,n}) = (\mathbf{1,1})$, for the four-layered symmetric $[(\mathbf{0}°, \mathbf{90}°)_1]_S$ cross-ply laminated square plate having thickness ratio of $\boldsymbol{a/h} = \mathbf{25}$ subjected to periodic longitudinal load having static load factor of $\boldsymbol{\alpha} = \mathbf{0}$ and dynamic load factor of $\boldsymbol{\beta} = \mathbf{0.3}$

regions, respectively shown in Figure 2.3 and the range of frequencies between these two solutions at $A = 0$ predicate the dynamically-unstable regions at this certain value of dynamic load factor β. So this figure shows graphically that unstable regions could be obtained by setting $A = 0$ in equation (2.40) and it could be considered as a validation of this non-linear part of dynamic instability analysis.

As another validation of the non-linear part of dynamic instability analysis i.e. both the stable- and unstable-solution amplitudes of steady-state vibrations, the present results are compared with those given by Ostiguy et al [19] for isotropic homogeneous rectangular plate in Figs. 2.5 and 2.6. To compare the results we set in our formulation the material property as $E_1 = E_2 = E = 4.83\ GPa$, $v_{12} = v = 0.38$ and $\rho = 1190\ kg/m^3$ and the geometry of the plate as $a = 50\ cm$, $b = 20.4\ cm$ and $h = 0.125\ cm$. The static component of the periodic longitudinal load in these two figures is cosidered as $F_s = -0.5\ N_{cr}^*$ and $F_s = -0.8\ N_{cr}^*$, respectively and the dynamic component is considered as $F_d = -0.2\ N_{cr}^*$ for both figures where N_{cr}^* is the buckling load according to Ostiguy et al [19] as follow:

44

$$N_{cr} = \frac{\pi^2 D}{b^2} \left(m_c \frac{b}{a} + \frac{1}{m_c} \frac{a}{b} \right)^2 \qquad (2.50a)$$

where

$$D = \frac{Eh^3}{12(1 - v_{12}^2)} \qquad (2.50b)$$

and m_c is the "number of half-waves of prevalent buckling mode" which "depends strongly on the aspect ratio of the plate" [19]. It is observed from these figures that there is an excellent agreement between the present results with those obtained by Ostiguy et al [19] and as one can see all the corresponding plots of $(m, n) = (3,1), (4,1)$ and $(5,1)$ completely coincide with each other and there is acceptable difference for the lower mode of $(m, n) = (2,1)$ between the present results and those by Ostiguy et al [19]. This difference could be due to considering the Navier's double Fourier series for displacement function $w_0(x, y, t)$ of simply supported boundary condition and using Airy's stress function for the in-plane force resultants that are finally obtained by applying compatibility equation in terms of this displacement function in the present work which is done for one term of displacement function for all values of m and n, still it is more accurate even for the lower value of $m = 2$ than the solution for the stress function which has been represented by a truncated double series consisting of Beam Functions in the later study that leads to "determination of the elasticity parameter, whose value is dependent on the number of terms taken in the double series" [19]. The authors of the later article also mentioned in their work that the convergence characteristic of that elasticity parameter indicates that more terms were needed for convergence as the order of (m) of the spatial mode is increased [19]. Hence their solution for lower values of m doesn't have sufficient accuracy so one can see from these two figures (Figs. 2.5 and 2.6) that once the upper limits of summation of m in the work by Ostiguy et al [19] increase to $m = 3, 4, 5, \dots$ an excellent agreement is achieved between these two studies.
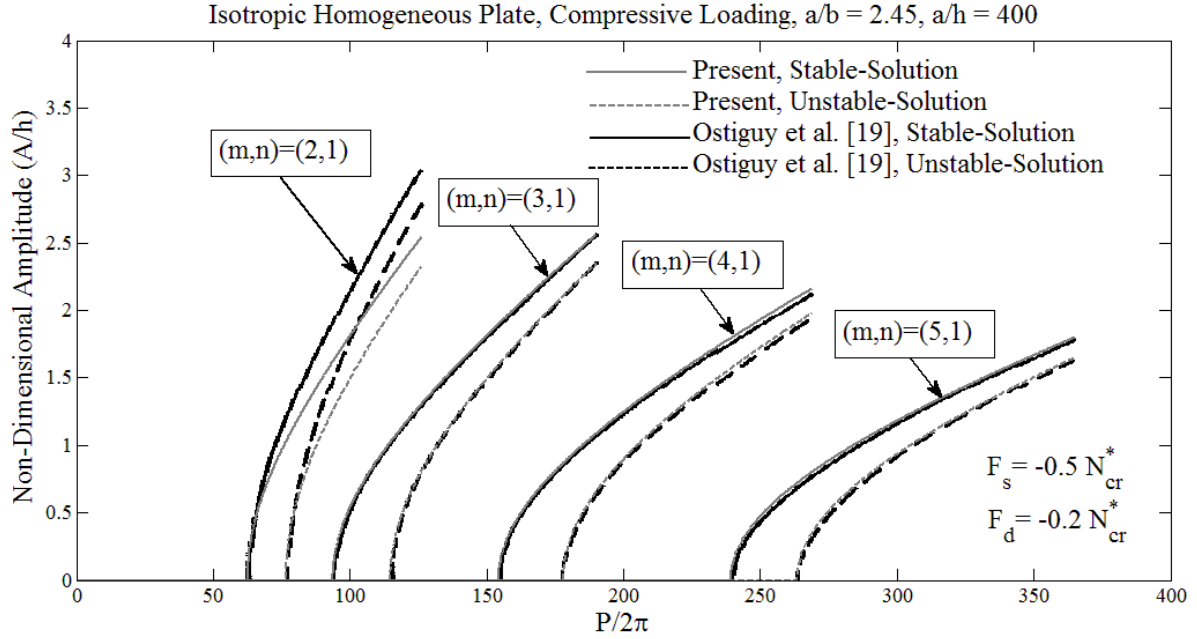
Figure 2.5 Comparison of both the stable- and unstable-solution amplitudes of steady-state vibrations of the present study with those of Ostiguy et al [19] for isotropic homogeneous rectangular plate having aspect ratios of $a/h = 400$ and $a/b = 2.45$ subjected to periodic longitudinal load having static component of $F_s = -0.5\ N_{cr}^*$ and dynamic component of $F_d = -0.2\ N_{cr}^*$
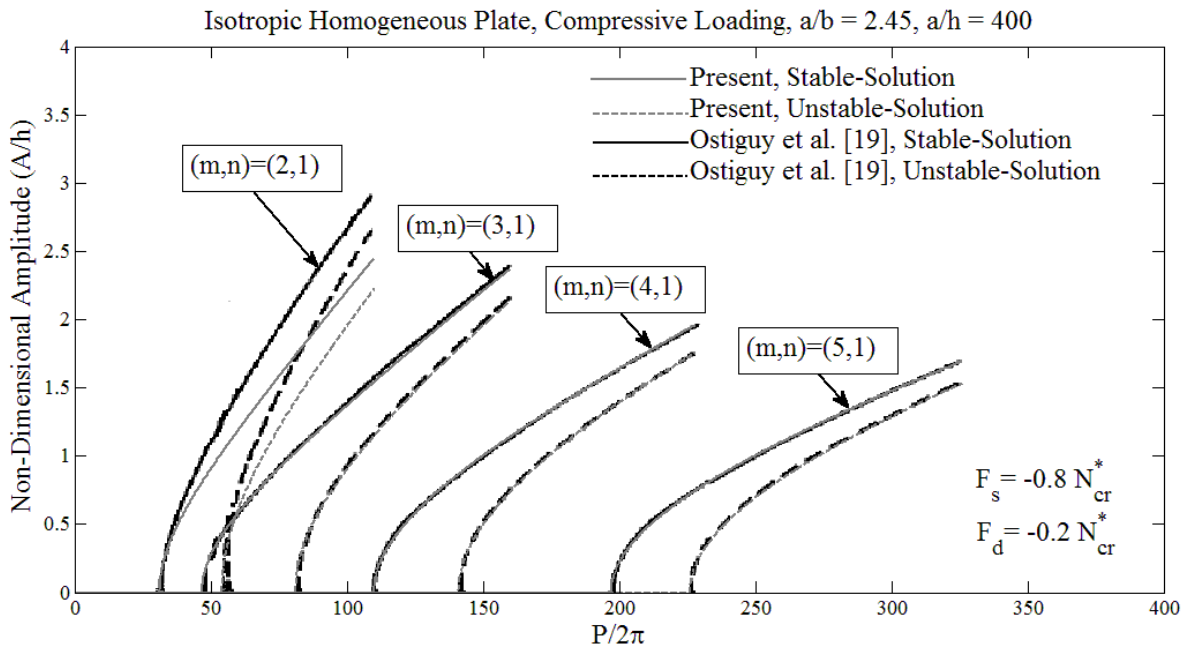
Figure 2.6 Comparison of both the stable- and unstable-solution amplitudes of steady-state vibrations of the present study with those of Ostiguy et al [19] for isotropic homogeneous rectangular plate having aspect ratios of $a/h = 400$ and $a/b = 2.45$ subjected to periodic longitudinal load having static component of $F_s = -0.8\ N_{cr}^*$ and dynamic component of $F_d = -0.2\ N_{cr}^*$

46

2.6.2 Effect of variation of lamination schemes

For isotropic plate the buckling load in terms of engineering constants is given by Timoshenko and Gere as [20]

$$N_{cr} = \frac{\pi^2 D}{b^2} \left(\frac{b}{a} + \frac{a}{b}\right)^2 \tag{2.51a}$$

where

$$D = \frac{Eh^3}{12(1-v^2)} \tag{2.51b}$$

The mechanism of dynamic buckling is similar to static buckling and the only difference is the additional considerations of the inertia force so that it leads to the dynamic buckling load to be lower than the static buckling load for the same structure. But the mechanism of dynamic instability is much more complex since in both static and dynamic buckling the main factor is only the critical static or dynamic load amplitude while in dynamic instability, not only the vibration amplitude of dynamic load, but also the vibration frequency together with the simulating frequency will play important roles. So the dynamic instability of the plate or shell structure will be occurred at much lower loads.

For laminated rectangular plates, the critical buckling load is approximated as

$$(N_{cr})_{Composite} = \frac{\pi^2 D^*}{b^2} \left(\frac{b}{a} + \frac{a}{b}\right)^2 \tag{2.52a}$$

where

$$D^* = \frac{E_2 h^3}{12(1-v_{12}v_{21})} \tag{2.52b}$$

This approximates the static buckling load for laminated rectangular plate and hence for the dynamic instability analysis both the static part of the load F_s and the periodic part F_d in Eq. (2.1) should be a percentage of this buckling load. This is why we have considered conservatively in the next tables and figures that $F_s = (0.1, 0.3, 0.5)N_{cr}$ and corresponding periodic part as $F_d = 0.3F_s$.

The dimensionless excitation frequency parameter p which is mentioned in the next figures and tables is introduced as follow:

$$p = 2\pi bP \sqrt{\frac{\rho_t}{A_{11}}} \tag{2.53}$$

To compare the results in the following tables we specified each unstable region by the non-dimensional frequency parameter p of the point of origin and the half angle of the unstable region as θ.

Here and in following figures, tables and discussions the first two primary steady-state vibrations (from left to right) refer to the first two modes.

The effects of variation of the lamination scheme on the first two modes, dynamically-unstable regions and both stable and unstable solutions amplitude of steady-state vibrations of antisymmetric cross-ply laminated rectangular plates are presented in Fig. 2.7, Fig. 2.8, and Tables 2.1-2.13. Figure 2.7 and 2.8 show the influence of the lamination scheme on the fundamental mode of dynamically-unstable regions and corresponding stable-solution amplitude-frequency curve of steady-state vibrations for antisymmetric cross-ply laminated plates, respectively. The plates are subjected to tensile loading of $F_s = 0.1N_{cr}$ and $F_d = 0.3F_s$. It is observed that the first mode unstable regions and amplitude of steady-state vibrations shift to the right along the frequency axis having higher frequencies of excitation as the number of layers are increased. This is probably due to the bending-extension coupling of lamination which is reduced by increasing the number of the plies in antisymmetric cross-ply laminates. This shifting to the right of frequency axis of both unstable regions and the steady-state amplitude (reducing the amplitude at a certain excitation frequency) is reduced once the number of layers is doubled and appears to converge at a certain value as can be observed from these figures that the unstable regions of eight- and ten-layered laminates are too close to each other and the amplitudes of eight- and ten-layered laminates almost coincide with each other.

Table 2.1 and Tables 2.2-2.12 also present a detailed study considering again the effects of variation of the lamination scheme on the first two modes of unstable regions and both stable and unstable solutions amplitude of steady-state vibrations of antisymmetric cross-ply laminated plate, respectively. In Table 2.1 the results have been listed for unstable regions which are specified by the points of origin and the half angle of the unstable region θ as mentioned before for the tensile load, $F_s = 0.1N_{cr}$. Tables 2.2-2.7 present the result for both stable and unstable solutions amplitude of steady-state vibrations for three different tensile loads, $F_s = 0.1N_{cr}$, $F_s = 0.3N_{cr}$ and $F_s = 0.5N_{cr}$ and the corresponding results for compressive loads, $F_s = -0.1N_{cr}$, $F_s = -0.3N_{cr}$ and $F_s = -0.5N_{cr}$ are tabulated in Tables 2.8-2.13. For the comparison studies the results in Tables 2.2-2.13 are normalized using the same non-dimensional excitation frequency $p = 1$. All the discussions and corresponding observations that were mentioned in the previous paragraph about Fig. 2.5 and Fig. 2.6 for unstable regions and amplitude of stead-state vibrations are also observed from Table 2.1 and
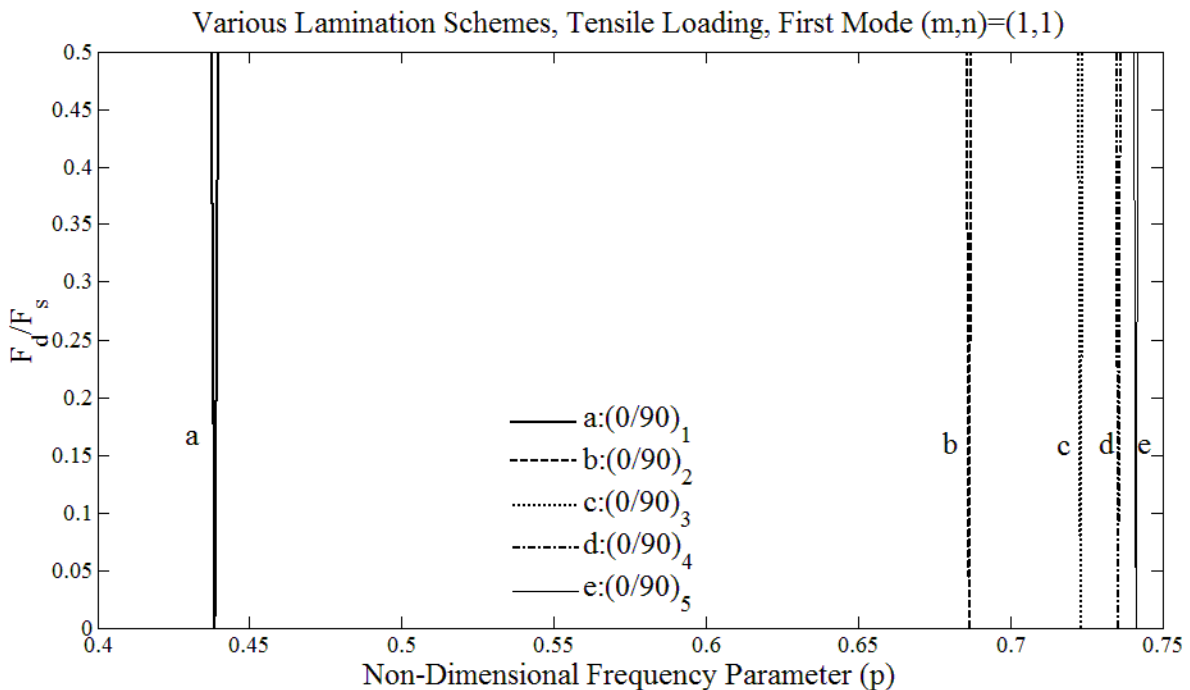
Figure 2.7 The first mode unstable region corresponding to various lamination schemes for the antisymmetric cross-ply laminated rectangular plate having aspect ratios of $a/b = 2$ and $a/h = 100$ subjected to tensile loading of $F_s = 0.1N_{cr}$
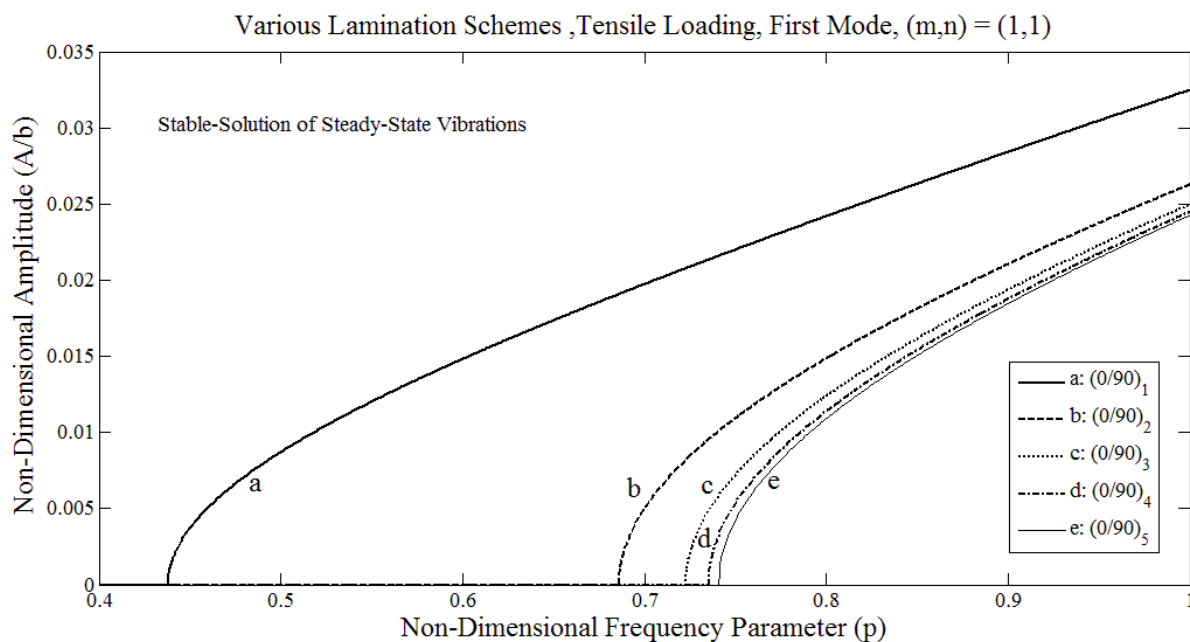
Figure 2.8 The stable-solution amplitude of steady-state vibrations of the first mode corresponding to various lamination schemes for the antisymmetric cross-ply laminated rectangular plate having aspect ratios of $a/b = 2$ and $a/h = 100$ subjected to tensile loading of $F_s = 0.1N_{cr}$ and $F_d = 0.3F_s$

Table 2.1 The first two unstable regions of an antisymmetric cross-ply laminated rectangular plate having aspect ratios of $a/b = 2$ and $a/h = 100$ subjected to tensile loading of $F_s = 0.1N_{cr}$

Lamination scheme		1st Mode, $(m,n) = (1,1)$	2nd Mode, $(m,n) = (1,2)$
2 Plies $(0°, 90°)$	Point of origin p $(\times 10^{-1})$	4.3867410	16.4443734
	θ $(\times 10^{-3})$	2.2243915	0.5940836
2 Plies $(90°, 0°)$	Point of origin p $(\times 10^{-1})$	4.3867410	16.4443734
	θ $(\times 10^{-3})$	2.2243915	0.5940836
4 Plies $(0°, 90°)_2$	Point of origin p $(\times 10^{-1})$	6.8654193	26.2730634
	θ $(\times 10^{-3})$	1.4223678	0.3718588
4 Plies $(90°, 0°)_2$	Point of origin p $(\times 10^{-1})$	6.8654193	26.2730634
	θ $(\times 10^{-3})$	1.4223678	0.3718588
6 Plies $(0°, 90°)_3$	Point of origin p $(\times 10^{-1})$	7.2317969	27.7132649
	θ $(\times 10^{-3})$	1.3503768	0.3525353
6 Plies $(90°, 0°)_3$	Point of origin p $(\times 10^{-1})$	7.2317969	27.7132649
	θ $(\times 10^{-3})$	1.3503768	0.3525353
8 Plies $(0°, 90°)_4$	Point of origin p $(\times 10^{-1})$	7.3557191	28.1999640
	θ $(\times 10^{-3})$	1.3276476	0.3464513
8 Plies $(90°, 0°)_4$	Point of origin p $(\times 10^{-1})$	7.3557191	28.1999640
	θ $(\times 10^{-3})$	1.3276476	0.3464513
10 Plies $(0°, 90°)_5$	Point of origin p $(\times 10^{-1})$	7.4123760	28.4224148
	θ $(\times 10^{-3})$	1.3175087	0.3437400
10 Plies $(90°, 0°)_5$	Point of origin p $(\times 10^{-1})$	7.4123760	28.4224148
	θ $(\times 10^{-3})$	1.3175087	0.3437400

Tables 2.2-2.13, respectively and hence are valid. In addition it is also observed from Table

2.1 and Tables 2.2-2.3 which are for the first two modes' unstable regions and amplitude of

50

steady-state vibrations, respectively, of the plate with stacking sequence of $(0^o/90^o/0^o ...)$ have exactly the same unstable regions and amplitude of steady-state vibrations both in stable- and unstable-solutions in comparison with the laminations with the stacking sequence of $(90^o/0^o/90^o ...)$. It means that these two different stacking sequences for the plate show equal rigidity although in the study of Ng et al [21] for dynamic unstable regions of laminated cylindrical shells it is revealed that $(0^o/90^o/0^o ...)$

laminate shows more rigidity. Hence in the following Tables 2.4-2.13 only the results are listed for one of these lamination stacking sequences i.e. the stacking sequence of $(0^o/90^o/0^o ...)$.

Table 2.2 The stable and unstable solution amplitudes corresponding to first mode, $(m, n) = (1, 1)$, of steady-state vibrations for an antisymmetric cross-ply laminated rectangular plate having aspect ratios of $a/b = 2$ and $a/h = 100$ subjected to tensile loading of $F_s = 0.1N_{cr}$ and $F_d = 0.3F_s$ under the excitation with non-dimensional frequency parameter $p = 1$.

Lamination scheme	Amplitude (A/b), Stable-Solutions ($\times 10^{-2}$)	Amplitude (A/b), Unstable-Solutions ($\times 10^{-2}$)
2 Plies $(0^{\circ}, 90^{\circ})$	3.248133736	3.245776765
2 Plies $(90^{\circ}, 0^{\circ})$	3.248133736	3.245776765
4 Plies $(0^{\circ}, 90^{\circ})_2$	2.628551757	2.625638661
4 Plies $(90^{\circ}, 0^{\circ})_2$	2.628551757	2.625638661
6 Plies $(0^{\circ}, 90^{\circ})_3$	2.49699994	2.493933187
6 Plies $(90^{\circ}, 0^{\circ})_3$	2.49699994	2.493933187
8 Plies $(0^{\circ}, 90^{\circ})_4$	2.449288107	2.446161538
8 Plies $(90^{\circ}, 0^{\circ})_4$	2.449288107	2.446161538
10 Plies $(0^{\circ}, 90^{\circ})_5$	2.426886808	2.423731342
10 Plies $(90^{\circ}, 0^{\circ})_5$	2.426886808	2.423731342

Table 2.3 The stable and unstable solution amplitudes corresponding to second mode, $(m, n) = (1, 2)$, of steady-state vibrations for an antisymmetric cross-ply laminated rectangular plate having aspect ratios of $a/b = 2$ and $a/h = 100$ subjected to tensile loading of $F_s = 0.1N_{cr}$ and $F_d = 0.3F_s$ under the excitation with non-dimensional frequency parameter $p = 3.5$

Lamination scheme	Amplitude (A/b), Stable-Solutions ($\times 10^{-2}$)	Amplitude (A/b), Unstable-Solutions ($\times 10^{-2}$)
2 Plies $(0^{\circ}, 90^{\circ})$	2.871214011	2.871037694
2 Plies $(90^{\circ}, 0^{\circ})$	2.871214011	2.871037694
4 Plies $(0^{\circ}, 90^{\circ})_2$	2.148992941	2.148992941
4 Plies $(90^{\circ}, 0^{\circ})_2$	2.148992941	2.148757363
6 Plies $(0^{\circ}, 90^{\circ})_3$	1.986641608	1.986386775
6 Plies $(90^{\circ}, 0^{\circ})_3$	1.986641608	1.986386775
8 Plies $(0^{\circ}, 90^{\circ})_4$	1.926589176	1.926326399
8 Plies $(90^{\circ}, 0^{\circ})_4$	1.926589176	1.926326399
10 Plies $(0^{\circ}, 90^{\circ})_5$	1.898150383	1.897883669
10 Plies $(90^{\circ}, 0^{\circ})_5$	1.898150383	1.897883669

Table 2.4 The stable and unstable solution amplitudes corresponding to first mode, $(m, n) = (1, 1)$, of steady-state vibrations for an antisymmetric cross-ply laminated rectangular plate having aspect ratios of $a/b = 2$ and $a/h = 100$ subjected to tensile loading of $F_s = 0.3N_{cr}$ and $F_d = 0.3F_s$ under the excitation with non-dimensional frequency parameter $p = 1$

Lamination scheme	Amplitude (A/b), Stable-Solutions ($\times 10^{-2}$)	Amplitude (A/b), Unstable-Solutions ($\times 10^{-2}$)
2 Plies $(0^\circ, 90^\circ)$	3.234754859	3.227649473
4 Plies $(0^\circ, 90^\circ)_2$	2.612001258	2.60319663
6 Plies $(0^\circ, 90^\circ)_3$	2.479571523	2.470294934
8 Plies $(0^\circ, 90^\circ)_4$	2.431517728	2.422057098
10 Plies $(90^\circ, 0^\circ)_5$	2.408951185	2.399401578

Table 2.5 The stable and unstable solution amplitudes corresponding to second mode, $(m, n) = (1, 2)$, of steady-state vibrations for an antisymmetric cross-ply laminated rectangular plate having aspect ratios of $a/b = 2$ and $a/h = 100$ subjected to tensile loading of $F_s = 0.3N_{cr}$ and $F_d = 0.3F_s$ under the excitation with non-dimensional frequency parameter $p = 3.5$

Lamination scheme	Amplitude (A/b), Stable-Solutions ($\times 10^{-2}$)	Amplitude (A/b), Unstable-Solutions ($\times 10^{-2}$)
2 Plies $(0^\circ, 90^\circ)$	2.870214739	2.869685571
4 Plies $(0^\circ, 90^\circ)_2$	2.147657656	2.146950405
6 Plies $(0^\circ, 90^\circ)_3$	1.985197125	1.984431973
8 Plies $(0^\circ, 90^\circ)_4$	1.925099634	1.924310586
10 Plies $(90^\circ, 0^\circ)_5$	1.896638506	1.895837613

Table 2.6 The stable and unstable solution amplitudes corresponding to first mode, $(m, n) = (1, 1)$, of steady-state vibrations for an antisymmetric cross-ply laminated rectangular plate having aspect ratios of $a/b = 2$ and $a/h = 100$ subjected to tensile loading of $F_s = 0.5N_{cr}$ and $F_d = 0.3F_s$ under the excitation with non-dimensional frequency parameter $p = 1$

Lamination scheme	Amplitude (A/b), Stable-Solutions ($\times 10^{-2}$)	Amplitude (A/b), Unstable-Solutions ($\times 10^{-2}$)
2 Plies $(0^\circ, 90^\circ)$	3.221320417	3.209419798
4 Plies $(0^\circ, 90^\circ)_2$	2.595345219	2.580559438
6 Plies $(0^\circ, 90^\circ)_3$	2.462019734	2.44642829
8 Plies $(0^\circ, 90^\circ)_4$	2.413616518	2.397710346
10 Plies $(90^\circ, 0^\circ)_5$	2.390881019	2.374822573

Table 2.7 The stable and unstable solution amplitudes corresponding to second mode, $(m, n) = (1, 2)$, of steady-state vibrations for an antisymmetric cross-ply laminated rectangular plate having aspect ratios of $a/b = 2$ and $a/h = 100$ subjected to tensile loading of $F_s = 0.5N_{cr}$ and $F_d = 0.3F_s$ under the excitation with non-dimensional frequency parameter $p = 3.5$

Lamination scheme	Amplitude (A/b), Stable-Solutions ($\times 10^{-2}$)	Amplitude (A/b), Unstable-Solutions ($\times 10^{-2}$)
2 Plies $(0^\circ, 90^\circ)$	2.869215118	2.86833281
4 Plies $(0^\circ, 90^\circ)_2$	2.146321541	2.145141924
6 Plies $(0^\circ, 90^\circ)_3$	1.98375159	1.982475243
8 Plies $(0^\circ, 90^\circ)_4$	1.923608938	1.922292658
10 Plies $(90^\circ, 0^\circ)_5$	1.895125423	1.893789346

Table 2.8 The stable and unstable solution amplitudes corresponding to first mode, $(m, n) = (1, 1)$, of steady-state vibrations for an antisymmetric cross-ply laminated rectangular plate having aspect ratios of $a/b = 2$ and $a/h = 100$ subjected to compressive loading of $F_s = -0.1N_{cr}$ and $F_d = 0.3F_s$ under the excitation with non-dimensional frequency parameter $p = 1$

Lamination scheme	Amplitude (A/b), Stable-Solutions ($\times 10^{-2}$)	Amplitude (A/b), Unstable-Solutions ($\times 10^{-2}$)
2 Plies $(0^\circ, 90^\circ)$	3.263803378	3.261457731
4 Plies $(0^\circ, 90^\circ)_2$	2.647890493	2.644998696
6 Plies $(0^\circ, 90^\circ)_3$	2.517349485	2.514307553
8 Plies $(0^\circ, 90^\circ)_4$	2.47003076	2.466930481
10 Plies $(90^\circ, 0^\circ)_5$	2.447819295	2.444690848

Table 2.9 The stable and unstable solution amplitudes corresponding to second mode, $(m, n) = (1, 2)$, of steady-state vibrations for an antisymmetric cross-ply laminated rectangular plate having aspect ratios of $a/b = 2$ and $a/h = 100$ subjected to compressive loading of $F_s = -0.1N_{cr}$ and $F_d = 0.3F_s$ under the excitation with non-dimensional frequency parameter $p = 3.5$

Lamination scheme	Amplitude (A/b), Stable-Solutions ($\times 10^{-2}$)	Amplitude (A/b), Unstable-Solutions ($\times 10^{-2}$)
2 Plies $(0^\circ, 90^\circ)$	2.872389181	2.872212936
4 Plies $(0^\circ, 90^\circ)_2$	2.150562803	2.150327397
6 Plies $(0^\circ, 90^\circ)_3$	1.988339656	1.988085041
8 Plies $(0^\circ, 90^\circ)_4$	1.928340105	1.928077567
10 Plies $(90^\circ, 0^\circ)_5$	1.899927521	1.899661056

Table 2.10 The stable and unstable solution amplitudes corresponding to first mode, $(m, n) = (1, 1)$, of steady-state vibrations for an antisymmetric cross-ply laminated rectangular plate having aspect ratios of $a/b = 2$ and $a/h = 100$ subjected to compressive loading of $F_s = -0.3N_{cr}$ and $F_d = 0.3F_s$ under the excitation with non-dimensional frequency parameter $p = 1$

Lamination scheme	Amplitude (A/b), Stable-Solutions ($\times 10^{-2}$)	Amplitude (A/b), Unstable-Solutions ($\times 10^{-2}$)
2 Plies $(0^\circ, 90^\circ)$	3.281730972	3.274727515
4 Plies $(0^\circ, 90^\circ)_2$	2.669956881	2.661343997
6 Plies $(0^\circ, 90^\circ)_3$	2.540549962	2.531496837
8 Plies $(0^\circ, 90^\circ)_4$	2.493671518	2.484447577
10 Plies $(90^\circ, 0^\circ)_5$	2.471672508	2.462366161

Table 2.11 The stable and unstable solution amplitudes corresponding to second mode, $(m, n) = (1, 2)$, of steady-state vibrations for an antisymmetric cross-ply laminated rectangular plate having aspect ratios of $a/b = 2$ and $a/h = 100$ subjected to compressive loading of $F_s = -0.3N_{cr}$ and $F_d = 0.3F_s$ under the excitation with non-dimensional frequency parameter $p = 3.5$

Lamination scheme	Amplitude (A/b), Stable-Solutions ($\times 10^{-2}$)	Amplitude (A/b), Unstable-Solutions ($\times 10^{-2}$)
2 Plies $(0^\circ, 90^\circ)$	2.873740033	2.873211514
4 Plies $(0^\circ, 90^\circ)_2$	2.152366729	2.151661025
6 Plies $(0^\circ, 90^\circ)_3$	1.99029062	1.989527427
8 Plies $(0^\circ, 90^\circ)_4$	1.930351711	1.929564811
10 Plies $(90^\circ, 0^\circ)_5$	1.901969177	1.901170529

Table 2.12 The stable and unstable solution amplitudes corresponding to first mode, $(m, n) = (1, 1)$, of steady-state vibrations for an antisymmetric cross-ply laminated rectangular plate having aspect ratios of $a/b = 2$ and $a/h = 100$ subjected to compressive loading of $F_s = -0.5N_{cr}$ and $F_d = 0.3F_s$ under the excitation with non-dimensional frequency parameter $p = 1$

Lamination scheme	Amplitude (A/b), Stable-Solutions ($\times 10^{-2}$)	Amplitude (A/b), Unstable-Solutions ($\times 10^{-2}$)
2 Plies $(0°, 90°)$	3.299561161	3.287943744
4 Plies $(0°, 90°)_2$	2.691842386	2.67758952
6 Plies $(0°, 90°)_3$	2.563540481	2.548570188
8 Plies $(0°, 90°)_4$	2.517090249	2.501842027
10 Plies $(90°, 0°)_5$	2.495297712	2.479915498

Table 2.13 The stable and unstable solution amplitudes corresponding to second mode, $(m, n) = (1, 2)$, of steady-state vibrations for an antisymmetric cross-ply laminated rectangular plate having aspect ratios of $a/b = 2$ and $a/h = 100$ subjected to compressive loading of $F_s = -0.5N_{cr}$ and $F_d = 0.3F_s$ under the excitation with non-dimensional frequency parameter $p = 3.5$

Lamination scheme	Amplitude (A/b), Stable-Solutions ($\times 10^{-2}$)	Amplitude (A/b), Unstable-Solutions ($\times 10^{-2}$)
2 Plies $(0°, 90°)$	2.875090249	2.874209745
4 Plies $(0°, 90°)_2$	2.154169145	2.152993827
6 Plies $(0°, 90°)_3$	1.992239674	1.990968768
8 Plies $(0°, 90°)_4$	1.932361222	1.931050909
10 Plies $(90°, 0°)_5$	1.904008644	1.902678805

2.6.3 Effect of magnitude and direction of the longitudinal loads

Comparing the results in the Tables 2.2-2.7 indicate that by increasing the magnitude of tensile longitudinal loading from $F_s = 0.1N_{cr}$ to $F_s = 0.5N_{cr}$ both the stable and unstable solutions of amplitudes decrease which means that the corresponding excitation frequency that causes instability shifts to the right along frequency axis having higher frequencies. Hence it can be expected that by increasing the tensile longitudinal load the plate stiffness is also increased. The inverse trend can be seen in the case of compressive loading. For the compressive loading the results for amplitudes have been listed in Tables 2.8-2.13. The plates have higher stable and unstable amplitudes as the magnitude of longitudinal compressive loading is increased from $F_s = -0.1N_{cr}$ to $F_s = -0.5N_{cr}$ meaning that the corresponding excitation frequency that causes instability shifts to the left along frequency axis having lower frequencies. This was expected since by increasing the magnitude of longitudinal compressive loading the plate stiffness reduces. To study these effects for first two modes of unstable regions

the results for points of origin and the corresponding angle of unstable region which predicate as a factor for magnitude of the areas of these regions, are listed in Tables 2.14 and 2.15 for a ten-layered antisymmetric laminated rectangular plate subjected to various magnitudes of tensile and compressive loads, respectively. The results illustrate that instability regions shift to the right along frequency axis having higher excitation frequencies once the magnitude of longitudinal tensile load is increased from $F_s = 0.1 N_{cr}$ to $F_s = 0.5 N_{cr}$. This also can be expected as was mentioned above that increasing the tensile longitudinal loads causes the plate's stiffness to increase. Although the results in Table 2.15 indicate that the inverse trend can be seen in the case of compressive loading, in compressive loading conditions increasing the absolute magnitude of compressive loads from $Fs = -0.1 Ncr$ to $Fs = -0.3 Ncr$ causes the instability region to shift to the left along frequency axis having lower excitation frequencies. This can be expected and noted in the above that by increasing the magnitude of longitudinal compressive loads plate's stiffness is reduced. It can be observed from these two tables that the widths of instability regions are increased once the absolute values of magnitude of longitudinal loads are increased for both tensile and compressive loading conditions. Comparing the results for symmetric laminates in Tables 2.16-2.19 with corresponding results for antisymmetric laminate in Tables 2.5, 2.6 , 2.11 and 2.12 also reveal that at the same non-dimensional frequency parameter (p) for both the tensile and compressive load conditions, symmetric laminates having stacking sequence of $[(0^\circ, 90^\circ)_n]_S$ have higher amplitudes (having lower excitation frequencies) than antisymmetric $(0^\circ/90^\circ/...)$ laminates even though this trend is inverse for the case of lamination schemes of symmetric $[(90^\circ, 0^\circ)_n]_S$ and antisymmetric $(90^\circ/0^\circ/...)$ laminates. This outcome is in good agreement with that reported by Najafov et. al [22] for non-linear free vibration of truncated orthotropic thin laminated conical shells. However we know that the present results are for laminated uniform plates and the results by

55

Najafov et. al [22] is for laminated conical shells but the trend of changes in both these two different case studies confirm together.

Table 2.14 The first two unstable regions of a ten-layered antisymmetric cross-ply laminated rectangular plate having aspect ratios of $a/b = 2$ and $a/h = 100$ subjected to various tensile loading

Lamination scheme		1st Mode, $(m,n) = (1,1)$	2nd Mode, $(m,n) = (1,2)$
$F_s = 0.1N_{cr}$	Point of origin p ($\times 10^{-1}$)	7.4123760	28.4224148
	θ ($\times 10^{-3}$)	1.3175087	0.3437400
$F_s = 0.3N_{cr}$	Point of origin p ($\times 10^{-1}$)	7.4649136	28.4361615
	θ ($\times 10^{-3}$)	3.9212851	1.0306588
$F_s = 0.5N_{cr}$	Point of origin p ($\times 10^{-1}$)	7.5170840	28.4499015
	θ ($\times 10^{-3}$)	6.4845977	1.7168306

Table 2.15 The first two unstable regions of a ten-layered antisymmetric cross-ply laminated rectangular plate having aspect ratios of $a/b = 2$ and $a/h = 100$ subjected to various compressive loading

Lamination scheme		1st Mode, $(m,n) = (1,1)$	2nd Mode, $(m,n) = (1,2)$
$F_s = -0.1N_{cr}$	Point of origin p ($\times 10^{-1}$)	7.3594633	28.4086614
	θ ($\times 10^{-3}$)	1.3269728	0.3439064
$F_s = -0.3N_{cr}$	Point of origin p ($\times 10^{-1}$)	7.3061675	28.3949014
	θ ($\times 10^{-3}$)	4.0062542	1.0321562
$F_s = -0.5N_{cr}$	Point of origin p ($\times 10^{-1}$)	7.2524800	28.3811348
	θ ($\times 10^{-3}$)	6.7201068	1.7209891

2.6.4   Effect of symmetry in variation of lamination schemes

To examine the effect of symmetry in lamination schemes of the studied laminated plate on both stable and unstable solutions amplitudes of the steady-state vibrations, the results are listed in Tables 2.16-2.17 and Tables 2.18-2.19 for the tensile and compressive axial loads respectively. A graphical presentation of Table 2.16 also has been provided in Fig. 2.9. The first and second modes in these tables refer to the modes (1,1) and (1,2) respectively which shows no change in terms of wave numbers in comparison with antisymmetric laminates which were listed in Tables 2.1-2.15. All the above discussions about Tables 2.6, 2.7, 2.12, and 2.13 and Fig. 2.8 are valid about Tables 2.16-2.19 and Fig. 2.9, respectively. It can also be observed from these tables and Fig. 2.9 again that by increasing the number of plies in symmetric laminate the amplitude of steady-state vibrations converges at a certain value where the non-dimentional amplitude vs non-dimentional frequency curves of twenty, twenty-four and
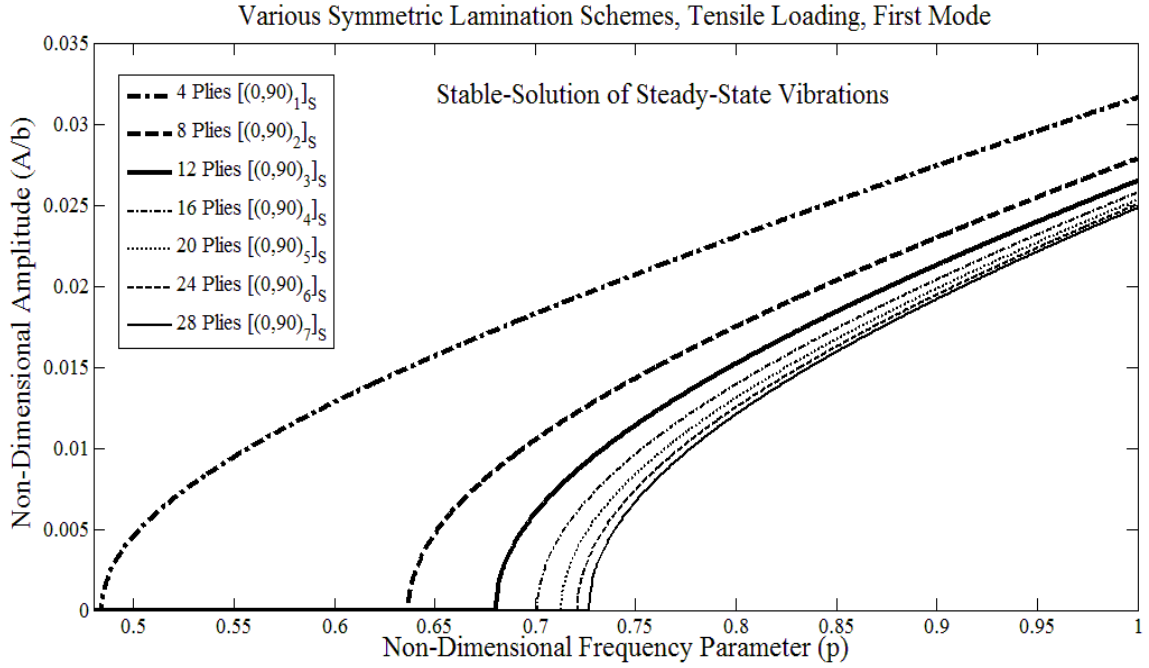
Figure 2.9 The stable-solution amplitude of steady-state vibrations of the first mode corresponding to various lamination schemes for the symmetric cross-ply laminated rectangular plate having aspect ratios of $a/b = 2$ and $a/h = 100$ subjected to tensile loading of $F_s = 0.5 N_{cr}$ and $F_d = 0.3 F_s$

Table 2.16 The stable and unstable solution amplitudes corresponding to first mode, $(m, n) = (1, 1)$, of steady-state vibrations for a symmetric cross-ply laminated rectangular plate having aspect ratios of $a/b = 2$ and $a/h = 100$ subjected to tensile loading of $F_s = 0.5 N_{cr}$ and $F_d = 0.3 F_s$ under the excitation with non-dimensional frequency parameter $p = 1$

Lamination scheme	Amplitude (A/b), Stable-Solutions ($\times 10^{-2}$)	Amplitude (A/b), Unstable-Solutions ($\times 10^{-2}$)
4 Plies $[(0°, 90°)_1]_S$	3.162137505	3.150013303
4 Plies $[(90°, 0°)_1]_S$	1.022314884	0.984173729
8 Plies $[(0°, 90°)_2]_S$	2.785788422	2.772018639
8 Plies $[(90°, 0°)_2]_S$	1.812077314	1.790836229
12 Plies $[(0°, 90°)_3]_S$	2.648481006	2.633993517
12 Plies $[(90°, 0°)_3]_S$	2.007433606	1.988280636
16 Plies $[(0°, 90°)_4]_S$	2.577085349	2.562194197
16 Plies $[(90°, 0°)_4]_S$	2.098302273	2.07998621
20 Plies $[(0°, 90°)_5]_S$	2.533282308	2.518132136
20 Plies $[(90°, 0°)_5]_S$	2.150981654	2.133117971
24 Plies $[(0°, 90°)_6]_S$	2.503654559	2.488324006
24 Plies $[(90°, 0°)_6]_S$	2.185395885	2.167815808
28 Plies $[(0°, 90°)_7]_S$	2.482275384	2.466811969
28 Plies $[(90°, 0°)_7]_S$	2.209649348	2.192263773

twenty-eight plies almost coincide with each other. It is also observed that in symmetric laminated plates both stable and unstable-solutions amplitude of steady-state vibration do not have the same values for stacking sequence of $[(0°, 90°)_n]_S$ and $[(90°, 0°)_n]_S$ although as it

was mentioned before these results have the same values in the case of antysymmetric lamianted plates. However by increasing the number of plies in symmetric laminate the difference is decreased.

Table 2.17 The stable and unstable solution amplitudes corresponding to second mode, $(m, n) = (1, 2)$, of steady-state vibrations for a symmetric cross-ply laminated rectangular plate having aspect ratios of $a/b = 2$ and $a/h = 100$ subjected to tensile loading of $F_s = 0.5N_{cr}$ and $F_d = 0.3F_s$ under the excitation with non-dimensional frequency parameter $p = 3.5$

Lamination scheme	Amplitude (A/b), Stable-Solutions ($\times 10^{-2}$)	Amplitude (A/b), Unstable-Solutions ($\times 10^{-2}$)
4 Plies $[(0°, 90°)_1]_S$	2.903888647	2.903016878
4 Plies $[(90°, 0°)_1]_S$	0	0
8 Plies $[(0°, 90°)_2]_S$	2.432149154	2.43110823
8 Plies $[(90°, 0°)_2]_S$	0.938568047	0.938568047
12 Plies $[(0°, 90°)_3]_S$	2.25305931	2.251935606
12 Plies $[(90°, 0°)_3]_S$	1.311481313	1.309549904
16 Plies $[(0°, 90°)_4]_S$	2.157948013	2.156774755
16 Plies $[(90°, 0°)_4]_S$	1.462709767	1.460978295
20 Plies $[(0°, 90°)_5]_S$	2.098813391	2.097607058
20 Plies $[(90°, 0°)_5]_S$	1.54636407	1.544726369
24 Plies $[(0°, 90°)_6]_S$	2.058446744	2.05721674
24 Plies $[(90°, 0°)_6]_S$	1.599705126	1.599705126
28 Plies $[(0°, 90°)_7]_S$	2.029121828	2.027874037
28 Plies $[(90°, 0°)_7]_S$	1.636741915	1.635194733

Table 2.18 The stable and unstable solution amplitudes corresponding to first mode, $(m, n) = (1, 1)$, of steady-state vibrations for a symmetric cross-ply laminated rectangular plate having aspect ratios of $a/b = 2$ and $a/h = 100$ subjected to compressive loading of $F_s = -0.5N_{cr}$ and $F_d = 0.3F_s$ under the excitation with non-dimensional frequency parameter $p = 1$

Lamination scheme	Amplitude (A/b), Stable-Solutions ($\times 10^{-2}$)	Amplitude (A/b), Unstable-Solutions ($\times 10^{-2}$)
4 Plies $[(0°, 90°)_1]_S$	3.241806939	3.229981801
4 Plies $[(90°, 0°)_1]_S$	1.247127238	1.247127238
8 Plies $[(0°, 90°)_2]_S$	2.875902599	2.862566325
8 Plies $[(90°, 0°)_2]_S$	1.947773811	1.928028274
12 Plies $[(0°, 90°)_3]_S$	2.743109598	2.729124488
12 Plies $[(90°, 0°)_3]_S$	2.130724832	2.112689876
16 Plies $[(0°, 90°)_4]_S$	2.674241485	2.659894308
16 Plies $[(90°, 0°)_4]_S$	2.216544846	2.199213782
20 Plies $[(0°, 90°)_5]_S$	2.632055827	2.617477427
20 Plies $[(90°, 0°)_5]_S$	2.266477597	2.249531264
24 Plies $[(0°, 90°)_6]_S$	2.603552338	2.588813432
24 Plies $[(90°, 0°)_6]_S$	2.299163717	2.282460077
28 Plies $[(0°, 90°)_7]_S$	3.241806939	3.229981801
28 Plies $[(90°, 0°)_7]_S$	1.247127238	1.247127238

Comparing the results of symmetric laminates in Tables 16-19 with corresponding results for antisymmetric laminate in Tables 2.5, 2.6 , 2.11 and 2.12 also reveal that at the same non-

dimensional frequency parameter (p) for the both tensile and compressive load conditions, symmetric laminates having stacking sequence of $[(0°, 90°)_n]_S$ have higher amplitudes (having lower excitation frequencies) than antisymmetric $(0°/90°/ ...)$ laminates even though this trend is inverse for the case of lamination schemes of symmetric $[(90°, 0°)_n]_S$ and antisymmetric $(90°/0°/ ...)$. This outcome is in good agreement with that reported by Najafov et. al [22] for non-linear free vibration of truncated orthotropic thin laminated conical shells.

Table 2.19 The stable and unstable solution amplitudes corresponding to second mode, $(m, n) = (1, 2)$, of steady-state vibrations for a symmetric cross-ply laminated rectangular plate having aspect ratios of $a/b = 2$ and $a/h = 100$ subjected to compressive loading of $F_s = -0.5N_{cr}$ and $F_d = 0.3F_s$ under the excitation with non-dimensional frequency parameter $p = 3.5$

Lamination scheme	Amplitude (A/b), Stable-Solutions ($\times 10^{-2}$)	Amplitude (A/b), Unstable-Solutions ($\times 10^{-2}$)
4 Plies $[(0°, 90°)_1]_S$	2.909693768	2.908823738
4 Plies $[(90°, 0°)_1]_S$	0	0
8 Plies $[(0°, 90°)_2]_S$	2.439077296	2.43803933
8 Plies $[(90°, 0°)_2]_S$	0.956377815	0.953727552
12 Plies $[(0°, 90°)_3]_S$	2.260536397	2.259416411
12 Plies $[(90°, 0°)_3]_S$	1.324285385	1.322372678
16 Plies $[(0°, 90°)_4]_S$	2.165753489	2.164584462
16 Plies $[(90°, 0°)_4]_S$	1.474200939	1.47248298
20 Plies $[(0°, 90°)_5]_S$	2.066628062	2.06540293
20 Plies $[(90°, 0°)_5]_S$	1.557238063	1.55561181
24 Plies $[(0°, 90°)_6]_S$	2.066628062	2.06540293
24 Plies $[(90°, 0°)_6]_S$	1.61021894	1.608646249
28 Plies $[(0°, 90°)_7]_S$	2.037420904	2.036178199
28 Plies $[(90°, 0°)_7]_S$	1.647019321	1.645481802

2.6.5 Effect of the length-to-width ratio

The effect of variation of the aspect ratio of the laminated plates i.e., length-to-width ratio a/b on the instability regions and stable-solution amplitudes of the steady-state vibrations for the ten-layered $(0°, 90°)_5$ cross-ply laminated plate having thickness ratio $a/h = 100$ subjected to longitudinal tensile loading of $F_s = 0.5N_{cr}$ are shown in Fig. 2.10, Table 2.20 and Fig. 2.11, respectively. The plots of amplitudes are depicted in Fig. 2.11 based on the dynamic
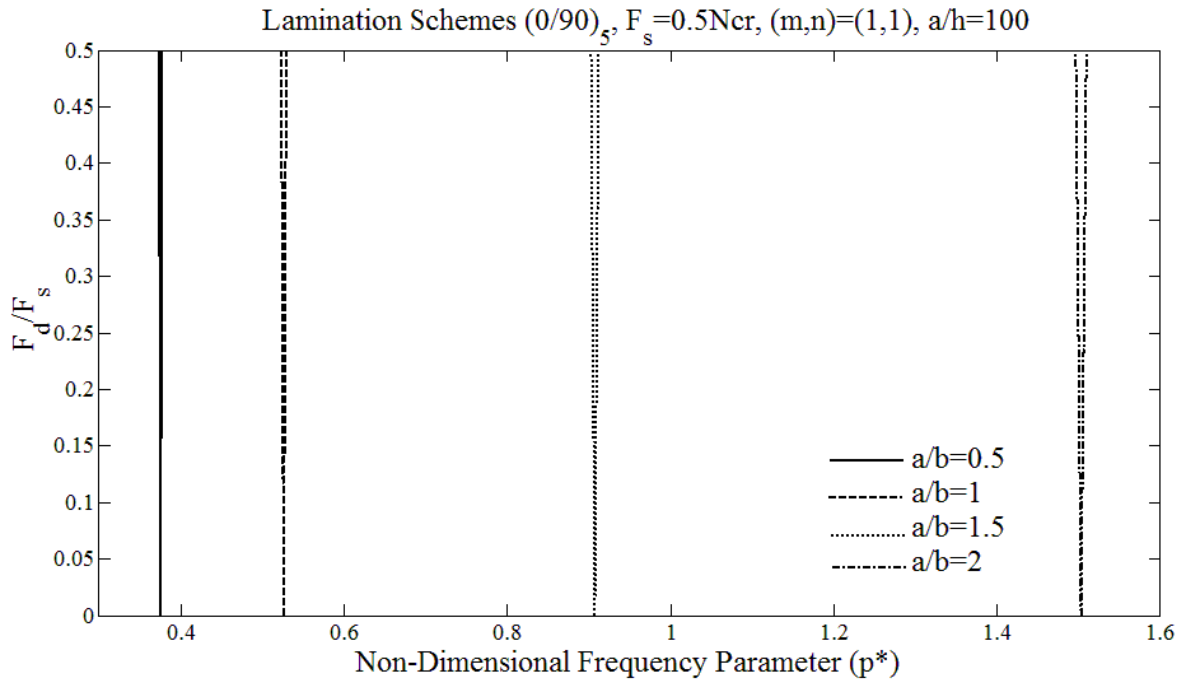
Figure 2.10 Variation of the first mode unstable region with plate's length of a ten-layered $(0°/90°)_5$ antisymmetric cross-ply laminated rectangular plate having thickness ratio $a/h = 100$ subjected to tensile loading of $F_s = 0.5N_{cr}^*$; N_{cr}^* corresponds to buckling load of the case $a/b = 2$
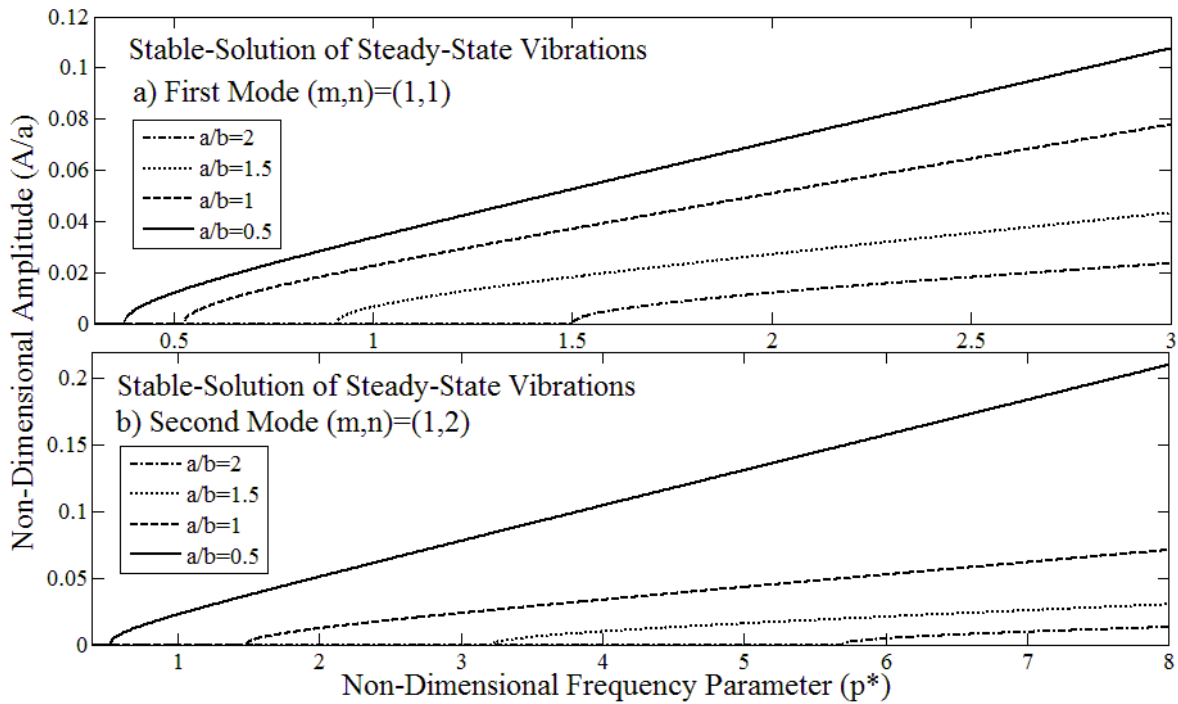
Figure 2.11 Variation of the first two stable-solution amplitudes of steady-state vibrations with plate's length of a ten-layered $(0°/90°)_5$ antisymmetric cross-ply laminated rectangular plate having thickness ratio $a/h = 100$ subjected to tensile loading of $F_s = 0.5N_{cr}^*$; N_{cr}^* corresponds to buckling load of the case $a/b = 2$ and $F_d = 0.3F_s$

term of the longitudinal load as $F_d = 0.3F_s$. Since here the length a of the plates is kept constant and to study the variation of aspect ratio the width of the plates b is varied the non-dimensional frequency parameter p^* is defined as follow:

$$p^* = 2\pi aP \sqrt{\frac{\rho t}{A_{11}}} \tag{2.54}$$

The results show that with a decrease in width of the plate, i.e. overall increase in aspect ratio of a/b, the plate's stiffness is increased as well, hence the dynamically-unstable regions shift to the right along frequency axis having higher frequencies of excitation of point of origins, the widths of instability regions are increased and also the amplitudes of steady-state vibrations at any specific frequency are decreased. In terms of point of origin of dynamically-unstable region. This is in full agreement with the corresponding study of Ramachandra et al [11] for dynamically-unstable regions.

Table 2.20 Variation of the first two unstable regions with plate's aspect ratio of a ten-layered $(0°/90°)_5$ antisymmetric cross-ply laminated plate having thickness ratio of $a/h = 100$ subjected to tensile loading of $F_s = 0.5N^*_{cr}$; N^*_{cr} corresponds to buckling load of the case $a/b = 2$

Lamination scheme		1st Mode, $(m,n) = (1,1)$	2nd Mode, $(m,n) = (1,2)$
$\frac{a}{b} = 0.5$	Point of origin p $(\times 10^{-1})$	3.7585420	5.1944527
	θ $(\times 10^{-3})$	3.2423329	2.3484589
$\frac{a}{b} = 1$	Point of origin p $(\times 10^{-1})$	5.2672968	14.8142034
	θ $(\times 10^{-3})$	5.9189258	2.1096994
$\frac{a}{b} = 1.5$	Point of origin p $(\times 10^{-1})$	9.0773696	32.2468704
	θ $(\times 10^{-3})$	9.0720438	2.5596828
$\frac{a}{b} = 2$	Point of origin p $(\times 10^{-1})$	15.0341680	56.8998031
	θ $(\times 10^{-3})$	12.9686501	3.4336510

2.6.6   Effect of the length-to-thickness ratio

Figure 2.12, Table 2.21 and Figure 2.13 present the effect of variation of the thickness ratio a/h on the instability regions and stable-solution amplitudes of the steady-state vibrations for the ten-layered $(0°, 90°)_5$ cross-ply laminated square plate subjected to longitudinal compressive loading of $F_s = -0.3N_{cr}$. The plots of amplitudes are depicted in Fig. 2.13 based
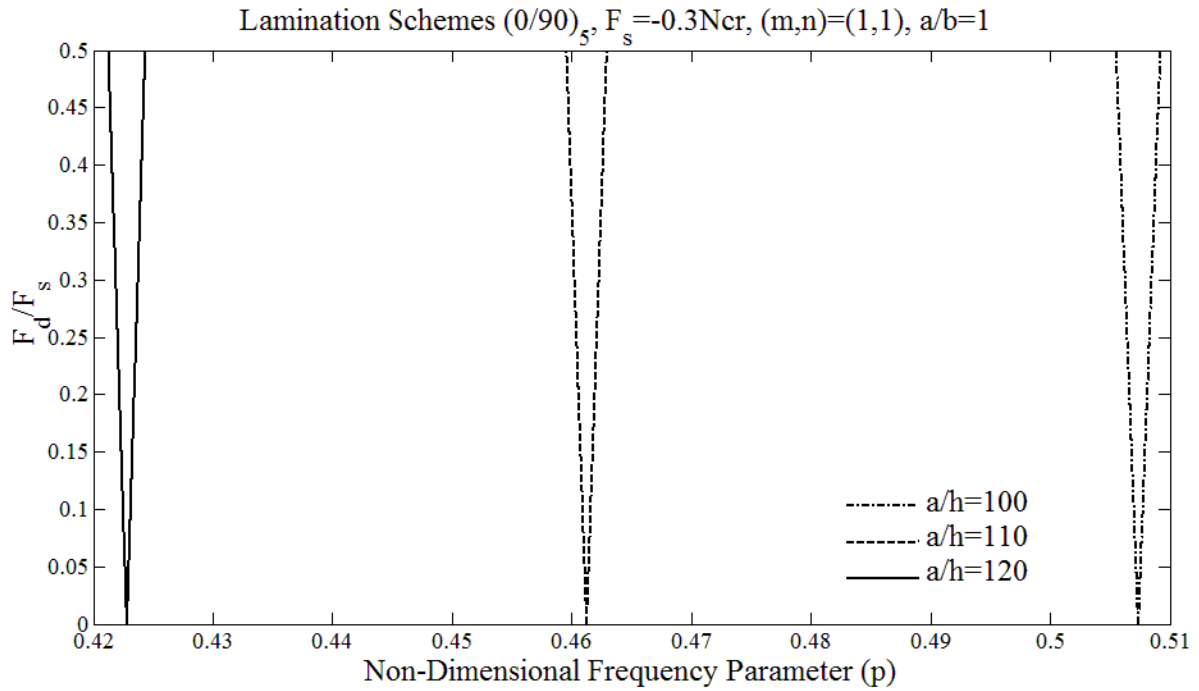
Figure 2.12 Variation of the first mode unstable region with plate's thickness of a ten-layered $(0°/90°)_5$ antisymmetric cross-ply laminated square plate subjected to compressive loading of $F_s = -0.3N_{cr}^*$; N_{cr}^* corresponds to buckling load of the case $a/h = 120$

Table 2.21 Variation of the first two dynamically-unstable regions with plate's thickness of a ten-layered $(0°/90°)_5$ antisymmetric cross-ply laminated square plate subjected to compressive loading of $F_s = -0.3N_{cr}^*$; N_{cr}^* corresponds to buckling load of the case $a/h = 120$

Lamination scheme		1st Mode, $(m,n) = (1,1)$	2nd Mode, $(m,n) = (1,2)$
$\frac{a}{h} = 100$	Point of origin p $(\times 10^{-1})$	5.0738029	14.7465143
	θ $(\times 10^{-3})$	3.6904626	1.2718097
$\frac{a}{h} = 110$	Point of origin p $(\times 10^{-1})$	4.6125480	13.4059221
	θ $(\times 10^{-3})$	3.3549686	1.1561907
$\frac{a}{h} = 120$	Point of origin p $(\times 10^{-1})$	4.2281690	12.2887619
	θ $(\times 10^{-3})$	3.0753897	1.0598416

on the dynamic term of the longitudinal load as $F_d = 0.3F_s$. It is observed that with a decrease in thickness of the plate, i.e. overall increasing the length-to-thickness ratio a/h, the dynamically-unstable regions shift to the left along the frequency axis having lower frequencies of point of origin, the widths of instability regions are decreased and also the amplitudes of steady-state vibrations at any specific frequency are increased. This is due to the fact that decreasing the thickness of plate makes the plate to be less stiff. This is also in full agreement with the corresponding study of Moorthy and Reddy [9]. This is also in full agreement with the

62
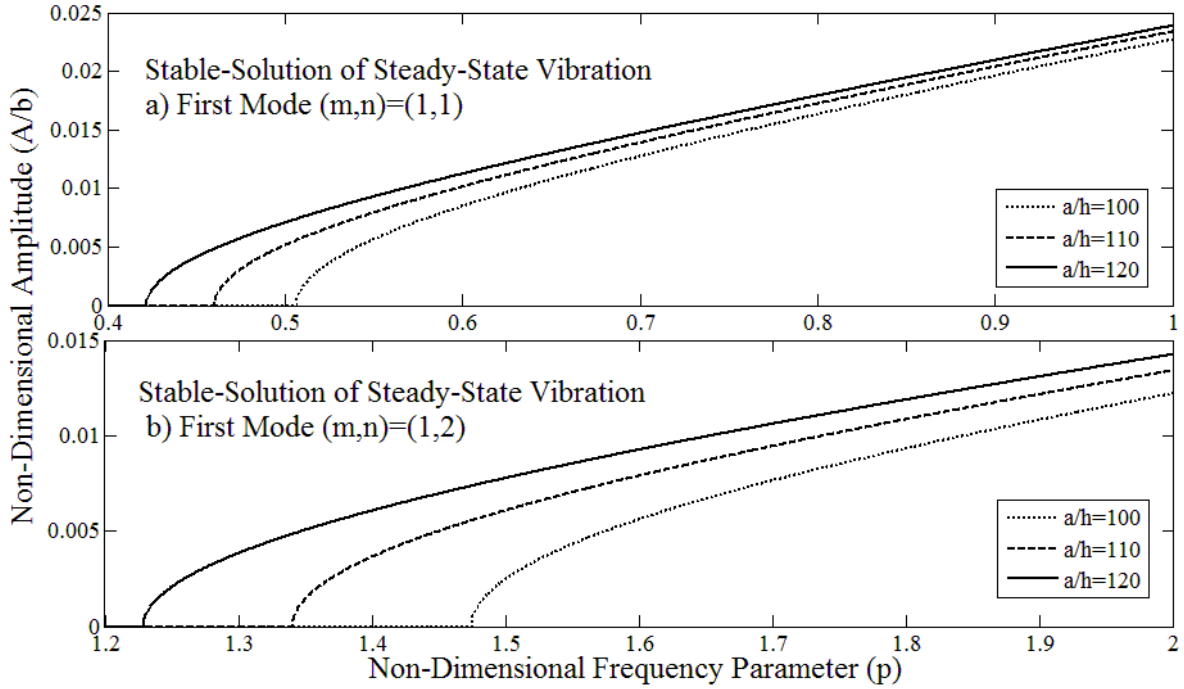
Figure 2.13 Variation of the first two stable-solution amplitudes of steady-state vibrations with plate's thickness of a ten-layered $(0°/90°)_5$ antisymmetric cross-ply laminated square plate subjected to compressive loading of $F_s = -0.3N^*_{cr}$; N^*_{cr} corresponds to buckling load of the case $a/h = 120$ and $F_d = 0.3F_s$

corresponding study of Lam and Ng [23] for dynamically-unstable regions of laminated composite cylindrical shells.

2.7 Conclusions

The non-linear dynamic stability of both antisymmetric and symmetric cross-ply laminated composite plates under combined static and periodic longitudinal loading has been studied. Equations of motion with von Karman-type of non-linearity were solved by employing Galerkin's technique. By applying Bolotin's method to the governing system of non-linear Mathieu-Hill equations the amplitudes of both stable and unstable solutions were obtained for steady-state vibrations. It is confirmed that instability regions and both stable and unstable solutions amplitudes of steady-state vibrations are significantly influenced by the lamination schemes including symmetric and antisymmetric lamination, the number and sequence of the plies, magnitude and direction of the longitudinal periodic loads, aspect ratios of the plate

including length-to-width and length-to-thickness ratios, and in-plane transverse wave number. Hence in any particular application specific configurations of laminate should be considered in design of composite plates. A comparative study of the present work with those available in literature shows a very good agreement. However, as the results of the present study reveal, the linear analysis carried out in available literature can only provide the information about the instability region and unable to predict the vibration amplitudes in these regions. The non-linear analysis developed in the present work can determine such vibration amplitudes. The present work has shown that there is vibration with steady-state amplitude in the instability region which approaches almost constant amplitude when the excitation frequencies are increased. Hence, for more perfect and complete studies of dynamic instability of laminated plates, the non-linear analysis is required to determine both the stable and unstable amplitudes of steady-state vibrations in addition to instability regions. Where the occurrence of dynamic instability is inevitable, in order to have a control on vibration amplitudes in the unstable regions the non-linear analysis is required. By adjusting the corresponding effective parameters as explained in the present work, steady-state vibrations with allowable amplitudes based on the design criteria can be achieved in the dynamically-unstable regions.

The major outcomes of the present study are summarized as follow:

- For both symmetric and antisymmetric laminated plates, amplitudes of steady-state vibrations are decreased, corresponding dynamically-unstable regions shift to the right along the frequency axis having higher frequencies of excitation, and the widths of the instability regions are decreased when the number of plies are increased. Convergence is also achieved at a specific number of the plies in each case.

- Increasing the magnitude of compressive longitudinal load causes increasing amplitude of steady-state vibrations, shifting dynamically-unstable regions to the left along the frequency axis, and increasing albeit the widths of instability regions.

- Increasing the magnitude of tensile longitudinal loads results in decreasing the amplitude of steady-state vibrations, shifting dynamically-unstable regions to the right along the frequency axis, and increasing albeit the widths of instability regions.

- With an increase in aspect ratio a/b of the plate, the dynamically-unstable regions shift to the right along frequency axis having higher frequencies of excitation of point of origin, the widths of instability regions are increased and also the amplitudes of steady-state vibrations are decreased.

- Increasing the thickness ratio a/h causes the dynamically-unstable regions shift to the left along frequency axis having lower frequencies of excitation of point of origin. Moreover the widths of instability regions are decreased and also the amplitudes of steady-state vibrations are increased.

The present work can be used as a bench mark study in future studies on dynamic instability of laminated composite plates.

CHAPTER 3

Non-linear vibration and dynamic instability of internally-thickness-tapered composite plates under parametric excitation

3.1 Introduction

Laminated composite plates are increasingly being used in aerospace, automotive, and civil engineering as well as in many other applications of modern engineering structures. The tailoring ability of fiber-reinforced polymer composite (FRPC) materials for the stiffness and strength properties with regard to reduction of structural weight made them superior compared with metals in such structures. One of the most efficient way to increase the stiffness and at the same time reduce the weight of the structures particularly in composite structures is the thickness-tapering of the structures. Also in some specific applications such as helicopter yokes and blades, wind mill blades and robot arms, the composite structure needs to be stiff at one location and flexible at another location. Tapered composites are formed by terminating or dropping-off some of the plies in the laminates which is an important method of stiffness tailoring and weight saving in these structures. Laminates are often thickness-tapered when changes in strength and stiffness along the length of the structure are required. Aircraft wing skins, helicopter yoke, flex-beams of helicopter rotor hubs, and near field joints in solid rocket boosters are few example applications of the tapered structures in aerospace industries. In order to design and use tapered composite structures in practical applications it is required to have a good knowledge of their mechanical and structural behavior such as deformations, stress distributions, natural frequencies, static and dynamic instabilities under various loading and boundary conditions. Due to the complexity of modeling and the analysis of tapered composite structures, limited research efforts have been devoted to this class of structures, which are described in terms of complex mechanical models. A detailed literature survey by He et.al. [24] studied research conducted before 2000 which focused on stress analysis, delamination

66

analysis and parametric study of the tapered composite structures. Ganesan and Zabihollah investigated the free un-damped vibration response of thickness-tapered composite beams, using higher-order finite element method [25, 26]. Steeves and Fleck [27] conducted experimental study on tapered laminates loaded in axial compression to investigate failures induced by either micro-buckling or delamination. Progressive failure and post buckling response of thickness-tapered composite plates under uni-axial compression were studied by Ganesan and Liu [28]. The buckling analysis was conducted by Ganesan and Akhlaque-E-Rasul for tapered composite shells [29]. A simplified non-linear buckling analysis of tapered curved composite plates was conducted [30] and the compressive response of tapered curved composite plates was investigated based on a nine-node composite shell element [31].

When lightweight structural components are subject to dynamic loading particularly periodic in-plane loads, and when the frequency of in-plane dynamic load and the frequency of vibration satisfy certain specific condition, parametric resonance will occur in the structure. This makes the plate enter into a state of dynamic instability [2, 32]. This instability is of concern because it can occur at load magnitudes that are much less than the static buckling load, so a component designed to withstand static buckling may fail in a periodic loading environment. Further, dynamic instability occurs over a range of forcing frequencies rather than at a single value [1, 32].

Forced vibration and dynamic stability of a rotating tapered composite Timoshenko shaft were studied by Kim et al. [33]. They studied the response and stability of high-speed extended length end-mill subjected to cutting forces typical of milling operations. To the best of authors' knowledge, the only available literature on the dynamic instability of internally-tapered composite plate is the thesis work conducted by Liu [34] under the supervision of the present Ph.D. research work. This thesis considered the linear dynamic instability analysis of a simplified problem using Ritz and FEM. The dynamic instability of structures based on linear

67

analysis can only determinate the dynamically-unstable regions. For more accurate, and comprehensive study of dynamic instability of laminated plates a non-linear analysis is required to determine both the stable and unstable amplitudes of steady-state vibrations in addition to instability regions [32].

The present work, the von Karman-type of plate equation is used to develop the equations of motion of the plate including geometric non-linearity for internally-thickness-tapered laminated composite plate subjected to harmonic in-plane loading. The in-plane displacements are determined from the two in-plane force-equilibrium equations of motion of non-linear large deflection tapered plate. Consequently, the in-plane force-resultants are obtained from the in-plane displacements and further applying the boundary conditions. Then the general Galerkin method is used for the moment-equilibrium equation of motion to satisfy spatial dependence in the partial differential equation of motion to produce a set of non-linear Mathieu-Hill equations which are ordinary differential equations with time-dependency. The dynamically-unstable regions, and both stable-, and unstable-solutions amplitudes of steady-state vibrations are determined by applying the Bolotin's method. A comprehensive parametric study is carried out to examine and compare the effects of the various taper configurations, taper angles, amplitudes of both tensile and compressive in-plane loads, aspect ratios of the tapered plate including length-to-width and length-to-thickness ratios and in particular the length-to-average-thickness ratio on the instability regions and the parametric resonance particularly the steady-state vibrations amplitude. The present results for the linear case show good agreement when compared with that available in the literature and hence can be used as benchmark results for future studies.

3.2 Formulation

A simply supported laminated composite rectangular internally-thickness-tapered plate, having length a and width b with respect to the Cartesian coordinates (x, y, z) which are assigned in the mid-plane of the plate is considered as shown in Fig.3.1.
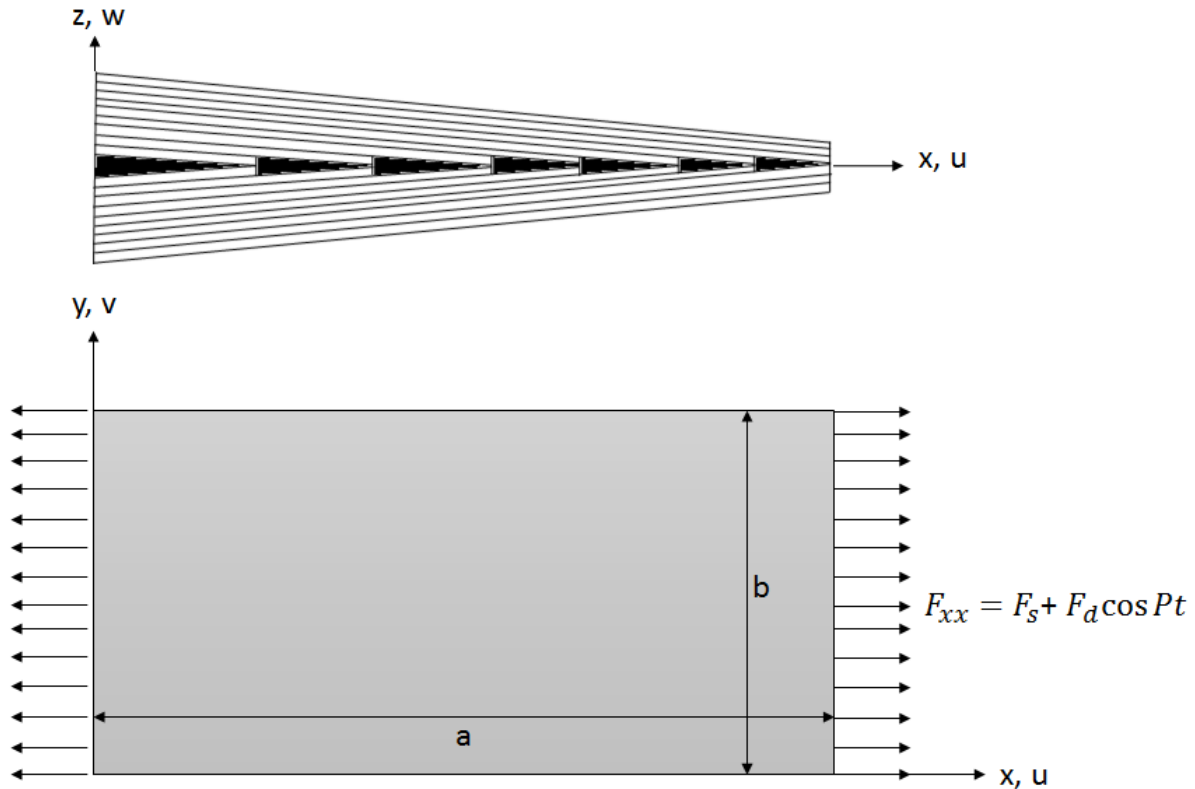
Figure 3.1 The geometry and loading condition of a laminated composite rectangular thickness-tapered plate

Here, u, v and w are the displacement components of the plate with reference to this coordinate system in the $x, y, and z$ directions, respectively.

The plate as shown in Fig.1 is subjected to a periodically pulsating load in the length direction with the longitudinal loading per unit length as follow:

$$F_{xx}(t) = F_s + F_d cosPt \qquad (3.1)$$

where F_s is a time invariant component, $F_d cosPt$ is the harmonically-pulsating component, and P denotes the frequency of excitation in radians per unit time.

As mentioned above the plate is considered to be internally-tapered in the thickness and has been designed with any one of the four different taper configurations shown in Fig.3.2.
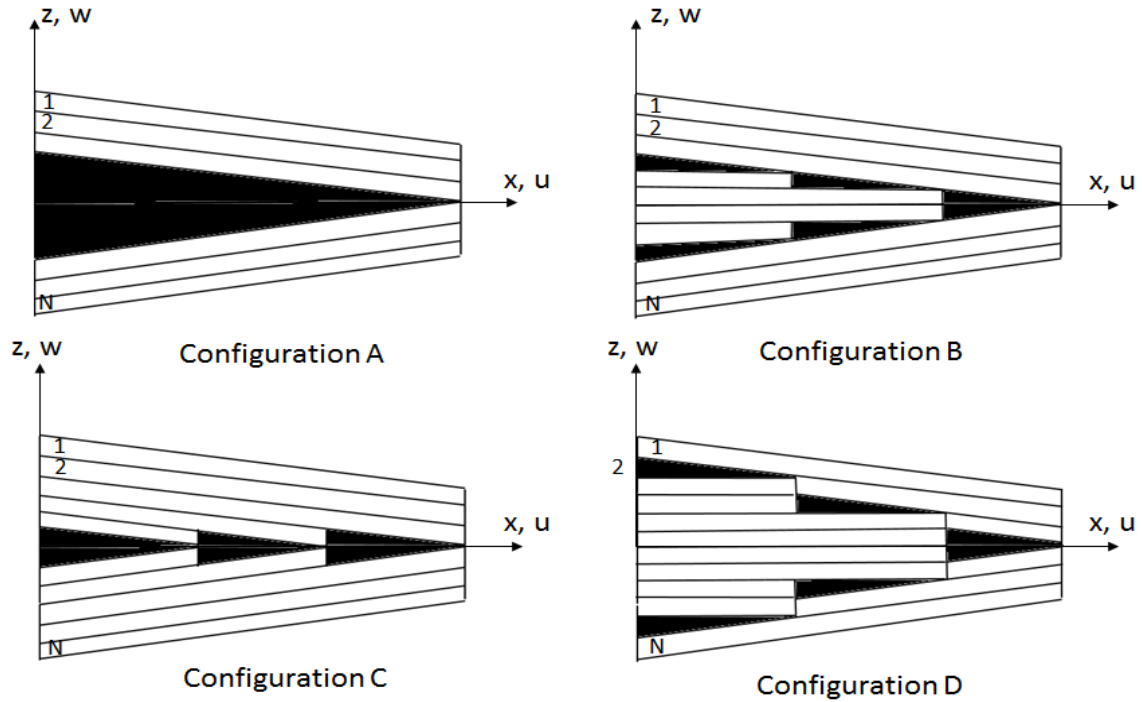
Figure 3.2 Taper configurations of the rectangular internally-thickness-tapered composite plate

Since $u_0 \ll w_0$ and $v_0 \ll w_0$ one can consider that $\rho_t \, {\partial^2 u_0}/{\partial t^2} \to 0$ and $\rho_t \, {\partial^2 v_0}/{\partial t^2} \to 0$. Therefore by neglecting the in-plane inertia forces the equations of motion for the plate, in the form that was originally presented by von Karman [16] and used in further development in Lagrangian coordinates by Fung [16, 17], under the in-plane pulsating load are given by

$$\frac{\partial N_{xx}}{\partial x} + \frac{\partial N_{xy}}{\partial y} = 0 \tag{3.2}$$

$$\frac{\partial N_{xy}}{\partial x} + \frac{\partial N_{yy}}{\partial y} = 0 \tag{3.3}$$

$$\frac{\partial^2 M_{xx}}{\partial x^2} + 2\frac{\partial^2 M_{xy}}{\partial x \partial y} + \frac{\partial^2 M_{yy}}{\partial y^2} + N_{xx}\frac{\partial^2 w_0}{\partial x^2} + 2N_{xy}\frac{\partial^2 w_0}{\partial x \partial y} + N_{yy}\frac{\partial^2 w_0}{\partial y^2} = \rho_t \frac{\partial^2 w_0}{\partial t^2} \tag{3.4}$$

where

$$\rho_t(x^1, x^0) = \sum_{k=1}^{N} \rho^{(k)}(h_k(x^1, x^0) - h_{k+1}(x^1, x^0)) \tag{3.5}$$

and (N_{xx}, N_{yy}, N_{xy}) are the total in-plane *force resultants and* (M_{xx}, M_{yy}, M_{xy}) are the total

moment resultants that are defined by

$$\begin{Bmatrix} N_{xx} \\ N_{yy} \\ N_{xy} \end{Bmatrix} = \int_{-h/2}^{h/2} \begin{Bmatrix} \sigma_{xx} \\ \sigma_{yy} \\ \sigma_{xy} \end{Bmatrix} dz \tag{3.6}$$

$$\begin{Bmatrix} M_{xx} \\ M_{yy} \\ M_{xy} \end{Bmatrix} = \int_{-h/2}^{h/2} \begin{Bmatrix} \sigma_{xx} \\ \sigma_{yy} \\ \sigma_{xy} \end{Bmatrix} Z \, dz \tag{3.7}$$

The non-zero von Karman strains associated with non-linear large deflections and curvatures

are given by

$$\begin{Bmatrix} \epsilon_{xx} \\ \epsilon_{yy} \\ \gamma_{xy} \end{Bmatrix} = \begin{Bmatrix} \epsilon_{xx}^{(0)} \\ \epsilon_{yy}^{(0)} \\ \gamma_{xy}^{(0)} \end{Bmatrix} + z \begin{Bmatrix} \epsilon_{xx}^{(1)} \\ \epsilon_{yy}^{(1)} \\ \gamma_{xy}^{(1)} \end{Bmatrix} \tag{3.8}$$

$$\{\epsilon^0\} = \begin{Bmatrix} \epsilon_{xx}^{(0)} \\ \epsilon_{yy}^{(0)} \\ \gamma_{xy}^{(0)} \end{Bmatrix} = \begin{Bmatrix} \frac{\partial u_0}{\partial x} + \frac{1}{2}\left(\frac{\partial w_0}{\partial x}\right)^2 \\ \frac{\partial v_0}{\partial y} + \frac{1}{2}\left(\frac{\partial w_0}{\partial y}\right)^2 \\ \frac{\partial u_0}{\partial y} + \frac{\partial v_0}{\partial x} + \frac{\partial w_0}{\partial x}\frac{\partial w_0}{\partial y} \end{Bmatrix} \tag{3.9}$$

$$\{\epsilon^1\} = \begin{Bmatrix} \epsilon_{xx}^{(1)} \\ \epsilon_{yy}^{(1)} \\ \gamma_{xy}^{(1)} \end{Bmatrix} = \begin{Bmatrix} -\frac{\partial^2 w_0}{\partial x^2} \\ -\frac{\partial^2 w_0}{\partial y^2} \\ -2\frac{\partial^2 w_0}{\partial x \partial y} \end{Bmatrix} \tag{3.10}$$

where ($\epsilon_{xx}^{(0)}, \epsilon_{yy}^{(0)}, \gamma_{xy}^{(0)}$) are the membrane strains, ($\epsilon_{xx}^{(1)}, \epsilon_{yy}^{(1)}, \gamma_{xy}^{(1)}$) are the flexural (bending)

strains and (u_0, v_0, w_0) are mid-plane displacements.

The rectangular thickness-tapered plate is considered to be constructed by a cross-ply

laminated composite material having density ρ. As shown in Fig. 3.3 the stiffness matrix of a

ply in the thickness-tapered laminate in the global coordinate system (x, y, z) is calculated by

using multiple transformations of the ply material stiffness matrix from principal material

coordinate system (x'', y'', z'') to local coordinate system (x', y', z'), and then to the global coordinate system (x, y, z) as follow:

$$[C]_{xyz} = [T_\Psi][T_\theta][C'']_{x''y''z''}[T_\theta]^T[T_\Psi]^T \tag{3.11}$$

where $[T_\theta]$ and $[T_\Psi]$ are the stress transformation matrices corresponding to the fiber orientation angle θ and ply angle Ψ respectively that are defined in Appendix (Eq. (A.5) and (A.6)). The ply angle Ψ for a ply located above the mid-plane is equal to the taper angle ϕ and for the ply located below the mid-plane it is equal to $-\phi$. The constitutive equation of the thickness-tapered laminate made of several orthotropic layers with the arbitrarily oriented material axes to the laminate coordinate can be obtained by the transformation of the stress-strain relations to the laminate coordinates as follow:

$$\begin{Bmatrix} \sigma_{xx} \\ \sigma_{yy} \\ \tau_{xy} \end{Bmatrix}^{(k)} = \begin{bmatrix} \bar{Q}_{11} & \bar{Q}_{12} & \bar{Q}_{16} \\ \bar{Q}_{12} & \bar{Q}_{22} & \bar{Q}_{26} \\ \bar{Q}_{16} & \bar{Q}_{26} & \bar{Q}_{66} \end{bmatrix}^{(k)} \begin{Bmatrix} \epsilon_{xx} \\ \epsilon_{yy} \\ \gamma_{xy} \end{Bmatrix} \tag{3.12}$$

where $[\bar{Q}]^{(k)}$ is the transformed reduced stiffness matrix defined as follow:

$$\bar{Q}_{11}{}^{(k)} = C_{11}(\theta^{(k)}, \Psi^{(k)}) - \frac{C_{13}(\theta^{(k)}, \Psi^{(k)}) * C_{13}(\theta^{(k)}, \Psi^{(k)})}{C_{33}(\theta^{(k)}, \Psi^{(k)})} \tag{3.13-a}$$

$$\bar{Q}_{12}{}^{(k)} = C_{12}(\theta^{(k)}, \Psi^{(k)}) - \frac{C_{13}(\theta^{(k)}, \Psi^{(k)}) * C_{23}(\theta^{(k)}, \Psi^{(k)})}{C_{33}(\theta^{(k)}, \Psi^{(k)})} \tag{3.13-b}$$

$$\bar{Q}_{22}{}^{(k)} = C_{22}(\theta^{(k)}, \Psi^{(k)}) - \frac{C_{23}(\theta^{(k)}, \Psi^{(k)}) * C_{23}(\theta^{(k)}, \Psi^{(k)})}{C_{33}(\theta^{(k)}, \Psi^{(k)})} \tag{3.13-c}$$

$$\bar{Q}_{16}{}^{(k)} = C_{16}(\theta^{(k)}, \Psi^{(k)}) - \frac{C_{13}(\theta^{(k)}, \Psi^{(k)}) * C_{63}(\theta^{(k)}, \Psi^{(k)})}{C_{33}(\theta^{(k)}, \Psi^{(k)})} \tag{3.13-d}$$

$$\bar{Q}_{26}{}^{(k)} = C_{26}(\theta^{(k)}, \Psi^{(k)}) - \frac{C_{23}(\theta^{(k)}, \Psi^{(k)}) * C_{63}(\theta^{(k)}, \Psi^{(k)})}{C_{33}(\theta^{(k)}, \Psi^{(k)})} \tag{3.13-e}$$

$$\bar{Q}_{66}{}^{(k)} = C_{66}(\theta^{(k)}, \Psi^{(k)}) - \frac{C_{63}(\theta^{(k)}, \Psi^{(k)}) * C_{63}(\theta^{(k)}, \Psi^{(k)})}{C_{33}(\theta^{(k)}, \Psi^{(k)})} \tag{3.13-f}$$
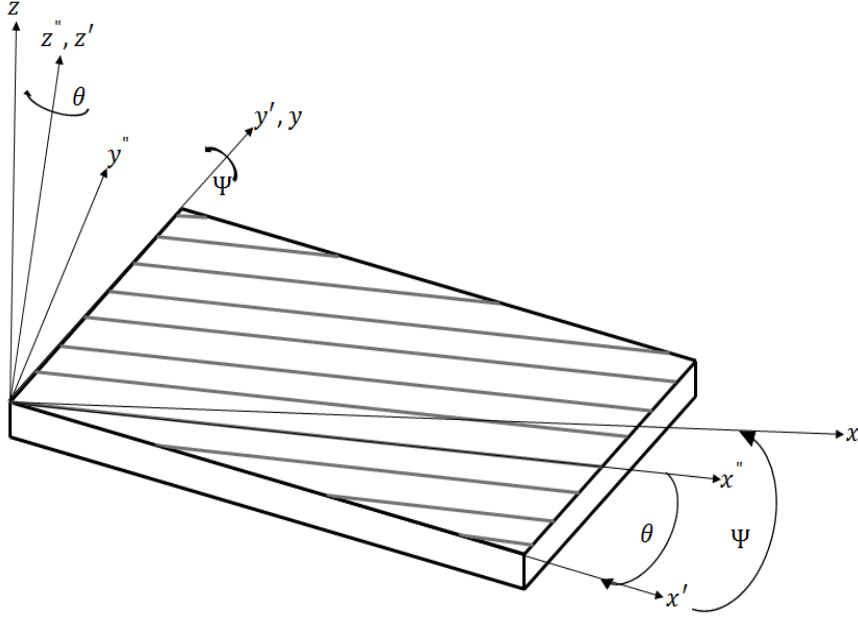
Figure 3.3 Transformation of the principal material coordinates to global coordinates

where $\bar{Q}_{16}{}^{(k)}$ and $\bar{Q}_{26}{}^{(k)}$ for the plies in the cross-ply laminate are zero and C_{ij} are elements of the stiffness matrix $[C]$ [35]. By following the equations (3.6)-(3.15) the force and moment resultants for the cross-ply symmetric laminated thickness-tapered plate are defined as

$$\begin{Bmatrix} N_{xx} \\ N_{yy} \\ N_{xy} \\ M_{xx} \\ M_{yy} \\ M_{xy} \end{Bmatrix} = \begin{bmatrix} \begin{matrix} A_{11} & A_{12} & 0 \\ A_{12} & A_{22} & 0 \\ 0 & 0 & A_{66} \end{matrix} & [0] \\ [0] & \begin{matrix} D_{11} & D_{12} & 0 \\ D_{12} & D_{22} & 0 \\ 0 & 0 & D_{66} \end{matrix} \end{bmatrix} \begin{Bmatrix} \epsilon_{xx}^{(0)} \\ \epsilon_{yy}^{(0)} \\ \gamma_{xy}^{(0)} \\ \epsilon_{xx}^{(1)} \\ \epsilon_{yy}^{(1)} \\ \gamma_{xy}^{(1)} \end{Bmatrix} \qquad (3.14)$$

where A_{ij} and D_{ij} denote the extensional and bending stiffnesses respectively.

$$A_{ij}(x^1, x^0) = \sum_{k=1}^{N} \bar{Q}_{ij}^{(k)}(h_k(x^1, x^0) - h_{k+1}(x^1, x^0)) \qquad , (i, j = 1, 2, 6) \qquad (3.15a)$$

$$D_{ij}(x^3, x^2, x^1, x^0) = \frac{1}{3} \sum_{k=1}^{N} \bar{Q}_{ij}^{(k)}((h_k(x^1, x^0))^3 - (h_{k+1}(x^1, x^0))^3) \qquad (3.15b)$$

where h_k and h_{k+1} are measured from the mid-plane to the outer and inner surfaces of the kth layer, respectively and calculated as follow:

$$h_k(x^1, x^0) = \begin{cases} (-\tan\phi) * x + z_k & IF \quad z_k > 0 \\ (\tan\phi) * x + z_k & IF \quad z_k < 0 \end{cases} \qquad (3.16)$$

Hence, although A_{ij} and D_{ij} are constant terms in uniform laminates, in the thickness-tapered laminates these extension- and bending-stiffnesses are linear and cubic functions of x-coordinate respectively. These functions are step functions for all configurations of the thickness-tapered plate except for configuration A. The number of the corresponding intervals, N_s, for the configurations B, C and D are expressed as follow:

$$N_s = \frac{1}{2}(N_L - N_R) \tag{3.17}$$

where N_L and N_R refer to the number of plies at the left (thick) and right (thin) sides of the thickness-tapered plate respectively.

3.3   Solution for laminated orthotropic thickness-tapered plates

Since the gradients of variations of extensional stiffnesses $A_{ij}(x^1, x^0)$ from the thickest to the thinnest sides of the thickness-tapered plate are too small in comparison to the corresponding variations of bending stiffnesses $D_{ij}(x^3, x^2, x^1, x^0)$, one can replace the $A_{ij}(x^1, x^0)$ terms in Eq. 14 by their average values as follow:

$$\bar{A}_{ij} = \frac{1}{a}\int_0^a A_{ij}(x^1, x^0)dx \qquad , (i, j = 1, 2, 6) \tag{3.18}$$

It should be noted here that since extensional stiffnesses, $A_{ij}(x^1, x^0)$, for all configurations of the thickness-tapered plate except for configuration A, are step functions, the integration in Eq. (3.18) over the length of the thickness-tapered plate should be step integration.

Substituting Eq. (3.9) and Eq. (3.18) into Eq. (3.14) the resultant membrane forces N_{xx}, N_{yy} and N_{xy} are defined and consequently the first-two equations of motion i.e. Eq. (3.2) and Eq. (3.3) are written in terms of the mid-plane displacement components i.e. $u_0(x, y, t)$, $v_0(x, y, t)$ and $w_0(x, y, t)$.

Considering the simply supported boundary condition for the laminated orthotropic thickness-tapered plate, the Navier's double Fourier series with the time dependent coefficient $q_{mn}(t)$ is chosen to describe the out-of-plane displacement function $w_0(x, y, t)$:

$$w_0 = \sum_{m=1}^{\infty}\sum_{n=1}^{\infty} q_{mn}(t) \sin \lambda_m x \sin \lambda_n y \quad , \quad \lambda_m = \frac{m\pi}{a} \text{ and } \lambda_n = \frac{n\pi}{b} \tag{19}$$

where m and n represent the number of longitudinal and transverse half-waves in corresponding standing wave pattern, respectively. Substituting Eq. (3.18) in the displacement form of Eq. (3.2) and Eq. (3.3) and applying appropriate trigonometric relations, the solution of the differential equation system has the form as follow:

$$u_0(x,y,t) = \sum_{m=1}^{\infty}\sum_{n=1}^{\infty} \zeta_1 \sin(2\lambda_m x) + \zeta_2 \sin(2\lambda_m x)\cos(2\lambda_n y) + u_c(x,y,t) \tag{3.20-a}$$

$$v_0(x,y,t) = \sum_{m=1}^{\infty}\sum_{n=1}^{\infty} \zeta_3 \sin(2\lambda_n y) + \zeta_4 \cos(2\lambda_m x)\sin(2\lambda_n y) + v_c(x,y,t) \tag{3.20-b}$$

Here ζ_1, ζ_2, ζ_3 and ζ_4 are unknown coefficients out of which ζ_1 and ζ_3 can be directly obtained from the displacement form of Eq. (3.2) and Eq. (3.3), respectively as follow:

$$\zeta_1 = -(\bar{A}_{11}\lambda_m{}^2 - \bar{A}_{12}\lambda_n{}^2)q_{mn}(t)^2/16\lambda_m\bar{A}_{11} \tag{3.21-a}$$

$$\zeta_3 = (\bar{A}_{12}\lambda_m{}^2 - \bar{A}_{22}\lambda_n{}^2)q_{mn}(t)^2/16\lambda_n\bar{A}_{22} \tag{3.21-b}$$

and also ζ_2 and ζ_4 can be solved from the displacement form of the system of equations (2 and 3) as follow:

$$\zeta_2 = \frac{1}{16}\lambda_m q_{mn}(t)^2 \tag{3.21-c}$$

$$\zeta_4 = \frac{1}{16}\lambda_n q_{mn}(t)^2 \tag{3.21-d}$$

$u_c(x,y,t)$ and $v_c(x,y,t)$ are homogeneous solutions of the differential equation system given as:

$$\bar{A}_{11}\frac{\partial^2 u_c}{\partial x^2} + (\bar{A}_{12} + \bar{A}_{66})\frac{\partial^2 v_c}{\partial x\partial y} + \bar{A}_{66}\frac{\partial^2 u_c}{\partial y^2} = 0 \tag{3.22-a}$$

$$\bar{A}_{66}\frac{\partial^2 v_c}{\partial x^2} + (\bar{A}_{12} + \bar{A}_{66})\frac{\partial^2 u_c}{\partial x\partial y} + \bar{A}_{22}\frac{\partial^2 u_c}{\partial y^2} = 0 \tag{3.22-b}$$

Since the solution should also satisfy the boundary conditions of the studied thickness-tapered plate which is subjected to in-plane loading, for the partial differential equation system of equations (3.22-a and b) the solution should have the forms as follow:

$$u_c(x,y,t) = \bar{A}_{11}(a - 2x)\xi_x(t) \tag{3.23-a}$$

$$v_c(x, y, t) = \bar{A}_{22}(b - 2y)\xi_y(t) \qquad \text{(3.23-b)}$$

where $\xi_x(t)$ and $\xi_y(t)$ are unknown functions of time that can be determined from the following boundary conditions:

$$\frac{1}{b}\int_0^b N_{xx}\ dy = F_{xx} \qquad at\ x = 0, a \qquad \text{(3.24-a)}$$

$$\frac{1}{a}\int_0^a N_{yy}\ dx = 0 \qquad at\ y = 0, b \qquad \text{(3.24-b)}$$

Hence by solving these two boundary condition equations, $\xi_x(t)$ and $\xi_y(t)$ are determined as follow:

$$\xi_x(t) = ((\bar{A}_{11}\bar{A}_{22} - \bar{A}_{12}{}^2)\lambda_m{}^2\ q_{mn}(t)^2 - 8\bar{A}_{22}F_{xx})/(16\bar{A}_{11}(\bar{A}_{11}\bar{A}_{22} - \bar{A}_{12}{}^2)) \qquad \text{(3.25-a)}$$

$$\xi_y(t) = ((\bar{A}_{11}\bar{A}_{22} - \bar{A}_{12}{}^2)\lambda_n{}^2\ q_{mn}(t)^2 + 8\bar{A}_{12}F_{xx})/(16\bar{A}_{22}(\bar{A}_{11}\bar{A}_{22} - \bar{A}_{12}{}^2)) \qquad \text{(3.25-b)}$$

and consequently the resultant membrane forces N_{xx}, N_{yy} and N_{xy} are determined as follow:

$$N_{xx} = F_{xx}b - (\bar{A}_{11}\bar{A}_{22} - \bar{A}_{12}{}^2)\ \lambda_m{}^2 q_{mn}(t)^2 \sin(2\lambda_n b)/16\lambda_n \bar{A}_{22} \qquad \text{(3.26-a)}$$

$$N_{yy} = -(\bar{A}_{11}\bar{A}_{22} - \bar{A}_{12}{}^2)\ \lambda_n{}^2 q_{mn}(t)^2 \sin(2\lambda_m a)/16\lambda_m \bar{A}_{11} \qquad \text{(3.26-b)}$$

$$N_{xy} = 0 \qquad \text{(3.26-c)}$$

By substituting the resultant membrane forces and the moment resultants from Eq. (3.14) that are in terms of the out-of-plane displacement, w_0, as defined in Eq.(3.19) into the third equation of motion i.e. Eq. (3.4), and then multiplying the governing equation by $\sin \lambda_m x \sin \lambda_n y$ and integrating over the mid-plane area of the thickness-tapered plate a system of $m \times n$ second-order ordinary differential equations is obtained. It should be noted again here that since bending stiffness for all configurations of the thickness-tapered plates except for configuration A, are step functions, hence the corresponding moment resultants are also step functions, therefore this integration over the area should be a step integration.

$$M_{mn}\ddot{q}_{mn}(t) + K_{mn}q_{mn}(t) - (F_s + F_d \cos pt)Q_{mn}q_{mn}(t) + \eta_{mn}q_{mn}^3(t) = 0 \qquad \text{(3.27)}$$

where M_{mn}, K_{mn}, Q_{mn} and η_{mn} are matrices and $\ddot{q}_{mn}(t)$, $q_{mn}(t)$ and $q_{mn}^3(t)$ are column vectors consisting of the $\ddot{q}_{mn}(t)$'s, $q_{mn}(t)$'s and $q_{mn}^3(t)$'s respectively. The subscripts m and n have the following ranges:

$$m, n = 1,2,3,4,..,N. \tag{3.28}$$

Introducing following notation:

$$\omega_{mn} = \sqrt{\frac{K_{mn}}{M_{mn}}} \tag{3.29a}$$

$$\gamma_{mn} = \frac{\eta_{mn}}{M_{mn}} \tag{3.29b}$$

$$N_* = \frac{K_{mn}}{Q_{mn}} \tag{3.29c}$$

Eq. (3.27) can be written in the form of the non-linear Mathieu-Hill equation as follow:

$$\ddot{q}_{mn}(t) + \Omega_{mn}^2 (1 - 2\mu_{mn}\cos pt)q_{mn}(t) + \gamma_{mn}q_{mn}^3(t) = 0 \tag{3.30}$$

where Ω_{mn} is the frequency of the free vibration of the plate loaded by a constant longitudinal force F_s,

$$\Omega_{mn} = \omega_{mn}\sqrt{1 - \frac{F_s}{N_*}} \tag{3.31}$$

and μ_{mn} is a quantity that is called the excitation parameter,

$$\mu_{mn} = \frac{F_d}{2(N_* - F_s)} \tag{3.32}$$

3.4 Amplitude of vibrations at the principal parametric resonance

As mentioned above Eq. (3.30) is a non-linear Mathieu-Hill equation where the non-linear term $\gamma q_{mn}^3(t)$ represents the effect of large deflection. According to the Liapunov Principle, the dynamically-unstable region is determined by the linear parts of the Eq. (3.30) [1], which will be discussed in the next section. Here the focus is set on the parametric resonance of the system. The basic solutions of Mathieu-Hill equation include two periodic solutions: i.e. periodic solutions of periods T and $2T$ with $T = 2\pi/P$. The solutions with period $2T$ are of greater practical importance as the widths of these unstable regions are usually larger than those

associated with solutions having period T. Using Bolotin's [1] method for parametric vibration, the solution of period $2T$ is given by the following equation:

$$q(t) = \sum_{k=1,3,5,\ldots}^{\infty} f_k \sin\frac{kPt}{2} + g_k \cos\frac{kPt}{2} \tag{3.33}$$

where f_k and g_k are arbitrary vectors. If one investigates the vibration at the principal resonance $\approx 2\Omega$, one can neglect the influence of higher harmonics in the expansion of above equation and can assume

$$q(t) = f \sin\frac{Pt}{2} + g \cos\frac{Pt}{2} \tag{3.34}$$

as an approximation. By substituting this function into Eq. (3.30) and equating the coefficients of $\sin(Pt/2)$, $\cos(Pt/2)$ terms and neglecting the terms containing higher harmonics, the following system of equations for the coefficients f and g remains:

$$\left[\Omega_{mn}^2(1 + \mu_{mn}) - \frac{P^2}{4}\right] f + \Gamma(f, g) = 0, \tag{3.35a}$$

$$\left[\Omega_{mn}^2(1 - \mu_{mn}) - \frac{P^2}{4}\right] g + \Psi(f, g) = 0, \tag{3.35b}$$

where $\Gamma(f, g)$ and $\Psi(f, g)$ are defined as coefficients of the terms including $\sin(Pt/2)$ and $\cos(Pt/2)$ which were obtained from the first approximation of expansion in a Fourier series as:

$$\Gamma(f, g) = \frac{3\gamma_{mn}}{4} A^2 f \tag{3.36a}$$

$$\Psi(f, g) = \frac{3\gamma_{mn}}{4} A^2 g \tag{3.36b}$$

where A is the amplitude of steady-state vibrations and is given by:

$$A = \sqrt{f^2 + g^2} \tag{3.37}$$

By substitution of Eqs. (36a, b) into Eqs. (35a, b) a system of two homogeneous linear equations with respect to f and g can be obtained. This system has solutions that differ from zero only in the case where the determinant composed of the coefficients vanishes:

78

$$\begin{vmatrix} 1 + \mu_{mn} - n_{mn}^2 + \frac{3\gamma_{mn}}{4\Omega_{mn}^2}A^2 & 0 \\ 0 & 1 - \mu_{mn} - n_{mn}^2 + \frac{3\gamma_{mn}}{4\Omega_{mn}^2}A^2 \end{vmatrix} = 0 \qquad (3.38)$$

where

$$n_{mn} = \frac{P}{2\Omega_{mn}} \qquad (3.39)$$

Expanding the determinant and solving the resulting equation with respect to the amplitude, A, of the steady-state vibrations the following equation is obtained:

$$A = \frac{2\Omega_{mn}}{\sqrt{3\gamma_{mn}}}\sqrt{n_{mn}^2 - 1 \pm \mu_{mn}} \qquad (3.40)$$

It can be proved that for the $\pm\mu_{mn}$ term in the above equation, only $+\mu_{mn}$ term yields the stable solution, and all the other terms yield unstable solutions.

3.5 Dynamic instability regions

The resonance curve is not influenced by the non-linearity of Eq. (3.28) and as mentioned in the previous section the dynamic instability regions are determined by linear part of the Mathieu-Hill equation, and so the Eq. (3.28) can be rewritten as follow:

$$M_{mn}\ddot{q}_{mn}(t) + (K_{mn}^* - Q_{mn}^* \cos pt)q_{mn}(t) + \eta_{mn}q_{mn}^3(t) = 0 \qquad (3.41)$$

where

$$K_{mn}^* = K_{mn} - F_s Q_{mn} \qquad (3.42)$$

and

$$Q_{mn}^* = F_d Q_{mn} \qquad (3.43)$$

The principal region of dynamic instability, which corresponds to the solution of the period, $2T$ is determined by substituting Eq. (3.34) into Eq. (3.41) and equating the determinant of the coefficient matrix of the linear part of the governing equation to zero as follow:

$$\begin{vmatrix} K_{mn}^* - \frac{Q_{mn}^*}{2} - \frac{M_{mn}}{4}P^2 & 0 \\ 0 & K_{mn}^* + \frac{Q_{mn}^*}{2} - \frac{M_{mn}}{4}P^2 \end{vmatrix} = 0 \qquad (3.44)$$

79

Comparing Eq. (3.44) with Eq. (3.38) by replacing μ_{mn}, n_{mn}, γ_{mn} and Ω_{mn} in terms of K^*_{mn}, Q^*_{mn} and M_{mn} reveals that the dynamic instability regions are determined by setting $A = 0$ in Eq. (3.38).

Equation (3.44) can be rearranged to the more simplified form of an eigenvalue problem as follow:

$$\begin{vmatrix} K^*_{mn} - \dfrac{Q^*_{mn}}{2} & 0 \\ 0 & K^*_{mn} + \dfrac{Q^*_{mn}}{2} \end{vmatrix} - P^2 \begin{vmatrix} \dfrac{M_{mn}}{4} & 0 \\ 0 & \dfrac{M_{mn}}{4} \end{vmatrix} = 0 \tag{3.45}$$

3.6 Numerical results and discussions

Non-linear dynamic stability characteristics of thickness-tapered cross-ply laminated composite rectangular plates subjected to combined static and periodic in-plane loads are studied here. The material properties used in the present analysis are listed in Table 3.1.

Table 3.1 Material properties of NCT/301 graphite-epoxy composite ply and epoxy materials

Composite Ply		Epoxy	
Material Properties	Value	Material Properties	Value
E_1	$113.9\ GPa$	$E_1 = E_2 = E_3$	$3.93\ GPa$
$E_2 = E_3$	$7.985\ GPa$	$\nu_{13} = \nu_{12} = \nu_{23}$	0.37
$\nu_{13} = \nu_{12}$	0.28	ρ	$1200\ Kg/m^3$
ν_{23}	0.4		
$G_{13} = G_{12}$	$3.1\ GPa$		
G_{23}	$2.8\ GPa$		
ρ	$1480\ Kg/m^3$		

The static and periodic components of the in-plane load are considered as $F_s = \alpha N_{cr}$ and $F_d = \beta N_{cr}$, respectively. The critical buckling load N_{cr} of the studied thickness-tapered composite plate has been calculated as follow:

$$|K_{mn} - N_{cr} Q_{mn}| = 0 \tag{3.46}$$

The fundamental frequency of the studied thickness-tapered plate is also calculated as follow:

$$|K^*_{mn} - \omega^2 M_{mn}| = 0 \tag{3.47}$$

In order to validate the present formulation, which is based on the non-linear analysis, we compare the dynamically-unstable regions with those given by Liu [34]. As it has been

mentioned and proved in Section 3.5 of the present study, the dynamic instability regions based on the large deflection formulation are achieved by either the linear part of the non-linear Mathieu-Hill equation or by setting $A = 0$ in equation (3.40). Once the stable- and unstable-solution amplitudes of steady-state vibrations is zero the corresponding excitation frequencies should coincide with the boundaries of the dynamically-unstable regions (having the same dynamic load factor β); therefore the accuracy of the amplitude-frequency curve is also confirmed by this comparison. Figures 3.4-3.11 give an illustrative graphical representation of dynamically-unstable region (Figs. 3.4a-3.11a) and also both stable- and unstable-solution amplitudes of steady-state vibrations (Figs. 3.4b-3.11b) of mode (1,1) of four different configurations, i.e. configurations A, B, C and D of the thickness-tapered plate. To compare the graphs with that given in [34] which considered the linear analysis and consequently lead only to the instability regions, for all configurations the thickness-tapered plate is a square plate having length $a = 0.24 \, m$, ply thickness $h_p = 0.138 \, mm$ ($a/h_{av} = 193.24$) and with 12 and 6 plies at the thick and thin sections of the thickness-tapered plate, respectively. The thickness-tapered composite plate is symmetric with stacking sequence of $[(0^{\circ}, 90^{\circ}, 0^{\circ}, ...)_1]_S$ and two comparative studies are considered having static loading amplitudes of $\alpha = 0.2$ and $\alpha = 0.8$ respectively, and also the amplitudes of steady-state vibrations (Figs. 3.4b-3.11b) are plotted for the same loading condition having the dynamic load factor of $\beta = 0.2$. As it can be observed from these figures (Figs. 3.4a-3.11a) each unstable region is separated by two lines with a common point of origin. Actually these two lines are not completely straight and they curved slightly outward. It is observed from these figures that there are excellent agreements between the present results and those obtained by Liu [34]. As it can be seen from these figures these agreements between the present results with the FEM analysis of their work are excellent although the Ritz analysis of their work deviate from these two agreements, particularly, the plots the configuration D subjected to the periodic axial loading having static load factor of
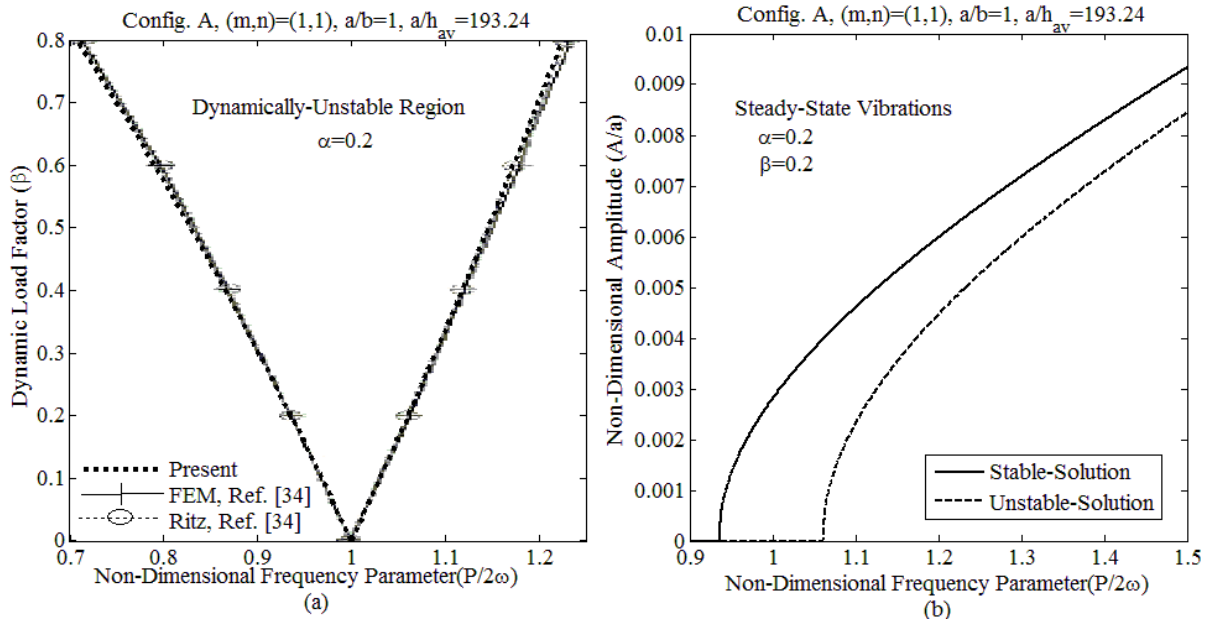
Figure 3.4 The first a) unstable region and b) both stable- and unstable-solution amplitudes of steady-state vibrations of a 12-6 layered symmetric $[(0°, 90°, 0°, (resin)_3)_1]_s$ cross-ply laminated square thickness-tapered plate with configuration A and thickness ratio of $a/h_{av} = 193.24$ subjected to periodic in-plane load having static load factor of $\alpha = 0.2$
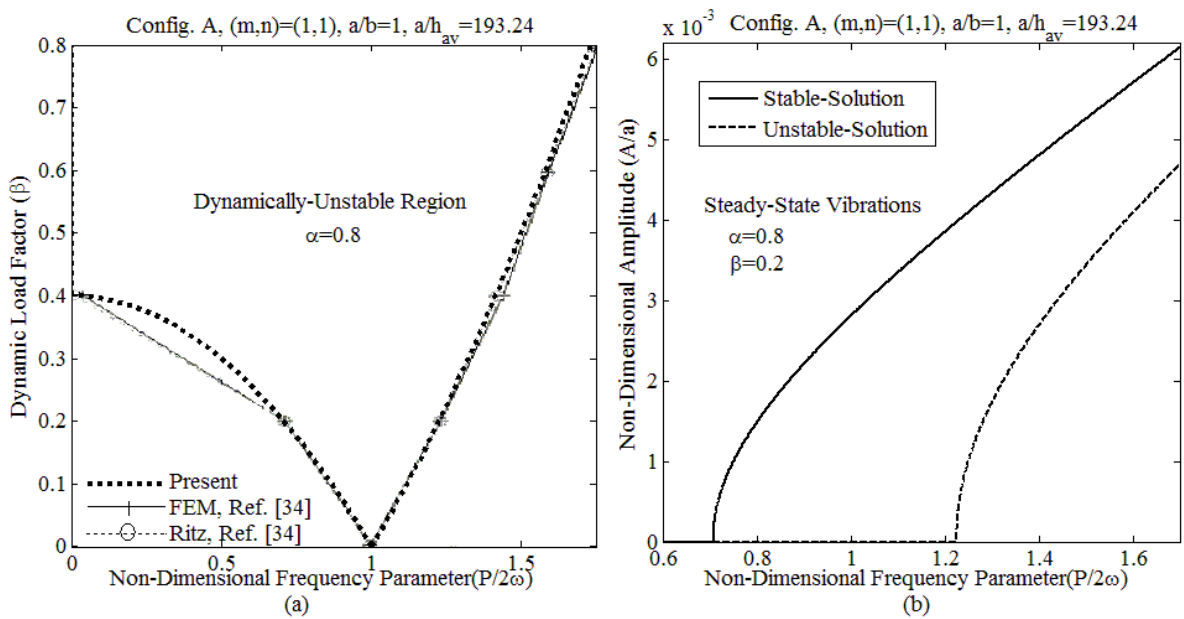
Figure 3.5 The first a) unstable region and b) both stable- and unstable-solution amplitudes of steady-state vibrations of a 12-6 layered symmetric $[(0°, 90°, 0°, (resin)_3)_1]_s$ cross-ply laminated square thickness-tapered plate with configuration A and thickness ratio of $a/h_{av} = 193.24$ subjected to periodic in-plane load having static load factor of $\alpha = 0.8$
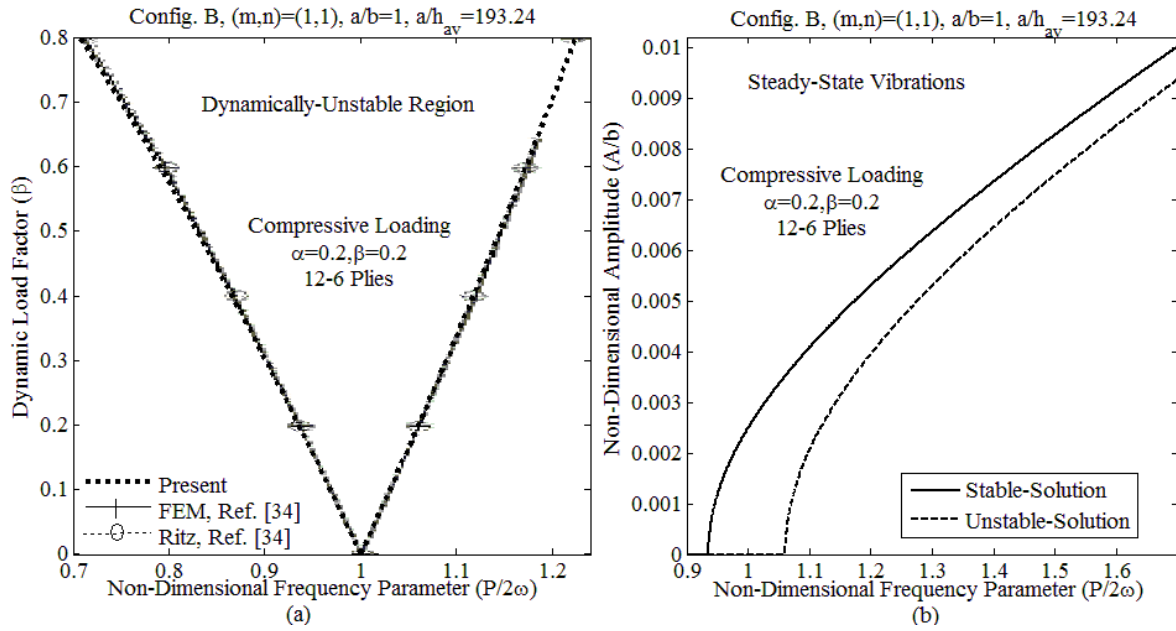
Figure 3.6 The first a) unstable region and b) both stable- and unstable-solution amplitudes of steady-state vibrations of a 12-6 layered symmetric $[(0°, 90°, 0°, \text{resin}, 0°, 90°)_1]_S$ cross-ply laminated square thickness-tapered plate with configuration B and thickness ratio of $a/h_{av} = 193.24$ subjected to periodic in-plane load having static load factor of $\alpha = 0.2$
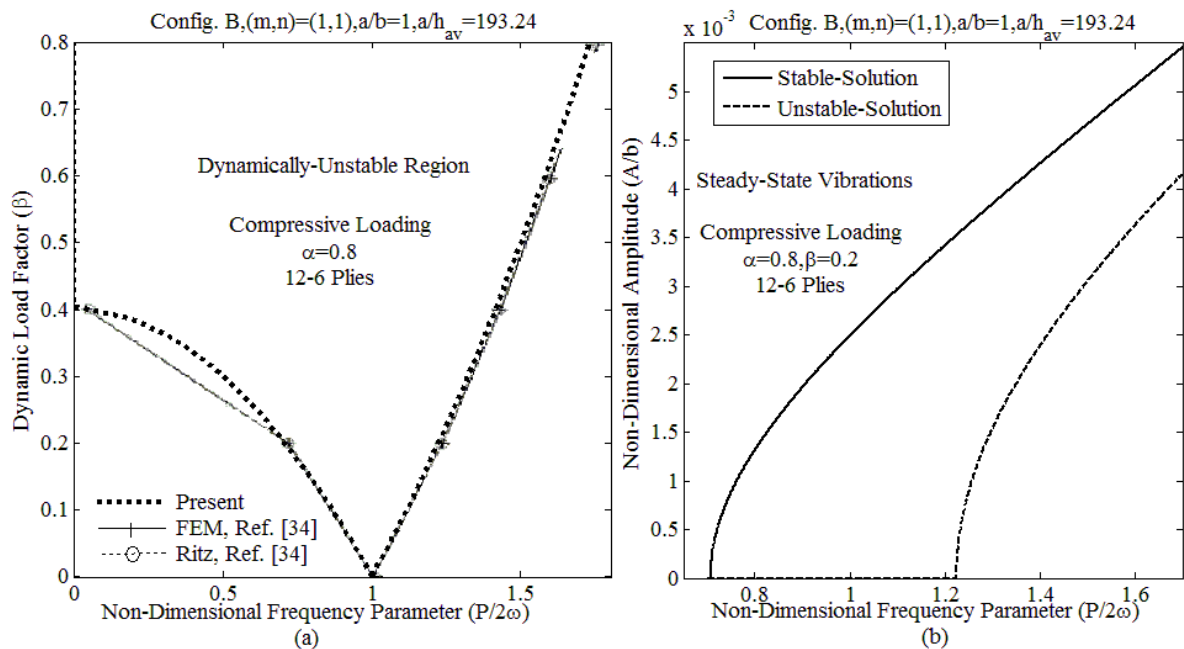
Figure 3.7 The first a) unstable region and b) both stable- and unstable-solution amplitudes of steady-state vibrations of a 12-6 layered symmetric $[(0°, 90°, 0°, \text{resin}, 0°, 90°)_1]_S$ cross-ply laminated square thickness-tapered plate with configuration B and thickness ratio of $a/h_{av} = 193.24$ subjected to periodic in-plane load having static load factor of $\alpha = 0.8$

83
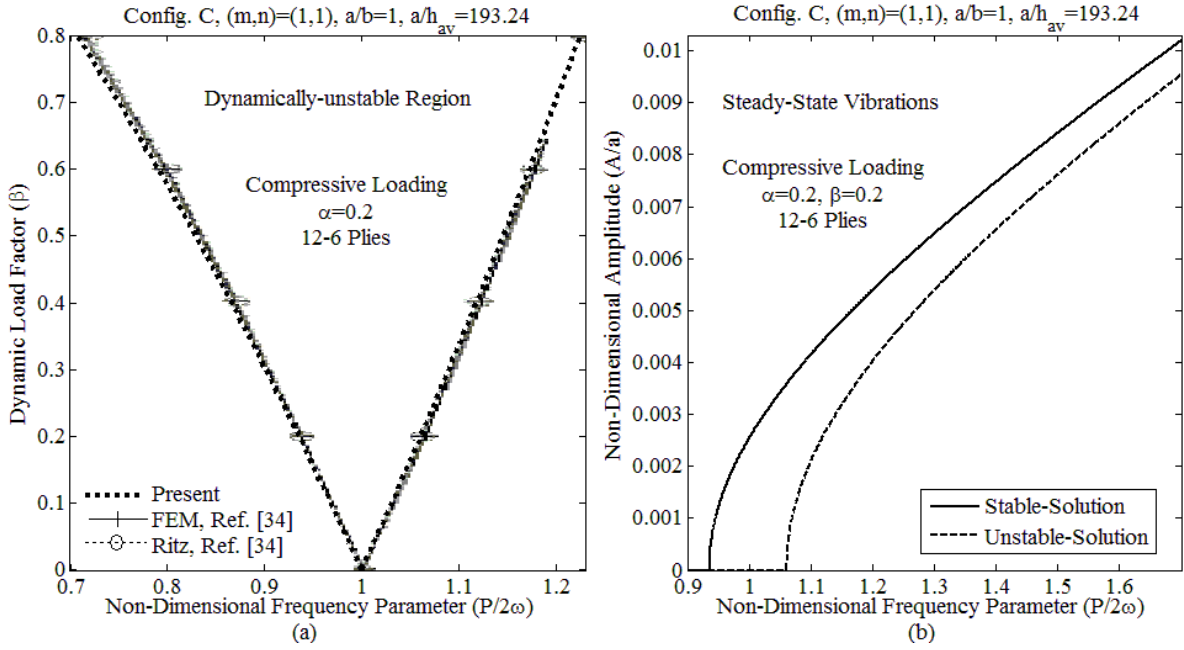
Figure 3.8 The first a) unstable region and b) both stable- and unstable-solution amplitudes of steady-state vibrations of a 12-6 layered symmetric $[(\mathbf{0^°, 90^°, 0^°, 90^°, 0^°, resin})_1]_S$ cross-ply laminated square thickness-tapered plate with configuration C and thickness ratio of $\boldsymbol{a/h_{av} = 193.24}$ subjected to periodic in-plane load having static load factor of $\boldsymbol{\alpha = 0.2}$
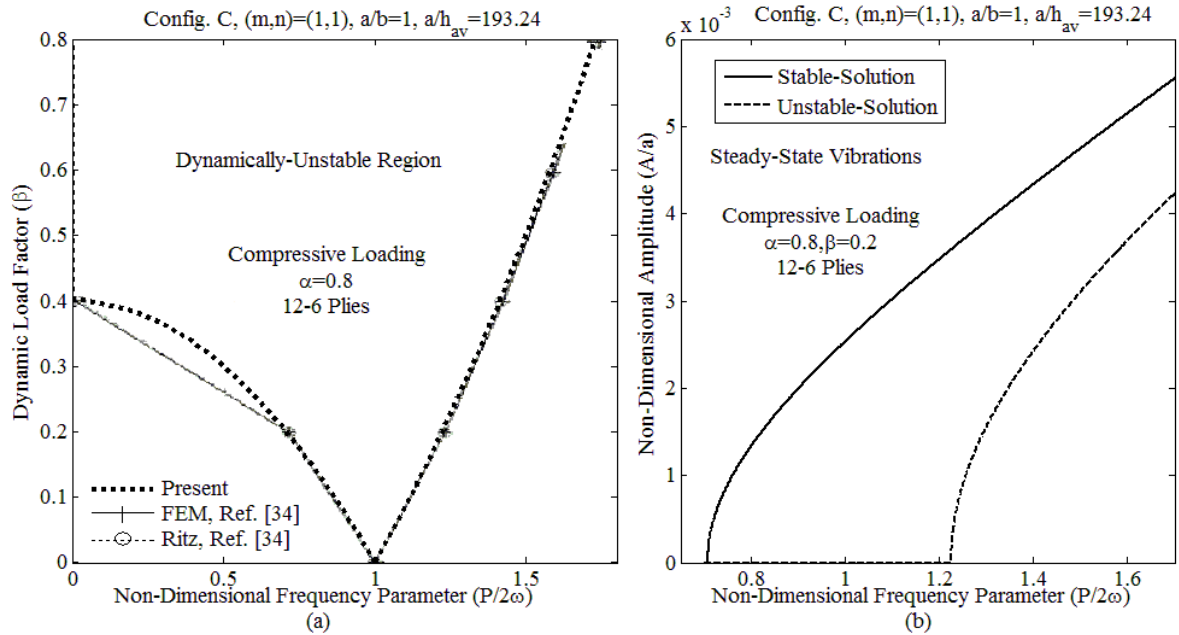
Figure 3.9 The first a) unstable region and b) both stable- and unstable-solution amplitudes of steady-state vibrations of a 12-6 layered symmetric $[(\mathbf{0^°, 90^°, 0^°, 90^°, 0^°, resin})_1]_S$ cross-ply laminated square thickness-tapered plate with configuration C and thickness ratio of $\boldsymbol{a/h_{av} = 193.24}$ subjected to periodic in-plane load having static load factor of $\boldsymbol{\alpha = 0.2}$

84
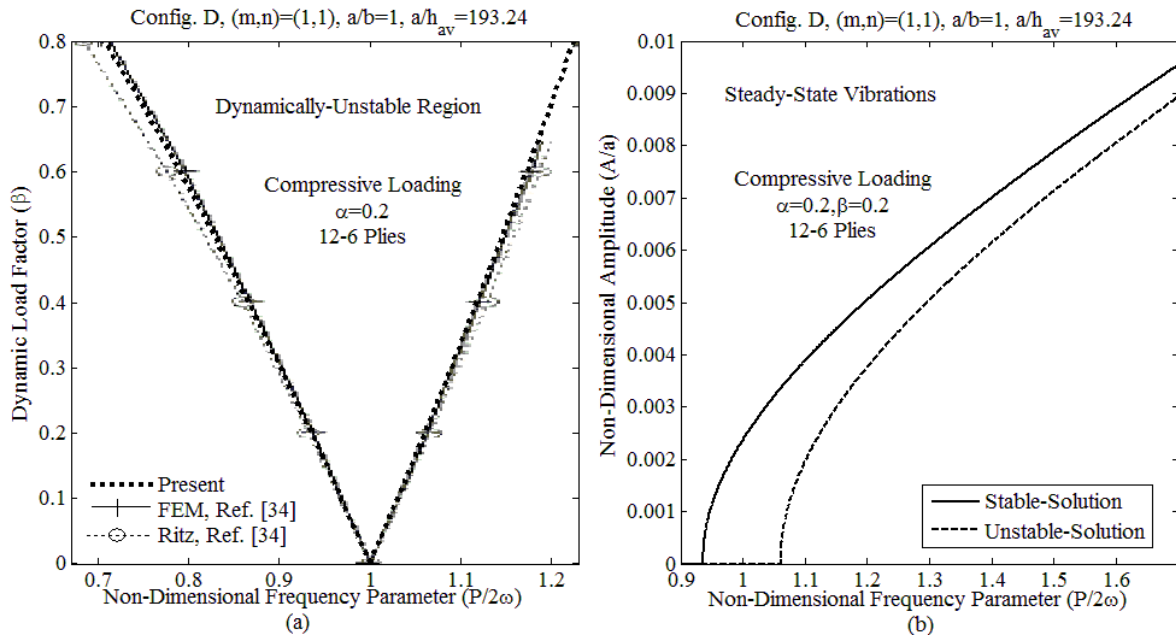
Figure 3.10 The first a) unstable region and b) both stable- and unstable-solution amplitudes of steady-state vibrations of a 12-6 layered symmetric cross-ply laminated square thickness-tapered plate with configuration D and thickness ratio of $a/h_{av} = 193.24$ subjected to periodic in-plane load having static load factor of $\alpha = 0.2$
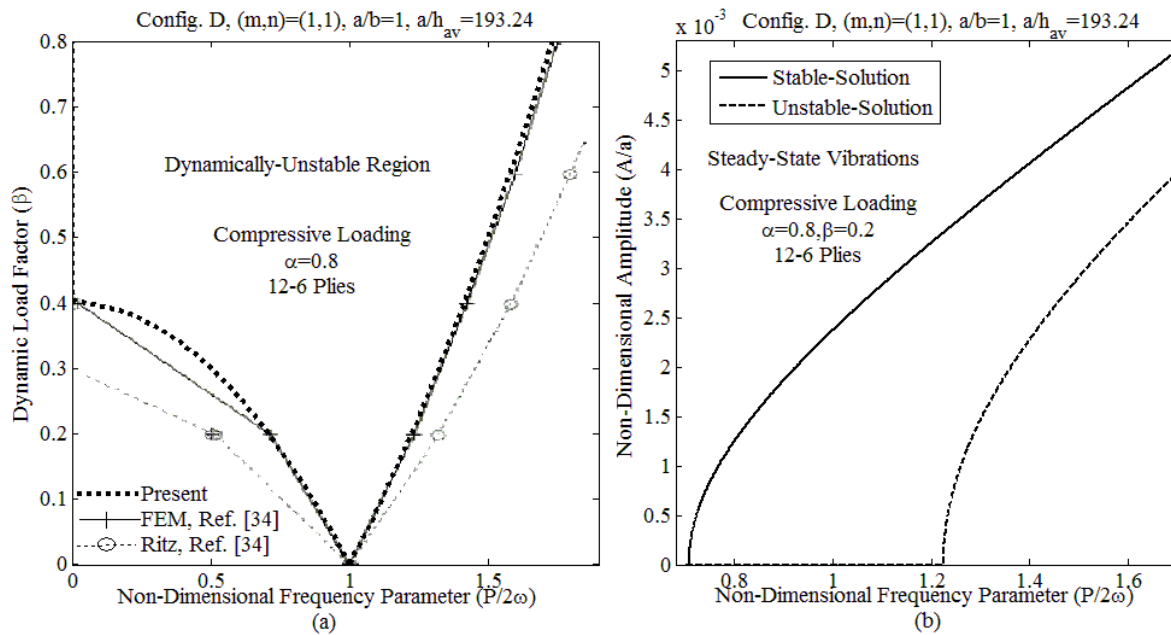
Figure 3.11 The first a) unstable region and b) both stable- and unstable-solution amplitudes of steady-state vibrations of a 12-6 layered symmetric cross-ply laminated square thickness-tapered plate with configuration D and thickness ratio of $a/h_{av} = 193.24$ subjected to periodic in-plane load having static load factor of $\alpha = 0.2$

85

$\alpha = 0.8$. As has been mentioned in [34] by the author Liu "the accuracy of their Ritz method depends on 1. the chosen approximate functions for deflections and their suitability for specific boundary conditions, and 2. the number of terms used. On the other hand, the finite element solution does not suffer from these limitations. Therefore, the finite element solution would be more accurate." So as can be seen from these figures this research work also confirms the accuracy of their FEM solution which is for linear analysis and only limited to dynamically-unstable regions and by these excellent agreements. There are not any specific reasons for the applied load factors and the modes except for comparison with the available results in that thesis research work by Liu [34]. Also, it is evident from these figures (Figs. 3.4b-3.11b) that once the amplitude is zero the corresponding excitation frequencies coincide with the boundaries of dynamically-unstable regions (Figs. 3.4a-3.11a), corresponding to the dynamic load factor of $\beta = 0.2$. The zero stable- and unstable-solution amplitudes of these figures (Figs. 3.4b-3.11b) exactly coincide with the left and right curves of the corresponding unstable regions (Figs. 3.4a-3.11a) respectively, and the range of frequencies between these two solutions at $A = 0$ predicate the dynamically-unstable regions at this certain value of dynamic load factor β. As a result, these figures show graphically that unstable regions could be obtained by setting $A = 0$ in Eq. (3.38) and hence, this could be considered as a validation of the non-linear part of the dynamic instability analysis.

The effects of various taper configurations on the first-two modes, dynamically-unstable regions and stable solution amplitudes of steady-state vibrations of symmetric thickness-tapered cross-ply laminated rectangular plates are presented in Figs. 3.12-3.15. All thickness-tapered configurations have 12 and 6 plies at the thick and thin section respectively, and also results are compared with the uniform plate having 9 plies (which is the average of 12 and 6 plies) and with the same length-to-average-thickness ratio i.e. $a/h_{av} = 100$ and length-to-width ratio of $a/b = 2$. Figures 3.12 and 3.13 correspond to the first-two modes, i.e. mode
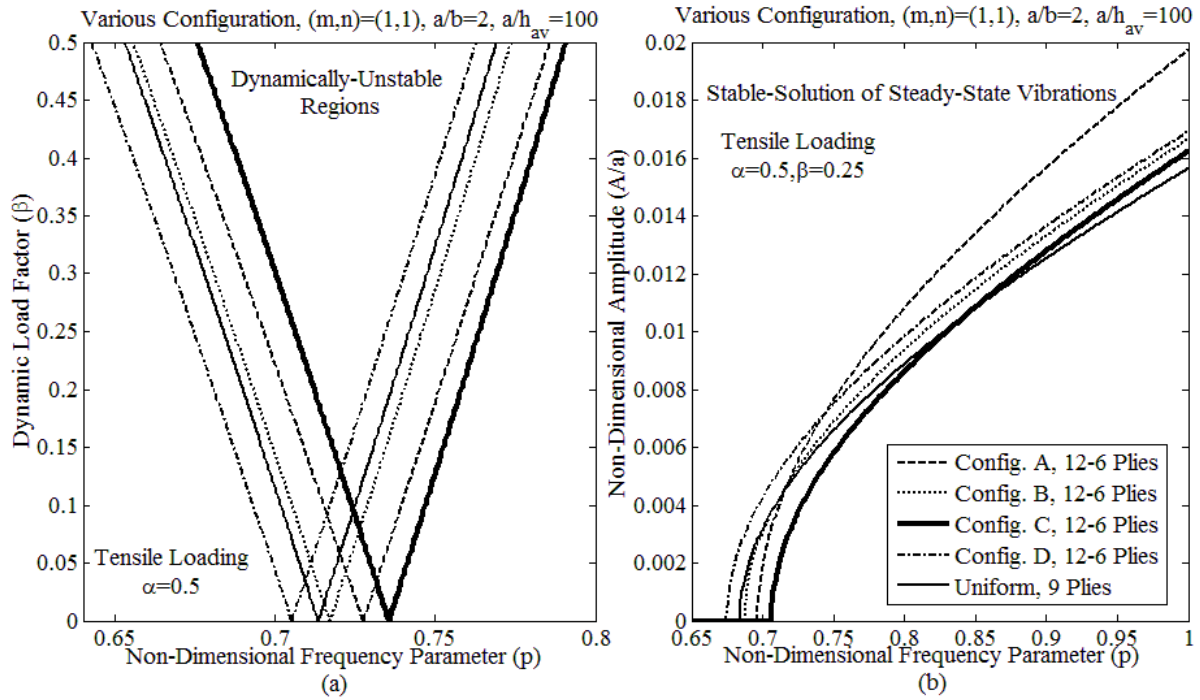
Figure 3.12 Effects of various taper configurations on the first mode a) unstable region and b) stable-solution amplitude of steady-state vibrations of a 12-6 layered symmetric cross-ply laminated rectangular thickness-tapered plate subjected to the tensile periodic in-plane loading
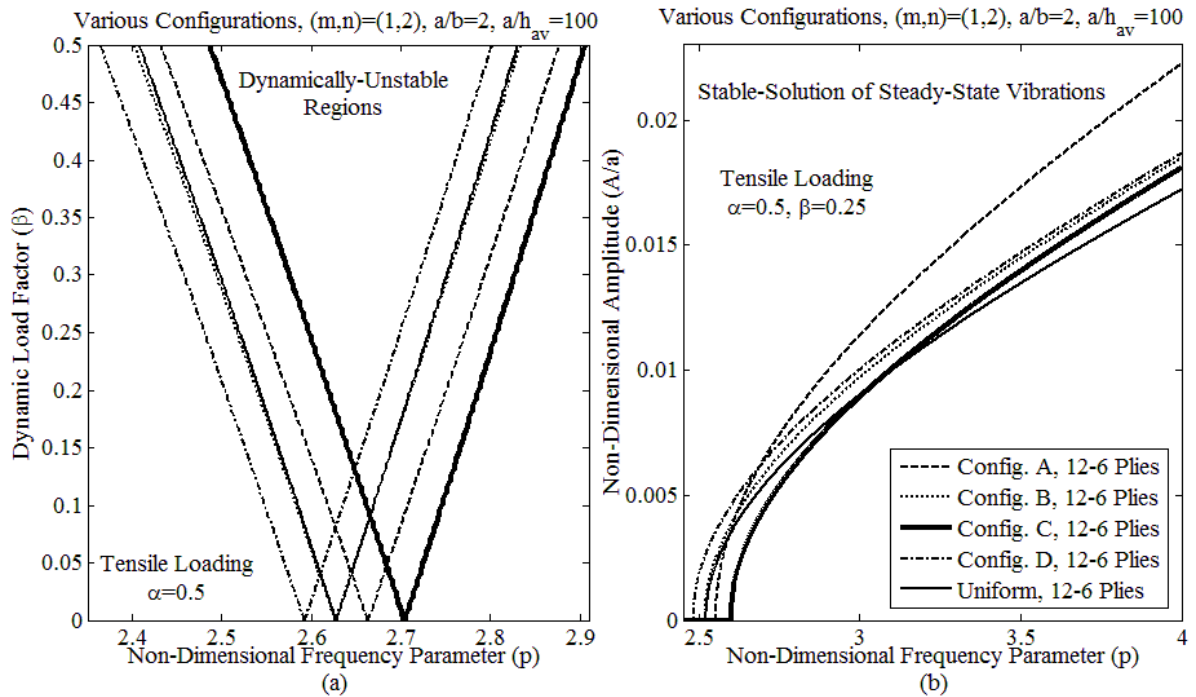
Figure 3.13 Effects of various tape configurations, on the second mode a) unstable region and b) stable-solution amplitude of steady-state vibrations of a 12-6 layered symmetric cross-ply laminated rectangular thickness-tapered plate subjected to the tensile periodic in-plane loading

87
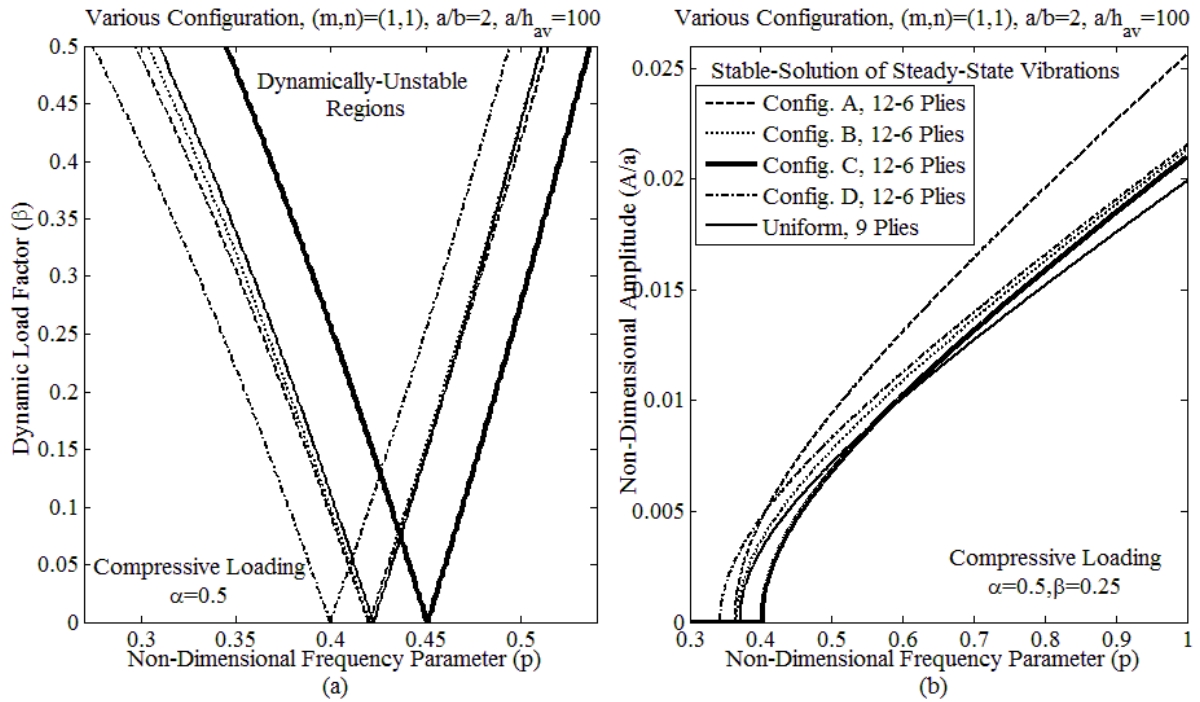
Figure 3.14 Effects of various taper configurations, on the first mode a) unstable region and b) stable-solution amplitude of steady-state vibrations of a 12-6 layered symmetric cross-ply laminated rectangular thickness-tapered plate subjected to the compressive periodic in-plane loading
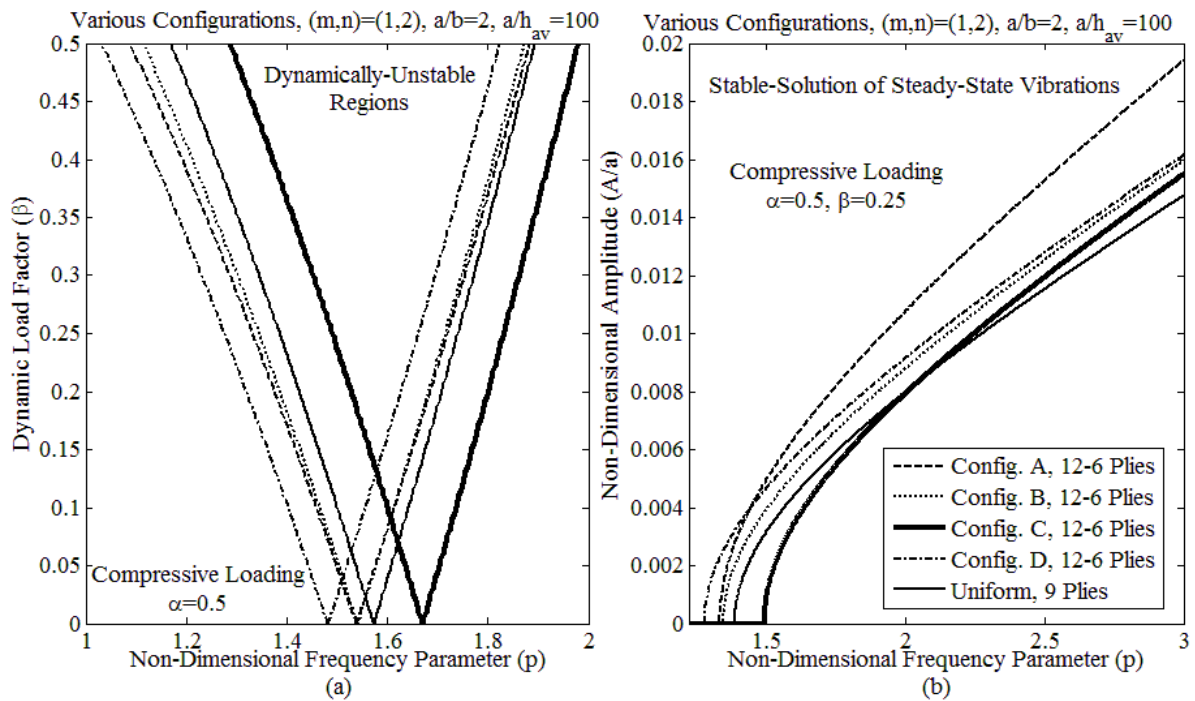
Figure 3.15 Effects of various taper configurations, on the second mode a) unstable region and b) stable-solution amplitude of steady-state vibrations of a 12-6 layered symmetric cross-ply laminated rectangular thickness-tapered plate subjected to the compressive periodic in-plane loading

(1,1) and mode (1,2), under tensile in-plane pulsating load having static load factor of $\alpha = 0.5$. From here onwards in all of the figures the amplitudes of the steady-state vibrations are plotted for the loading conditions having dynamic load factor of $\beta = 0.25$. The corresponding graphs for the compressive loading are represented in Fig. 3.14 and Fig. 3.15 respectively. It is also worthwhile to note here that in the tensile loading case we consider the absolute value of critical buckling load $|N_{cr}|$ for both static and dynamic components of the in-plane harmonically-pulsating load, while in the compressive case we use the actual value of critical buckling load N_{cr} which is negative with respect to the assigned coordinate system shown in Fig. 3.1. In the comparative study of various configurations, the applied in-plane harmonically pulsating load for all configurations and the uniform plate is based on the critical buckling load of the configuration A. Here and in the following figures and tables, the dimensionless excitation frequency parameter p is introduced as follow:

$$p = Pa\sqrt{\frac{\rho_c}{E_2}} \qquad\qquad (3.48)$$

where ρ_c is the mass density of the composite plies. It is observed that thickness-tapered composite plate having configuration C, has the highest frequency of excitation or in other words the most-shifted to the right along the frequency axis of both dynamically-unstable regions and amplitudes of steady-state vibrations among the other configurations. So consequently, it has the lowest amplitudes of steady-state vibrations at any specific excitation frequency. To provide a more detailed and a better comparison the corresponding results for the first-two modes of dynamically-unstable regions also are listed in Tables 3.2 and 3.3 corresponding to tensile and compressive in-plane loadings respectively. To compare the results in these and the following tables we specified each unstable region by the non-dimensional frequency parameter p of the point of origin and the half angle of the unstable region as δ. It is also observed from these figures and tables that configuration C has the smallest δ i.e. smallest width of the instability regions. All of these observations are confirmed

89

Table 3.2 Effects of various taper configurations on the first-two modes of the dynamically-unstable regions of a 12-6 layered symmetric cross-ply laminated rectangular thickness-tapered plate subjected to the tensile periodic in-plane loading

Taper Configuration	Mode (1,1) of Dynamically-Unstable Region		Mode (1,2) of Dynamically-Unstable Region	
	Point of origin p ($\times 10^{-1}$)	δ ($\times 10^{-1}$)	Point of origin p ($\times 10^{-1}$)	δ ($\times 10^{-1}$)
A (12-6 Plies)	7.273486753	1.160318234	26.63182834	4.033661837
B (12-6 Plies)	7.170241789	1.127398507	26.26533989	3.928456527
C (12-6 Plies)	7.354430072	1.101373713	27.04124281	3.833745441
D (12-6 Plies)	7.051689571	1.144781922	25.92035233	3.971943926
Uniform (9 Plies)	7.134012328	1.109899102	26.27473998	3.855409063

Table 3.3 Effects of various taper configurations on the first-two modes of the dynamically-unstable regions of a 12-6 layered symmetric cross-ply laminated rectangular thickness-tapered plate subjected to the compressive periodic in-plane loading

Taper Configuration	Mode (1,1) of Dynamically-Unstable Region		Mode (1,2) of Dynamically-Unstable Region	
	Point of origin p ($\times 10^{-1}$)	δ ($\times 10^{-1}$)	Point of origin p ($\times 10^{-1}$)	δ ($\times 10^{-1}$)
A (12-6 Plies)	4.199349535	1.865614554	15.37589326	6.047485315
B (12-6 Plies)	4.202132441	1.793216102	15.40576975	5.854713696
C (12-6 Plies)	4.509234017	1.693038991	16.69426471	5.550619329
D (12-6 Plies)	3.996482897	1.86644874	14.80994015	6.004155401
Uniform (9 Plies)	4.224835457	1.751863448	15.7271826	5.687899224

even when changing the mode from the mode (1,1) to the mode (1,2) or loading directions from tensile to compressive. Hence, configuration C shows the most rigidity among all configurations and this can be expected since in this configuration the resin pockets are located very close to mid-plane of the plate and therefore its bending stiffnesses are less decreased due to the smaller bending stiffnesses of the resin pocket in comparison to the composite plies. It is also noted that although the amplitudes of steady-state vibrations of the configuration C in the initial stages of the excitation is lower than that of the uniform laminate, this trend is changed at the higher excitation frequencies that can be due to the existence of the resin pocket in configuration C while there isn't any such resin pocket in uniform plate. Due to the less mass density of the resin (epoxy) to the graphite composite plies, overall it makes that the uniform plate be heavier than the thickness-tapered laminates or particularly here the thickness-tapered having configuration C (the total mass of plates having configuration A, B, C, D and the uniform plate with the same length-to-average-thickness ratio i.e. $a/h_{av} = 100$ and length-to-

width ratio of $a/b = 2$ are 13.28, 13.88, 13.88, 13.88 and 14.18 grams, respectively. However it should be noted here that for the same size of uniform plate with 12 plies the total mass would be 18.91 grams.). So to summarize these, increasing the stiffnesses makes the instability regions or excitation to start at higher frequencies but the same time reducing the weight of the structures causes the speed of increasing of the amplitudes of steady-state vibrations be increased. However, as can be observed from these figures the increase of the amplitudes at those higher excitation frequencies are very small to compared amplitudes of the uniform laminate. Therefore it is concluded that configuration C is the most stable laminated plate under parametric excitation among all taper configurations and even uniform laminate. Another observation from these figures and tables reveal that since configuration D has the lowest stiffness due to the location of the resin pockets far from the mid-plane, its dynamically-unstable regions or the parametric excitations start at the lowest frequencies. But since configuration A has the lowest total weight due to the largest amount of the resin pockets in this configuration, its amplitudes of steady-state vibrations are increased much faster than any other configuration and consequently reach the highest amplitudes of steady-state vibrations at higher frequencies.

Figures 3.16 and 3.17 show the effects of the amplitudes of the tensile and compressive in-plane harmonically pulsating load on the dynamically-unstable regions (Figs. 3.16a and 3.17a) and the stable-solution amplitudes of the steady-state vibrations (Figs. 3.16b and 3.17b), respectively. Here the graphs are plotted for thickness-tapered laminated plate with configuration C having 40 and 10 plies at the thickest and the thinnest sides, respectively. Therefore according to the Eq. (3.17) this reduction of the plies from 40- to 10-plies are performed in 15 steps. The depicted graphs are for three different loading amplitudes having static load factors of $\alpha = 0.1$, $\alpha = 0.3$ and $\alpha = 0.5$ respectively. In all of these three cases of loadings for both the tensile and compressive load conditions the thickness-tapered

laminated plate has aspect and thickness ratios of $a/b = 2$ and $a/h_{av} = 50$ respectively, and also the graphs has been depicted for the first mode i.e. the mode (1,1). From Fig.16 it can be realized that increasing the magnitude of the tensile in-plane loading results in shifting the instability regions to the higher frequencies along the frequency axis (Fig. 3.16a), and consequently decreasing the stable-solution amplitudes of steady-state vibrations (Fig. 3.16b) and also decreasing very slightly the widths of dynamically-unstable regions (Fig. 3.16a). However increasing the magnitude of the compressive in-plane loading results in shifting the instability regions to the lower frequencies along the frequency axis (Fig. 3.17a), and consequently increasing the stable-solution amplitudes of the steady-state vibrations (Fig.3.17b) and also increasing the widths of dynamically-unstable regions (Fig. 3.17a). These
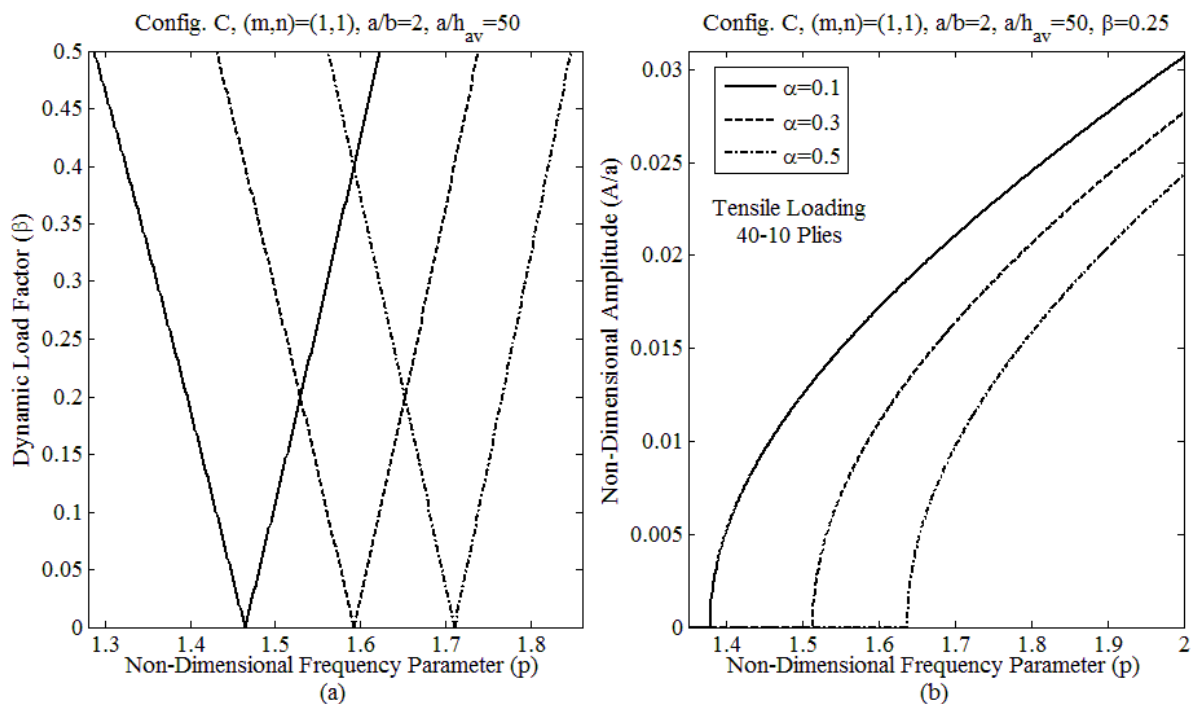
Figure 3.16 Effects of the amplitude of tensile in-plane harmonically pulsating loads, on the first mode a) unstable region and b) stable-solution amplitude of steady-state vibrations of a 40-10 layered symmetric cross-ply laminated thickness-tapered plate having configuration C
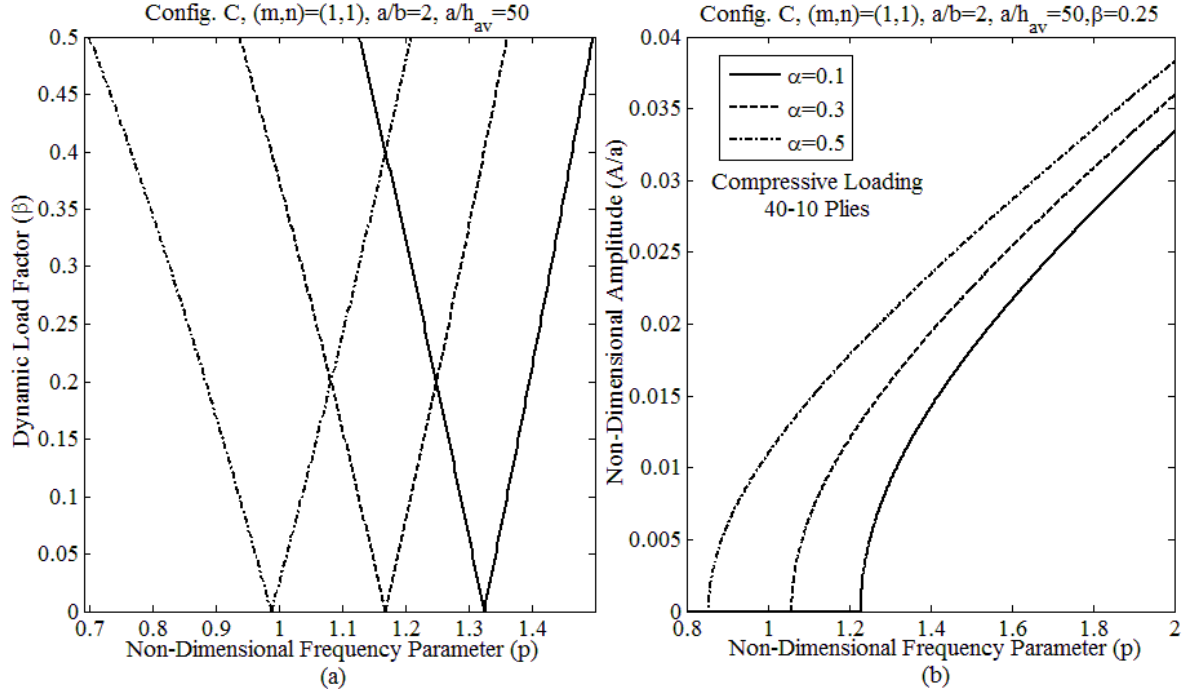
Figure 3.17 Effects of the amplitude of compressive in-plane harmonically pulsating loads, on the first mode a) unstable region and b) stable-solution amplitude of steady-state vibrations of a 40-10 layered symmetric cross-ply laminated thickness-tapered plate having configuration C

outcomes can be expected because increasing the tensile in-plane load makes the plate to be stiffer, and contrarily increasing the compressive in-plane load results in decreasing the plate's stiffness.

One of the most important parameters in the design of thickness-tapered plates is the taper angle ϕ. In the very few works on the mechanical and structural behavior of thickness-tapered plates, most of the researchers in order to investigate the effect of this parameter decreased the length of the thickness-tapered plate [29, 31]. Although it is clear that decreasing the length of the plate and keeping the thickness of the thickness-tapered plate unchanged, overall the length-thickness ratio is changed while this ratio is also another important parameter for both uniform and thickness-tapered plates that should be investigated independently. Here to avoid this interference of these two important parameters we introduce the following formulation which only changes the taper angles by keeping the length-to-average-thickness ratio as constant:

$$\phi = \tan^{-1}((N_L - N_R)/((a/h_{av})(N_L + N_R)))$$
(3.49)

93

Hence by keeping the a/h_{av} ratio as constant in this equation and changing the number of plies at the thickest (here the left) and the thinnest (here the right) sides of the thickness-tapered plate respectively, the taper angle is changed without changing the length-thickness ratio. Variation of both the length a and the thickness h do not influence the response of the structure if the overall length-thickness ratio remains unchanged. Here to study the effect of taper angle we keep the number of plies at the thickest side of the taperd plate $N_L = 40$ for all cases and by decresing the number of plies at the thinnest side of the taperd plate i.e. N_R while we keep the length-to-average-thickness ratio as constant as $a/h_{av} = 50$ in Figures 18 and 20 and Tables 3.4 and 3.6 or $a/h_{av} = 10$ in Figures 3.19 and 3.21 and Tables 3.5 and 3.7, the taper angle is increased. In addition, as it can be seen from Eq. (3.49) the taper angle also is increased by
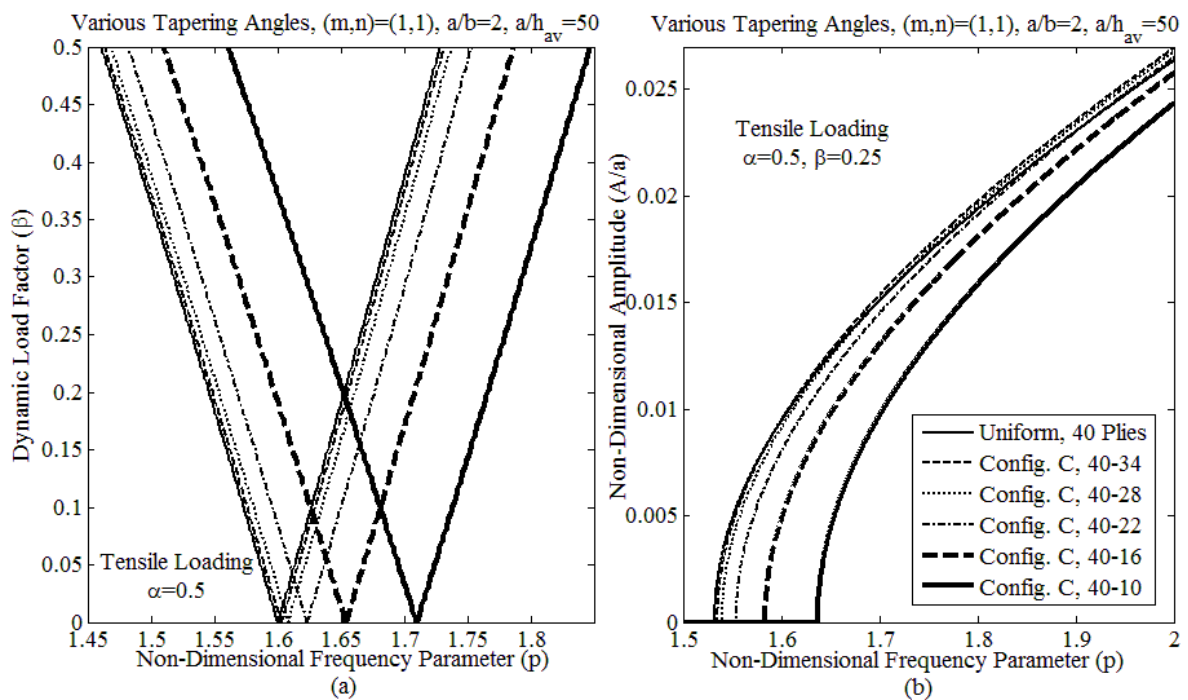
Figure 3.18 Effects of the taper angle on the first mode a) unstable region and b) stable-solution amplitude of steady-state vibrations of symmetric cross-ply laminated thickness-tapered plates having configuration C, aspect ratios of $a/b = 2$ and $a/h_{av} = 50$ subjected to the tensile periodic in-plane loading
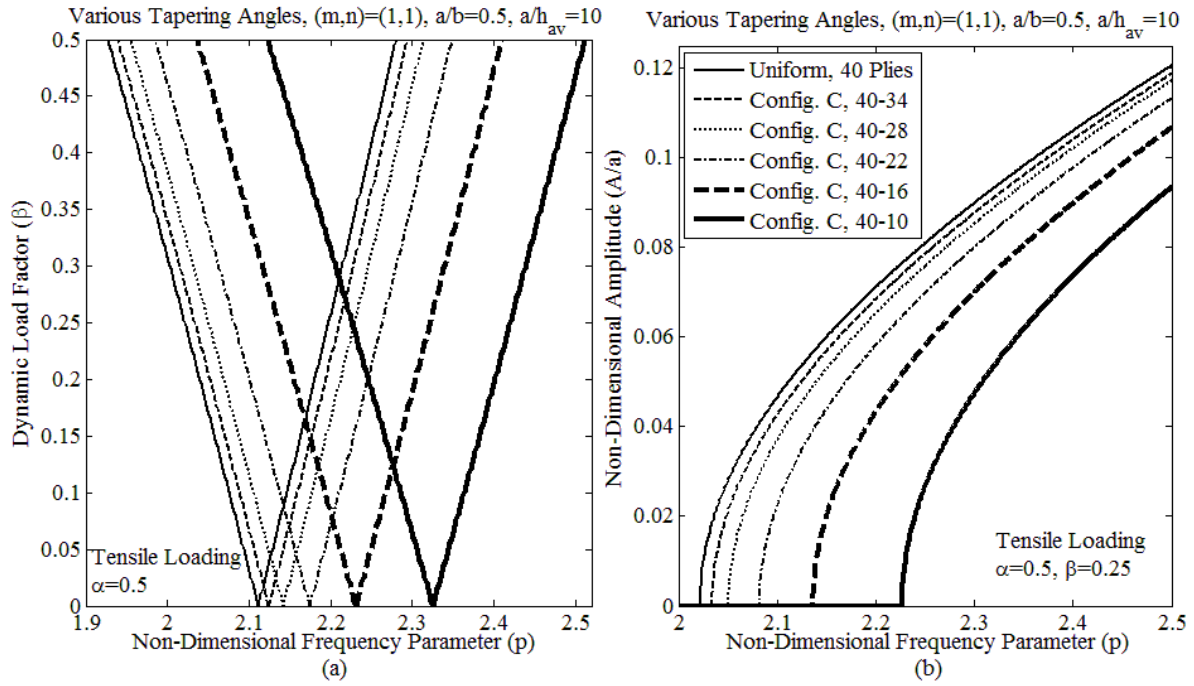
Figure 3.19 Effects of the taper angle on the first mode a) unstable region and b) stable-solution amplitude of steady-state vibrations of symmetric cross-ply laminated thickness-tapered plates having configuration C, aspect ratios of $a/b = 0.5$ and $a/h_{av} = 10$ subjected to the tensile periodic in-plane loading
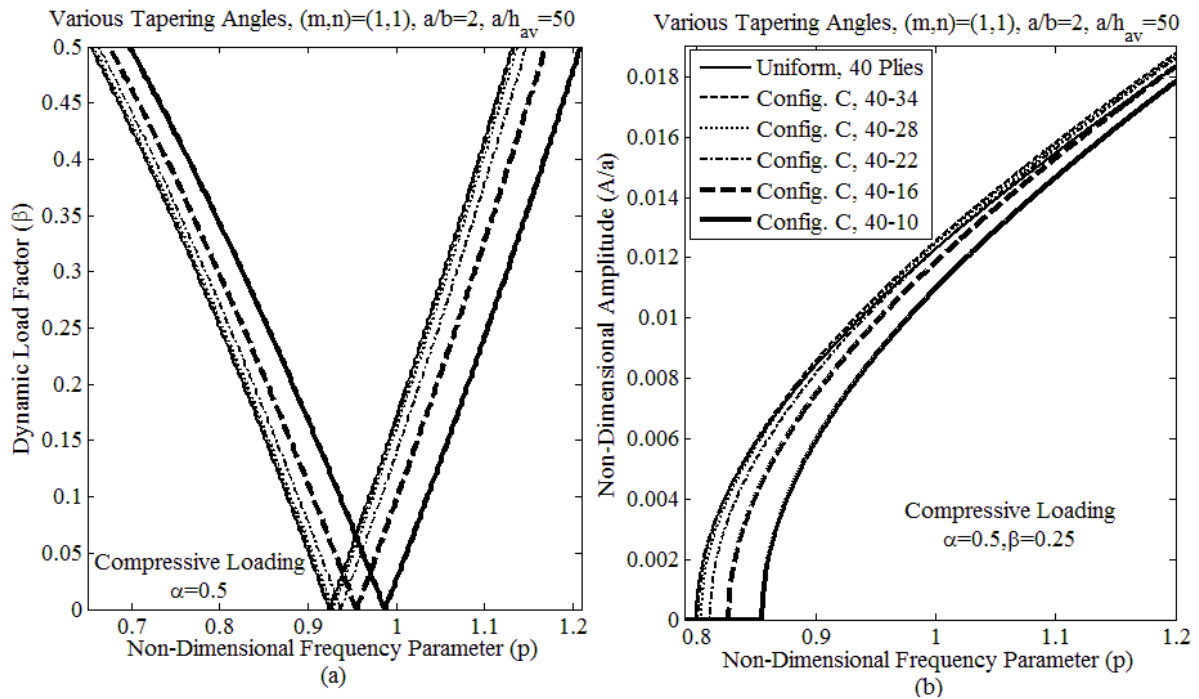
Figure 3.20 Effects of the taper angle on the first mode a) unstable region and b) stable-solution amplitude of steady-state vibrations of symmetric cross-ply laminated thickness-tapered plate having configuration C, aspect ratios of $a/b = 2$ and $a/h_{av} = 50$ subjected to the compressive periodic in-plane loading
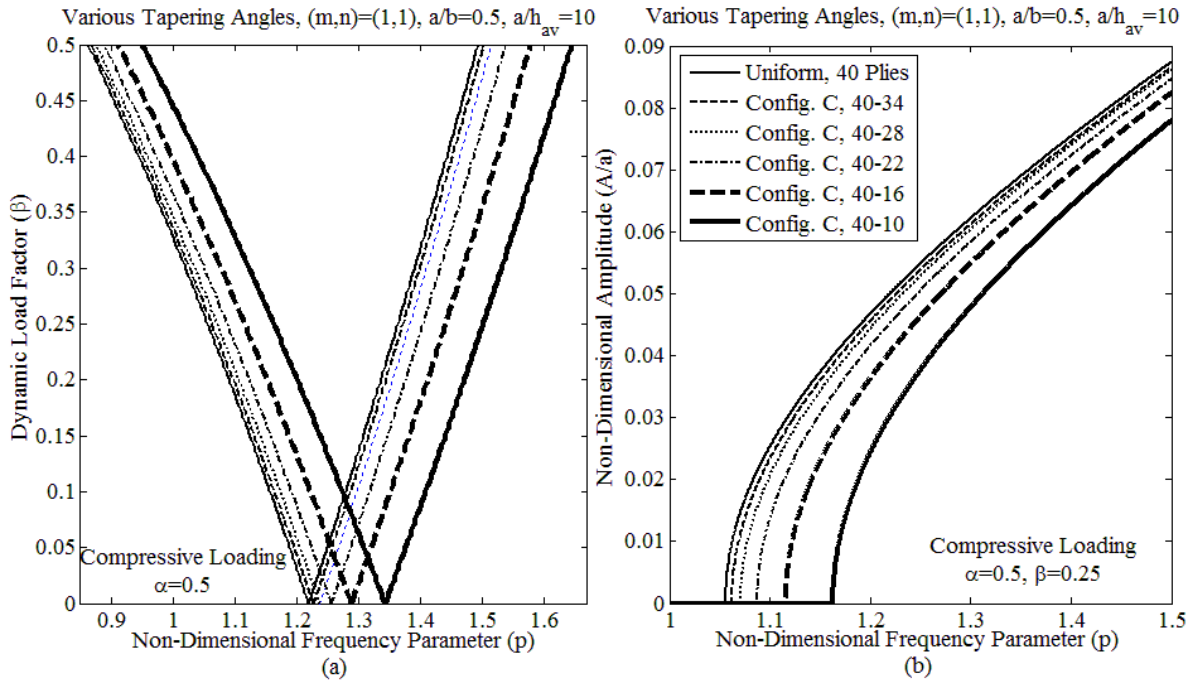
Figure 3.21 Effects of the taper angle on the first mode a) unstable region and b) stable-solution amplitude of steady-state vibrations of symmetric cross-ply laminated thickness-tapered plate having configuration C, aspect ratios of $a/b = 0.5$ and $a/h_{av} = 10$ subjected to the compressive periodic in-plane loading

decreasing the length-to-average-thickness ratio i.e. a/h_{av} therefore the reults are presented in these firgures and tables for $a/h_{av} = 50$ and $a/h_{av} = 10$ respectively. It is also noted here that by knowing the number of plies at the thickest and the thinnest sides and also the ply thickness h_p, the h_{av} of the thickness-tapered plate can be obtained. Then considering the length of the plate either $a = 50h_{av}$ or $a = 10h_{av}$, the length of the plate is also determined. The effects of the taper angle on both dynamically-unstable regions and the stable-solution amplitudes of steady-state vibartions are shown in Figures 3.18-3.21 that correspond to the tensile and compressive in-plane periodic loadings, respectivly.

taperd laminated plate from 40 plies, which also correponds to the number of plies in the uniform plate, to 10 plies, the corresponding taper angle is increased from zero to $0.6875°$ in the plates having $a/h_{av} = 50$ and from zero to $3.434°$ in the plates having $a/h_{av} = 10$. Although we consider the static load factor $\alpha = 0.5$ for all these six taper ratios i.e. 40-40, 40-34, 40-28, 40-22, 40-16 and 40-10 plies, it should be noted that corresponding dimensionless

critical bucklig loads, i.e. $(N_{cr})_{ND}$, which is $N_{cr}a^2/E_1 h_{av}{}^3$, are also increased. Both tensile (Figs. 3.18 and 3.19 and Tables 3.4 and 3.5) and compressive (Figs. 3.20 and 3.21 and Tables 3.6 and 3.7) loading confirm that increasing the taper angle causes shifting the dynamically-unstable regions to the higher frequencies along the frequency axis (Figs. 3.18a-3.21a, Tables 3.4-3.7), and consequently decreasing the stable-solution amplitudes of the steady-state vibrations (Figs. 3.18b- 3.21b) and also decreasing very slightly the widths of dynamically-unstable regions (Figs. 3.18a-3.21a, Tables 3.4-3.7). This is due to the fact that increasing taper angles results in higher stiffness of the plate. Another important outcome of these figures and tables is that these variations of dynamic instability response, highly deviate from thickness-tapered plate having 40-10 to 40-16 and 40-22 plies but it shows the convergence of the response of the thickness-tapered plates having 40-28 plies and 40-34 plies with the uniform laminated plate having 40 plies.

Figure 3.22 shows the variation of the both extension- and bending-stiffnesses ratios of the left (thick) side to the right (thin) side of symmetric cross-ply laminated thickness-tapered plate having configuration C with the taper ratio (N_L/N_R). The results also are listed in Table 3.8. As it has been mentioned been mentioned in section 2 (Formulation) of this work in the thickness-tapered laminates the extension- and bending-stiffnesses are linear and cubic functions of x-coordinate respectively. So these stiffnesses are maximum in the left (thickest) side and minimum in the right (thinnest) side. However increasing the taper angle by varying $a/h_{av} = 50$ to $a/h_{av} = 10$ only the speed of reaching from that maximum to minimum will accelerate without changing those maximum and minimum values of stifnesses from the thickest to the thinnest side at any specific N_L and N_R. As it is clear from this figure and table the extension-stiffnesses ratio vs N_L/N_R has almost linear distribution and increased linearly from $N_L/N_R = 34/40$ to $N_L/N_R = 10/40$ that all of those stiffness ratios are less than 4.4.
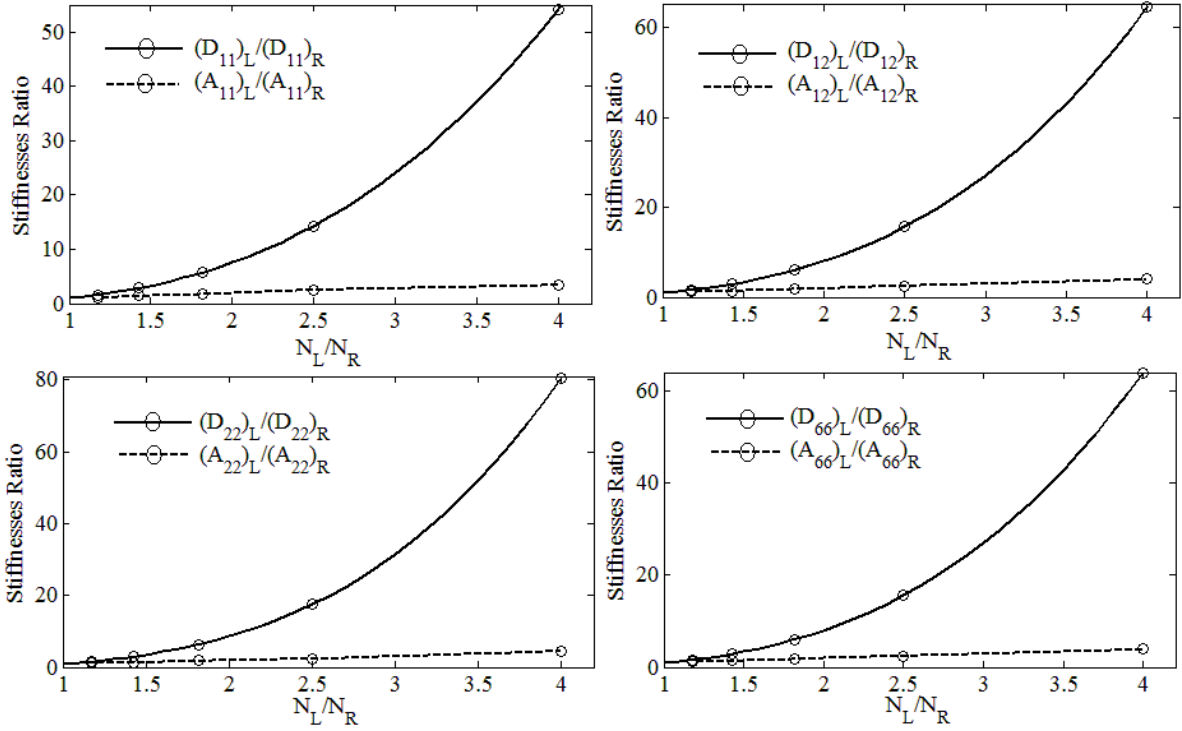
Figure 3.22 Variation of the both extension- and bending-stiffnesses ratios of the left (thick) side to the right (thin) side of symmetric cross-ply laminated thickness-tapered plate having configuration C with the taper ratio (N_L/N_R)

However the bending-stiffnesses ratio vs N_L/N_R has cubic distribution and increased non-linearly from $N_L/N_R = 34/40$ to $N_L/N_R = 10/40$ that those stiffness ratio are increased up to 80.5. On the other hand instability of structures either statically or dynamically are actually bending deflections rather than extensional deflections. So as also mentioned before we can take the average of extension-stiffnesses to solving the in-plane displacements i.e. $u_0(x, y, t)$ and $v_0(x, y, t)$ in terms of transverse displacement $w_0(x, y, t)$ in the displacement form of Eqs. (3.2 and 3.3) and further Eqs. (3.22-a and b). To examin the effect of aspect ratio b/a (as the ratio of the width of loaded edge to the width of unloaded edge) on the dynamic instability of thickness-tapered plate the graphs are presented in Figs. 3.23 and 3.24 corresponding to the tensile and compressive periodic in-plane loadings, respectively. Here a is kept constant and b is varied and the length-to-average-thickness ratio is $a/h_{av} = 50$.

Table 3.4 Effects of the taper angle on the first mode of dynamically-unstable region of symmetric cross-ply laminated thickness-tapered plate having configuration C, aspect ratios of $a/b = 2$ and $a/h_{av} = 50$ subjected to the tensile periodic in-plane loading

Plate Configuration	Tap. Angle ϕ^o ($\times 10^{-1}$)	$(N_{cr})_{ND}$	Point of origin p ($\times 10^{-1}$)	δ ($\times 10^{-1}$)
Uniform (40 Plies)	0.00000	-7.57787	16.00123	2.51007
C (40-34 Plies)	0.92912	-7.56606	16.02980	2.51436
C (40-28 Plies)	2.02220	-7.61167	16.08169	2.52216
C (40-22 Plies)	3.32681	-7.75019	16.23175	2.54470
C (40-16 Plies)	4.91095	-8.04095	16.53886	2.59074
C (40-10 Plies)	6.87516	-8.58747	17.09866	2.67437

* Non-dimensional critical buckling load, $(N_{cr})_{ND} = (N_{cr}a^2)/(E_1 h_{av}^3)$

Table 3.5 Effects of the taper angle on the first mode of dynamically-unstable region of symmetric cross-ply laminated thickness-tapered plate having configuration C, aspect ratios of $a/b = 0.5$ and $a/h_{av} = 10$ subjected to the tensile periodic in-plane loading

Plate Configuration	Tap. Angle ϕ^o ($\times 10^{-1}$)	$(N_{cr})_{ND}$	Point of origin p ($\times 10^{-1}$)	δ ($\times 10^{-1}$)
Uniform (40 Plies)	0.00000	-0.52769	21.11247	3.26233
C (40-34 Plies)	4.64550	-0.53144	21.24169	3.28089
C (40-28 Plies)	10.10997	-0.54003	21.41759	3.30613
C (40-22 Plies)	16.62959	-0.55632	21.74416	3.35287
C (40-16 Plies)	24.54032	-0.58521	22.30880	3.43333
C (40-10 Plies)	34.33630	-0.63529	23.25326	3.56688

* Non-dimensional critical buckling load, $(N_{cr})_{ND} = (N_{cr}a^2)/(E_1 h_{av}^3)$

Table 3.6 Effects of the taper angle on the first mode of dynamically-unstable region of symmetric cross-ply laminated thickness-tapered plate having configuration C, aspect ratios of $a/b = 2$ and $a/h_{av} = 50$ subjected to the compressive loading

Plate Configuration	Tap. Angle ϕ^o ($\times 10^{-1}$)	$(N_{cr})_{ND}$	Point of origin p ($\times 10^{-1}$)	δ ($\times 10^{-1}$)
Uniform (40 Plies)	0.00000	-7.57787	9.23832	3.93586
C (40-34 Plies)	0.92912	-7.56606	9.25481	3.94218
C (40-28 Plies)	2.02220	-7.61167	9.28477	3.95365
C (40-22 Plies)	3.32681	-7.75019	9.37140	3.98677
C (40-16 Plies)	4.91095	-8.04095	9.54872	4.05427
C (40-10 Plies)	6.87516	-8.58747	9.87191	4.17630

* Non-dimensional critical buckling load, $(N_{cr})_{ND} = (N_{cr}a^2)/(E_1 h_{av}^3)$

Table 3.7 Effects of the taper angle on the first mode of dynamically-unstable region of symmetric cross-ply laminated thickness-tapered plate having configuration C, aspect ratios of $a/b = 0.5$ and $a/h_{av} = 10$ subjected to the compressive loading

Plate Configuration	Tap. Angle ϕ^o ($\times 10^{-1}$)	$(N_{cr})_{ND}$	Point of origin p ($\times 10^{-1}$)	δ ($\times 10^{-1}$)
Uniform (40 Plies)	0.00000	-0.52769	12.18929	5.01227
C (40-34 Plies)	4.64550	-0.53144	12.26390	5.03802
C (40-28 Plies)	10.10997	-0.54003	12.36545	5.07296
C (40-22 Plies)	16.62959	-0.55632	12.55399	5.13748
C (40-16 Plies)	24.54032	-0.58521	12.87999	5.24792
C (40-10 Plies)	34.33630	-0.63529	13.42528	5.42954

* Non-dimensional critical buckling load, $(N_{cr})_{ND} = (N_{cr}a^2)/(E_1 h_{av}^3)$

Table 3.8 Variation of the both extension- and bending-stiffnesses ratios of the left (thick) side to the right (thin) side of symmetric cross-ply laminated thickness-tapered plate having configuration C with the taper ratio (N_L/N_R)

stiffnesses ratios	40-34 Plies	40-28 Plies	40-22 Plies	40-16 Plies	40-10 Plies
$(A_{11})_L/(A_{11})_R$	1.12	1.42	1.68	2.49	3.40
$(A_{12})_L/(A_{12})_R$	1.16	1.41	1.80	2.47	3.98
$(A_{22})_L/(A_{22})_R$	1.13	1.30	1.80	2.28	4.41
$(A_{66})_L/(A_{66})_R$	1.14	1.39	1.77	2.43	3.89
$(D_{11})_L/(D_{11})_R$	1.61	2.84	5.73	14.31	54.23
$(D_{12})_L/(D_{12})_R$	1.63	2.92	6.01	15.66	64.50
$(D_{22})_L/(D_{22})_R$	1.65	3.00	6.37	17.45	80.53
$(D_{66})_L/(D_{66})_R$	1.63	2.92	6.01	15.62	64.00

Again we keep the static load factor $\alpha = 0.5$ for all these six aspect ratios i.e., $b/a = 2, 1, 2/3, 0.5, 2/5$ and $1/3$. It should be noted that the corresponding dimensionless critical bucklig loads are increased by decreasing the width-to-length ratio. The graphs indicate that with a decrease in width of the plate, i.e. overall decrease in aspect ratio of b/a, the thickness-tapered plate's stiffness is increased as well, hence the dynamically-unstable regions shift to the right along the frequency axis having higher frequencies of excitations of points of origins (Figs. 3.23a and 3.24a), and consequently the amplitudes of steady-state vibrations at any specific frequency are decreased (Figs. 3.23b and 3.24b) and further, the widths of instability regions are also increased (Figs. 3.23a and 3.24a). It is noticed that increase in the widths of instability regions are more influenced by the compressive loading (Fig. 3.24a) than the tensile loading (Fig. 3.23a). However the points of origins of dynamically-unstable regions are more influenced by the tensile loading (Fig. 3.23a) than the compressive loading (Fig. 3.24a). These are in full agreement qualitatively with the corresponding study of Ramachandra and Panda [11] for dynamically-unstable regions of uniform laminated plates. In order to investigate the effect of the variation of the length-to-average-thickness ratio, a/h_{av}, on the instability regions and the stable-solution amplitudes of steady-state vibrations, as it has been mentioned above since the taper angle and length-thickness ratio are influenced by each other, here to avoid this interference of these two important parameters we keep the length a of the thickness-
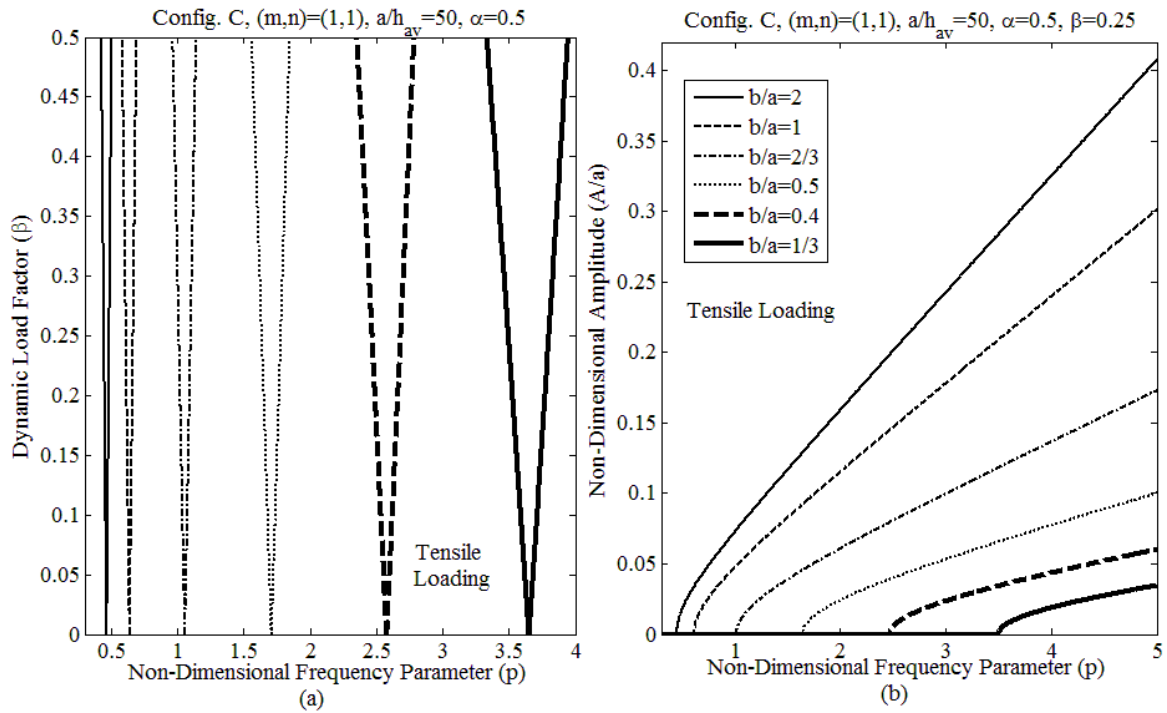
Figure 3.23 Effects of the variation of the length-to-width ratio, on the first mode a) unstable region and b) stable-solution amplitude of steady-state vibrations of 40-10 layered symmetric cross-ply laminated thickness-tapered plate having configuration C and $a/h_{av} = 50$ subjected to the tensile periodic in-plane loading
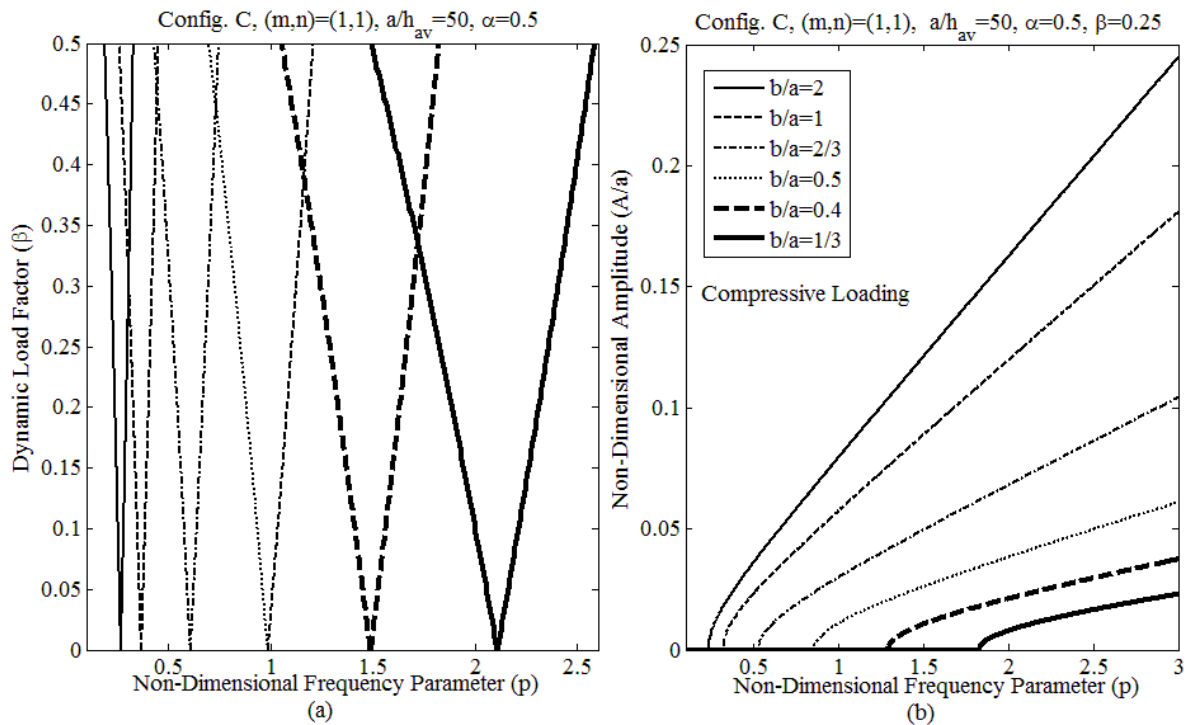
Figure 3.24 Effects of the variation of the length-to-width ratio, on the first mode a) unstable region and b) stable-solution amplitude of steady-state vibrations of 40-10 layered symmetric cross-ply laminated thickness-tapered plate having configuration C and $a/h_{av} = 50$ subjected to the compressive periodic in-plane loading
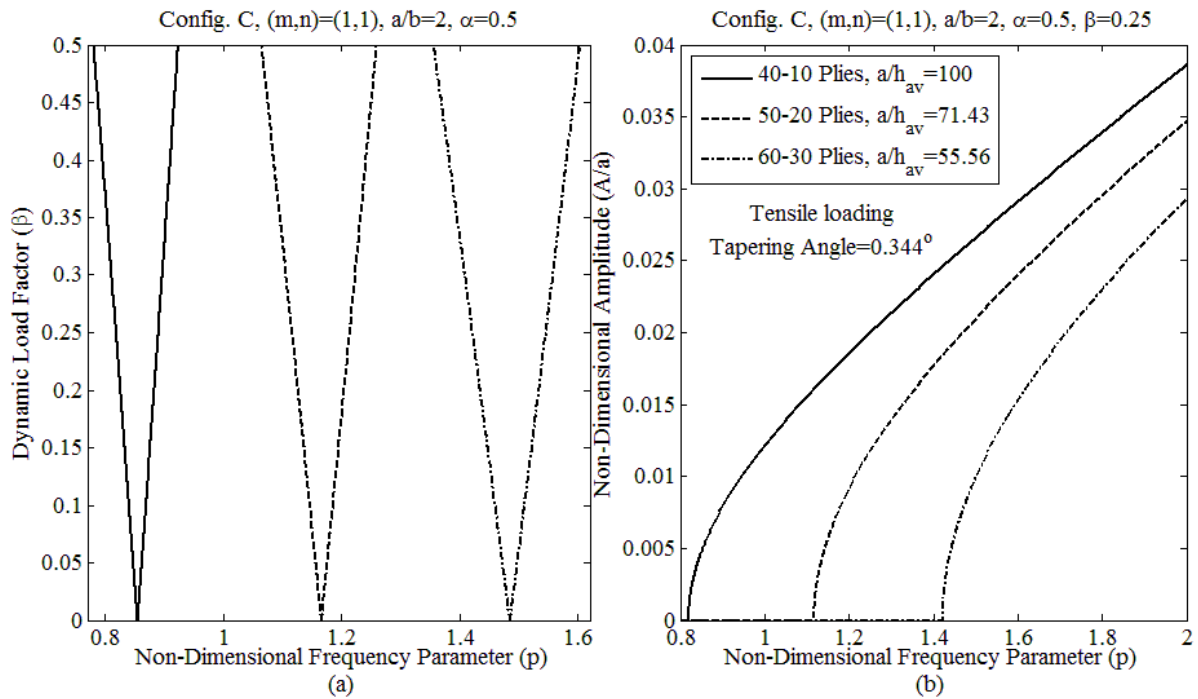
Figure 3.25 Effects of the variation of the length-to-average-thickness ratio on the first mode a) unstable region and b) stable-solution amplitude of steady-state vibrations of 40-10 layered symmetric cross-ply laminated thickness-tapered plate having configuration C and aspect ratios of $a/b = 0.5$ subjected to the tensile periodic in-plane loading
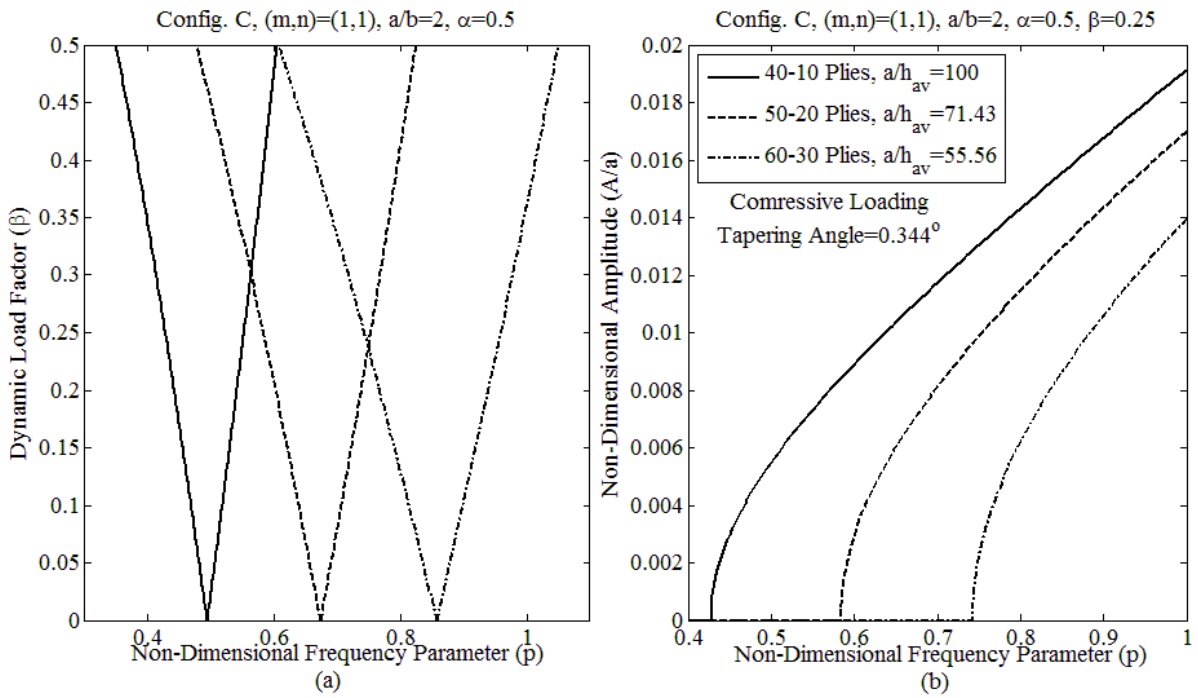
Figure 3.26 Effects of the variation of the length-to-average-thickness ratio, on the first mode a) unstable region and b) stable-solution amplitude of steady-state vibrations of 40-10 layered symmetric cross-ply laminated thickness-tapered plate having configuration C and aspect ratios of $a/b = 0.5$ subjected to the compressive periodic in-plane loading

102

tapered plate constant and change the length-to-average-thickness ratio by increasing the number of plies. Figures 3.25 and 3.26 present a graphical illustration of the effect of length-to-average-thickness ratio on dynamic instability of thickness-tapered plate with configuration C having three different numbers of plies i.e. 40-10 plies, 50-20 plies and 60-30 plies. The taper angle for all these three different thickness-tapered plates remains constant as $\phi = 0.344^{\circ}$. The length-to-width ratio $a/b = 2$ and the static load factor $\alpha = 0.5$ for all these three diferent thickness ratios i.e., $a/h_{av} = 100, 71.43 \ and \ 55.56$ corresponding to the 40-10 plies, 50-20 plies and 60-30 plies, respectively. It is confirmed that in both tensile (Fig. 3.25) and compressive (Fig. 3.26) loading conditions with increasing the number of plies, i.e. with decreasing the length-to-average-thickness ratio a/h_{av} , the dynamically-unstable regions (Figs. 3.25a and 3.26a) shift to the right along the frequency axis having higher excitation frequencies, and consequently decreasing the stable-solution amplitudes of steady-state vibrations (Figs. 3.25b and 3.26b) and also increasing the widths of dynamically-unstable regions (Figs 25a and 26a). It should be noted here again that increase in the widths of instability regions is more influenced by the compressive loading (Fig. 3.26a) than the tensile loading (Fig. 3.25a). However the points of origins of dynamically-unstable regions are more influenced by the tensile loading (Fig. 3.25a) than the compressive loading (Fig. 3.26a). These outcomes are also due to the fact that increasing the thickness of plate makes the plate stiffer.

3.7   Conclusions

When the plate is subjected to periodically-varying in-plane loading, the parametric instability can occur, and the nature of this instability is flutter. Here the non-linear vibration and dynamic instability of thickness-tapered laminated composite plates under parametric in-plane excitation have been studied. The non-linear von Karman strains associated with large deflections are considered. The in-plane displacements are determined from the force-equilibrium equations of motion in the x and y direction of non-linear large deflection

thickness-tapered plate. Consequently, the in-plane force-resultants are obtained from the in-plane displacements and further applying the boundary conditions. Then the general Galerkin method is used for the moment-equilibrium equation of motion to satisfy the spatial dependence in the partial differential equation of motion and to produce a set of non-linear Mathieu-Hill equations. These equations are ordinary differential equations with time-dependency. Applying Bolotin's method to these set of equations, the dynamically-unstable regions and both stable-, and unstable-solutions amplitudes of the steady-state vibrations are obtained. It was confirmed that instability regions, stable-, and unstable-solutions amplitudes of steady-state vibrations are significantly influenced by taper configurations, taper angles, magnitudes of both tensile and compressive in-plane loads, aspect ratios of the thickness-tapered plate including length-to-width and length-to-thickness ratios and particularly here length-to-average-thickness ratio. Hence in any particular application specific considerations of all these important parameters should be taken into account in the design of thickness-tapered composite plates. A comparative study of the present work with those available in literature shows a very good agreement. However, as the results of the present study reveal, the linear analysis carried out in available literature can only provide the information about the instability region and is unable to predict the vibration amplitudes in these regions. The non-linear analysis developed in the present work can determine such vibration amplitudes. The present work has shown that there is vibration with steady-state amplitude in the instability region which approaches almost constant amplitude when the excitation frequencies are increased. Hence, for more perfect and complete studies of dynamic instability of laminated plates, the non-linear analysis is required to determine both the stable and unstable amplitudes of steady-state vibrations in addition to instability regions. Where the occurrence of dynamic instability is inevitable, in order to have a control on vibration amplitudes in the unstable regions non-linear analysis is required. By adjusting the corresponding effective parameters as

explained in the present work, design criteria based on and in terms of the steady-state vibrations with allowable amplitudes in the dynamically-unstable regions can be established for thickness-tapered composite plates in practice.

The major outcomes of the present study are summarized as follow:

- Both dynamically-unstable regions and corresponding amplitudes of the steady-state vibrations are significantly influenced by taper configurations. The results show that configuration C is the most stable thickness-tapered plate under parametric excitation among all the thickness-tapered configurations i.e. configurations A, B, C and D, and also the uniform-thickness laminate having the thickness equal in value to the average thickness of the corresponding thickness-tapered plate. Overall, tapering the plate makes the plate's stiffness to be increased although its total weight might be decreased due to the existence of resin pockets. Increasing the stiffness of the thickness-tapered plate results in the shifting of the dynamically-unstable regions toward higher frequencies and consequently decreasing both stable- and unstable-solutions amplitudes of the steady-state vibrations and also decreasing the widths of these regions. Although reducing the total weight of the thickness-tapered structures causes the rate of increase of the amplitudes of the steady-state vibrations be increased. Hence in comparison to the uniform plate, although the thickness-tapered plate with configuration C has the amplitude of steady-state vibrations lower than the uniform laminate in the initial stages of the excitation, by increasing the excitation frequencies this trend is changed; Influenced by the lower total weight of the thickness-tapered plate (configuration C) at the higher level of the excitation frequencies, the steady-state vibration amplitude is very slightly increased from the steady-state vibration amplitude of the uniform plate.

- The other most important parameter in the design of thickness-tapered plates is the taper angle. The higher the taper angle is, the higher the excitation frequencies corresponding to the dynamically-unstable regions are, and consequently the lower is the amplitude of the steady-

state vibrations. Also the widths of dynamically-unstable regions decrease very slightly for higher values of taper angles. This is due to the fact that increasing the taper angle results in higher stiffness of the plate. The variation of dynamic instability response of thickness-tapered plate from that of the uniform plate is very smooth for smaller taper angles but the rates of the deviations are high for increasing values of taper angle.

- Increasing the amplitude of the tensile in-plane harmonically-pulsating load results in the shifting of the instability regions to higher frequencies along the frequency axis, and consequently decreasing the amplitudes of the steady-state vibrations and also decreasing very slightly the widths of the dynamically-unstable regions. However, increasing the amplitude of the compressive in-plane load results in the shifting of the instability regions to lower frequencies along the frequency axis, and consequently increasing the amplitudes of the steady-state vibrations and also increasing the widths of the dynamically-unstable regions. These outcomes can be expected because increasing the tensile in-plane load makes the plate to be stiffer, and contrarily increasing the compressive in-plane load results in decreasing the plate's stiffness.

- The results indicate that with a decrease in width b, i.e. overall decrease in aspect ratio b/a, the thickness-tapered plate's stiffness is increased as well, hence the dynamically-unstable regions shift to the right along the frequency axis having higher frequencies of excitation, and consequently decreasing the amplitudes of steady-state vibrations and further, the widths of instability regions are also increased. It is also noticed that increase in the widths of instability regions is more influenced by the compressive loading than the tensile loading. However, the points of origins of dynamically-unstable regions are more influenced by the tensile loading than the compressive loading.

- It is confirmed that in both tensile and compressive loading conditions with increasing the number of plies, i.e. with decreasing the length-to-average-thickness ratio a/h_{av}, the

106

dynamically-unstable regions shift to the right along the frequency axis having higher excitation frequencies, and consequently decreasing the amplitudes of steady-state vibrations and also increasing the widths of dynamically-unstable regions. Increase in the widths of instability regions is more influenced by the compressive loading than the tensile loading. However, the points of origins of dynamically-unstable regions are more influenced by the tensile loading than the compressive loading. These outcomes are also due to the fact that increasing the thickness of plate makes the plate stiffer.

The thickness-tapered plates, through increasing the stiffness and at the same time decreasing the weight, bring upon more complicated structural behavior as exhibited by their vibration response and dynamic instability characteristics, in comparison to the uniform plate. All of the parametric study results indicate that the thickness-tapered plates having configuration C is more stable and have better vibrational behavior in comparison to any other thickness-tapered configurations (A, B or D) and even in comparison to the uniform plate having the thickness as the average-thickness of the corresponding thickness-tapered plate having configuration C. It can also be concluded that the superiority of the thickness-tapered plate with configuration C could further be improved by decreasing the sizes of the resin pockets. The present work can be used as a benchmark study in future studies on the dynamic instability of laminated thickness-tapered composite plates.

CHAPTER 4

Non-linear dynamic instability of internally-thickness-tapered composite cylindrical panels subjected to parametric excitation

4.1 Introduction

According to the literature survey done by Sahu and Datta [36] on the research advances in the dynamic stability behavior of plates and shells, Faraday was the first who observed dynamic instability in the liquid (wine) in a cylinder (wineglass) that oscillated with half of the frequency of the exciting force movement of moist fingers around the glass edge and the first mathematical explanation to this phenomenon was given by Rayleigh. However the dynamic instability of the elastic systems via governing systems of differential equations of the Mathieu–Hill type was presented in the bibliography of the works by Bolotin [1] and Ewan-Iwanowski [37]. The dynamic instability of a structure subjected to periodic axial forces has been a very important topic in structural dynamics and is of practical importance in different engineering disciplines. Structural components under periodic loads can undergo parametric resonance which may occur over a range of forcing frequencies and has become a popular subject of study. A detailed research survey on the dynamic stability behavior of plates and shells in which the literature from 1987 to 2005 has been reviewed can be found in the review paper by Sahu and Datta [36]. By searching and reviewing through available literature it can be observed that considerable number of studies have been devoted to the dynamic instability of flat plates and either cylindrical or conical shells. However, very few studies considered the dynamic instability of curved panels particularly laminated composite curved panels. Dynamic stability of simply-supported, isotropic cylindrical panels under combined static and periodic axial forces was investigated by Ng et.al, [38]. They used an extension of Donnell's shell theory to a first-order shear deformation theory that via a normal-mode expansion a system of

Mathieu-Hill equations were derived and consequently by applying Bolotin's method the parametric resonance response was obtained and analyzed. Ganapathi et. al. [39] established finite element method using C^0 shear flexible continuous, nine-nodded quadrilateral (QUAD-9) shell element to study the dynamic instability of laminated composite curved panels. Dynamic instability of laminated composite curved panels with cutouts subjected to in-plane static and periodic compressive loads was studied by Sahu and Datta [40]. They also implemented finite element method using a generalized shear deformable Sanders' theory. Liew et. al. [41] used the mesh-free kp-Ritz method in which the mesh-free kernel particle estimate is employed to approximate the 2D transverse displacement filed then a system of Mathieu-Hill equations is obtained via applying the Ritz minimization procedure to the energy expressions to investigate the dynamic instability of laminated cylindrical panels. All the above mentioned literature for the curved panels are based on linear analysis that can only provide the information about the instability region and unable to predict the vibration amplitudes in these regions for which non-linear analysis is required.

Due to the high strength-to-weight and stiffness-to-weight ratios of engineering composite structures they are increasingly being used in aerospace, mechanical and automotive industries. Considerable experimental, numerical and analytical studies in the past few decades were devoted to the mechanical behavior of these structures including stress analysis, fatigue and fracture, buckling, and vibrations. Dynamic stability has been considered in few of the works mentioned in the above. In all those studies the stiffness of the structure remain constant along the length and width of the beams, plates or shells. But in practical and in some specific applications a large number of those structures are tapered such as aircraft wing skins, turbine blades, helicopter yokes and blades, robot arms and satellite antennas, flex-beams of helicopter rotor hubs, and near field joints in solid rocket boosters, wherein the stiffness of the structure needs to be varied along the length of the structure. Tapered composite structures are formed

by terminating or dropping-off some of the plies in the laminates which is an important method of stiffness tailoring and weight saving in these structures. In these structures both the stiffness and the weight of the structure are varying along the tapering direction and makes that the structure be stiff at one end and flexible at another and. However such variation of the stiffnesses brings much complexity to their mechanical behavior and the analysis of such tapered structures mentioned in the above.

So far, to the best of the authors' knowledge, there is no work available in the published literature on the dynamic instability of internally-thickness-tapered composite curved panels subjected to in-plane periodically pulsating loads. In this work the dynamically-unstable regions, and both stable-, and unstable-solutions amplitudes of steady-state vibrations at these regions of internally-thickness-tapered composite cylindrical panels are investigated based on non-linear analysis. The non-linear von Karman strains associated with large deflections and curvatures are considered. Considering the simply supported boundary condition the in-plane displacements are determined in terms of the out-of-plane displacement function. The in-plane force-resultants which are determined based on those in-plane displacements and corresponding boundary conditions are substituted in the moment-equilibrium equation of motion with the moment-resultants which directly are defined in terms of the out-of-plane displacement function. Then the general Galerkin method are applied to the resultant equation and a set of non-linear Mathieu-Hill equations are obtained. Eventually the principal dynamically-unstable regions, stable-, and unstable-solutions amplitudes of the steady-state vibrations at these regions are calculated via Bolotin's first approximation. Numerical comparisons are made with those available in literature to validate the present methodology. Four different configurations of internally-thickness-tapered panels are considered for the studied laminated cylindrical panels. A comprehensive parametric study is carried out to examine and compare the effects of the various taper configurations, taper angles, amplitudes

of both tensile and compressive axial loads, panel curvature or in particular radius-to-width ratio, aspect ratios of the tapered cylindrical panel including the loaded-to-unloaded width and length-to-thickness ratios which is in particular the length-to-average-thickness ratio on the instability regions and the parametric resonance particularly the steady-state vibrations amplitude. The present results show good agreement when compared with those available in the literature and hence can be used as benchmark results for future studies.

4.2 Formulation

A simply supported laminated composite internally-thickness-tapered cylindrical panel, having length a, width b and radius R with respect to the Cartesian coordinates (x, y, z) which are assigned in the mid-plane of the plate is considered as shown in Fig. 4.1.
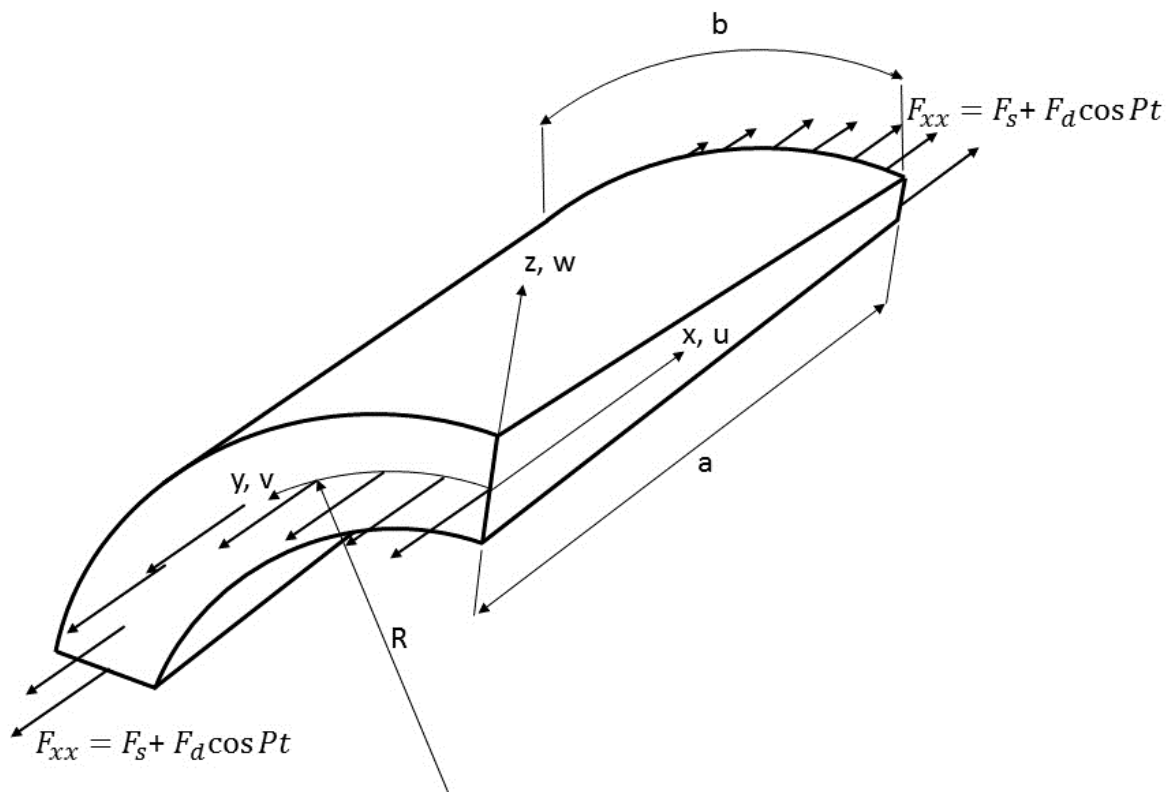
Figure 4.1 The geometry and loading condition of a laminated composite cylindrical thickness-tapered panel

Here, u, v and w are the displacement components of the cylindrical panel with reference to this coordinate system in the x, y, and z directions, respectively. The cylindrical panel as shown in Fig.1 is subjected to a periodically pulsating load in the length direction with the axial loading per unit length as follow:

$$F_{xx}(t) = F_s + F_d cosPt \qquad (4.1)$$

where F_s is a time invariant component, $F_d cosPt$ is the harmonically-pulsating component, and P denotes the frequency of excitation in radians per unit time.

As mentioned above the panel is considered to be internally-tapered in the thickness and has been designed with any one of the four different taper configurations shown in Fig. 4.2.
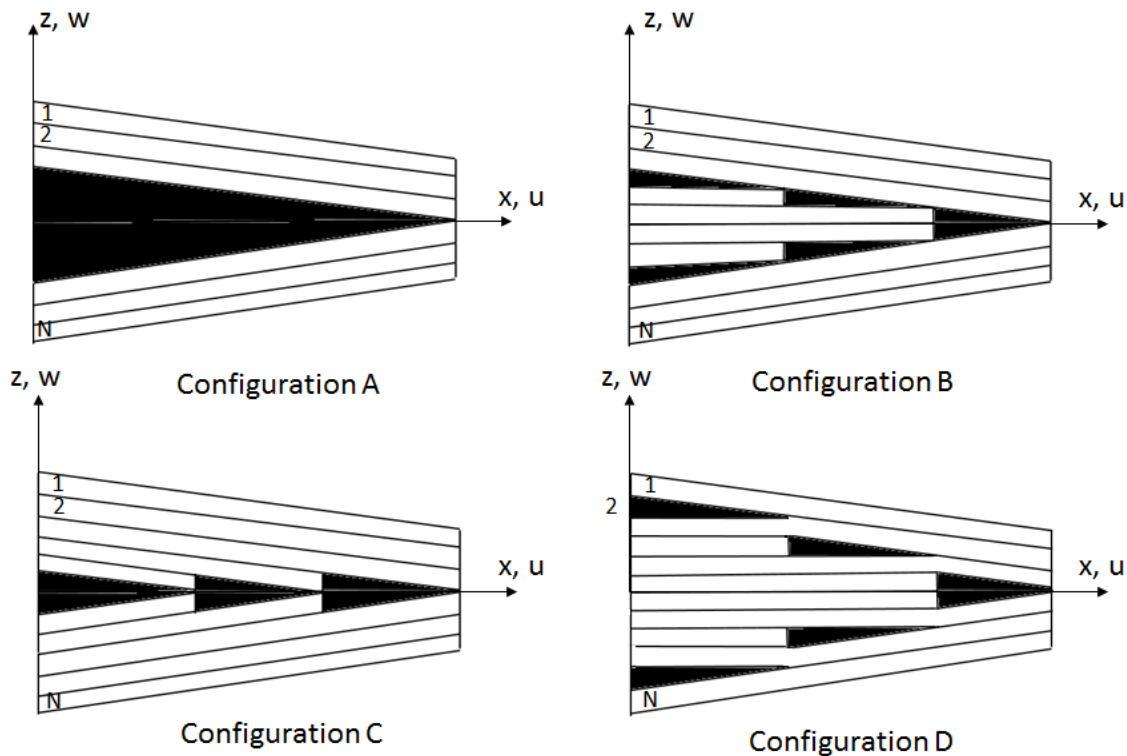
Figure 4.2 Taper configurations of the internally-thickness-tapered composite cylindrical panel

The rectangular thickness-tapered cylindrical panel is considered to be constructed by a cross-ply laminated composite material having density$\rho^{(k)}$ of each lamina or the resin pockets and k refers to the corresponding lamina's number. Therefore the mass per unit length per unit width of the laminated thickness-tapered cylindrical panel can be calculated as

$$\rho_t = \rho_t(x^1, x^0) = \sum_{k=1}^{N} \rho^{(k)}(h_k(x^1, x^0) - h_{k+1}(x^1, x^0)) \tag{4.2}$$

where h_k and h_{k+1} are measured from the mid-plane to the outer and inner surfaces of the kth layer, respectively and calculated as follow:

$$h_k(x^1, x^0) = \begin{cases} (-\tan\phi) * x + z_k & IF & z_k > 0 \\ (\tan\phi) * x + z_k & IF & z_k < 0 \end{cases} \tag{4.3}$$

Hence, although ρ_t is a constant parameter for uniform laminate, for thickness-tapered laminate it is a linear function of x-coordinate. This function consists of step functions for all taper configurations of the thickness-tapered cylindrical panel except for the configuration A. The number of the corresponding intervals, N_s, for the configurations B, C and D are expressed as follow:

$$N_s = \frac{1}{2}(N_L - N_R) \tag{4.4}$$

where N_L and N_R refer to the number of plies at the left (thick) and right (thin) sides of the thickness-tapered plate respectively.

The displacements of a generic point of the mid-plane of the cylindrical panel are denoted by u_0, v_0 and w_0 in $x, y, and\ z$ directions, respectively; the corresponding displacements of a generic point of the cylinder panel at distance z from the mid-plane are denoted by u, v and w, which are defined based on Kirchhoff hypotheses as follow:

$$u = u_0(x, y, t) - z\frac{\partial w_0(x,y,t)}{\partial x} \tag{4.5}$$

$$v = v_0(x, y, t) - z\frac{\partial w_0(x,y,t)}{\partial y} \tag{4.6}$$

$$w = w_0(x, y, t) \tag{4.7}$$

The strain components ϵ_{xx}, ϵ_{yy} and γ_{xy} at an arbitrary point of the curved panel are related to the membrane strains (mid-plane strains) $\epsilon_{xx}^{(0)}$, $\epsilon_{yy}^{(0)}$ and $\gamma_{xy}^{(0)}$ and to the bending curvatures in the x and y directions and twisting curvature of the mid-plane which are denoted as $\epsilon_{xx}^{(1)}$, $\epsilon_{yy}^{(1)}$ and $\gamma_{xy}^{(1)}$, are obtained as follow:

$$\begin{Bmatrix} \epsilon_{xx} \\ \epsilon_{yy} \\ \gamma_{xy} \end{Bmatrix} = \begin{Bmatrix} \epsilon_{xx}^{(0)} \\ \epsilon_{yy}^{(0)} \\ \gamma_{xy}^{(0)} \end{Bmatrix} + z \begin{Bmatrix} \epsilon_{xx}^{(1)} \\ \epsilon_{yy}^{(1)} \\ \gamma_{xy}^{(1)} \end{Bmatrix} \tag{4.8}$$

For von Karman hypothesis, the in-plane displacements u_0 and v_0 are infinitesimal, and in the strain-displacement relations only those non-linear terms that depend on w_0 need to be retained. Hence all other non-linear terms may be neglected and the following membrane strains and the flexural (bending) strains are given by

$$\{\epsilon^0\} = \begin{Bmatrix} \epsilon_{xx}^{(0)} \\ \epsilon_{yy}^{(0)} \\ \gamma_{xy}^{(0)} \end{Bmatrix} = \begin{Bmatrix} \frac{\partial u_0}{\partial x} + \frac{1}{2}\left(\frac{\partial w_0}{\partial x}\right)^2 \\ \frac{\partial v_0}{\partial y} + \frac{w_0}{R} + \frac{1}{2}\left(\frac{\partial w_0}{\partial y}\right)^2 \\ \frac{\partial u_0}{\partial y} + \frac{\partial v_0}{\partial x} + \frac{\partial w_0}{\partial x}\frac{\partial w_0}{\partial y} \end{Bmatrix} \tag{4.9}$$

$$\{\epsilon^1\} = \begin{Bmatrix} \epsilon_{xx}^{(1)} \\ \epsilon_{yy}^{(1)} \\ \gamma_{xy}^{(1)} \end{Bmatrix} = \begin{Bmatrix} -\frac{\partial^2 w_0}{\partial x^2} \\ -\frac{\partial^2 w_0}{\partial y^2} \\ -2\frac{\partial^2 w_0}{\partial x \partial y} \end{Bmatrix} \tag{4.10}$$

The total in-plane force resultants which are forces per unit length, and the total moment resultants, which are moments per unit length are defined respectively as

$$\begin{Bmatrix} N_{xx} \\ N_{yy} \\ N_{xy} \end{Bmatrix} = \int_{-\frac{h}{2}}^{\frac{h}{2}} \begin{Bmatrix} \sigma_{xx} \\ \sigma_{yy} \\ \sigma_{xy} \end{Bmatrix} dz \tag{4.11}$$

$$\begin{Bmatrix} M_{xx} \\ M_{yy} \\ M_{xy} \end{Bmatrix} = \int_{-\frac{h}{2}}^{\frac{h}{2}} \begin{Bmatrix} \sigma_{xx} \\ \sigma_{yy} \\ \sigma_{xy} \end{Bmatrix} Z \, dz \tag{4.12}$$

which are based on Kirchhoff stresses σ_{ij} and are referred to the initial undeformed configuration of the cylindrical panel.

As shown in Fig.4.3 the stiffness matrix of a ply in the thickness-tapered laminate in the global coordinate system (x, y, z) is calculated by using multiple transformations of the ply material stiffness matrix from principal material coordinate system (x'', y'', z'') to local coordinate system (x', y', z'), and then to the global coordinate system (x, y, z) as follow:

114
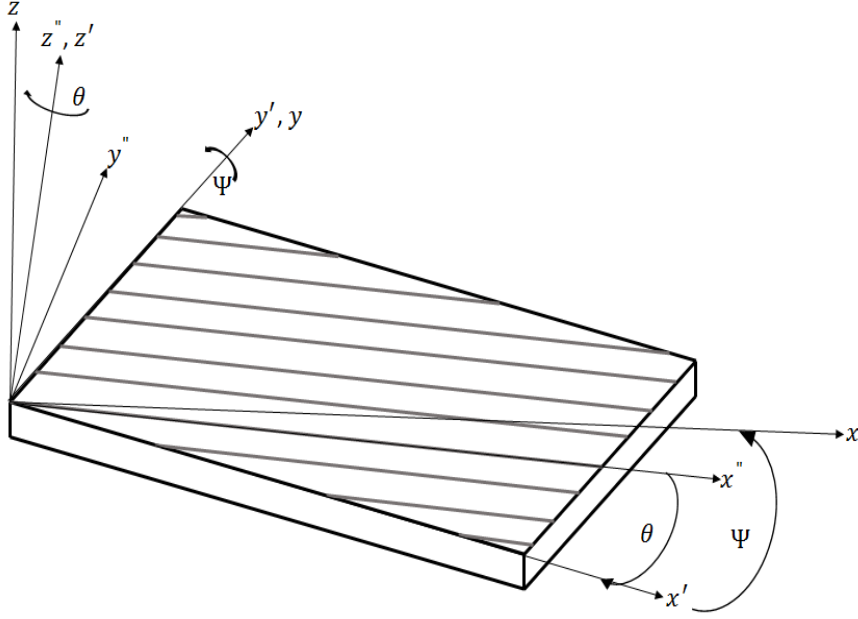
Figure 4.3 Transformation of the principal material coordinates to global coordinates

$$[C]_{xyz} = [T_\Psi][T_\theta][C^{''}]_{x''y''z''}[T_\theta]^T[T_\Psi]^T \tag{4.13}$$

where $[T_\theta]$ and $[T_\Psi]$ are the stress transformation matrices corresponding to the fiber orientation angle θ and ply angle Ψ respectively that are defined in Appendix (Eqs. (A.5) and (A.6)). The ply angle Ψ for a ply located above the mid-plane is equal to the taper angle ϕ and for the ply located below the mid-plane it is equal to $-\phi$. The constitutive equation of the thickness-tapered laminate made of several orthotropic layers with the arbitrarily oriented material axes to the laminate coordinate can be obtained by the transformation of the stress-strain relations to the laminate coordinates as follow:

$$\begin{Bmatrix} \sigma_{xx} \\ \sigma_{yy} \\ \tau_{xy} \end{Bmatrix}^{(k)} = \begin{bmatrix} \bar{Q}_{11} & \bar{Q}_{12} & \bar{Q}_{16} \\ \bar{Q}_{12} & \bar{Q}_{22} & \bar{Q}_{26} \\ \bar{Q}_{16} & \bar{Q}_{26} & \bar{Q}_{66} \end{bmatrix}^{(k)} \begin{Bmatrix} \epsilon_{xx} \\ \epsilon_{yy} \\ \gamma_{xy} \end{Bmatrix} \tag{4.14}$$

where $[\bar{Q}]^{(k)}$ is the transformed reduced stiffness matrix defined as follow:

$$\bar{Q}_{11}^{(k)} = C_{11}(\theta^{(k)}, \Psi^{(k)}) - \frac{C_{13}(\theta^{(k)}, \Psi^{(k)}) * C_{13}(\theta^{(k)}, \Psi^{(k)})}{C_{33}(\theta^{(k)}, \Psi^{(k)})} \tag{4.15-a}$$

$$\bar{Q}_{12}^{(k)} = C_{12}(\theta^{(k)}, \Psi^{(k)}) - \frac{C_{13}(\theta^{(k)}, \Psi^{(k)}) * C_{23}(\theta^{(k)}, \Psi^{(k)})}{C_{33}(\theta^{(k)}, \Psi^{(k)})} \tag{4.15-b}$$

115

$$\bar{Q}_{22}^{(k)} = C_{22}\left(\theta^{(k)}, \Psi^{(k)}\right) - \frac{C_{23}\left(\theta^{(k)}, \Psi^{(k)}\right) * C_{23}\left(\theta^{(k)}, \Psi^{(k)}\right)}{C_{33}\left(\theta^{(k)}, \Psi^{(k)}\right)} \tag{4.15-c}$$

$$\bar{Q}_{16}^{(k)} = C_{16}\left(\theta^{(k)}, \Psi^{(k)}\right) - \frac{C_{13}\left(\theta^{(k)}, \Psi^{(k)}\right) * C_{63}\left(\theta^{(k)}, \Psi^{(k)}\right)}{C_{33}\left(\theta^{(k)}, \Psi^{(k)}\right)} \tag{4.15-d}$$

$$\bar{Q}_{26}^{(k)} = C_{26}\left(\theta^{(k)}, \Psi^{(k)}\right) - \frac{C_{23}\left(\theta^{(k)}, \Psi^{(k)}\right) * C_{63}\left(\theta^{(k)}, \Psi^{(k)}\right)}{C_{33}\left(\theta^{(k)}, \Psi^{(k)}\right)} \tag{4.15-e}$$

$$\bar{Q}_{66}^{(k)} = C_{66}\left(\theta^{(k)}, \Psi^{(k)}\right) - \frac{C_{63}\left(\theta^{(k)}, \Psi^{(k)}\right) * C_{63}\left(\theta^{(k)}, \Psi^{(k)}\right)}{C_{33}\left(\theta^{(k)}, \Psi^{(k)}\right)} \tag{4.15-f}$$

where $\bar{Q}_{16}^{(k)}$ and $\bar{Q}_{26}^{(k)}$ for the plies in the cross-ply laminate are zero and C_{ij} are elements of the stiffness matrix $[C]$ [35]. By following the equations (4.11)-(4.15) the force and moment resultants for the cross-ply symmetric laminated thickness-tapered cylindrical panel are defined as

$$\begin{Bmatrix} N_{xx} \\ N_{yy} \\ N_{xy} \\ M_{xx} \\ M_{yy} \\ M_{xy} \end{Bmatrix} = \begin{bmatrix} A_{11} & A_{12} & 0 & & & \\ A_{12} & A_{22} & 0 & & [0] & \\ 0 & 0 & A_{66} & & & \\ & & & D_{11} & D_{12} & 0 \\ & [0] & & D_{12} & D_{22} & 0 \\ & & & 0 & 0 & D_{66} \end{bmatrix} \begin{Bmatrix} \epsilon_{xx}^{(0)} \\ \epsilon_{yy}^{(0)} \\ \gamma_{xy}^{(0)} \\ \epsilon_{xx}^{(1)} \\ \epsilon_{yy}^{(1)} \\ \gamma_{xy}^{(1)} \end{Bmatrix} \tag{4.16}$$

where A_{ij} and D_{ij} denote the extensional and bending stiffnesses respectively.

$$A_{ij}(x^1, x^0) = \sum_{k=1}^{N} \bar{Q}_{ij}^{(k)}\left(h_k(x^1, x^0) - h_{k+1}(x^1, x^0)\right) \quad , (i, j = 1, 2, 6) \tag{4.17a}$$

$$D_{ij}(x^3, x^2, x^1, x^0) = \frac{1}{3} \sum_{k=1}^{N} \bar{Q}_{ij}^{(k)}\left((h_k(x^1, x^0))^3 - (h_{k+1}(x^1, x^0))^3\right) \tag{4.17b}$$

Hence, although A_{ij} and D_{ij} are constant terms for the uniform laminate, for the thickness-tapered laminate these extension- and bending-stiffnesses are linear and cubic functions of x-coordinate respectively. These functions are step functions for all configurations of the thickness-tapered cylindrical panel except for the configuration A. The number of the corresponding intervals, N_s, as mentioned before for the configurations B, C and D are obtained from Eq. (4.4).

As mentioned above since $u_0 \ll w_0$ and $v_0 \ll w_0$ one can consider that $\rho_t \, \partial^2 u_0 / \partial t^2 \to 0$

and $\rho_t \, \partial^2 v_0 / \partial t^2 \to 0$. Therefore by neglecting the in-plane inertia forces the equations of

motion for the cylindrical panel [42] under the in-plane pulsating load are given by

$$\frac{\partial N_{xx}}{\partial x} + \frac{\partial N_{xy}}{\partial y} = 0 \tag{4.18}$$

$$\frac{\partial N_{xy}}{\partial x} + \frac{\partial N_{yy}}{\partial y} = 0 \tag{4.19}$$

$$\frac{\partial^2 M_{xx}}{\partial x^2} + 2 \frac{\partial^2 M_{xy}}{\partial x \partial y} + \frac{\partial^2 M_{yy}}{\partial y^2} - \frac{1}{R} N_{yy} + \frac{\partial}{\partial x}\left(N_{xx}\frac{\partial w_0}{\partial x} + N_{xy}\frac{\partial w_0}{\partial y}\right) + \frac{\partial}{\partial y}\left(N_{xy}\frac{\partial w_0}{\partial x} + N_{yy}\frac{\partial w_0}{\partial y}\right) =$$

$$\rho_t \frac{\partial^2 w_0}{\partial t^2} \tag{4.20}$$

4.3   Solution for laminated orthotropic thickness-tapered panels

Since the gradients of variations of extensional stiffnesses $A_{ij}(x^1, x^0)$ from the thickest to

the thinnest sides of the thickness-tapered plate are too small in comparison to the

corresponding variations of bending stiffnesses $D_{ij}(x^3, x^2, x^1, x^0)$ (see the figure (Fig. A.1)

and corresponding table (Table A.1) in Appendix), one can replace the $A_{ij}(x^1, x^0)$ terms in Eq.

4.14 by their average values as follow:

$$\bar{A}_{ij} = \frac{1}{a}\int_0^a A_{ij}(x^1, x^0)dx \qquad , (i,j = 1, 2, 6) \tag{4.21}$$

It should be noted here that since extensional stiffnesses, $A_{ij}(x^1, x^0)$, for all configurations of

the thickness-tapered plate except for configuration A, are step functions, the integration in

Eq. (4.21) over the length of the thickness-tapered plate should be step integration.

Substituting Eq. (4.9) and Eq. (4.21) into Eq. (4.16) the resultant membrane forces N_{xx} , N_{yy}

and N_{xy} are defined and consequently the first-two equations of motion i.e. Eq. (4.18) and Eq.

(4.19) are written in terms of the mid-plane displacement components i.e. $u_0(x, y, t)$,

$v_0(x, y, t)$ and $w_0(x, y, t)$.

Considering the simply supported boundary condition for the laminated orthotropic thickness-tapered cylindrical panel, the Navier's double Fourier series with the time dependent coefficient $q_{mn}(t)$ is chosen to describe the out-of-plane displacement function $w_0(x,y,t)$:

$$w_0 = \sum_{m=1}^{\infty}\sum_{n=1}^{\infty} q_{mn}(t)\sin\lambda_m x \sin\lambda_n y \quad, \quad \lambda_m = \frac{m\pi}{a} \text{ and } \lambda_n = \frac{n\pi}{b} \qquad (4.22)$$

where m and n represent the number of longitudinal and transverse half-waves in corresponding standing wave pattern, respectively. Substituting Eq. (4.21) in the displacement form of Eq. (4.18) and Eq. (4.19) and applying appropriate trigonometric relations, the solution of the differential equation system has the form as follow:

$u_0(x,y,t) = \sum_{m=1}^{\infty}\sum_{n=1}^{\infty} \zeta_1 \sin(2\lambda_m x) +$

$\zeta_2 \cos(\lambda_m x)\sin(\lambda_n y) + \zeta_3 \sin(2\lambda_m x)\cos(2\lambda_n y) + u_c(x,y,t)$ (4.23-a)

$v_0(x,y,t) = \sum_{m=1}^{\infty}\sum_{n=1}^{\infty} \zeta_4 \sin(2\lambda_n y) +$

$\zeta_5 \sin(\lambda_m x)\cos(\lambda_n y) + \zeta_6 \cos(2\lambda_m x)\sin(2\lambda_n y) + v_c(x,y,t)$ (4.23-b)

Here ζ_1 , ζ_2, ζ_3, ζ_4, ζ_5 and ζ_6 are unknown coefficients out of which ζ_1 and ζ_4 can be directly obtained from the displacement form of Eq. (18) and Eq. (19) , respectively as follow:

$$\zeta_1 = (\bar{A}_{11}\lambda_m^{~2} - \bar{A}_{12}\lambda_n^{~2})q_{mn}(t)^2/16\lambda_m \bar{A}_{11} \qquad (4.24\text{-a})$$

$$\zeta_4 = (\bar{A}_{12}\lambda_m^{~2} - \bar{A}_{22}\lambda_n^{~2})q_{mn}(t)^2/16\lambda_n \bar{A}_{22} \qquad (4.24\text{-b})$$

and also ζ_2 and ζ_5 can be solved from the displacement form of the system of equations (4.18 and 4.19) as follow:

$$\zeta_2 = \frac{(\bar{A}_{12}\lambda_m^{~2} - \bar{A}_{22}\lambda_n^{~2})\bar{A}_{66}\lambda_m q_{mn}(t)}{\Delta} \qquad (4.24\text{-c})$$

$$\zeta_5 = \frac{(\bar{A}_{11}\bar{A}_{22}\lambda_m^{~2} - \bar{A}_{12}^{~2}\lambda_m^{~2} - \bar{A}_{12}\bar{A}_{66}\lambda_m^{~2} + \bar{A}_{22}\bar{A}_{66}\lambda_n^{~2})\lambda_n q_{mn}(t)}{\Delta} \qquad (4.24\text{-d})$$

where

$$\Delta = R(\bar{A}_{11}\bar{A}_{22}\lambda_m^{~2}\lambda_n^{~2} + \bar{A}_{11}\bar{A}_{66}\lambda_m^{~4} - \bar{A}_{12}^{~2}\lambda_m^{~2}\lambda_n^{~2} - 2\bar{A}_{12}\bar{A}_{66}\lambda_m^{~2}\lambda_n^{~2} + \bar{A}_{22}\bar{A}_{66}\lambda_n^{~4})$$

(4.24-e)

and similarly ζ_3 and ζ_6 can be solved from again the displacement form of the system of equations (4.18 and 4.19) as follow:

$$\zeta_3 = \frac{1}{16}\lambda_m q_{mn}(t)^2 \tag{4.24-f}$$

$$\zeta_6 = \frac{1}{16}\lambda_n q_{mn}(t)^2 \tag{4.24-g}$$

$u_c(x, y, t)$ and $v_c(x, y, t)$ are homogeneous solutions of the differential equation system given as:

$$\bar{A}_{11}\frac{\partial^2 u_c}{\partial x^2} + (\bar{A}_{12} + \bar{A}_{66})\frac{\partial^2 v_c}{\partial x \partial y} + \bar{A}_{66}\frac{\partial^2 u_c}{\partial y^2} = 0 \tag{4.25-a}$$

$$\bar{A}_{66}\frac{\partial^2 v_c}{\partial x^2} + (\bar{A}_{12} + \bar{A}_{66})\frac{\partial^2 u_c}{\partial x \partial y} + \bar{A}_{22}\frac{\partial^2 u_c}{\partial y^2} = 0 \tag{4.25-b}$$

Since the solution should also satisfy the boundary conditions of the studied thickness-tapered cylindrical panel which is subjected to in-plane loading, for the partial differential equation system of equations (4.25-a and b) the solution should have the forms as follow:

$$u_c(x, y, t) = \bar{A}_{11}(a - 2x)\xi_x(t) \tag{4.26-a}$$

$$v_c(x, y, t) = \bar{A}_{22}(b - 2y)\xi_y(t) \tag{4.26-b}$$

where $\xi_x(t)$ and $\xi_y(t)$ are unknown functions of time that can be determined from the following boundary conditions:

$$\frac{1}{b}\int_0^b N_{xx} \, dy = F_{xx} \qquad at \; x = 0, a \tag{4.27-a}$$

$$\frac{1}{a}\int_0^a N_{yy} \, dx = 0 \qquad at \; y = 0, b \tag{4.27-b}$$

Hence by solving these two boundary condition equations, $\xi_x(t)$ and $\xi_y(t)$ are determined as follow:

$$\xi_x(t) = ((\bar{A}_{11}\bar{A}_{22} - \bar{A}_{12}{}^2)\lambda_m{}^2 q_{mn}(t)^2 - 8\bar{A}_{22}F_{xx})/(16\bar{A}_{11}(\bar{A}_{11}\bar{A}_{22} - \bar{A}_{12}{}^2)) \tag{4.28-a}$$

$$\xi_y(t) = ((\bar{A}_{11}\bar{A}_{22} - \bar{A}_{12}{}^2)\lambda_n{}^2 q_{mn}(t)^2 + 8\bar{A}_{12}F_{xx})/(16\bar{A}_{22}(\bar{A}_{11}\bar{A}_{22} - \bar{A}_{12}{}^2)) \tag{4.28-b}$$

and consequently the resultant membrane forces N_{xx}, N_{yy} and N_{xy} are determined and all the three are too long functions. All the described calculations and following algorithm were

119

performed with the Symbolic Toolbox of Maple, which incorporates symbolic computations into the numeric environment of MATLAB.

By substituting the resultant membrane forces and the moment resultants from Eq. (4.16) that are in terms of the out-of-plane displacement, w_0, as defined in Eq. (4.22) into the third equation of motion i.e. Eq. (4.20), and then multiplying the governing equation by $\sin \lambda_m x \sin \lambda_n y$ and integrating over the mid-plane area of the thickness-tapered cylindrical panel a system of $m \times n$ second-order ordinary differential equations is obtained. It should be noted again here that since bending stiffness for all configurations of the thickness-tapered cylindrical panel except for configuration A, are step functions, hence the corresponding moment resultants are also step functions, therefore this integration over the area should be a step integration.

$$M_{mn}\ddot{q}_{mn}(t) + K_{mn}q_{mn}(t) - (F_s + F_d \cos pt)Q_{mn}q_{mn}(t) + \eta_{mn}q^3_{mn}(t) = 0 \quad (4.29)$$

where M_{mn}, K_{mn} , Q_{mn} and η_{mn} are matrices and $\ddot{q}_{mn}(t)$, $q_{mn}(t)$ and $q^3_{mn}(t)$ are column vectors consisting of the terms $\ddot{q}_{mn}(t)$'s, $q_{mn}(t)$'s and $q^3_{mn}(t)$'s respectively. The subscripts m and n have the following ranges:

$$m, n = 1,2,3,4,..,N. \quad (4.30)$$

It should be noted here that for the case with $m = n = 1,3,5, ...$ an additional term appears as $K'_{mn}q^2_{mn}(t)$ in the Eq. (4.29) which is due to the geometric asymmetry of curved panel and it doesn't have any contribution either on the dynamically-unstable regions or amplitudes of the steady-state vibrations at the principal parametric resonance, so by introducing the following notation:

$$\omega_{mn} = \sqrt{\frac{K_{mn}}{M_{mn}}} \quad (4.31a)$$

$$\gamma_{mn} = \frac{\eta_{mn}}{M_{mn}} \quad (4.31b)$$

$$N_* = \frac{K_{mn}}{Q_{mn}} \quad (4.31c)$$

Eq. (4.29) can be written in the form of the non-linear Mathieu-Hill equation as follow:

$$\ddot{q}_{mn}(t) + \Omega^2_{mn}(1 - 2\mu_{mn}\cos pt)q_{mn}(t) + \gamma_{mn}q^3_{mn}(t) = 0 \tag{4.32}$$

where Ω_{mn} is the frequency of the free vibration of the plate loaded by a constant longitudinal force F_s,

$$\Omega_{mn} = \omega_{mn}\sqrt{1 - \frac{F_s}{N_*}} \tag{4.33}$$

and μ_{mn} is a quantity that is called the excitation parameter,

$$\mu_{mn} = \frac{F_d}{2(N_* - F_s)} \tag{4.34}$$

4.4 Dynamic instability regions

The resonance curve is not influenced by the non-linearity of Eq. (4.32) and according to the Liapunov theorem [1] the trivial solution of the non-linear system is stable everywhere except in the regions of excitation of the linear system. Therefore, the dynamically-unstable regions are determined by the linear parts of the Eq. (4.32) [1] so it is more convenient to write the non-linear Mathieu-Hill equation (4.32) in the following form which only includes the linear parts:

$$M_{mn}\ddot{q}_{mn}(t) + (K^*_{mn} - Q^*_{mn}\cos pt)q_{mn}(t) = 0 \tag{4.35}$$

where

$$K^*_{mn} = K_{mn} - F_sQ_{mn} \tag{4.36}$$

and

$$Q^*_{mn} = F_dQ_{mn} \tag{4.37}$$

The basic solutions of Mathieu-Hill equation include two periodic solutions: i.e. periodic solutions of periods T and $2T$ with $T = 2\pi/P$. The solutions with period $2T$ are of greater practical importance as the widths of these unstable regions are usually larger than those

associated with solutions having period T. Using Bolotin's method [1] for parametric vibration, the solution of period $2T$ is given by the following equation:

$$q(t) = \sum_{k=1,3,5,...}^{\infty} f_k \sin\frac{kPt}{2} + g_k \cos\frac{kPt}{2} \qquad (4.38)$$

where f_k and g_k are arbitrary vectors. If one investigates the instability at the principal resonance $\approx 2\Omega$, one can neglect the influence of higher harmonics in the expansion of the above equation and can assume

$$q(t) = f \sin\frac{Pt}{2} + g \cos\frac{Pt}{2} \qquad (4.39)$$

The principal region of dynamic instability, which corresponds to the solution of the period, $2T$ is determined by substituting Eq. (4.39) into Eq. (4.35) and equating the determinant of the coefficient matrix of the linear part of the governing equation to zero as follow:

$$\begin{vmatrix} K_{mn}^* - \frac{Q_{mn}^*}{2} - \frac{M_{mn}}{4}P^2 & 0 \\ 0 & K_{mn}^* + \frac{Q_{mn}^*}{2} - \frac{M_{mn}}{4}P^2 \end{vmatrix} = 0 \qquad (4.40)$$

Equation (4.40) can be rearranged to the more simplified form of an eigenvalue problem as follow:

$$\begin{vmatrix} K_{mn}^* - \frac{Q_{mn}^*}{2} & 0 \\ 0 & K_{mn}^* + \frac{Q_{mn}^*}{2} \end{vmatrix} - P^2 \begin{vmatrix} \frac{M_{mn}}{4} & 0 \\ 0 & \frac{M_{mn}}{4} \end{vmatrix} = 0 \qquad (4.41)$$

4.5 Amplitude of vibrations at the principal parametric resonance

As mentioned above, Eq. (4.32) is a non-linear Mathieu-Hill equation where the non-linear term $\gamma q_{mn}^3(t)$ represents the effect of large deflection. As also mentioned in the previous section, the dynamically-unstable region is determined by the linear parts of the Eq. (4.32) and correspondingly leads to the eigenvalue problem which is governed by Eq. (4.41). Here the focus is set on the parametric resonance of the system. Again using Bolotin's first approximation, considering the case of the vibration_at the principal resonance $\approx 2\Omega$, substituting Eq. (4.39) into Eq. (4.32) and equating the coefficients of $\sin(Pt/2),\cos(Pt/2)$

terms and neglecting the terms containing higher harmonics, the following system of equations for the coefficients f and g remains:

$$\left[\Omega_{mn}^2(1 + \mu_{mn}) - \frac{P^2}{4}\right]f + \Gamma(f,g) = 0, \tag{4.42a}$$

$$\left[\Omega_{mn}^2(1 - \mu_{mn}) - \frac{P^2}{4}\right]g + \Psi(f,g) = 0, \tag{4.42b}$$

where $\Gamma(f,g)$ and $\Psi(f,g)$ are defined as coefficients of the terms including $\sin(Pt/2)$ and $\cos(Pt/2)$ which were obtained from the first approximation of expansion in a Fourier series as:

$$\Gamma(f,g) = \frac{3\gamma_{mn}}{4}A^2 f \tag{4.43a}$$

$$\Psi(f,g) = \frac{3\gamma_{mn}}{4}A^2 g \tag{4.43b}$$

where A is the amplitude of steady-state vibrations and is given by:

$$A = \sqrt{f^2 + g^2} \tag{4.44}$$

By substitution of Eqs. (4.43a, b) into Eqs. (4.42a, b) a system of two homogeneous linear equations with respect to f and g can be obtained. This system has solutions that differ from zero only in the case where the determinant composed of the coefficients vanishes:

$$\begin{vmatrix} 1 + \mu_{mn} - n_{mn}^2 + \frac{3\gamma_{mn}}{4\Omega_{mn}^2}A^2 & 0 \\ 0 & 1 - \mu_{mn} - n_{mn}^2 + \frac{3\gamma_{mn}}{4\Omega_{mn}^2}A^2 \end{vmatrix} = 0 \tag{4.45}$$

where

$$n_{mn} = \frac{P}{2\Omega_{mn}} \tag{4.46}$$

Expanding the determinant and solving the resulting equation with respect to the amplitude, A, of the steady-state vibrations the following equation is obtained:

$$A = \frac{2\Omega_{mn}}{\sqrt{3\gamma_{mn}}}\sqrt{n_{mn}^2 - 1 \pm \mu_{mn}} \tag{4.47}$$

It can be proved that for the $\pm\mu_{mn}$ term in the above equation, only $+\mu_{mn}$ term yields the stable solution, and all the other terms yield unstable solutions.

Comparing Eq. (4.45) with Eq. (4.40) by replacing μ_{mn}, n_{mn}, γ_{mn} and Ω_{mn} in terms of K^*_{mn}, Q^*_{mn} and M_{mn} reveals that the dynamic instability regions can also be determined by setting $A = 0$ in Eq. (4.45).

4.6 Numerical results and discussions

Non-linear dynamic stability characteristics of thickness-tapered cross-ply laminated composite cylindrical panels subjected to combined static and periodic in-plane loads are studied here. The material properties used in the present analysis are listed in Table 4.1.

Table 4.1 Material properties of NCT/301 graphite-epoxy composite ply and epoxy materials

Composite Ply		Epoxy	
Material Properties	Value	Material Properties	Value
E_1	$113.9\ GPa$	$E_1 = E_2 = E_3$	$3.93\ GPa$
$E_2 = E_3$	$7.985\ GPa$	$v_{13} = v_{12} = v_{23}$	0.37
$v_{13} = v_{12}$	0.28	ρ	$1200\ Kg/m^3$
v_{23}	0.4		
$G_{13} = G_{12}$	$3.1\ GPa$		
G_{23}	$2.8\ GPa$		
ρ	$1480\ Kg/m^3$		

The static and periodic components of the in-plane load are considered as $F_s = \alpha N_{cr}$ and $F_d = \beta N_{cr}$, respectively. The critical buckling load N_{cr} of the studied thickness-tapered composite plate has been calculated as follow:

$$|K_{mn} - N_{cr}Q_{mn}| = 0 \tag{4.48}$$

The fundamental frequency of the studied thickness-tapered plate is also calculated as follow:

$$|K^*_{mn} - \omega^2 M_{mn}| = 0 \tag{4.49}$$

4.6.1 Validation

To validate the present formulation, which is based on the non-linear analysis, we compare the dynamically-unstable regions of the present formulation with those given by Liew et al. [41] in Fig. 4.4a. To compare the graphs with that given in [41] which has considered the linear analysis and consequently leads only to the instability regions, a four layered uniform
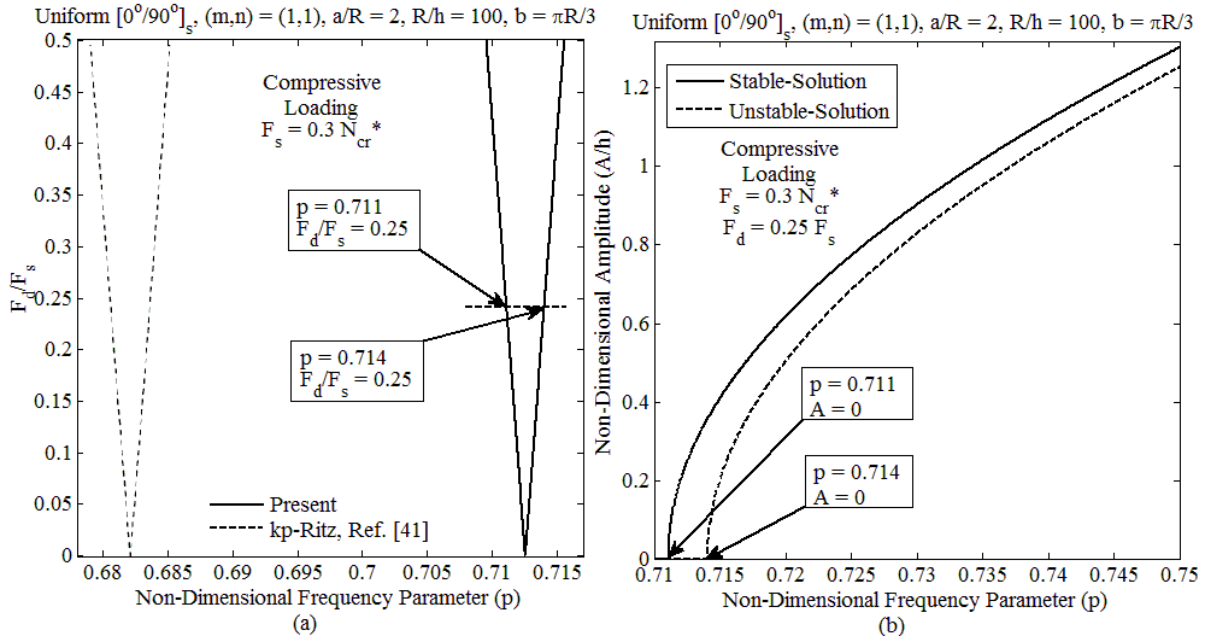
Figure 4.4 The first a) unstable region and b) both stable- and unstable-solution amplitudes of steady-state vibrations of a four layered symmetric $[0°, 90°]_S$ cross-ply laminated cylindrical panel with the geometry of $a/R = 2$, $R/h = 100$ and $b = \pi R/3$, subjected to compressive periodic axial load having static component of $F_s = 0.3\,N_{cr}^*$

symmetric $[0°, 90°]_S$ cross-ply laminated cylindrical panel with the geometry of $a/R = 2$, $R/h = 100$ and $b = \pi R/3$, is subjected to compressive periodic in-plane load having static component of $F_s = 0.3\,N_{cr}^*$. Here N_{cr}^* is the critical buckling load that is approximated for laminated cylindrical panel by Liew et al. [41] based on the critical buckling load of isotropic cylindrical panel which has been given by Timoshenko and Gere [20] as follow:

$$N_{cr}^* = \frac{E_2 h^2}{[3(1-\nu_{12}\nu_{21})]^{1/2} R} \tag{4.50}$$

As it can be observed from this figure (Fig. 4.4a) each unstable region is separated by two lines with a common point of origin. Actually these two lines are not completely straight and they curved slightly outward. To compare the graphs here and in the following figures and tables we specified each unstable region by the non-dimensional frequency parameter p of the point of origin and the half angle of the unstable region as δ which is a parameter that indicates the width of dynamically unstable region. Here the dimensionless excitation frequency parameter p is introduced as follow:

125

$$p = PR\sqrt{\frac{\rho_c(1-\nu_{12}\nu_{21})}{E_2}} \qquad (4.52)$$

where ρ_c is the mass density of the composite plies. The point of origin and the half angle of unstable region of the present formulation are $p = 0.7126$ and $\delta = 0.343°$, respectively and those values with the kp-Ritz method obtained by Liew et al. [41] are $p = 0.6821$ and $\delta = 0.355°$, respectively. The difference between these two studies are 4.47% and 3.38% for the point of origin and the width of unstable regions, respectively; hence it shows a good agreement between the present formulation and that by Liew et al. [41] and the small differences could be due to the numerical method used by the later and neglecting the in-plane inertia forces in the present study. In Fig. 4.4b the amplitudes of the steady-state vibrations are plotted for the same loading conditions and having harmonic component load of $F_d = 0.25 \, F_s$. In the analysis of dynamic stability of plates and shells, there exists simultaneously the stable- and unstable solutions. The difference between these two solutions refers to the required magnitudes of frequency and amplitude to stimulate a parametric resonance. If this difference between them is small, then there might be the possibility of parametric resonance occurring. If the difference is large, it means high values of vibration frequency and amplitude are needed to stimulate a possible parametric resonance. The dynamic stability of such a plate or shell system is said to be good [2, 43]. As it has been mentioned and proved in Section 5 of the present study, the dynamic instability regions based on the large deflection formulation are achieved by either the linear part of the non-linear Mathieu-Hill equation or by setting $A = 0$ in equation (4.45). Once the stable- and unstable-solution amplitudes of steady-state vibrations is zero the corresponding excitation frequencies should coincide with the boundaries of the dynamically-unstable regions (having the same harmonic component of $F_{xx}(t)$ i.e. the same value of F_d). As can be seen from Fig. 4.4b when the amplitude of steady-state vibrations i.e. $A = 0$ the corresponding excitation frequencies are $p = 0.711$ and $p = 0.714$ for stable- and unstable-solutions,

respectively which exactly coincide with that for $F_d/F_s = 0.25$ in the Fig. 4.4a with the left and right curves of the corresponding unstable regions, respectively, and the range of frequencies between these two solutions at $A = 0$ predicate the dynamically-unstable regions at this certain ratio of harmonic-to-static component of the pulsating longitudinal load. Hence, this could be considered as a validation of the non-linear part of the dynamic instability analysis too.

As an another validation of the non-linear part of dynamic instability analysis i.e. both the stable- and unstable-solution amplitudes of steady-state vibrations, the present results which are for laminated cylindrical panel are compared with those given by Ostiguy et al [19] for isotropic homogeneous rectangular plate in Figs. 4.5-4.10. To compare the results we set in our formulation the material property as $E_1 = E_2 = E = 4.83\ GPa$, $v_{12} = v = 0.38$ and $\rho = 1190\ kg/m^3$ and the geometry of
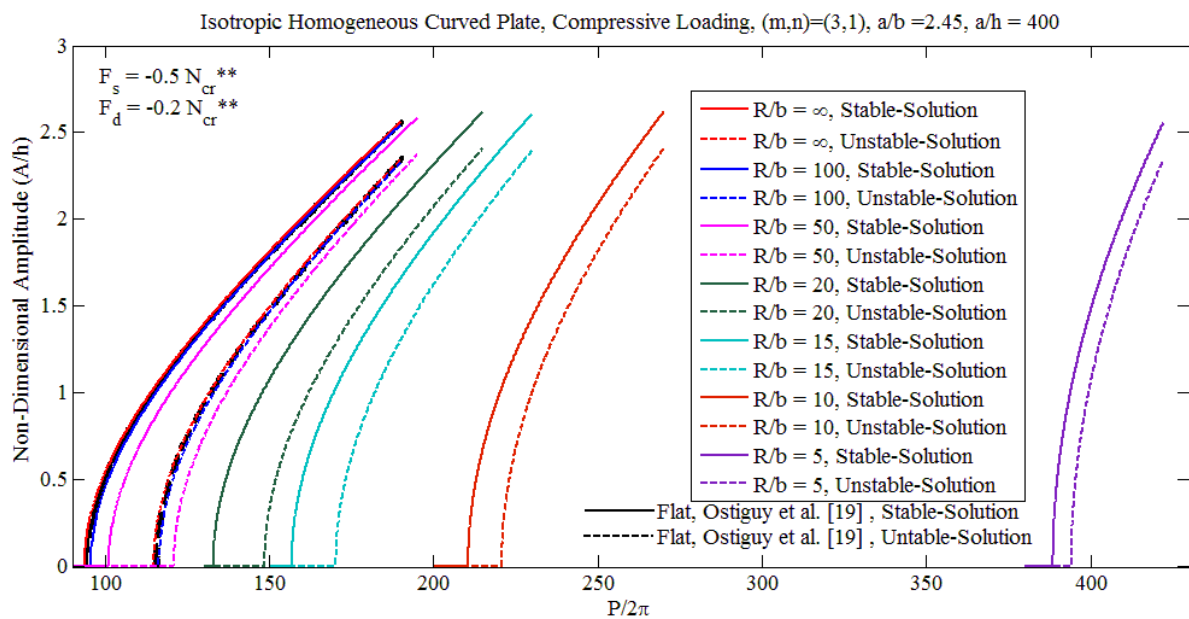
Figure 4.5 Comparison of both the stable- and unstable-solution amplitudes of steady-state vibrations of the present cylindrical panel with those of Ostiguy et al **[19]** for isotropic homogeneous rectangular plate in the mode $(\boldsymbol{m,n}) = (\mathbf{3,1})$, having aspect ratios of $\boldsymbol{a/h} = \mathbf{400}$ and $\boldsymbol{a/b} = \mathbf{2.45}$ subjected to periodic in-plane load having static component of $\boldsymbol{F_s} = -\mathbf{0.5}\ \boldsymbol{N_{cr}^*}$ and dynamic component of $\boldsymbol{F_d} = -\mathbf{0.2}\ \boldsymbol{N_{cr}^*}$
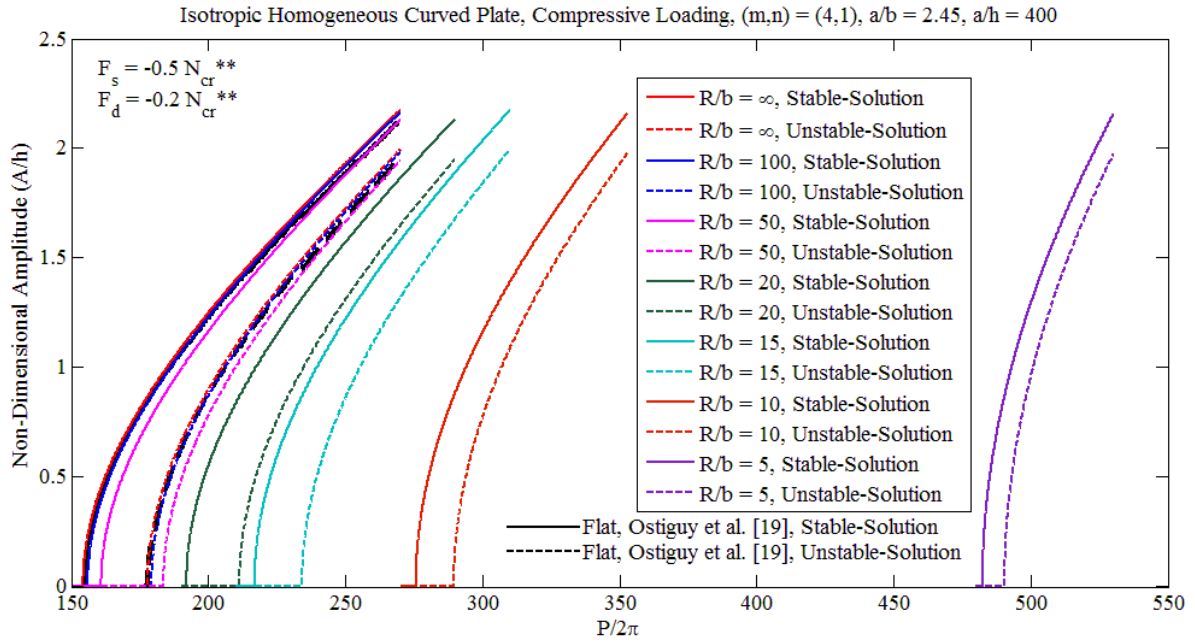
Figure 4.6 Comparison of both the stable- and unstable-solution amplitudes of steady-state vibrations of the present cylindrical panel with those of Ostiguy et al [19] for isotropic homogeneous rectangular plate in the mode $(m, n) = (4, 1)$, having aspect ratios of $a/h = 400$ and $a/b = 2.45$ subjected to periodic in-plane load having static component of $F_s = -0.5 N^*_{cr}$ and dynamic component of $F_d = -0.2 N^*_{cr}$
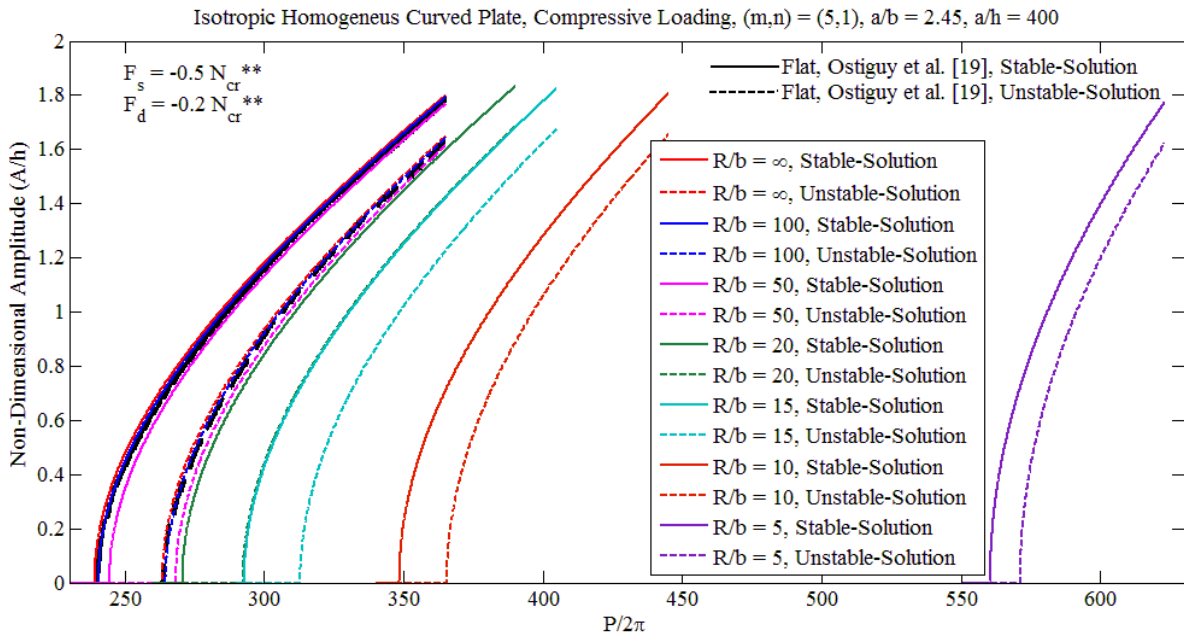
Figure 4.7 Comparison of both the stable- and unstable-solution amplitudes of steady-state vibrations of the present cylindrical panel with those of Ostiguy et al [19] for isotropic homogeneous rectangular plate in the mode $(m, n) = (5, 1)$, having aspect ratios of $a/h = 400$ and $a/b = 2.45$ subjected to periodic in-plane load having static component of $F_s = -0.5 N^*_{cr}$ and dynamic component of $F_d = -0.2 N^*_{cr}$

128
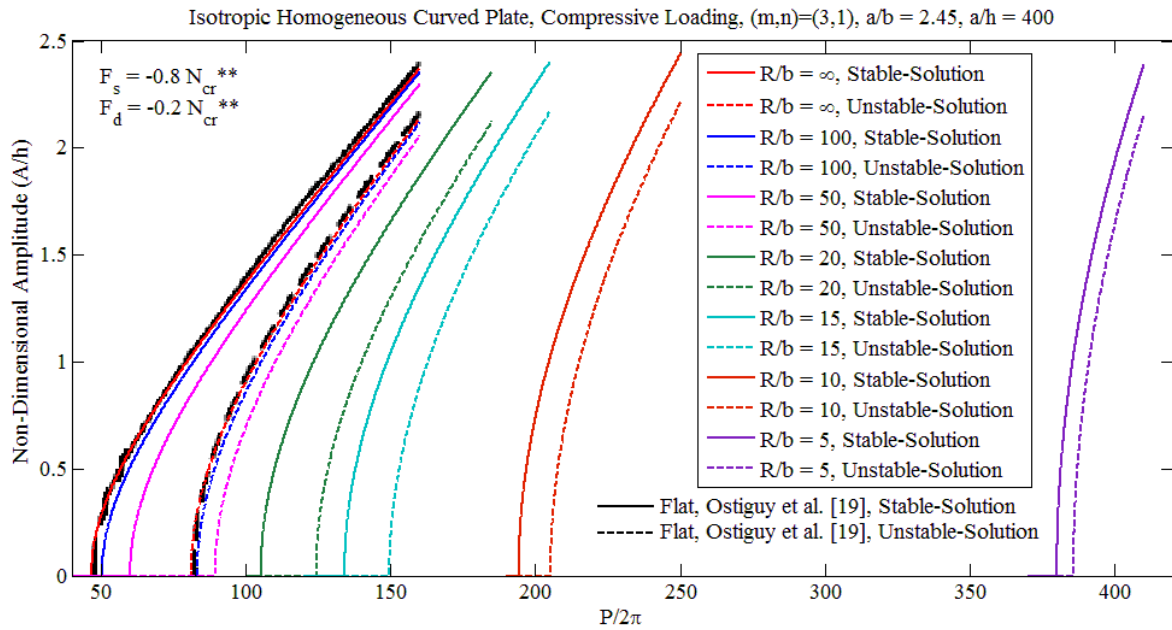
Figure 4.8 Comparison of both the stable- and unstable-solution amplitudes of steady-state vibrations of the present cylindrical panel with those of Ostiguy et al [19] for isotropic homogeneous rectangular plate in the mode $(m, n) = (3, 1)$, having aspect ratios of $a/h = 400$ and $a/b = 2.45$ subjected to periodic in-plane load having static component of $F_s = -0.8 \, N_{cr}^*$ and dynamic component of $F_d = -0.2 \, N_{cr}^*$
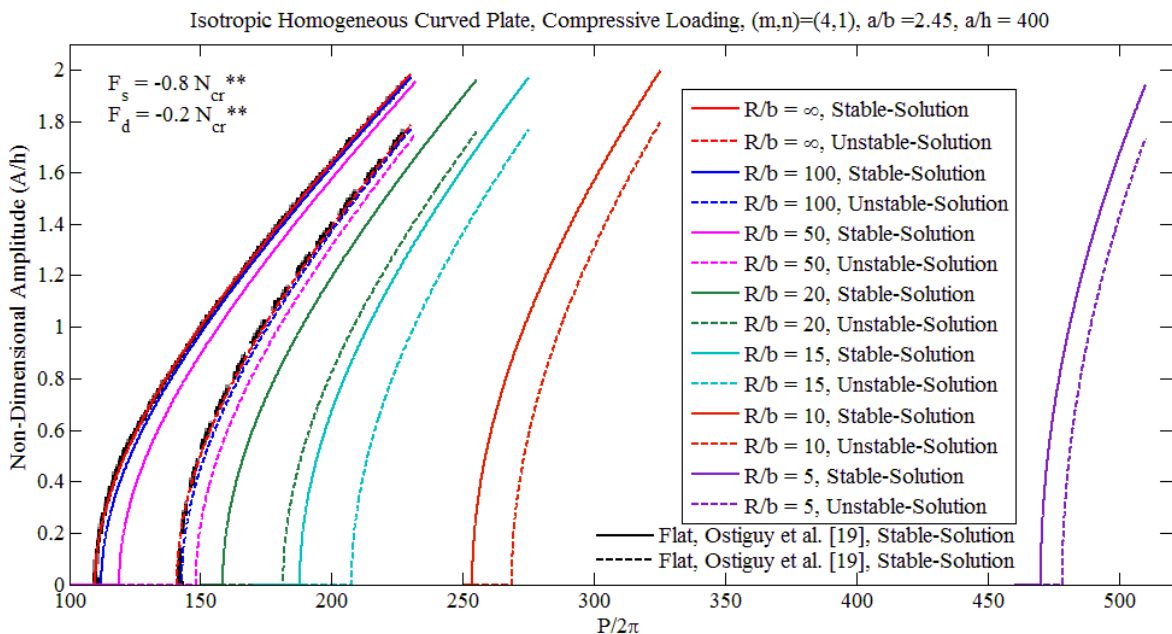
Figure 4.9 Comparison of both the stable- and unstable-solution amplitudes of steady-state vibrations of the present cylindrical panel with those of Ostiguy et al [19] for isotropic homogeneous rectangular plate in the mode $(m, n) = (4, 1)$, having aspect ratios of $a/h = 400$ and $a/b = 2.45$ subjected to periodic in-plane load having static component of $F_s = -0.8 \, N_{cr}^*$ and dynamic component of $F_d = -0.2 \, N_{cr}^*$
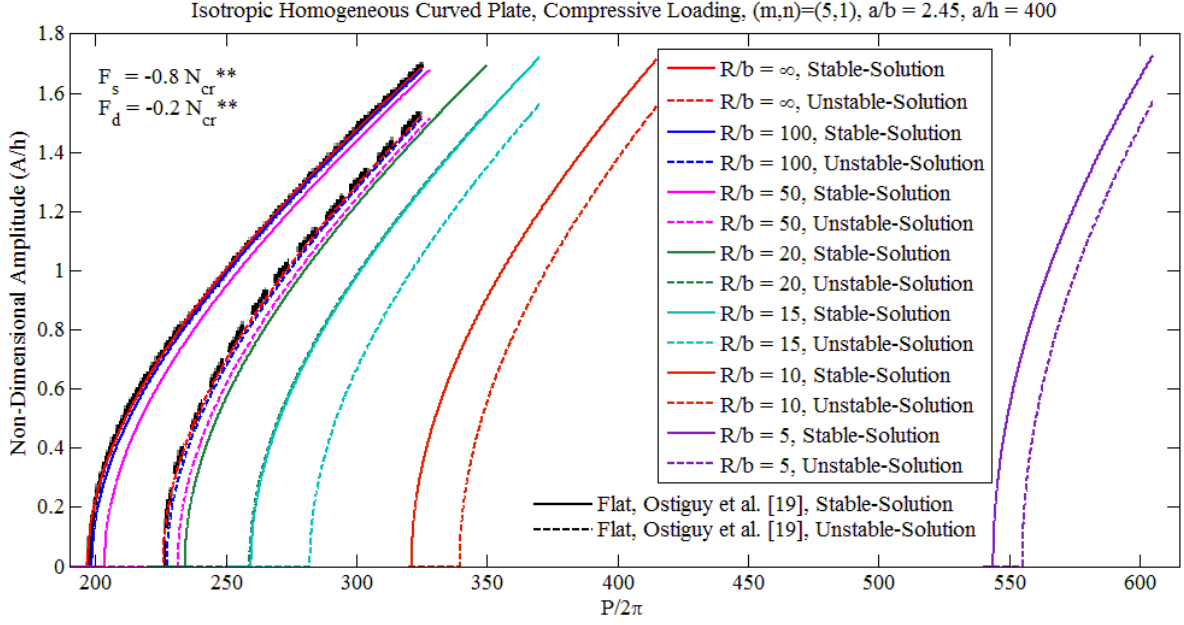
Figure 4.10 Comparison of both the stable- and unstable-solution amplitudes of steady-state vibrations of the present cylindrical panel with those of Ostiguy et al [19] for isotropic homogeneous rectangular plate in the mode $(m, n) = (5, 1)$, having aspect ratios of $a/h = 400$ and $a/b = 2.45$ subjected to periodic in-plane load having static component of $F_s = -0.8 \, N_{cr}^*$ and dynamic component of $F_d = -0.2 \, N_{cr}^*$

the plate as $a = 50 \, cm$, $b = 20.4 \, cm$ and $h = 0.125 \, cm$. Since there is only one layer in both

the left (thickest) and the right (thinnest) sides of the cylindrical tapered panel so the number

of layers in these two sides of the cylindrical tapered panel is the same, consequently the taper

angle is zero. Figures 4.5-4.7 are for the modes $(m, n) = (3,1)$, $(m, n) = (4,1)$, $(m, n) = (5,1)$, respectively where the static component of the periodic longitudinal load is $F_s = -0.5 \, N_{cr}^{**}$ and the dynamic component is $F_d = -0.2 \, N_{cr}^{**}$. Figures 4.8-4.10 are for the modes

$(m, n) = (3,1)$, $(m, n) = (4,1)$, $(m, n) = (5,1)$, respectively where in these figures the static

component of the periodic longitudinal load is $F_s = -0.8 \, N_{cr}^{**}$ and the dynamic component is

$F_d = -0.2 \, N_{cr}^{**}$ where N_{cr}^{**} in these figures is the buckling load according to Ostiguy et al [19]

as follow:

$$N_{cr}^{**} = \frac{\pi^2 D}{b^2} \left(m_c \frac{b}{a} + \frac{1}{m_c} \frac{a}{b} \right)^2 \tag{4.51a}$$

where

$$D = \frac{E h^3}{12(1 - v_{12}^2)} \tag{4.51b}$$

130

and m_c is the "number of half-waves of prevalent buckling mode" which "depends strongly on the aspect ratio of the plate" [19]. It is observed from these figures that increasing the radius of the cylindrical panel results that both stable- and unstable solution amplitude-frequency curve of steady-state vibrations shift to the left along the frequency axis having lower frequencies of excitation. This shifting to the left of frequency axis of the steady-state amplitude (increasing the amplitude at a certain excitation frequency) is fast for the smaller radius (larger curvature) i.e. $R/b = 5, 10, 15$ but very slightly approaches once the radius increases as $R/b = 20\ to\ 50$ and appears to converge at a certain value as can be observed from these figures that the amplitude-frequency curve of steady-state vibrations of $R/b = 100\ to\ \infty$ are too close to each other and almost completely coincide with each other and actually overlap the plot on the corresponding curve given by Ostiguy et al [19]. This gradual convergence by decreasing the curvature and coinciding with those by Ostiguy et al [19] for very small curvature of $R/b = 100$ and for completely flat plate i.e. $R/b = \infty$ validates the present study and shows an excellent agreement with Ostiguy et al [19] for all the different modes and loading conditions. The reason for the chosen modes and loading conditions is only due to the comparison of the present study with those available in the literature which is the article by Ostiguy et al [19] here.

4.6.2   Comparison of influences of various taper configurations

In Figs. 4.11-4.14 for the first-two modes, dynamically-unstable regions and stable solution amplitudes of steady-state vibrations of four different configurations of symmetric thickness-tapered cross-ply laminated cylindrical panel (as shown in Fig. 4.2) are compared together and with the uniform cylindrical panel. Here all those four taper configurations have 12 and 6 plies at the thick and thin section respectively and the uniform panel has 9 plies (which is the average of 12 and 6 plies) with the same length-to-average-thickness ratio i.e. $a/h_{av} = 100$, length-to-width ratio of $a/b = 2$ and the same radius-to-width ratio of $R/b = 2$.
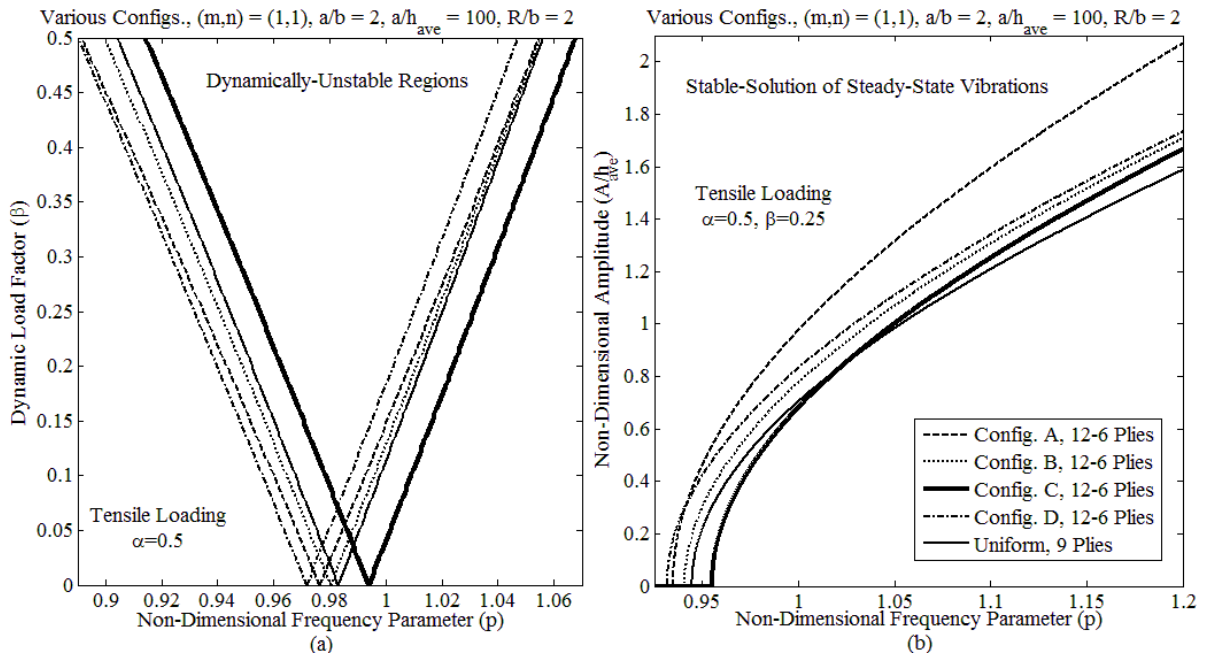
Figure 4.11 Comparison of various taper configurations, on the first mode a) unstable region and b) stable-solution amplitude of steady-state vibrations of a 12-6 layered symmetric cross-ply laminated thickness-tapered cylindrical panel subjected to the tensile periodic in-plane loading
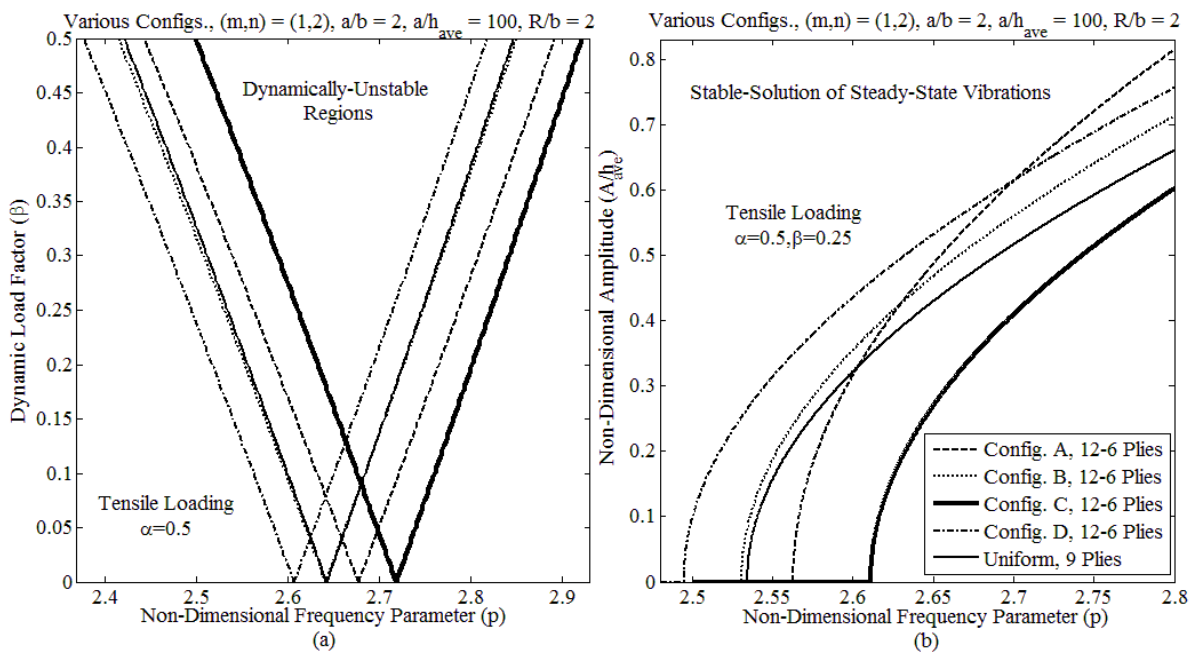
Figure 4.12 Comparison of various taper configurations, on the second mode a) unstable region and b) stable-solution amplitude of steady-state vibrations of a 12-6 layered symmetric cross-ply laminated thickness-tapered cylindrical panel subjected to the tensile periodic in-plane loading

132
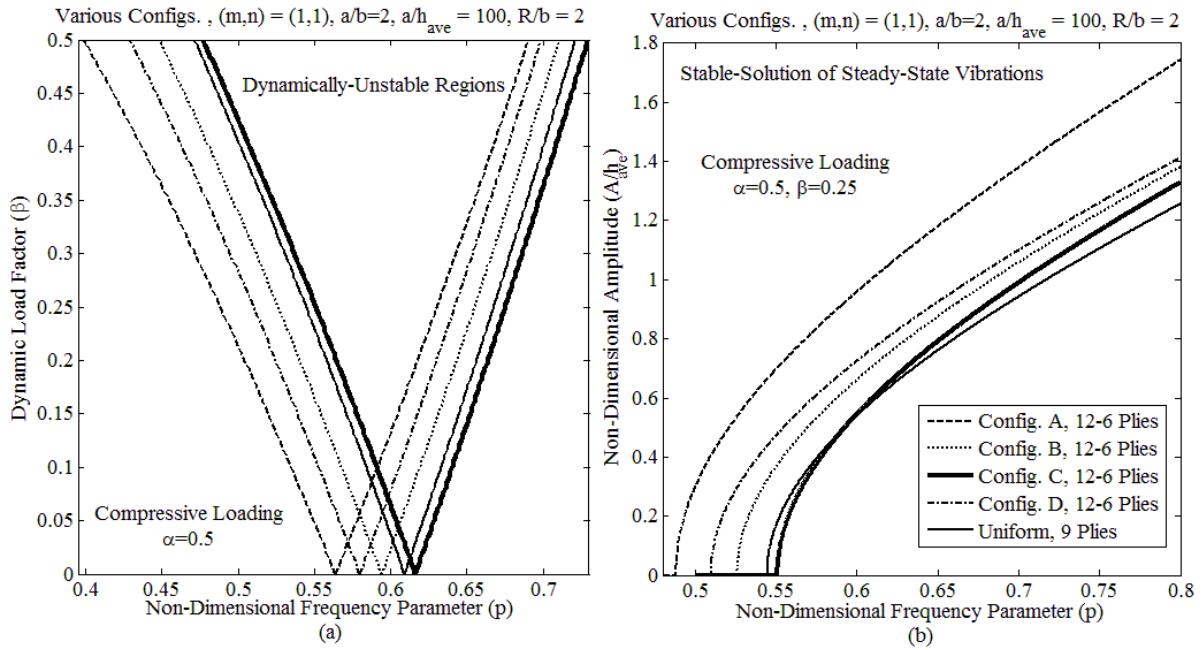
Figure 4.13 Comparison of various taper configurations, on the first mode a) unstable region and b) stable-solution amplitude of steady-state vibrations of a 12-6 layered symmetric cross-ply laminated thickness-tapered cylindrical panel subjected to the compressive periodic in-plane loading
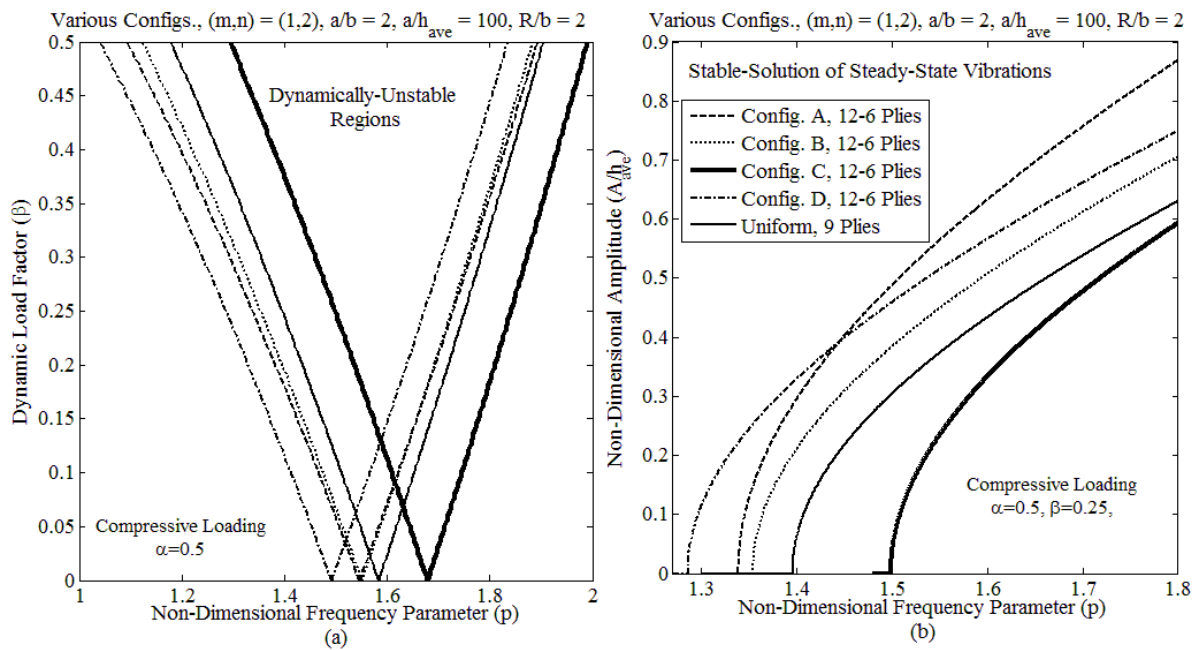
Figure 4.14 Comparison of various taper configurations, on the second mode a) unstable region and b) stable-solution amplitude of steady-state vibrations of a 12-6 layered symmetric cross-ply laminated thickness-tapered cylindrical panel subjected to the compressive periodic in-plane loading

133

Figures 4.11 and 4.12 correspond to the first-two modes, i.e. mode (1,1) and mode (1,2), under tensile in-plane pulsating load having static load factor of $\alpha = 0.5$. From here onwards in all figures the

amplitudes of the steady-state vibrations are plotted for the loading conditions having dynamic load factor of $\beta = 0.25$. The corresponding graphs for the compressive loading are represented in Fig. 4.13 and Fig. 4.14 respectively. It is also worthwhile to note here that in the tensile loading case we consider the absolute value of critical buckling load $|N_{cr}|$ for both static and dynamic components of the in-plane harmonically-pulsating load, while in the compressive case we use the actual value of critical buckling load N_{cr} which is negative with respect to the assigned coordinate system shown in Fig. 4.1. In the comparative study of various configurations, the applied in-plane harmonically pulsating load for all configurations and the uniform plate is based on the critical buckling load of the configuration A. Here and in the following figures and tables, the dimensionless excitation frequency parameter p is introduced as follow:

$$p = Pa\sqrt{\frac{\rho_c}{E_2}} \tag{4.52}$$

It is observed that thickness-tapered composite cylindrical panel having configuration C, has the highest frequency of excitation or in other words the most-shifted to the right along the frequency axis of both dynamically-unstable regions and amplitudes of steady-state vibrations among the other configurations. So consequently, it has the lowest amplitudes of steady-state vibrations at any specific excitation frequency. To provide a more detailed and a better comparison the corresponding results for the first-two modes of dynamically-unstable regions also are listed in Tables 4.2 and 4.3 corresponding to tensile and compressive in-plane loadings respectively. It is also observed from these figures and tables that configuration C has the smallest δ i.e. smallest width of the instability regions among all other configurations and uniform one except in the first mode i.e. mode (1,1) that uniform one is very slightly smaller

than configuration C. All of these observations are confirmed even when changing loading directions from tensile to compressive. Hence, configuration C shows the most rigidity among all configurations and this can be expected since in this configuration the resin pockets are located very close to mid-plane of the cylindrical panel and therefore its bending stiffnesses are less decreased due to the smaller bending stiffnesses of the resin pocket in comparison to the composite plies. It is also noted that although the amplitudes of steady-state vibrations of the configuration C in the initial stages of the excitation is lower than that of the uniform laminate, this trend is changed at the higher excitation frequencies that can be due to the existence of the resin pocket in configuration C while there isn't any such resin pocket in uniform cylindrical panel. Due to the less mass density of the resin (epoxy) to the graphite composite plies, overall it makes that the uniform cylindrical panel be heavier than the thickness-tapered laminates or particularly here the thickness-tapered laminate having configuration C (the total mass of plates having configuration A, B, C, D and the uniform panel with the same length-to-average-thickness ratio i.e. $a/h_{av} = 100$, length-to-width ratio of $a/b = 2$ and the radius-to-width ratio of $R/b = 2$ are 13.28, 13.88, 13.88, 13.88 and 14.18 grams, respectively. However it should be noted here that for the same size of uniform panel with 12 plies the total mass would be 18.91 grams.). So to summarize these, increasing the stiffnesses makes the instability regions or excitation to start at higher frequencies but at the same time reducing the weight of the structure causes the speed of increasing of the amplitudes of steady-state vibrations very slightly be increased. However, as can be observed from these figures once comparing both configuration C and uniform one at those higher excitation frequencies the increase of the amplitudes are very small. Therefore it is concluded that configuration C is the most stable laminated cylindrical panel under parametric excitation among all taper configurations and even uniform laminate.

Another observation from these figures and tables reveal that since configuration D has the lowest stiffness due to the location of the resin pockets far from the mid-plane, its dynamically-unstable regions or the parametric excitations start at the lowest frequencies except in the first mode i.e. mode (1,1) under compressive load that the dynamically-unstable region or the parametric excitations of configuration A starts at the lowest frequencies. But since configuration A has the lowest total weight due to the largest amount of the resin pockets in this configuration, its amplitudes of steady-state vibrations are increased much faster than any other configuration and consequently reach the highest amplitudes of steady-state vibrations at higher frequencies.

Table 4.2 Effects of various taper configurations on the first-two modes of the dynamically-unstable regions of a 12-6 layered symmetric cross-ply laminated cylindrical thickness-tapered panel subjected to the tensile periodic in-plane loading

Taper Configuration	Mode (1,1) of Dynamically-Unstable Region		Mode (1,2) of Dynamically-Unstable Region	
	Point of origin p ($\times 10^{-1}$)	δ ($\times 10^{-1}$)	Point of origin p ($\times 10^{-1}$)	δ ($\times 10^{-1}$)
A (12-6 Plies)	9.763303022	1.581653529	26.76816776	4.12239619
B (12-6 Plies)	9.802930381	1.510221573	26.41098446	4.012912881
C (12-6 Plies)	9.938445085	1.490670764	27.18273024	3.914163511
D (12-6 Plies)	9.716555286	1.522945597	26.06792482	4.058302518
Uniform (9 Plies)	9.829966074	1.475642672	26.42380154	3.936854735

Table 4.3 Effects of various taper configurations on the first-two modes of the dynamically-unstable regions of a 12-6 layered symmetric cross-ply laminated cylindrical thickness-tapered panel subjected to the compressive periodic in-plane loading

Taper Configuration	Mode (1,1) of Dynamically-Unstable Region		Mode (1,2) of Dynamically-Unstable Region	
	Point of origin p ($\times 10^{-1}$)	δ ($\times 10^{-1}$)	Point of origin p ($\times 10^{-1}$)	δ ($\times 10^{-1}$)
A (12-6 Plies)	5.636845628	2.602393063	15.45460886	6.306150135
B (12-6 Plies)	5.93956602	2.389706164	15.50369371	6.095758611
C (12-6 Plies)	6.160656719	2.314283771	16.78467282	5.762438002
D (12-6 Plies)	5.79589916	2.441220958	14.911778	6.260495975
Uniform (9 Plies)	6.089968055	2.292536076	15.83199303	5.913413684

4.6.3   Effects of magnitude and direction of in-plane loads

Figures 4.15-4.18 show the effects of the amplitudes of the tensile and compressive in-plane harmonically pulsating load on the dynamically-unstable regions (Figs. 4.15a-4.18a) and the
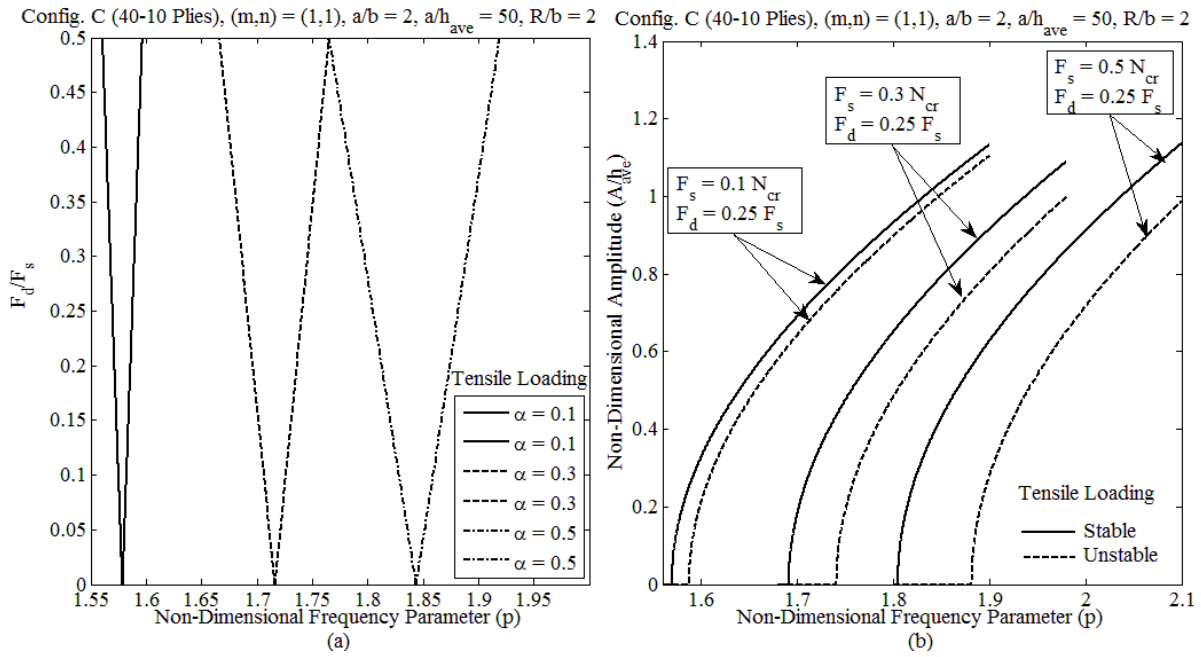
Figure 4.15 Effects of the amplitude of tensile in-plane harmonically pulsating loads, on the first mode a) unstable region and b) stable-solution amplitude of steady-state vibrations of a 40-10 layered symmetric cross-ply laminated thickness-tapered cylindrical panel having configuration C
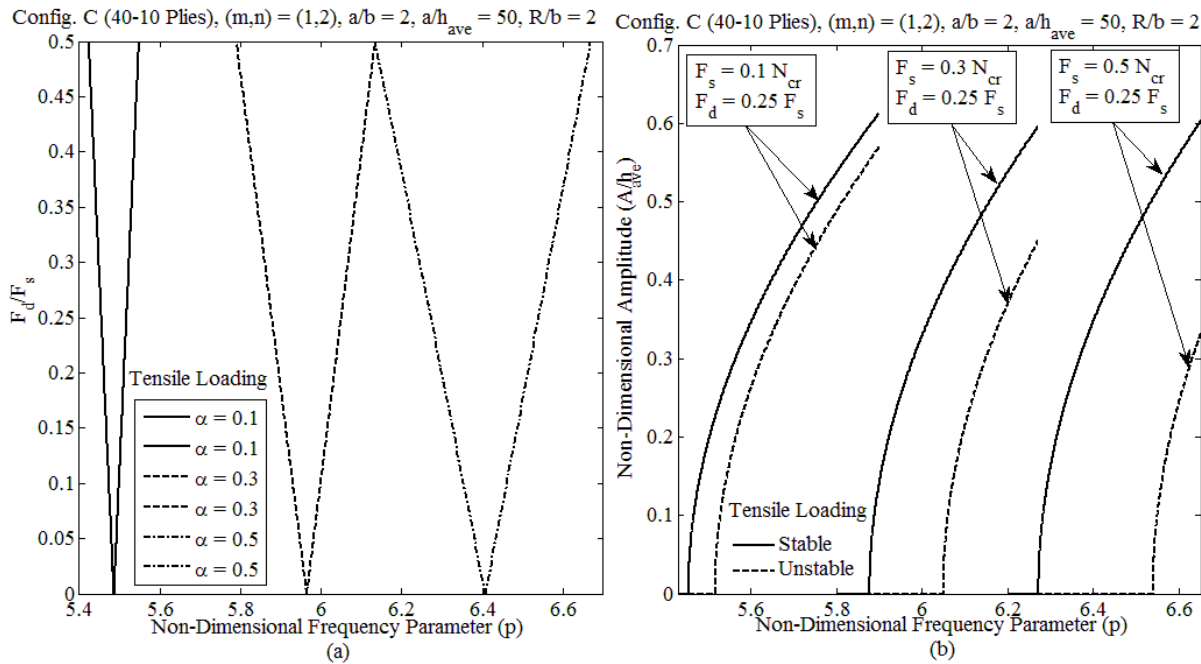
Figure 4.16 Effects of the amplitude of tensile in-plane harmonically pulsating loads, on the second mode a) unstable region and b) stable-solution amplitude of steady-state vibrations of a 40-10 layered symmetric cross-ply laminated thickness-tapered cylindrical panel having configuration C
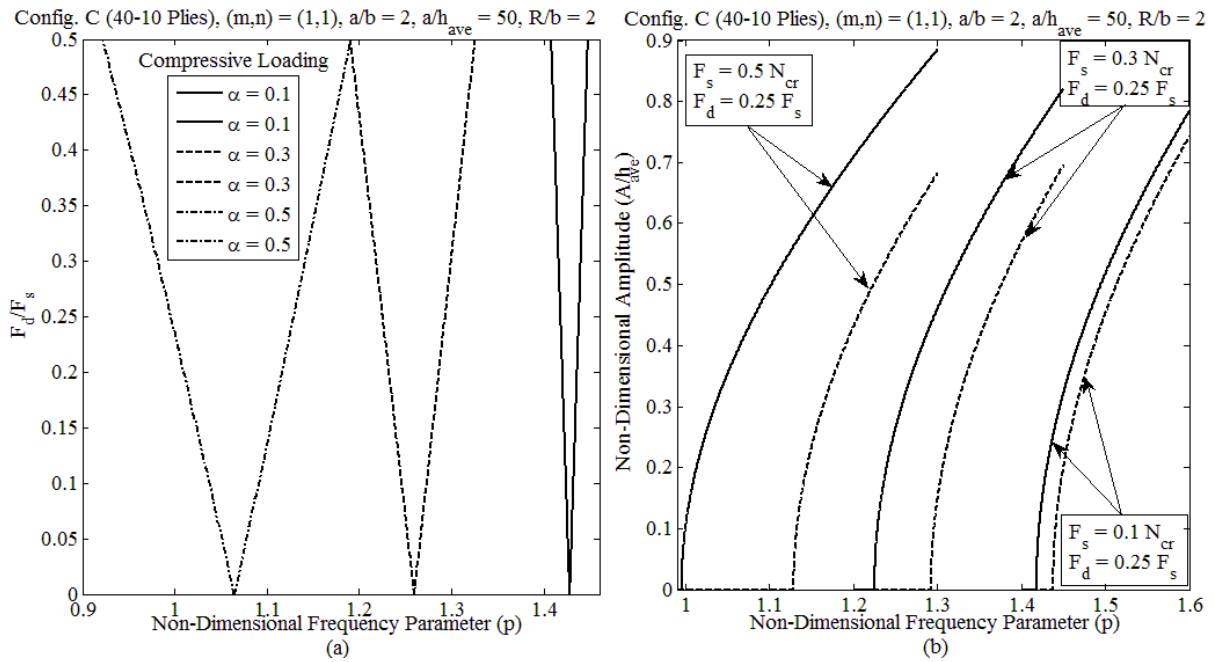
Figure 4.17 Effects of the amplitude of compressive in-plane harmonically pulsating loads, on the first mode a) unstable region and b) stable-solution amplitude of steady-state vibrations of a 40-10 layered symmetric cross-ply laminated thickness-tapered cylindrical panel having configuration C
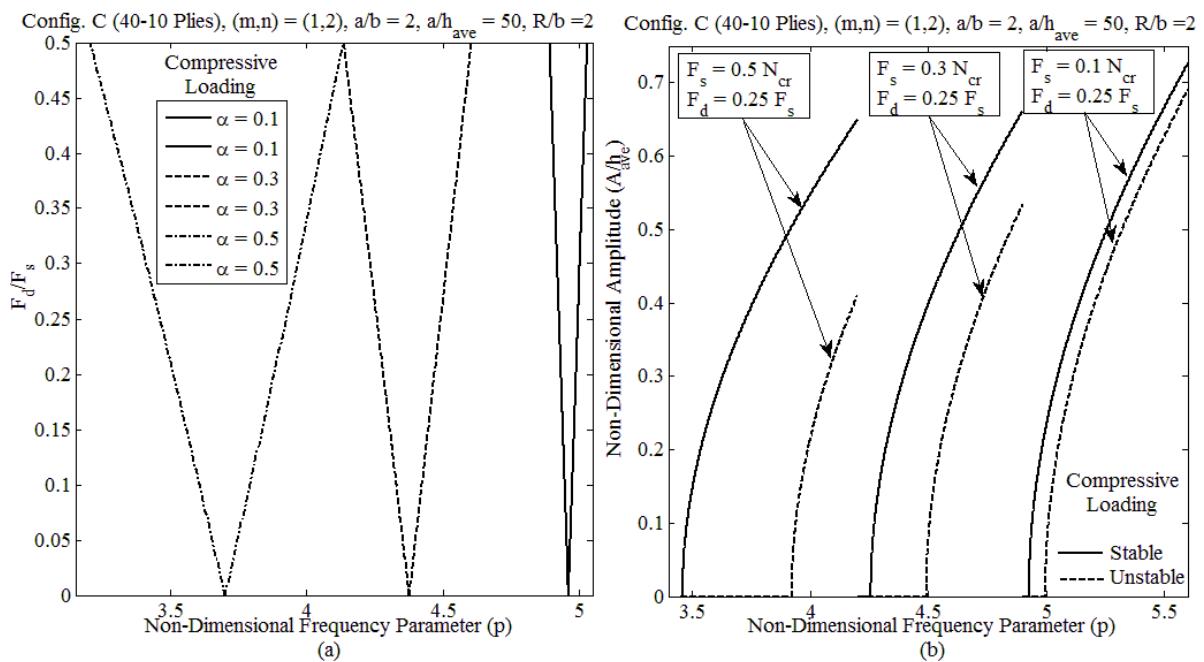
Figure 4.18 Effects of the amplitude of compressive in-plane harmonically pulsating loads, on the second mode a) unstable region and b) stable-solution amplitude of steady-state vibrations of a 40-10 layered symmetric cross-ply laminated thickness-tapered cylindrical panel having configuration C

138

stable-solution amplitudes of the steady-state vibrations (Figs. 4.15b-4.18b), respectively. Here the graphs are plotted for thickness-tapered laminated cylindrical panel with configuration C having 40 and 10 plies at the thickest and the thinnest sides, respectively. Therefore according to the Eq. (4.17) this reduction of the plies from 40- to 10-plies are performed in 15 steps. The depicted graphs are for three different loading amplitudes having static load factors of $= 0.1$, $\alpha = 0.3$ and $\alpha = 0.5$ respectively. In all these three cases of loadings for both the tensile and compressive load conditions the thickness-tapered laminated cylindrical panel has aspect and thickness ratios of $a/b = 2$ and $a/h_{av} = 50$, respectively and radius-to-width ratio of $R/b = 2$, and also the graphs have been depicted for the first-two modes i.e. the modes (1,1) and (1,2). From Figs. 4.15 and 4.16 it can be realized that increasing the magnitude of the tensile in-plane loading results in shifting the instability regions to the higher frequencies along the frequency axis (Fig. 4.15a and 4.16a), and consequently decreasing the stable-solution amplitudes of steady-state vibrations (Figs. 4.15b and 4.16b). However increasing the magnitude of the compressive in-plane loading results in shifting the instability regions to the lower frequencies along the frequency axis (Fig. 4.17a and 4.18a), and consequently increasing the stable-solution amplitudes of the steady-state vibrations (Fig. 4.17b and 4.18b). These outcomes can be expected because increasing the tensile in-plane load makes the cylindrical panel to be stiffer, and contrarily increasing the compressive in-plane load results in decreasing the cylindrical panel's stiffness. Also it can be observed from these figures (Figs. 4.16a-4.18a) that the width of instability regions are increased once the absolute value of magnitude of in-plane loads are increased for both tensile and compressive loading conditions. All these outcomes are in an excellent conformance with those reported by Ng et al. [21] for the dynamic instability of cylindrical shells where their analysis are based on linear analysis and consequently limited to only the dynamically-unstable regions so their results and corresponding outcomes are for only instability regions and not the amplitudes of the steady-state vibrations at this regions.

4.6.4 Effects of taper angle

One of the most important parameters in the design of thickness-tapered panels is the taper angle ϕ. Decreasing the length of the thickness-tapered panel makes the taper angle to increase but it is clear that decreasing the length of the panel and keeping the thickness of the thickness-tapered panel unchanged, the overall length-to-thickness ratio is changed while this ratio is also another important parameter for both uniform and thickness-tapered panels that should be investigated independently. Here to avoid this interference of these two important parameters i.e. taper angle and length-to-thickness ratio we introduce the following formulation which only changes the taper angles by keeping the length-to-average-thickness ratio as constant:

$$\phi = \tan^{-1}((N_L - N_R)/((a/h_{av})(N_L + N_R)))$$ (4.53)

Hence by keeping the a/h_{av} ratio as constant in this equation and changing the number of plies at the thickest (here the left) and the thinnest (here the right) sides of the thickness-tapered cylindrical panel respectively, the taper angle is changed without changing the length-thickness ratio. Variation of both the length a and the thickness h do not influence the response of the structure if the overall length-thickness ratio remains unchanged. Here to study the effect of taper angle we keep the number of plies at the thickest side of the taperd plate $N_L = 40$ for all cases and by decresing the number of plies at the thinnest side of the taperd plate i.e. N_R while we keep the length-to-average-thickness ratio as constant as $a/h_{av} = 10$ in Figs. 4.19-4.22 and Tables 4.4-4.7, the taper angle is increased. It is also noted here that by knowing the number of plies at the thickest and the thinnest sides and also the ply thickness h_p, the h_{av} of the thickness-tapered cylindrical panel can be obtained. Then considering the length of the cylindrical panel as $a = 10h_{av}$, the length of the cylindrical panel is also determined; consequently setting $b = 2a$ and $R = 2b$ we keep the loaded-to-unloaded width ratio (a/b) and radius-to-width ratio (R/b) unchanged, respectively. The effects of the taper angle on both

Figure 4.19 Effects of the taper angle on the first mode a) unstable region and b) stable-solution amplitude of steady-state vibrations of symmetric cross-ply laminated thickness-tapered cylindrical panels having configuration C, aspect ratios of $a/b = 2$ and $a/h_{av} = 10$, and radius-to-width ratio of $R/b = 2$ subjected to the tensile periodic in-plane loading
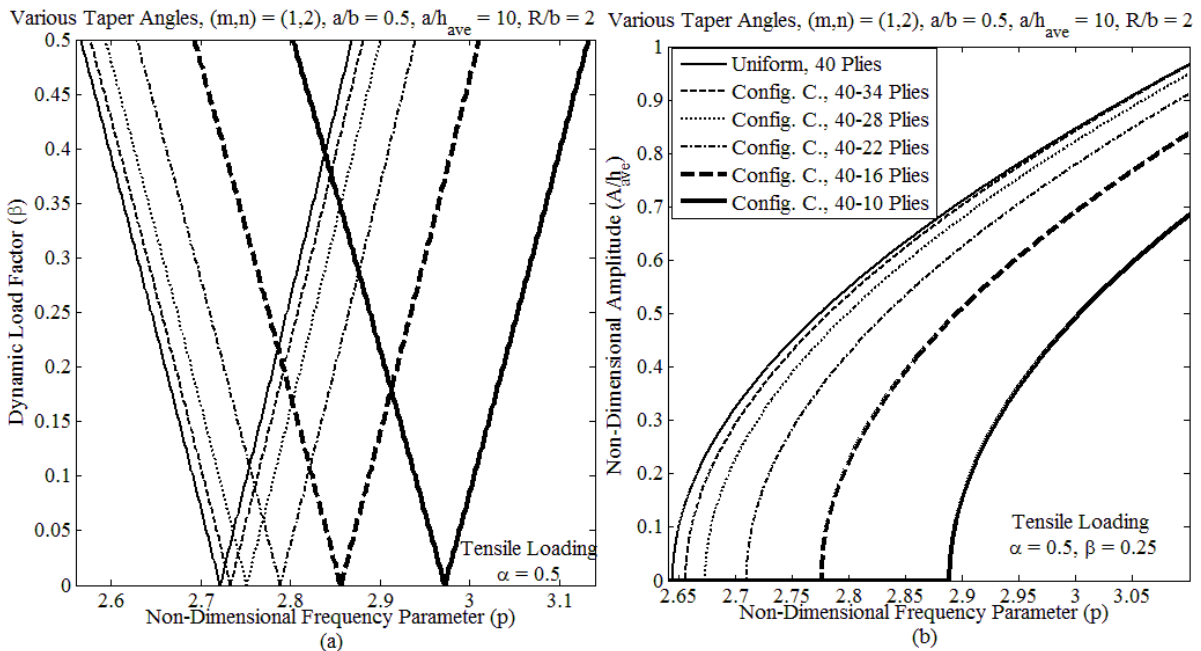
Figure 4.20 Effects of the taper angle on the second mode a) unstable region and b) stable-solution amplitude of steady-state vibrations of symmetric cross-ply laminated thickness-tapered cylindrical panels having configuration C, aspect ratios of $a/b = 2$ and $a/h_{av} = 10$, and radius-to-width ratio of $R/b = 2$ subjected to the tensile periodic in-plane loading

141
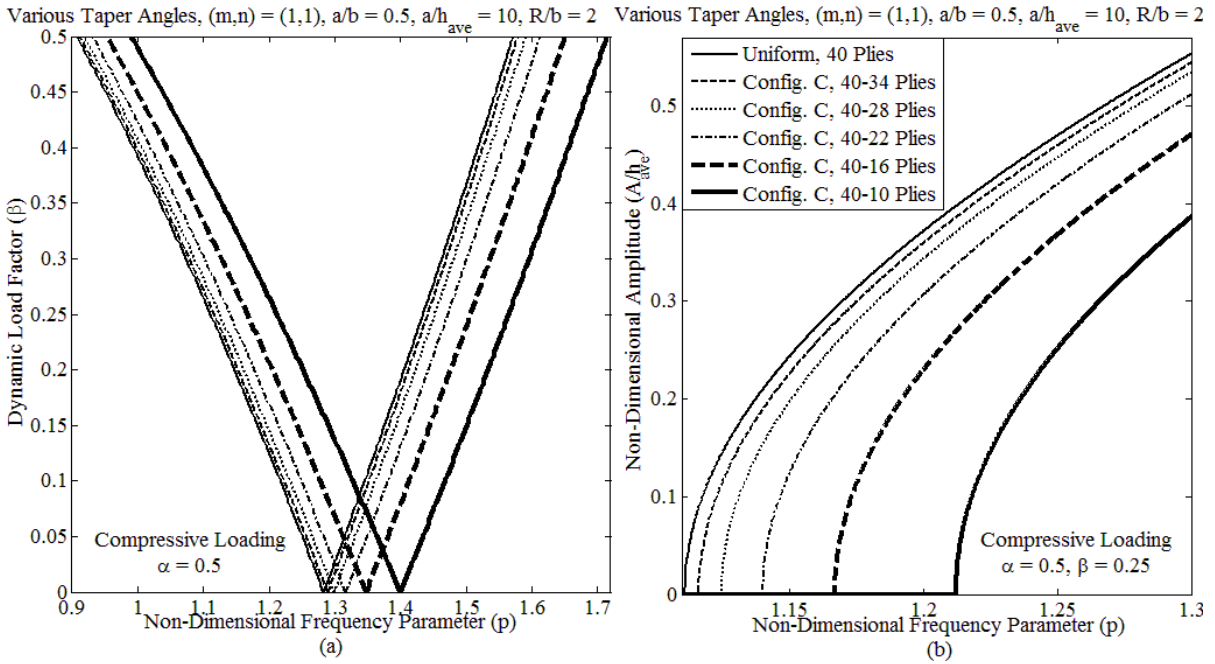
Figure 4.21 Effects of the taper angle on the first mode a) unstable region and b) stable-solution amplitude of steady-state vibrations of symmetric cross-ply laminated thickness-tapered cylindrical panels having configuration C, aspect ratios of $a/b = 2$ and $a/h_{av} = 10$, and radius-to-width ratio of $R/b = 2$ subjected to the compressive periodic in-plane loading
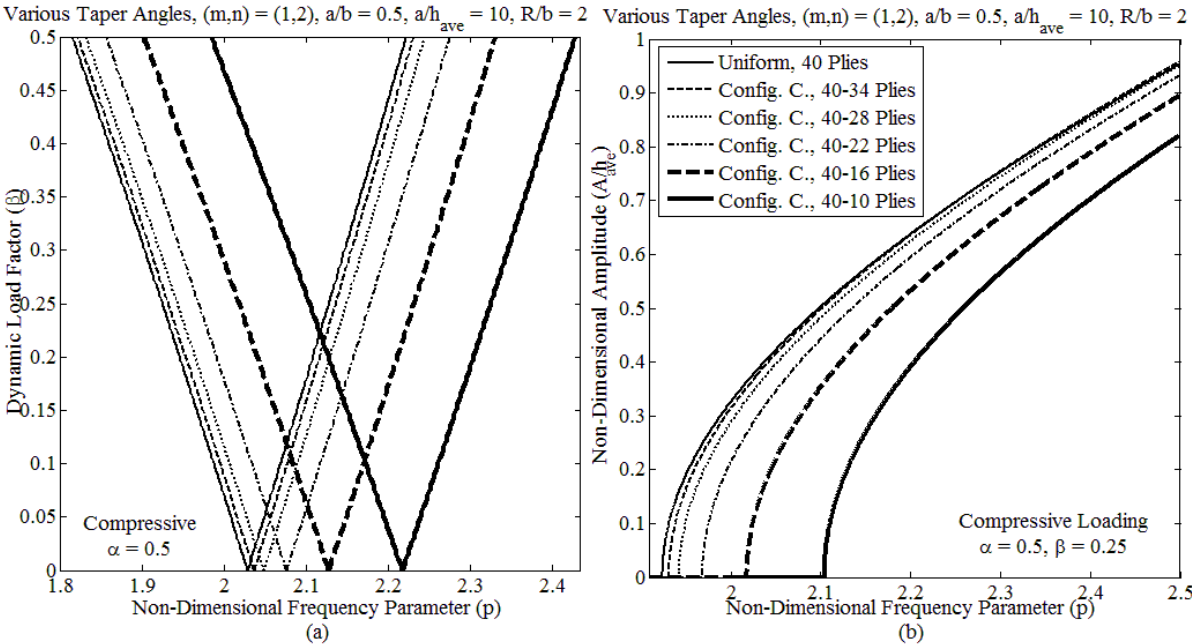
Figure 4.22 Effects of the taper angle on the second mode a) unstable region and b) stable-solution amplitude of steady-state vibrations of symmetric cross-ply laminated thickness-tapered cylindrical panels having configuration C, aspect ratios of $a/b = 2$ and $a/h_{av} = 10$, and radius-to-width ratio of $R/b = 2$ subjected to the compressive periodic in-plane loading

Table 4.4 Effects of the taper angle on the first mode dynamically-unstable region of symmetric cross-ply laminated thickness-tapered cylindrical panel having configuration C aspect ratios of $a/b = 2$ and $a/h_{av} = 10$, and radius-to-width ratio of $R/b = 2$ subjected to the tensile periodic in-plane loading

Plate Configuration	Tap. Angle ϕ^o ($\times 10^{-1}$)	$-(N_{cr})_{ND}$	Point of origin p ($\times 10^{-1}$)	δ ($\times 10^{-1}$)
Uniform (40 Plies)	0.00000	0.584591658	22.22165	3.42094
C (40-34 Plies)	4.64550	0.587117143	22.32675	3.43588
C (40-28 Plies)	10.10997	0.595681653	22.49410	3.45964
C (40-22 Plies)	16.62959	0.611819331	22.80294	3.50337
C (40-16 Plies)	24.54032	0.640578634	23.34040	3.57914
C (40-10 Plies)	34.33630	0.690443031	24.24172	3.70524

* Non-dimensional critical buckling load, $(N_{cr})_{ND} = (N_{cr}a^2)/(E_1 h_{av}^3)$

Table 4.5 Effects of the taper angle on the second mode dynamically-unstable region of symmetric cross-ply laminated thickness-tapered cylindrical panel having configuration C aspect ratios of $a/b = 2$ and $a/h_{av} = 10$, and radius-to-width ratio of $R/b = 2$ subjected to the tensile periodic in-plane loading

Plate Configuration	Tap. Angle ϕ^o ($\times 10^{-1}$)	$-(N_{cr})_{ND}$	Point of origin p ($\times 10^{-1}$)	δ ($\times 10^{-1}$)
Uniform (40 Plies)	0.00000	0.584591658	27.21238	2.86376
C (40-34 Plies)	4.64550	0.587117143	27.32758	2.87785
C (40-28 Plies)	10.10997	0.595681653	27.50923	2.90043
C (40-22 Plies)	16.62959	0.611819331	27.88241	2.93843
C (40-16 Plies)	24.54032	0.640578634	28.55980	3.00175
C (40-10 Plies)	34.33630	0.690443031	29.72121	3.10501

* Non-dimensional critical buckling load, $(N_{cr})_{ND} = (N_{cr}a^2)/(E_1 h_{av}^3)$

Table 4.6 Effects of the taper angle on the first mode of dynamically-unstable region of symmetric cross-ply laminated thickness-tapered cylindrical panel having configuration C aspect ratios of $a/b = 2$ and $a/h_{av} = 10$, and radius-to-width ratio of $R/b = 2$ subjected to the compressive periodic in-plane loading

Plate Configuration	Tap. Angle ϕ^o ($\times 10^{-1}$)	$(N_{cr})_{ND}$	Point of origin p ($\times 10^{-1}$)	δ ($\times 10^{-1}$)
Uniform (40 Plies)	0.00000	-0.584591658	12.82967	5.23096
C (40-34 Plies)	4.64550	-0.587117143	12.89035	5.25141
C (40-28 Plies)	10.10997	-0.595681653	12.98698	5.28386
C (40-22 Plies)	16.62959	-0.611819331	13.16528	5.34343
C (40-16 Plies)	24.54032	-0.640578634	13.47559	5.44610
C (40-10 Plies)	34.33630	-0.690443031	13.99596	5.61545

* Non-dimensional critical buckling load, $(N_{cr})_{ND} = (N_{cr}a^2)/(E_1 h_{av}^3)$

Table 4.7 Effects of the taper angle on the second mode dynamically-unstable region of symmetric cross-ply laminated thickness-tapered cylindrical panel having configuration C aspect ratios of $a/b = 2$ and $a/h_{av} = 10$, and radius-to-width ratio of $R/b = 2$ subjected to the compressive periodic in-plane loading

Plate Configuration	Tap. Angle ϕ^o ($\times 10^{-1}$)	$(N_{cr})_{ND}$	Point of origin p ($\times 10^{-1}$)	δ ($\times 10^{-1}$)
Uniform (40 Plies)	0.00000	-0.584591658	20.28085	3.69520
C (40-34 Plies)	4.64550	-0.587117143	20.35864	3.71387
C (40-28 Plies)	10.10997	-0.595681653	20.48010	3.74391
C (40-22 Plies)	16.62959	-0.611819331	20.75523	3.79147
C (40-16 Plies)	24.54032	-0.640578634	21.27156	3.86818
C (40-10 Plies)	34.33630	-0.690443031	22.17152	3.99074

* Non-dimensional critical buckling load, $(N_{cr})_{ND} = (N_{cr}a^2)/(E_1 h_{av}^3)$

dynamically-unstable regions and the stable-solution amplitudes of steady-state vibartions are shown in Figs. 4.19-4.22 that correspond to the first two modes of the cylindrical panel subjected to the tensile and compressive in-plane periodic loadings, respectivly. To more clearly compare the dynamic instability regions particularlly the width of dynamically-unstable regions the tabular presentation is also provided in the Tables 4.4-4.7 corresponding to the first two modes of dynamic intability of the cylindrical panel subjected to the tensile and compressive loadings, respectivly. In those tables the variation of taper angles from zero (uniform) to that for the most tapered panel which is cylindrical panel having 40 and 10 plies at the thickest and thinest sides respectivly are listed and corresponding buckling loads as well. Although we consider the static load factor $\alpha = 0.5$ for all these six taper ratios i.e. 40-40, 40-34, 40-28, 40-22, 40-16 and 40-10 plies, it should be noted that corresponding dimensionless critical bucklig loads, i.e. $(N_{cr})_{ND}$, which is $N_{cr}a^2/E_1\,h_{av}{}^3$, are also increased. For the second mode i.e. mode $(1,2)$ the loading is considered based on the critical bucklig loads which actually corresponds to the first mode $(1,1)$ so it means that the loading conditions in both tensile and compressive cases are the same for both first two modes. Both tensile (Figs. 4.19 and 4.20 and Tables 4.4 and 4.5) and compressive (Figs. 4.21 and 4.22 and Tables 4.6 and 4.7) loadings confirm that increasing the taper angle causes shifting the dynamically-unstable regions to the higher frequencies along the frequency axis (Figs. 4.19a-4.22a, Tables 4.4-4.7), and consequently decreasing the stable-solution amplitudes of the steady-state vibrations (Figs. 4.19b-4.22b) and also increasing very slightly the widths of dynamically-unstable regions (Figs. 4.19a-4.22a, Tables 4.4-4.7). This is due to the fact that increasing taper angles results in higher stiffness of the cylindrical panel. Another important outcome of these figures and tables is that these variations of dynamic instability response, highly deviate from thickness-tapered cylindrical panel having 40-10 to 40-16 and 40-22 plies but it shows the convergence

of the response of the thickness-tapered cylindrical panel having 40-28 plies and 40-34 plies with the uniform laminated cylindrical panel having 40 plies.

4.6.5   Variation of curvature

Figures 4.23 and 4.24 present the effects of the radius-to-width ratio on the first mode dynamic instability of thickness-tapered squer cylindrical panel subjected to the tensile and compressive periodic in-plane loadings, respectively. Here b is kept constant and the radius of the square cylindrical panel is varied and the length-to-average-thickness ratio is $a/h_{ave} = 50$. We keep the static load factor $\alpha = 0.5$ for all these five radius-to-width ratios i.e., $R/b = 1, 3, 5, 10 \ and \ \infty$ (flat plate) and the critical buckling load is the same for all those five cylindrical panels and corresponds to the critical buckling load of the flat plate. We can clearly observe from these figures that in both tensile and compressive loading cases decreasing the curvature or increasing the overal radius-to-width of the laminated tapered cylindrical panel results in shifting dynamically-unstable regions to the left along the frequenccy axis having lower frequencies of excitations of origins (Figs. 4.23a and 4.24a), increasing the width of instability regions (Figs. 4.23a and 4.24a) and also increasing the amplitudes of steady-state vibrations at any specific frequency (Figs. 4.23b and 4.24b). These behaviors confirm the corresponding conclusions of Ref. [39] for dynamically-unstable regions of uniform curved panels. However their study, corresponding results and conclusions are only about the dynamically-unstable regions based on the linear analysis done in their works. It is to be noted that the amplitude of steady-state vibrations in the dynamically-unstable regions can only be determined by a non-linear analysis, as is done in the present work. Results of the present sub-section also confirm that increasing the curvature of the laminated tapered cylindrical panel makes the panel stiffer.
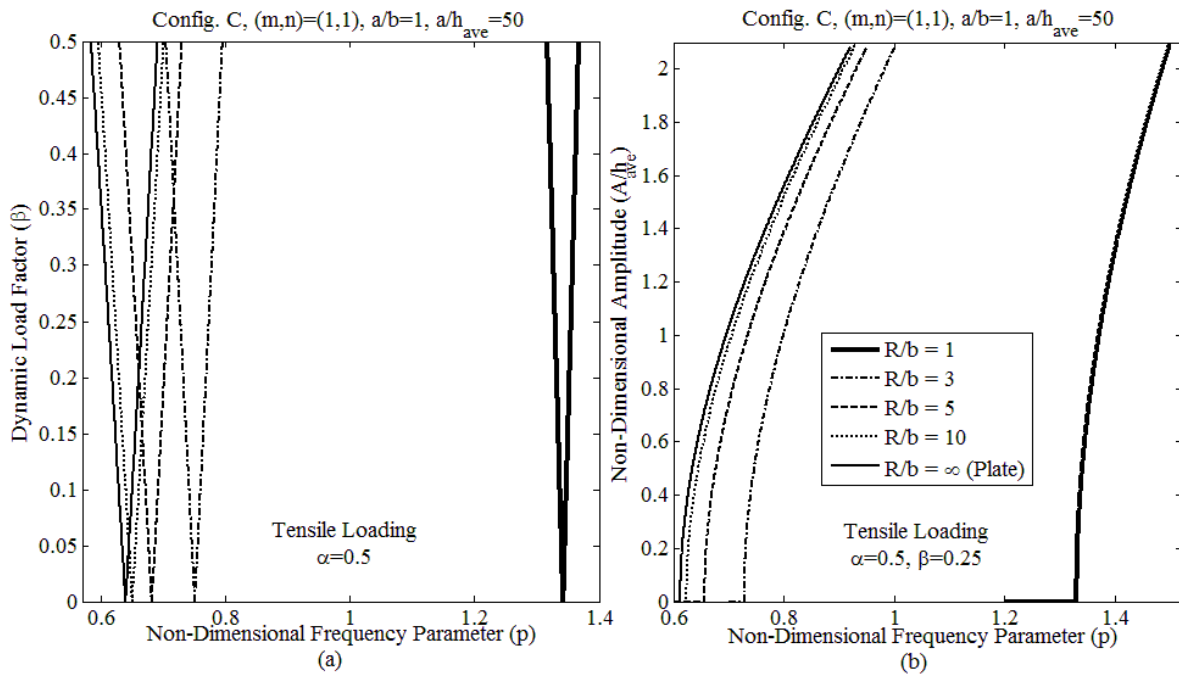
Figure 4.23 Effects of the variation of curvature on the first mode a) unstable region and b) stable-solution amplitude of steady-state vibrations of symmetric cross-ply laminated thickness-tapered square cylindrical panels having configuration C, length-to-thickness ratios of $a/h_{av} = 10$ subjected to the tensile periodic in-plane loading
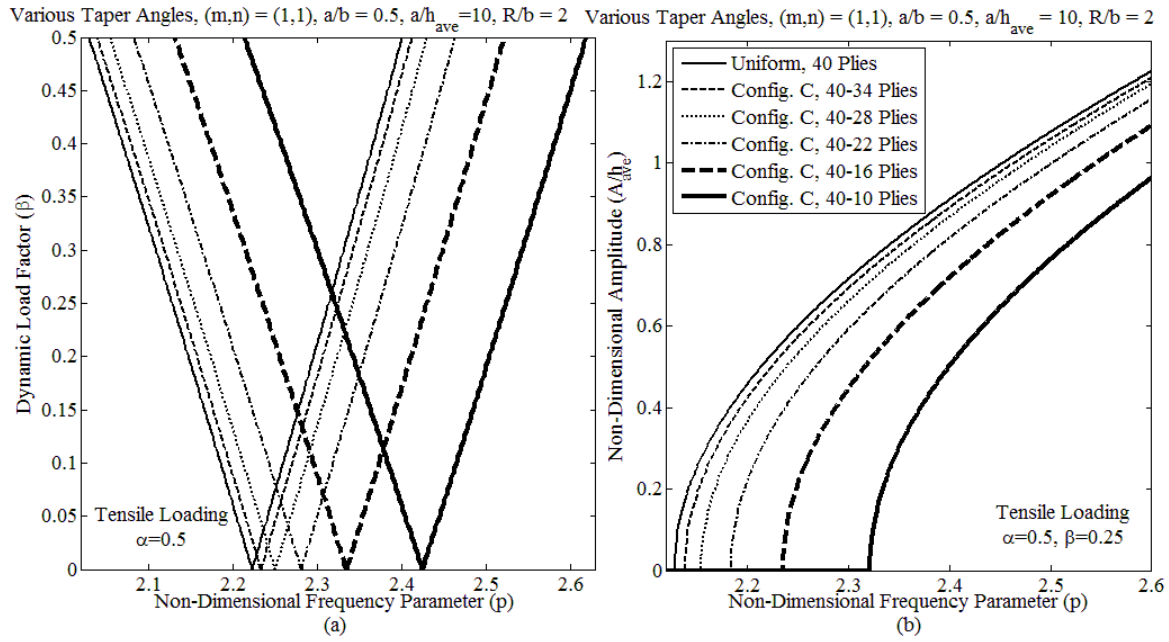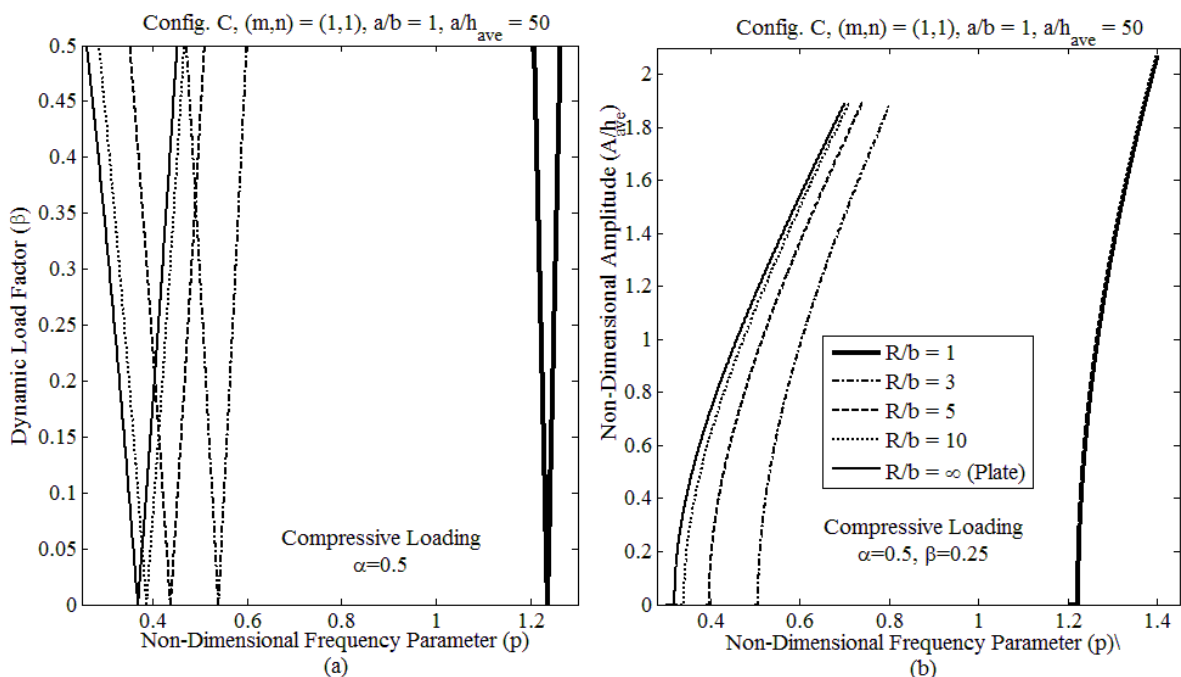

Figure 4.24 Effects of the variation of curvature on the first mode a) unstable region and b) stable-solution amplitude of steady-state vibrations of symmetric cross-ply laminated thickness-tapered square cylindrical panels having configuration C, length-to-thickness ratios of $a/h_{av} = 10$ subjected to the compressive periodic in-plane loading

146

4.6.6 Effect of the loaded-to-unloaded width ratio

Here in Figs. 4.25 and 4.26 corresponding to the tensile and compressive periodic in-plane loadings, respectively we examine the effect of width-to-length aspect ratio b/a which is the ratio of the width of loaded edge to the width of unloaded edge on the dynamic instability of thickness-tapered cylindrical panel with configuration C having 40-10 plies. The length a is kept constant and the width b is varied; the length-to-average-thickness ratio and the radius-to-width ratio are $a/h_{av} = 50$ and $R/b = 2$, respectively. Again we keep the static load factor $\alpha = 0.5$ for all these six aspect ratios i.e. $b/a = 2, 1, 2/3, 0.5, 2/5 \ and \ 1/3$. It should be noted
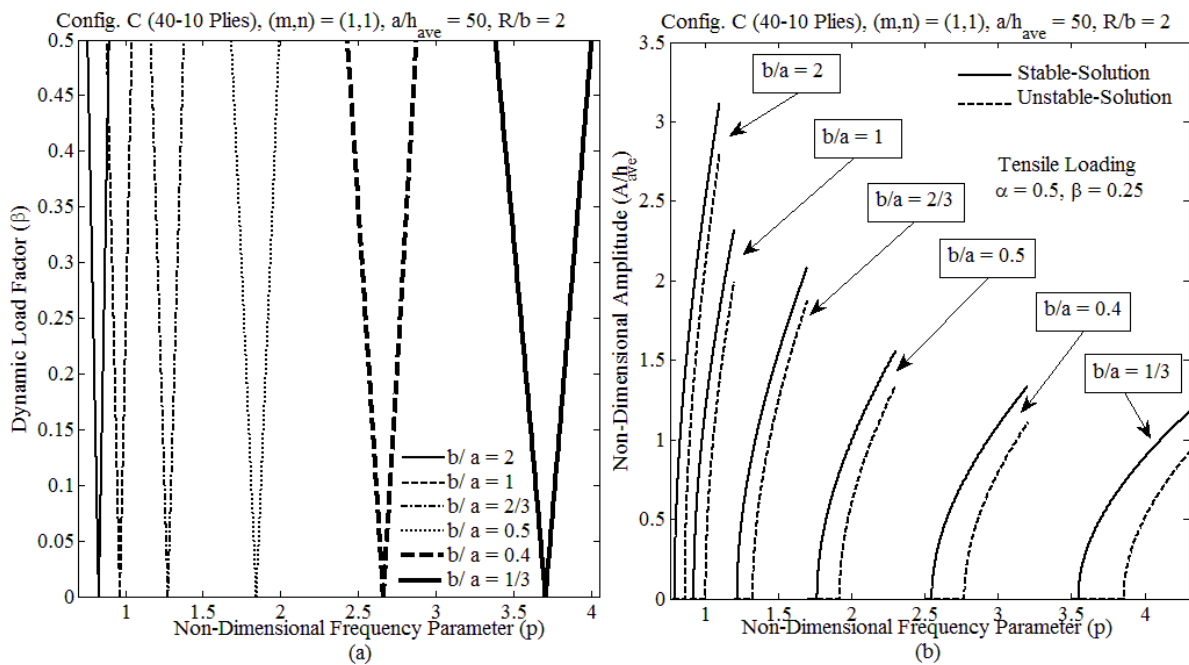
Figure 4.25 Effects of the variation of the loaded-to-unloaded width ratio, on the first mode a) unstable region and b) both stable-and unstable-solution amplitude of steady-state vibrations of 40-10 layered symmetric cross-ply laminated thickness-tapered cylindrical panel having configuration C, $a/h_{av} = 50$ and $R/b = 2$ subjected to the tensile periodic in-plane loading
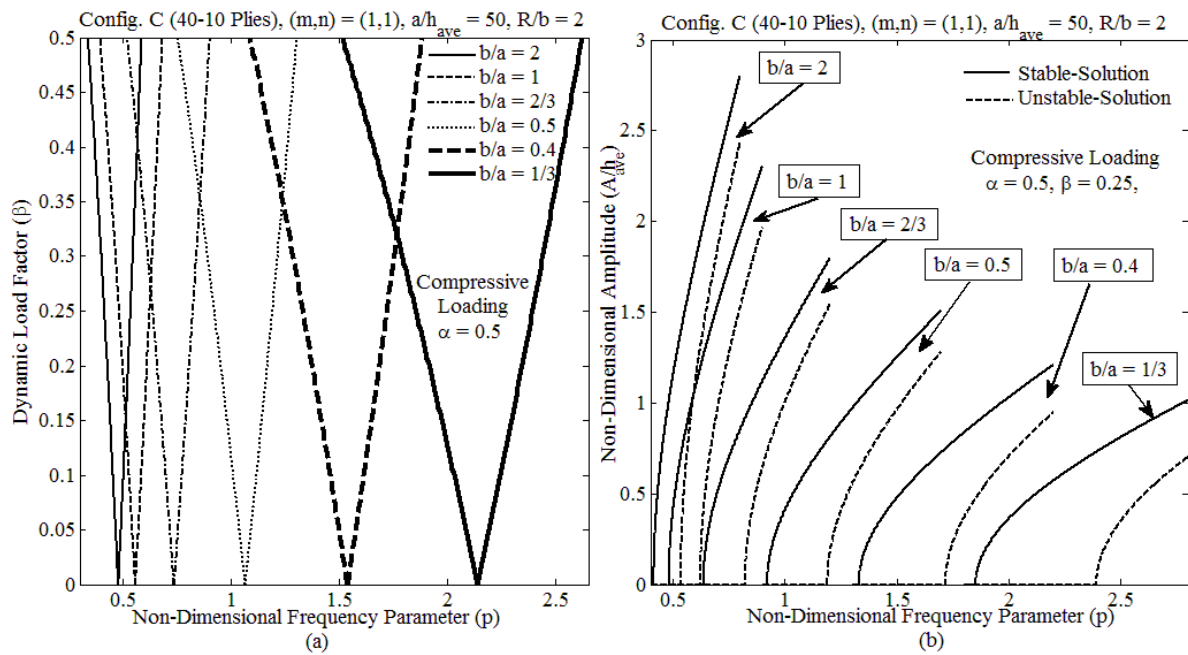
Figure 4.26 Effects of the variation of the loaded-to-unloaded width ratio, on the first mode a) unstable region and b) both stable-and unstable-solution amplitude of steady-state vibrations of 40-10 layered symmetric cross-ply laminated thickness-tapered cylindrical panel having configuration C, $a/h_{av} = 50$ and $R/b = 2$ subjected to the compressive periodic in-plane loading

that the corresponding dimensionless critical bucklig loads are increased by decreasing the loaded-to-unloaded width. The graphs indicate that in both tensile and compressive loadings with a decrease in width of the cylindrical panel, i.e. overall decrease in aspect ratio of b/a , the thickness-tapered cylindrical panel's stiffness is increased as well, hence the dynamically-unstable regions shift to the right along the frequency axis having higher frequencies of excitations of points of origins (Figs. 4.25a and 4.26a), and consequently both the stable- and unstable solutions amplitudes of steady-state vibrations at any specific frequency are decreased (Figs. 4.25b and 4.26b) and further, the widths of instability regions are also increased (Figs. 4.24a and 4.26a). It is noticed that increase in the widths of instability regions are more influenced by the compressive loading (Fig. 4.25a) than the tensile loading (Fig. 4.26a) and also most affected by the loads i.e. as mentioned above by decreasing the width-to length aspect ratio dimensionless critical bucklig loads are increased therefor it makes that the widths of instability region be increased too. However the points of origins of dynamically-unstable regions are more influenced by the tensile loading (Fig. 4.25a) than the compressive loading

(Fig. 4.26a). These are in full agreement qualitatively with the corresponding study of Ramachandra and Panda [11] for dynamically-unstable regions of uniform laminated plates. However again their study, corresponding results and conclusions are only about the dynamically-unstable regions based on the linear analysis done in their works and doesn't lead to the amplitude of steady-state vibrations at these regions.

4.6.7 Effect of the length-to-thickness ratio

As the final parametric study in Figs. 4.27 and 4.28 we investigate the effect of the variation of the length-to-average-thickness ratio, a/h_{ave} , on the instability regions and the both stable- and unstable-solution amplitudes of steady-state vibrations subjected to the tensile and compressive periodic in-plane loadings respectively. As it has been mentioned above since the taper angle and length-thickness ratio are influenced by each other, here to avoid this
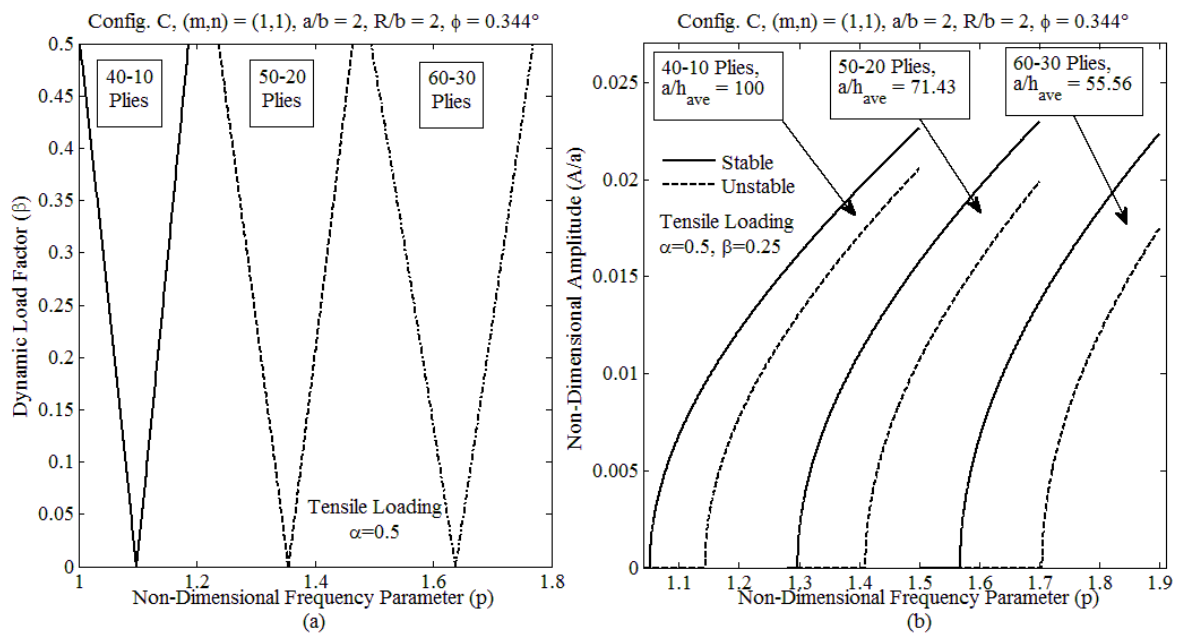
Figure 4.27 Effects of the variation of the length-to-average-thickness ratio on the first mode a) unstable region and b) both stable-and unstable-solution amplitude of steady-state vibrations of 40-10 layered symmetric cross-ply laminated thickness-tapered cylindrical panel having configuration C, $a/b = 2$ and $R/b = 2$ subjected to the tensile periodic in-plane loading

149
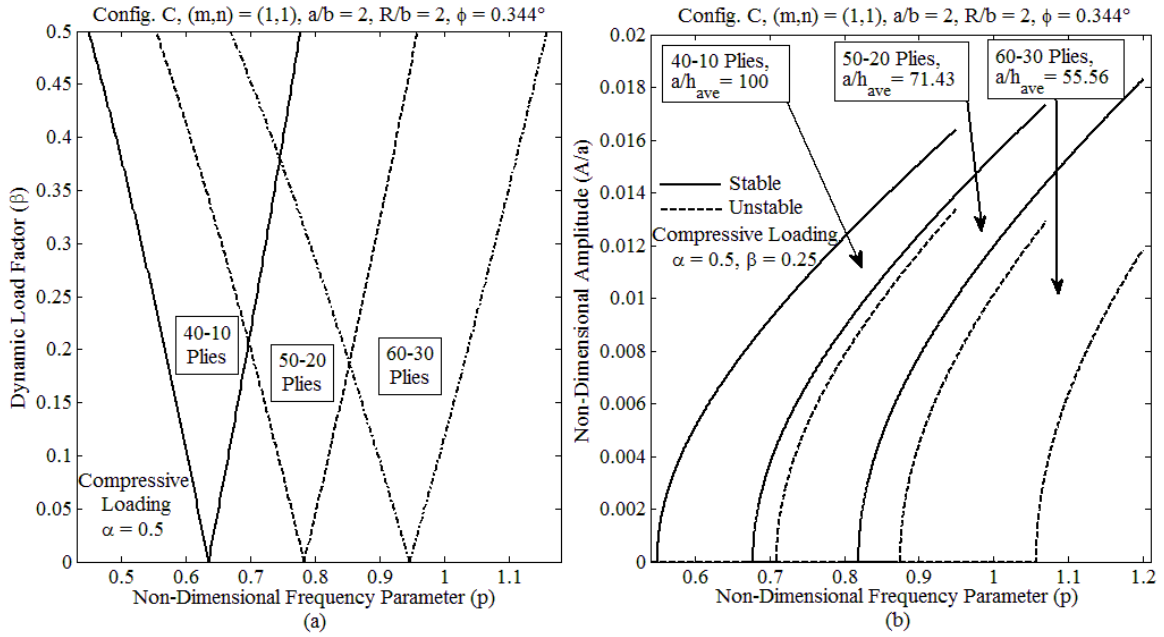
Figure 4.28 Effects of the variation of the length-to-average-thickness ratio on the first mode a) unstable region and b) both stable-and-unstable-solution amplitude of steady-state vibrations of 40-10 layered symmetric cross-ply laminated thickness-tapered cylindrical panel having configuration C, $a/b = 2$ and $R/b = 2$ subjected to the compressive periodic in-plane loading

interference of these two important parameters in Eq. (4.50) we keep the length a of the thickness-tapered cylindrical panel constant and change the length-to-average-thickness ratio by increasing the number of plies. These figures present a graphical illustration of the effect of length-to-average-thickness ratio on dynamic instability of thickness-tapered cylindrical panel with configuration C having three different numbers of plies i.e. 40-10 plies, 50-20 plies and 60-30 plies where the taper angle for all these three different thickness-tapered plates remains constant as $\phi = 0.344°$. The length-to-width ratio $a/b = 2$ and the static load factor $\alpha = 0.5$ for all these three diferent thickness ratios i.e., $a/h_{av} = 100, 71.43$ and 55.56 corresponding to the 40-10 plies, 50-20 plies and 60-30 plies, respectively. It is confirmed that in both tensile (Fig. 4.27) and compressive (Fig. 4.28) loading conditions with increasing the number of plies, i.e. with decreasing the length-to-average-thickness ratio a/h_{av}, the dynamically-unstable regions (Figs. 4.27a and 4.28a) shift to the right along the frequency axis having higher excitation frequencies, and consequently decreasing both the stable- and unstable-solution

150

amplitudes of steady-state vibrations (Figs. 4.27b and 4.28b) and also increasing the widths of dynamically-unstable regions (Figs 4.27a and 4.28a). It should be noted here again that increase in the widths of instability regions is more influenced by the compressive loading (Fig. 4.28a) than the tensile loading (Fig. 4.27a). However the points of origins of dynamically-unstable regions are more influenced by the tensile loading (Fig. 4.27a) than the compressive loading (Fig. 4.28a). These outcomes are also due to the fact that increasing the thickness of cylindrical panel makes the panel stiffer.

4.7   Conclusions

A displacement approach taking into account the non-linear von Karman strains associated with large deflections and curvatures was applied to investigate parametric instability of internally thickness-tapered laminated composite cylindrical panels having four different taper configurations. Considering the simply supported boundary condition the in-plane displacements were determined in terms of the out-of-plane displacement function. The in-plane force-resultants were determined based on the in-plane displacements and corresponding boundary conditions, and the moment-resultants were directly defined in terms of the out-of-plane displacement function after substituting it in the moment-equilibrium equation of motion. Applying the general Galerkin method to the resultant equation a set of non-linear Mathieu-Hill equations were obtained. Eventually the principal dynamically-unstable regions, stable-, and unstable-solutions amplitudes of the steady-state vibrations at these regions were calculated via Bolotin's first approximation. Numerical comparisons were made with those results available in literature, and the present methodology was validated. Based on the parametric studies, the following observations are made:

- Both dynamically-unstable regions and corresponding amplitudes of the steady-state vibrations are significantly influenced by taper configurations. The results show that configuration C is the most stable thickness-tapered cylindrical panel under parametric excitation among all the

thickness-tapered configurations i.e. configurations A, B, C and D, and also the uniform-thickness laminate having the thickness equal in value to the average thickness of the corresponding thickness-tapered cylindrical panel. Overall, tapering the cylindrical panel makes the panel's stiffness to be increased although its total weight might be decreased due to the existence of resin pockets. Higher stiffness of the thickness-tapered cylindrical panel results in the shifting of the dynamically-unstable regions toward higher frequencies and consequently decreasing both stable- and unstable-solutions amplitudes of the steady-state vibrations. However, almost the same widths of instability regions as that of uniform cylindrical panel having its thickness as the average thickness of the tapered plate are obtained, although reducing the total weight of the thickness-tapered structure causes the rate of increase of the amplitudes of the steady-state vibrations be increased. Hence in comparison to the uniform cylindrical panel, although the thickness-tapered cylindrical panel with configuration C has the amplitude of steady-state vibrations lower than that of the uniform laminate in the initial stages of the excitation, by increasing the excitation frequencies this trend is changed; influenced by the lower total weight of the thickness-tapered cylindrical panel (configuration C) at the higher level of the excitation frequencies, the first mode steady-state vibration amplitude is very slightly increased from the first mode steady-state vibration amplitude of the uniform cylindrical panel.

- Taper angle is the other most important parameter in the design of thickness-tapered cylindrical panel which, as observed from the results obtained, makes the cylindrical panel stiffer. The higher the taper angle is, the higher the excitation frequencies corresponding to the dynamically-unstable regions are, and consequently the lower is the amplitude of the steady-state vibrations. Also the widths of dynamically-unstable regions decrease very slightly for higher values of taper angles. The variation of dynamic instability response of thickness-

152

tapered cylindrical panel from that of the uniform one is very smooth for smaller taper angles but the rates of the deviations are high for increasing values of taper angle.

- Dynamically-unstable regions occur later with an increase of the amplitude of the tensile in-plane harmonically-pulsating load for laminated thickness-tapered cylindrical panel, with narrower width of instability regions, and consequently the lower amplitudes of the steady-state vibrations. However, with an increase of the amplitude of the compressive in-plane load, dynamically-unstable regions occur earlier with wider width of instability regions, and consequently the higher amplitudes of the steady-state vibrations. These outcomes can be expected because increasing the tensile in-plane load makes the cylindrical panel to be stiffer, and contrarily increasing the compressive in-plane load makes the cylindrical panel be less stiff.

- Thickness-tapered cylindrical panel with higher values of curvature have greater dynamic stability strength. In both tensile and compressive loadings decreasing the curvature or increasing the overal radius-to-width of the laminated tapered cylindrical panel results in shifting dynamically-unstable regions to the left along the frequenccy axis having lower frequencies of excitations of origins, increasing the width of instability regions and also increasing the amplitudes of steady-state vibrations at any specific frequency. This shifting to the left along the frequency axis of the dynamically-unstable regions, increasing steady-state amplitudes and the width of instability regions is very fast for values from $R/b = 1$ to $R/b = 3$, is moderate thereafter until $R/b = 5$ and is very slow until $R/b = 10$ and appears to have converged to a certain value thereafter. The dynamic instability's parameters are too close to each other for $R/b = 10$ and $R/b = \infty$ (flat plate).

- The results in both tensile and compressive loading conditions indicate that with a decrease in width b, i.e. overall decrease in aspect ratio b/a, the thickness-tapered cylindrical panel's stiffness is increased as well, hence the dynamically-unstable regions shift to the right along

the frequency axis having higher frequencies of excitation, and consequently decreasing the amplitudes of steady-state vibrations and further, the widths of instability regions are also increased. It is also noticed that increase in the widths of instability regions is more influenced by the compressive loading than the tensile loading. However, the points of origins of dynamically-unstable regions are more influenced by the tensile loading than the compressive loading.

- It is confirmed that in both tensile and compressive loading conditions with increasing the number of plies, i.e. with decreasing the length-to-average-thickness ratio a/h_{av} , the dynamically-unstable regions shift to the right along the frequency axis having higher excitation frequencies, and consequently decreasing the amplitudes of steady-state vibrations and also increasing the widths of dynamically-unstable regions. Increase in the widths of instability regions is more influenced by the compressive loading than the tensile loading. However, the points of origins of dynamically-unstable regions are more influenced by the tensile loading than the compressive loading. These outcomes are also due to the fact that increasing the thickness of plate makes the plate stiffer.

The thickness-tapered cylindrical panels, through increasing the stiffness and at the same time decreasing the weight, brings upon more complicated structural behavior as exhibited by their vibration response and dynamic instability characteristics, in comparison to the uniform cylindrical panels. All of the parametric study results indicate that the thickness-tapered cylindrical panels having configuration C is more stable and have better vibrational behavior in comparison to any other thickness-tapered configurations (A, B or D) and even in comparison to the uniform cylindrical panels having the thickness as the average-thickness of the corresponding thickness-tapered cylindrical panels having configuration C. It can also be concluded that the superiority of the thickness-tapered cylindrical panels with configuration C could further be improved by decreasing the sizes of the resin pockets. The present work can

be used as a benchmark study in future studies on the dynamic instability of laminated thickness-tapered composite cylindrical panels.

CHAPTER 5

Non-linear dynamic instability analysis of laminated composite cylindrical shells subjected to periodic axial loads

5.1 Introduction

Composite structures have been progressed from almost an engineering curiosity to widely used structures in aerospace, automotive, and civil engineering as well as in many other applications in everyday life. Advantages of fiber-reinforced composite materials including their outstanding strength and stiffness particularly the specific stiffness which is the stiffness-to-density make them more attractive for use in weight-sensitive structures such as aircraft or spacecraft structures [44].

When the lightweight structural components are subjected to dynamic loading particularly periodic loads, when the frequency of in-plane dynamic load and the frequency of vibration satisfy certain specific condition, parametric resonance will occur in the structure, which makes the plate or shell structure to enter into a state of dynamic instability [2]. This instability is of concern because it can occur at load magnitudes that are much less than the static buckling load, so a component designed to withstand static buckling may fail in a periodic loading environment. Further, the dynamic instability occurs over a range of forcing frequencies rather than at a single value [2, 3].

The interest to study the dynamic stability behavior of engineering structures dates back to the text by Bolotin [1] which addresses numerous problems on the stability of structures under pulsating loads. According to the general theory of dynamic stability of elastic systems by using Bolotin's method a set of differential equations of the Mathieu-Hill type are derived, and by seeking periodic solutions using Fourier series expansion the boundaries of unstable regions are determined. An extensive bibliography of the earlier works on parametric response of structures was presented by Evan-Iwanowsky [4].

156

A detailed research survey on the dynamic stability behavior of plates and shells in which the literature from 1987 to 2005 has been reviewed can be found in the review paper by Sahu and Datta [5].

The dynamic instability regions of laminated anisotropic cylindrical shells were studied by Argento and Scott [3, 45] using a perturbation technique. The shell's ends were clamped and subjected to axial periodic loading. In the numerical part [45] they discussed the effect of circumferential wave number and magnitude of external axial load on instability regions. Argento [46] then extended this work to compare the instability regions of the shell subjected to pure axial, pure torsional, and combined axial and torsional loadings. Extensive studies of dynamic stability of laminated composite cylindrical shells have been carried out by Ng. et al. [21, 23, 38, 41, 47, 48], using Love's classical thin shell theory for antisymmetric cross-ply laminate to investigate the effects of different lamination schemes and magnitude of the axial periodic loading [21], and length-to-radius and thickness-to radius ratios [23]. A comparison of different thin shell theories namely, Donnell's , Love's and Flugge's shell theories in predicting dynamically unstable regions of cross-ply laminated cylindrical shells has been provided [49]. Cylindrical panels with transverse shear effects have been studied using Donnell's shell theory and then extended using first-order shear deformation theory [47]. Donnell's equation has been used to study thin rotating isotropic cylindrical shells subjected to periodic axial loading [48] and, dynamic instability of laminated cylindrical shells has been studied via the mesh-free kp-Ritz method [50]. Fazilati and Ovesy used finite strip method to study the parametric instability of laminated composite plates and shells [51] , subjected to non-uniform in-plane loads [52] , moderately thick cylindrical panels with internal cutouts [53] and longitudinally stiffened curved panels with cutout [54] as well.

All these mentioned works are based on linear analysis and so lead to dynamic instability regions. Stability analysis based on classical linear theories provided only an outline of the

parameter regimes where non-linear effects are of importance. According to Popov [12] without adequate non-linear analysis the results in some cases can be inaccurate. "According to linear theory, one expects the vibration amplitudes in the regions of dynamic instability to increase unboundedly with time indeed very rapidly so as to increase exponentially. However, this conclusion contradicts experimental results which reveal that vibrations with steady-state amplitudes exist in the instability regions. As the amplitude increases, the character of the vibrations changes; the speed of the amplitude growth gradually decreases until vibrations of constant (or almost constant) amplitude are finally established" [1].

Some non-linear problems of laminated shells have been addressed in literature including initial post-buckling behavior [55], and free vibration and dynamic analysis of cylindrical and conical shells [56-60].

A comprehensive literature review covering the period 2003- 2013 on non-linear vibrations of shells has been done by Alijani and Amabili [13]

Few works have been conducted considering the non-linear shell theories for dynamic stability problems. Cheng-Ti and Li-Dong [18] used Hamilton principle to derive the equation of motion and solved this equation with variational methods to study the effect of large deflection which leads to non-linear dynamic instability for three typical laminated composite cylindrical shells, viz, Graphite epoxy, E-glass epoxy and ARAAL shells. Their studies were limited to overall trend of variation of the amplitude with these three composites.

To the present authors' knowledge a comprehensive study which considers the effects of stacking sequence and aspect ratios has not been carried out on the non-linear dynamic instability of thin laminated shells. In the present part of the thesis, the Donnell's shallow-shell theory with von Karman-type of non-linearity is considered for thin, laminated composite cylindrical shell subjected to harmonic axial loading. Galerkin's technique is then employed to solve the non-linear large deflection shallow-shell equations of motion and a system of non-

linear Mathieu-Hill equations are derived. The steady-state amplitudes of both stable and unstable solutions are determined by applying the Bolotin's method. The parametric studies are performed to investigate and compare the effects of different lamination schemes of symmetric and antisymmetric cross-ply laminated shells, the magnitude of axial loads both tensile and compressive loads, different aspect ratios of the shell including length-to-radius and thickness-to-radius ratios and different circumferential wave numbers as well on the parametric resonance particularly of the steady-state vibrations. The present results show good agreement when compared with that available in the literature and hence can be used as bench mark results for future studies.

5.2 Formulation

A thin simply supported laminated composite cylindrical shell, having length L and radius R with respect to the curvilinear coordinates (X, θ, Z) which are assigned in the mid-surface of the shell is considered as shown in Fig. 5.1.

Here, u, v and w are the displacement components of the shell with reference to this coordinate system in the X, θ, Z, directions, respectively.

The cylindrical shell is subjected to a periodically pulsating load in the axial direction with the axial loading per unit length as follow:

$$F_{xx}(t) = F_s + F_d cosPt \tag{5.1}$$

where F_s is a time invariant component, $F_d cosPt$ is the harmonically pulsating component, and P denotes the frequency of excitation in radians per unit time.

Donnell's theory for thin cylindrical shells is employed for this analysis. Thus the equations of motion under the axial pulsating load are given by

$$\frac{\partial N_{xx}}{\partial x} + \frac{1}{R}\frac{\partial N_{x\theta}}{\partial x} = \rho_t \frac{\partial^2 u_0}{\partial t^2} \tag{5.2}$$

$$\frac{\partial N_{x\theta}}{\partial x} + \frac{1}{R}\frac{\partial N_{\theta\theta}}{\partial \theta} = \rho_t \frac{\partial^2 v_0}{\partial t^2} \tag{5.3}$$

159
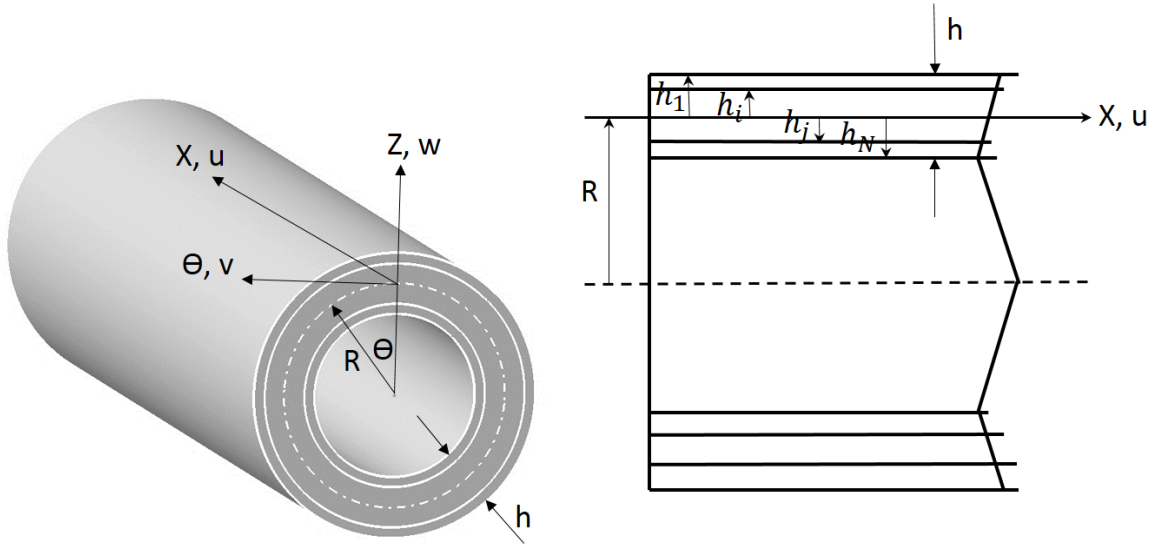
Figure 5.1 The geometry of a laminated composite cylindrical shell and the cross-sectional view

$$\frac{\partial^2 M_{xx}}{\partial x^2} + \frac{2}{R}\frac{\partial^2 M_{x\theta}}{\partial x \partial \theta} + \frac{1}{R^2}\frac{\partial^2 M_{\theta\theta}}{\partial \theta^2} - \frac{1}{R}N_{\theta\theta} + N_{xx}\frac{\partial^2 w_0}{\partial x^2} = \rho_t \frac{\partial^2 w_0}{\partial t^2} \tag{5.4}$$

where

$$\rho_t = \int_{-h/2}^{h/2} \rho\, dz, \tag{5.5}$$

and $(N_{xx}, N_{\theta\theta}, N_{x\theta})$ are the total in-plane force resultants and $(M_{xx}, M_{\theta\theta}, M_{x\theta})$ are the total

moment resultants that are defined by

$$\begin{Bmatrix} N_{xx} \\ N_{\theta\theta} \\ N_{x\theta} \end{Bmatrix} = \int_{\frac{-h}{2}}^{\frac{h}{2}} \begin{Bmatrix} \sigma_{xx} \\ \sigma_{\theta\theta} \\ \sigma_{x\theta} \end{Bmatrix} dz \tag{5.6}$$

$$\begin{Bmatrix} M_{xx} \\ M_{\theta\theta} \\ M_{x\theta} \end{Bmatrix} = \int_{\frac{-h}{2}}^{\frac{h}{2}} \begin{Bmatrix} \sigma_{xx} \\ \sigma_{\theta} \\ \sigma_{x\theta} \end{Bmatrix} Z\, dz \tag{5.7}$$

The nonzero von Karman strains associated with non-linear large deflections and curvatures

according to Donnell's theory are given by

$$\begin{Bmatrix} \epsilon_{xx} \\ \epsilon_{\theta\theta} \\ \gamma_{x\theta} \end{Bmatrix} = \begin{Bmatrix} \epsilon_{xx}^{(0)} \\ \epsilon_{\theta\theta}^{(0)} \\ \gamma_{x\theta}^{(0)} \end{Bmatrix} + z \begin{Bmatrix} \epsilon_{xx}^{(1)} \\ \epsilon_{\theta\theta}^{(1)} \\ \gamma_{x\theta}^{(1)} \end{Bmatrix} \tag{5.8}$$

160

$$\{\epsilon^0\} = \begin{Bmatrix} \epsilon_{xx}^{(0)} \\ \epsilon_{\theta\theta}^{(0)} \\ \gamma_{x\theta}^{(0)} \end{Bmatrix} = \begin{Bmatrix} \frac{\partial u_0}{\partial x} + \frac{1}{2}(\frac{\partial w_0}{\partial x})^2 \\ \frac{1}{R}(\frac{\partial v_0}{\partial \theta} + w_0) + \frac{1}{2R^2}(\frac{\partial w_0}{\partial \theta})^2 \\ \frac{1}{R}\frac{\partial u_0}{\partial \theta} + \frac{\partial v_0}{\partial x} + \frac{1}{R}\frac{\partial w_0}{\partial x}\frac{\partial w_0}{\partial \theta} \end{Bmatrix} \tag{5.9}$$

$$\{\epsilon^1\} = \begin{Bmatrix} \epsilon_{xx}^{(1)} \\ \epsilon_{\theta\theta}^{(1)} \\ \gamma_{x\theta}^{(1)} \end{Bmatrix} = \begin{Bmatrix} -\frac{\partial^2 w_0}{\partial x^2} \\ -\frac{1}{R^2}\frac{\partial^2 w_0}{\partial \theta^2} \\ -\frac{2}{R}\frac{\partial^2 w_0}{\partial x \partial \theta} \end{Bmatrix} \tag{5.10}$$

where $(\epsilon_{xx}^{(0)}, \epsilon_{\theta\theta}^{(0)}, \gamma_{x\theta}^{(0)})$ are the membrane strains, $(\epsilon_{xx}^{(1)}, \epsilon_{\theta\theta}^{(1)}, \gamma_{x\theta}^{(1)})$ are the flexural (bending) strains and (u_0, v_0, w_0) are mid-plane displacements.

The thin shell is constructed by a cross-ply laminated composite material having density ρ. Hence the state of stress is governed by the generalized Hooke's law. The linear constitutive relations for the kth orthotropic lamina in the principal material coordinates of a lamina are

$$\begin{Bmatrix} \sigma_1 \\ \sigma_2 \\ \sigma_6 \end{Bmatrix}^{(k)} = \begin{bmatrix} Q_{11} & Q_{12} & 0 \\ Q_{12} & Q_{22} & 0 \\ 0 & 0 & Q_{66} \end{bmatrix}^{(k)} \begin{Bmatrix} \epsilon_1 \\ \epsilon_2 \\ \epsilon_6 \end{Bmatrix} \tag{5.11}$$

where $[Q]^{(k)}$ is the reduced stiffness matrix of the kth lamina and its components $Q_{ij}^{(k)}$ are known in terms of the engineering constants of the kth layer, as

$$Q_{11} = \frac{E_{11}}{1 - v_{12}v_{21}} \tag{5.12a}$$

$$Q_{12} = \frac{v_{12}E_{22}}{1 - v_{12}v_{21}} \tag{5.12b}$$

$$Q_{22} = \frac{E_{22}}{1 - v_{12}v_{21}} \tag{5.12c}$$

$$Q_{66} = G_{12} \tag{5.12d}$$

where E_{11} and E_{22} are the elastic moduli in the principal material coordinates, G_{12} is the shear modulus and v_{12} and v_{21} are the Poisson's ratios.

The constitutive equation of the laminate which is made of several orthotropic layers, with the arbitrarily oriented material axes to the laminate coordinate, can be obtained by the transformation of the stress-strain relations to the laminate coordinates as follow:

$$\begin{Bmatrix} \epsilon_x \\ \epsilon_\theta \\ \gamma_{x\theta} \end{Bmatrix}^{(k)} = \begin{bmatrix} \bar{Q}_{11} & \bar{Q}_{12} & \bar{Q}_{16} \\ \bar{Q}_{12} & \bar{Q}_{22} & \bar{Q}_{26} \\ \bar{Q}_{16} & \bar{Q}_{26} & \bar{Q}_{66} \end{bmatrix}^{(k)} \begin{Bmatrix} \epsilon_{xx} \\ \epsilon_{\theta\theta} \\ \gamma_{x\theta} \end{Bmatrix} \qquad (5.13)$$

where $[\bar{Q}]^{(k)}$ is the transformed reduced stiffness matrix defined as follow:

$$[\bar{Q}] = [T]^{-1}[Q][T]^{-T} \qquad (5.14)$$

where $[T]$ is the transformation matrix for the principal material coordinates and the shell's coordinates given by

$$[T] = \begin{bmatrix} \cos^2 \alpha & \sin^2 \alpha & 2\cos \alpha \sin \alpha \\ \sin^2 \alpha & \cos^2 \alpha & -2\cos \alpha \sin \alpha \\ -\cos \alpha \sin \alpha & 2\cos \alpha \sin \alpha & \cos^2 \alpha - \sin^2 \alpha \end{bmatrix} \qquad (5.15)$$

and α is the angular orientation of the fibers. By following the equations (6)-(15) the force and moment resultants are defined as

$$\begin{Bmatrix} N_{xx} \\ N_{\theta\theta} \\ N_{x\theta} \\ M_{xx} \\ M_{\theta\theta} \\ M_{x\theta} \end{Bmatrix} = \begin{bmatrix} A_{11} & A_{12} & A_{16} & B_{11} & B_{12} & B_{16} \\ A_{12} & A_{22} & A_{26} & B_{12} & B_{22} & B_{26} \\ A_{16} & A_{26} & A_{66} & B_{16} & B_{26} & B_{66} \\ B_{11} & B_{12} & B_{16} & D_{11} & D_{12} & D_{16} \\ B_{12} & B_{22} & B_{26} & D_{12} & D_{22} & D_{26} \\ B_{16} & B_{26} & B_{66} & D_{16} & D_{26} & D_{66} \end{bmatrix} \begin{Bmatrix} \epsilon_{xx}^{(0)} \\ \epsilon_{\theta\theta}^{(0)} \\ \gamma_{x\theta}^{(0)} \\ \epsilon_{xx}^{(1)} \\ \epsilon_{\theta\theta}^{(1)} \\ \gamma_{x\theta}^{(1)} \end{Bmatrix} \qquad (5.16)$$

where A_{ij} denote the extensional stiffnesses, D_{ij} the bending stiffnesses, and B_{ij} the bending-extensional coupling stiffnesses

$$A_{ij} = \sum_{k=1}^{N} \bar{Q}_{ij}^{(k)} (h_k - h_{k+1}) \qquad , (i,j = 1,2,6) \qquad (5.17a)$$

$$B_{ij} = \frac{1}{2} \sum_{k=1}^{N} \bar{Q}_{ij}^{(k)} (h_k^2 - h_{k+1}^2) \qquad (5.17b)$$

$$D_{ij} = \frac{1}{3} \sum_{k=1}^{N} \bar{Q}_{ij}^{(k)} (h_k^3 - h_{k+1}^3) \qquad (5.17c)$$

where h_k and h_{k+1} are measured from the shell reference surface to the outer and inner surfaces of the kth layer, respectively, as shown in Fig. 1. From Eq.(5.16) the strains can be written as

162

$$\begin{Bmatrix} \epsilon_{xx}^{(0)} \\ \epsilon_{\theta\theta}^{(0)} \\ \gamma_{x\theta}^{(0)} \end{Bmatrix} = [A_{ij}]^{-1} \begin{Bmatrix} N_{xx} \\ N_{\theta\theta} \\ N_{x\theta} \end{Bmatrix} - [A_{ij}]^{-1} [B_{ij}] \begin{Bmatrix} \epsilon_{xx}^{(1)} \\ \epsilon_{\theta\theta}^{(1)} \\ \gamma_{x\theta}^{(1)} \end{Bmatrix} = \begin{Bmatrix} a_1 N_{xx} + a_2 N_{\theta\theta} + a_3 \epsilon_{xx}^{(1)} + a_4 \epsilon_{\theta\theta}^{(1)} \\ a_2 N_{xx} + a_1 N_{\theta\theta} + a_4 \epsilon_{xx}^{(1)} + a_3 \epsilon_{\theta\theta}^{(1)} \\ a_5 N_{x\theta} + a_6 \gamma_{x\theta}^{(1)} \end{Bmatrix}$$

$$(5.18)$$

where

$$a_1 = \Delta A_{22} \ , \ a_2 = D_{12} \ , \ a_3 = \Delta(A_{12}B_{12} - A_{22}B_{11})$$

$$a_4 = \Delta(A_{12}B_{22} - A_{22}B_{12}) \ , \ a_5 = \frac{1}{A_{66}} \ , \ a_6 = -\frac{B_{66}}{A_{66}}$$

$$\Delta = \frac{1}{(A_{11}^2 - A_{12}^2)} \tag{5.19}$$

The moment resultants also can be written from Eq.(16) as

$$\begin{Bmatrix} M_{xx} \\ M_{\theta\theta} \\ M_{x\theta} \end{Bmatrix} = [b_{ij}]^T \begin{Bmatrix} N_{xx} \\ N_{\theta\theta} \\ N_{x\theta} \end{Bmatrix} + [d_{ij}] \begin{Bmatrix} \epsilon_{xx}^{(1)} \\ \epsilon_{\theta\theta}^{(1)} \\ \gamma_{x\theta}^{(1)} \end{Bmatrix} = \begin{Bmatrix} b_1 N_{xx} + b_2 N_{\theta\theta} + b_3 \epsilon_{xx}^{(1)} + b_4 \epsilon_{\theta\theta}^{(1)} \\ b_2 N_{xx} + b_1 N_{\theta\theta} + b_4 \epsilon_{xx}^{(1)} + b_3 \epsilon_{\theta\theta}^{(1)} \\ b_5 N_{x\theta} + b_6 \gamma_{x\theta}^{(1)} \end{Bmatrix} \tag{5.20}$$

where

$$[b_{ij}] = [A_{ij}]^{-1} [B_{ij}] \tag{5.21a}$$

$$[d_{ij}] = -[B_{ij}][b_{ij}] + [D_{ij}] \tag{5.21b}$$

$$b_1 = -a_3 \ , \ b_2 = -a_4 \ , \ b_3 = a_3 B_{11} + a_4 B_{12} + D_{11}$$

$$b_4 = a_4 B_{12} + a_3 B_{22} + D_{22} \ , \ b_5 = a_6 \ , \ b_6 = a_6 B_{66} + D_{66} \tag{5.21c}$$

Here we define the membrane forces in terms of Airy's stress function φ as

$$N_{xx} = \frac{1}{R^3} \frac{\partial^2 \phi}{\partial \theta^2} \tag{5.22a}$$

$$N_{\theta\theta} = \frac{\partial^2 \phi}{\partial x^2} \tag{5.22b}$$

$$N_{x\theta} = -\frac{1}{R} \frac{\partial^2 \phi}{\partial x \partial \theta} \tag{5.22c}$$

Substituting Equations (5.10) and (5.26) into equations (5.18) and (5.20) the strains and moment resultants are given in terms of the Airy's stress function ϕ and w_0.

By combining the mid-plane strains, the compatibility equation can be expressed as

$$\frac{\partial^2 \epsilon_{\theta\theta}^{(0)}}{\partial x^2} + \frac{1}{R^2}\frac{\partial^2 \epsilon_{xx}^{(0)}}{\partial \theta^2} - \frac{1}{R}\frac{\partial^2 \gamma_{x\theta}^{(0)}}{\partial x \partial \theta} = \frac{1}{R}\frac{\partial^2 w}{\partial x^2}\frac{\partial^2 w_0}{\partial \theta^2} + \frac{1}{R^2}\frac{\partial^2 w_0}{\partial x \partial \theta} \tag{5.23}$$

Replacing the strains in terms of the Airy's stress function ϕ from Eq. (18) and w_0 into Eq.(5.23) the non-linear equation of compatibility can be derived as:

$$a_1\frac{\partial^4 \phi}{\partial x^4} + \frac{a_1}{R^4}\frac{\partial^4 \phi}{\partial \theta^4} + \frac{1}{R^2}(2a_2 + a_5)\frac{\partial^4 \phi}{\partial x^2 \partial \theta^2} - a_4\frac{\partial^4 w_0}{\partial x^4} - \frac{a_4}{R^4}\frac{\partial^4 w_0}{\partial \theta^4} + \frac{2}{R^2}(a_6 - a_3)\frac{\partial^4 w_0}{\partial x^2 \partial \theta^2} =$$

$$\frac{1}{R}\frac{\partial^2 w_0}{\partial x^2} - \frac{1}{R^2}\frac{\partial^2 w_0}{\partial x^2}\frac{\partial^2 w_0}{\partial \theta^2} + \frac{1}{R^2}\frac{\partial^2 w_0}{\partial x \partial \theta} \tag{5.24}$$

5.3   Solution for laminated orthotropic shells

Considering the simply supported boundary condition for the studied laminated orthotropic cylindrical shell, the Navier's double Fourier series with the time-dependent coefficient $q_{mn}(t)$ is chosen to describe the transverse displacement function $w_0(x, \theta, t)$:

$$w_0 = \sum_{m=1}^{\infty}\sum_{n=1}^{\infty} q_{mn}(t) \sin\frac{m\pi}{L}x \cos n\theta \tag{5.25}$$

where m, n represent the number of axial half waves in corresponding standing wave pattern and the circumferential wave number, respectively.

F_{xx} is the average axial force at the edge, thus the stress function has to satisfy the following condition

$$\frac{1}{2\pi R^2}\int_0^{2\pi}\frac{\partial^2 \phi}{\partial \theta^2}d\theta = F_{xx} \quad at \ x = 0, L \tag{5.26}$$

Airy's stress function can be governed by substituting Eq. (25) into Eq. (24) and applying different trigonometric relations, as:

$$\phi = \frac{1}{2}R^2 F_{xx}\theta^2 + \sum_{m=1}^{\infty}\sum_{n=1}^{\infty}\left\{\frac{1}{2}A_{mn}q_{mn}(t)\xi_1[\sin(\lambda_m x - n\theta) + \sin(\lambda_m x + n\theta)] + \right.$$

$$\left.\frac{1}{32}B_{mn}q_{mn}^2(t)[\xi_2\cos(2\lambda_m x) - \xi_3\cos(2n\theta)]\right\} \tag{5.27}$$

where $\lambda_m = m\pi/L$ and

$$A_{mn} = \frac{1}{R^4}a_4 n^4 - \frac{2}{R^2}(a_6 - a_3)\lambda_m^2 n^2 - \frac{1}{R}\lambda_m^2 + a_4\lambda_m^4 \tag{5.28a}$$

$$B_{mn} = \frac{1}{R}\lambda_m^2 n^2 \tag{5.28b}$$

$$\xi_1 = {1} \Big/ {\left(\frac{1}{R^4} a_1 n^4 + \frac{1}{R^2} (2a_2 + a_5) \lambda_m{}^2 n^2 + a_1 \lambda_m{}^4 \right)}$$ (5.28c)

$$\xi_2 = {1} \Big/ {(a_1 \lambda_m{}^4)}$$ (5.5.28d)

$$\xi_3 = {R^4} \Big/ {(a_1 n^4)}$$ (5.28e)

Taking the inertia forces $\rho_t \, \partial^2 u_0 / \partial t^2 \to 0$ and $\rho_t \, \partial^2 v_0 / \partial t^2 \to 0$ into consideration since $u_0 \ll w_0$ and $v_0 \ll w_0$ and substituting the relations (5.22a-c) in Eqs. (5.2) and (5.3), these equations are satisfied automatically. With the definitions (5.22a-c), the membrane forces N_{xx}, $N_{\theta\theta}$ and $N_{x\theta}$ are computable by this solution and the boundary condition (5.26) is satisfied. As mentioned before by substituting Eqs. (5.10) and (5.22a-c) into equations (5.20) the moments are given in terms of the Airy's stress function ϕ and w_0; so by inserting these functions the moment resultants M_{xx}, $M_{\theta\theta}$ and $M_{x\theta}$ are also computable. By substituting these stress and moment resultants and the transverse displacement as defined in Eq.(5.25) into the third equation of motion (5.4) and after multiplying the governing equation by $\sin \frac{m\pi}{L} x \cos n\theta$ and integrating over the shell area, a system of $m \times n$ second-order ordinary differential equations is obtained:

$$M_{mn} \ddot{q}_{mn}(t) + K_{mn} q_{mn}(t) - (F_s + F_d \cos pt) Q_{mn} q_{mn}(t) + \eta_{mn} q_{mn}^3(t) = 0$$ (5.29)

where M_{mn}, K_{mn}, Q_{mn} and η_{mn} are matrices that are defined in the Appendix ((Eqs.(A.7)-(A.10))) and $\ddot{q}_{mn}(t)$, $q_{mn}(t)$ and $q_{mn}^3(t)$ are column vectors consisting of the $\ddot{q}_{mn}(t)$'s, $q_{mn}(t)$'s and $q_{mn}^3(t)$'s respectively. The subscripts m and n have the following ranges:

$$m, n = 1,2,3,4,.., N.$$ (5.30)

Introducing following notation:

$$\omega_{mn} = \sqrt{\frac{K_{mn}}{M_{mn}}}$$ (5.31a)

$$\gamma_{mn} = \frac{\eta_{mn}}{M_{mn}} \tag{5.31b}$$

$$N_* = \frac{K_{mn}}{Q_{mn}} \tag{5.31c}$$

Eq.(5.29) can be written in the form of the non-linear Mathieu equation as follow:

$$\ddot{q}_{mn}(t) + \Omega_{mn}^2 (1 - 2\mu_{mn}\cos pt)q_{mn}(t) + \gamma_{mn}q_{mn}^3(t) = 0 \tag{5.32}$$

where Ω_{mn} is the frequency of the free vibration of the shell loaded by a constant longitudinal force F_s,

$$\Omega_{mn} = \omega_{mn}\sqrt{1 - \frac{F_s}{N_*}} \tag{5.33}$$

and μ_{mn} is a quantity that is called the excitation parameter,

$$\mu_{mn} = \frac{F_d}{2(N_* - F_s)} \tag{5.34}$$

5.4 Amplitude of vibrations at the principal parametric resonance

As mentioned above Eq. (5.32) is a non-linear Mathieu equation where the non-linear term $\gamma q_{mn}^3(t)$ represents the effect of large deflection. According to Liapunov Principle, dynamically unstable region is determined by the linear parts of the Eq. (5.32) [1] which will be discussed in the next section. Here the focus is set on the parametric resonance of the system. The basic solutions of Mathieu equation include two periodic solutions: i.e. periodic solutions of T and $2T$ with $T = 2\pi/P$. The solutions with period $2T$ are of greater practical importance as the widths of these unstable regions are usually larger than those associated with solutions having period T. Using Bolotin's [1] method for parametric vibration, the solution of period $2T$ is given by the following equation:

$$q(t) = \sum_{k=1,3,5,\ldots}^{\infty} a_k \sin\frac{kPt}{2} + b_k \cos\frac{kPt}{2} \tag{5.35}$$

where a_k and b_k are arbitrary vectors. If we investigate the vibration for the principal resonance $P \approx 2\Omega$, we can neglect the influence of higher harmonics in the expansion of above equation and can assume

$$q(t) = a \sin \frac{Pt}{2} + b \cos \frac{Pt}{2} \qquad (5.36)$$

as an approximation. By substituting this function into Eq. (5.32) and equating the coefficients

of $\sin(Pt/2)$ and $\cos(Pt/2)$ terms and neglecting terms containing higher harmonics, the

following system of equations for the coefficients a and b remains:

$$\left[\Omega_{mn}^2 (1 + \mu_{mn}) - \frac{P^2}{4} \right] a + \Gamma(a, b) = 0, \qquad (5.37a)$$

$$\left[\Omega_{mn}^2 (1 - \mu_{mn}) - \frac{P^2}{4} \right] b + \Psi(a, b) = 0, \qquad (5.37b)$$

where $\Gamma(a, b)$ and $\Psi(a, b)$ are defined as coefficients of the terms including $\sin(Pt/2)$ and

$\cos(Pt/2)$ which were obtained from the first approximation of expansion in a Fourier series

as:

$$\Gamma(a, b) = \frac{3\gamma_{mn}}{4} A^2 a \qquad (5.38a)$$

$$\Psi(a, b) = \frac{3\gamma_{mn}}{4} A^2 b \qquad (5.38b)$$

where A is the amplitude of steady-state vibrations and is given by:

$$A = \sqrt{a^2 + b^2} \qquad (5.39)$$

By substitution of Eqs. (5.38a, b) into Eq. (5.37a, b) a system of two homogeneous linear

equations with respect to a and b can be obtained. This system has solutions that differ from

zero only in the case where the determinant composed of the coefficients is equal to zero:

$$\begin{vmatrix} 1 + \mu_{mn} - n_{mn}^2 + \frac{3\gamma_{mn}}{4\Omega_{mn}^2} A^2 & 0 \\ 0 & 1 - \mu_{mn} - n_{mn}^2 + \frac{3\gamma_{mn}}{4\Omega_{mn}^2} A^2 \end{vmatrix} = 0 \qquad (5.40)$$

where

$$n_{mn} = \frac{P}{2\Omega_{mn}} \qquad (5.41)$$

Expanding the determinant and solving the resulting equation with respect to the amplitude, A,

of the steady-state vibrations the following equation is obtained:

$$A = \frac{2\Omega_{mn}}{\sqrt{3\gamma_{mn}}} \sqrt{n_{mn}^2 - 1 \pm \mu_{mn}} \qquad (5.42)$$

167

It can be proved that in the $\pm \mu_{mn}$ term of the above equation, only $+\mu_{mn}$ term is the stable

solution, and all the other terms are unstable solutions.

5.5 Dynamic instability regions

The resonance curve is not influenced by non-linearity of Eq. (5.29) and as mentioned in the

previous section the dynamic instability regions are determined by linear part of Mathieu-Hill

equation, and so the equation (5.29) can be rewritten as follow:

$$M_{mn}\ddot{q}_{mn}(t) + (K_{mn}^* - Q_{mn}^* \cos pt)q_{mn}(t) + \eta_{mn}q_{mn}^3(t) = 0 \qquad (5.43)$$

where

$$K_{mn}^* = K_{mn} - F_s Q_{mn} \qquad (5.44)$$

and

$$Q_{mn}^* = F_d Q_{mn} \qquad (5.45)$$

The principal region of dynamic instability which corresponds to solution of period $2T$ is

determined by substituting Eq. (5.36) into Eq. (5.43) and equating the determinant of the

coefficient matrix of linear part of the governing equation to zero as follow:

$$\begin{vmatrix} K_{mn}^* - \dfrac{Q_{mn}^*}{2} - \dfrac{M_{mn}}{4}P^2 & 0 \\ 0 & K_{mn}^* + \dfrac{Q_{mn}^*}{2} - \dfrac{M_{mn}}{4}P^2 \end{vmatrix} = 0 \qquad (5.46)$$

Comparing equations (5.46) and (5.40) by replacing μ_{mn}, n_{mn}, γ_{mn} and Ω_{mn} in terms of

K_{mn}^*, Q_{mn}^* and M_{mn} reveals that the dynamic instability regions are determined by setting $A =$

0 in equation (5.40).

Equation (5.46) can be rearranged to the more simplified form of an eigenvalue problem as

follow:

$$\begin{vmatrix} K_{mn}^* - \dfrac{Q_{mn}^*}{2} & 0 \\ 0 & K_{mn}^* + \dfrac{Q_{mn}^*}{2} \end{vmatrix} - P^2 \begin{vmatrix} \dfrac{M_{mn}}{4} & 0 \\ 0 & \dfrac{M_{mn}}{4} \end{vmatrix} = 0 \qquad (5.47)$$

168

5.6 Numerical results and discussion

Non-linear dynamic stability characteristics of cross-ply laminated composite cylindrical shells subjected to combined static and periodic axial loads are studied here. The material properties used in the present analysis are chosen in accordance with Ng et al. [21] as $E_1/E_2 = 40$, $G_{12}/E_2 = 0.5$ and $v_{12} = 0.25$.

For isotropic cylindrical shells the critical static buckling load in terms of engineering constants is given by Timoshenko and Gere as [20]

$$N_{buc} = \frac{Eh^2}{R\sqrt{[3(1-v^2)]}} \qquad (5.48)$$

The mechanism of dynamic buckling is similar to static buckling and the only difference is the additional considerations of the inertia force so that it leads to the dynamic buckling load to be lower than the static buckling load for the same structure. But the mechanism of dynamic instability is much more complex since in both static and dynamic buckling the main factor is only the critical static or dynamic load amplitude while in dynamic instability, not only the vibration amplitude of dynamic load, but also the vibration frequency together with the stimulating frequency will play important roles. So the dynamic instability of the plate or shell structures will occur at much lower loads.

For laminated circular cylindrical shells, the critical static buckling load is approximated as [50]

$$N_{cr} = \frac{E_2 h^2}{R\sqrt{[3(1-v_{12}v_{21})]}} \qquad (5.49)$$

This approximates the static buckling load for laminated cylindrical shell and hence for the dynamic instability analysis both the static part of the load F_s and the periodic part F_d in Eq. (5.1) should be a percentage of this buckling load. This is why we have considered conservatively in the following tables and figures that $F_s = (0.1, 0.2, 0.3, 0.5)N_{cr}$ and corresponding periodic part as $F_d = (0...0.5)F_s$.

169

In order to compare the results, the following dimensionless excitation frequency parameter p is considered according to the references [21, 23]

$$p = 2\pi RP \sqrt{\frac{\rho_t}{A_{11}}} \qquad (5.50)$$

As mentioned before the main objective of this work is to study the influence of geometric non-linearity on the dynamic instability of laminated composite cylindrical shells which leads to the non-linear Mathieu-Hill equation as Eqs. (5.29) and (5.32). In section 5 it was observed that the dynamic instability regions based on the large deflection formulation are achieved by either linear part of the non-linear Mathieu-Hill equation or by setting $A = 0$ in equation (5.40). So to validate the present formulation which is based on the non-linear analysis first we obtain the numerical results that corresponds to the dynamically unstable regions to compare with those in available in literatures [21, 23] for cross-ply laminated composite cylindrical shells.

Figure 5.2 displays the boundaries of the first (from left to the right of the frequency's axis) dynamically unstable region of a two- layered $(90^o/0^o)$ cross-ply laminated cylindrical shell having aspect ratios of $L/R = 2$ and $R/h = 200$ subjected to tensile loading of $F_s = 0.1N_{cr}$ As it can be observed from this figure each unstable region is separated by two lines with a common point of origin. Actually these two lines are not completely straight and they curved slightly outward. To compare the results in the following tables we specified each unstable regions by the non-dimensional frequency parameter p of the point of origins and the half angle of the unstable regions as θ.
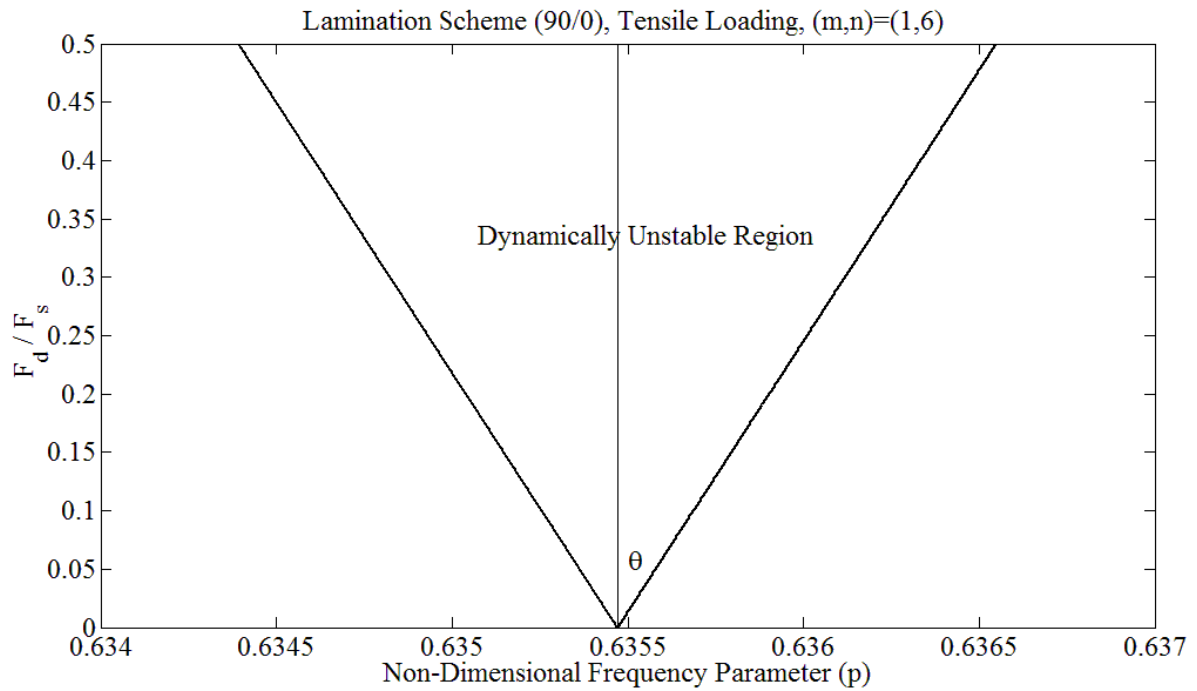
Figure 5.2 Dynamically unstable region corresponding to the first transverse mode, mode (1, 6) of a two-layered ($90^o/0^o$) cross-ply laminated cylindrical shell having aspect ratios of $L/R = 2$ and $R/h = 200$ subjected to tensile loading of $F_s = 0.1N_{cr}$
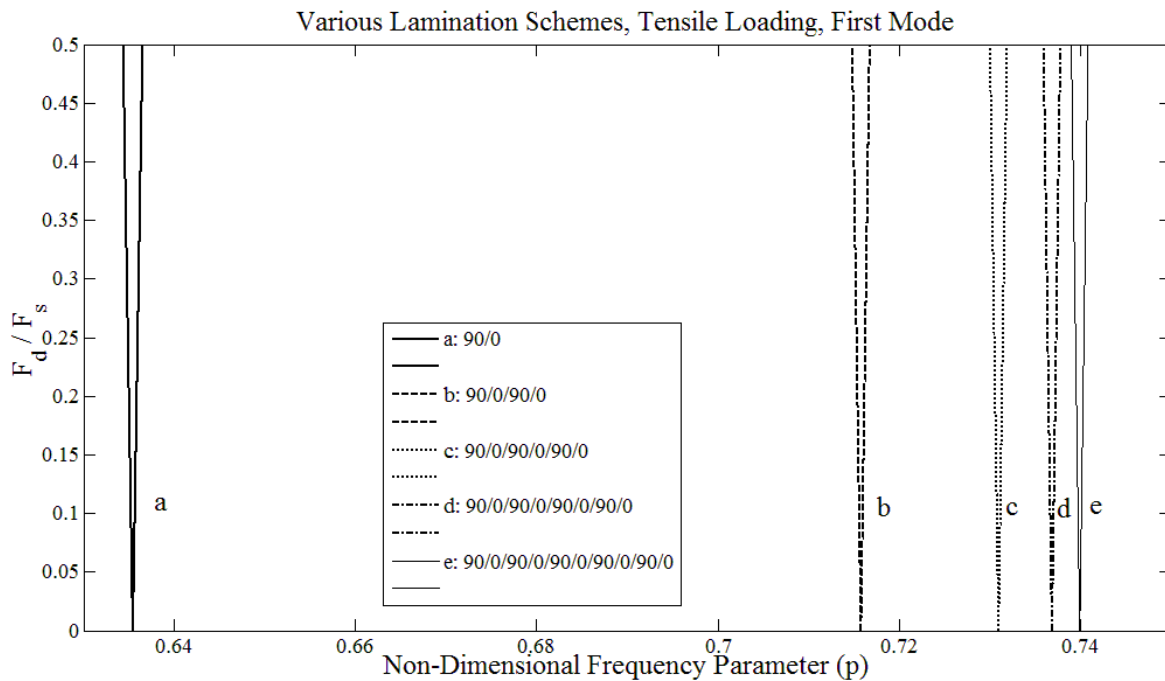
Figure 5.3 Variation of the first mode unstable regions with different lamination schemes for the antisymmetric cross-ply laminated cylindrical shell having aspect ratios of $L/R = 2$ and $R/h = 200$ subjected to tensile loading of $F_s = 0.1N_{cr}$

Figure 5.3 shows a graphical representation of the influence of lamination schemes on the distribution of dynamically unstable regions. The graphs have been plotted for various number of plies for antisymmetric cross-ply laminated cylindrical shells subjected to tensile loading of $F_s = 0.1N_{cr}$. It is observed that the first unstable regions shifts to the right along the frequency axis so as to have higher frequencies of excitation as the number of layers are increased. This is probably due to the bending-extension coupling of lamination which is reduced by increasing the number of the plies in antisymmetric cross-ply laminates. This shifting to the right of the frequency axis of the unstable regions is reduced once the number of layers is doubled and appears to converge at a certain value as can be observed from this figure. The instability regions of eight- and ten-layered laminates are too closed to each other in comparison with those for two- and four-layered laminates. To compare these results in more detail with the corresponding one of the work of Ng et al. [21] they have been listed in Table 5.1. The results are for the first two dynamically unstable regions. In addition to all discussions about Fig. 3, it is also observed that for the studied antisymmetric cylindrical shell, the shells with stacking sequence of $(0^o/90^o/0^o \dots)$ generally have slightly higher excitation frequency and smaller unstable region than that for the laminations having the stacking sequence of $(90^o/0^o/90^o \dots)$. So it can be concluded that $(0^o/90^o/0^o \dots)$ laminate shows more rigidity. All these outcomes are in excellent agreement with those reported by Ng et al. [21] and also in terms of the accuracy of the results there are good agreements between these two studies. The major differences between them have been originated from the neglecting of the in plane inertia forces in the present study although as it can be observed from the table the differences are very small particularly when the number of the plies are increased. The differences between the present work with those by Ng et al. [21] for eight layered laminated composite cylindrical shells having stacking sequence of $(90^o/0^o/90^o \dots)$ for the point of origins of the first two modes are 6.9% and 5.4% respectively, and the corresponding results for the width of dynamically-

unstable regions as the half-angle of the unstable regions i.e. θ are 6.4% and 5.1%

respectively.

Table 5.1 The first two unstable regions of an antisymmetric cross-ply laminated cylindrical shells having aspect ratios of $L/R = 2$ and $R/h = 200$ subjected to tensile loading of $F_s = 0.1N_{cr}$

Lamination scheme			1st Mode	2nd Mode
2 Plies $(0°, 90°)$	Point of origin p $(\times 10^{-1})$	Present	6.9016008	6.9705860
		Ref. [21]	5.7294728	6.0209359
	θ $(\times 10^{-3})$	Present	1.9845085	1.9648964
		Ref. [21]	2.3895200	2.2740400
2 Plies $(90°, 0°)$	Point of origin p $(\times 10^{-1})$	Present	6.3547085	6.3959595
		Ref. [21]	5.6544179	5.9596621
	θ $(\times 10^{-3})$	Present	2.1550190	2.1411435
		Ref. [21]	2.4209600	2.2971400
4 Plies $(0°, 90°)_2$	Point of origin p $(\times 10^{-1})$	Present	7.4216213	7.9993525
		Ref. [21]	6.7444835	7.2631657
	θ $(\times 10^{-3})$	Present	1.8456368	1.7124891
		Ref. [21]	2.0304200	1.8856600
4 Plies $(90°, 0°)_2$	Point of origin p $(\times 10^{-1})$	Present	7.1582175	7.7424176
		Ref. [21]	6.7139982	7.2272139
	θ $(\times 10^{-3})$	Present	1.9134623	1.7692547
		Ref. [21]	2.0395200	1.8949200
6 Plies $(0°, 90°)_3$	Point of origin p $(\times 10^{-1})$	Present	7.4831878	7.9920178
		Ref. [21]	6.8675170	7.4502604
	θ $(\times 10^{-3})$	Present	1.8304709	1.7140591
		Ref. [21]	1.9941000	1.8382800
6 Plies $(90°, 0°)_3$	Point of origin p $(\times 10^{-1})$	Present	7.3101192	7.8215051
		Ref. [21]	6.8471840	7.4332544
	θ $(\times 10^{-3})$	Present	1.8737527	1.7513850
		Ref. [21]	1.9999200	1.8424200
8 Plies $(0°, 90°)_4$	Point of origin p $(\times 10^{-1})$	Present	7.4982173	7.9831185
		Ref. [21]	6.9092540	7.4640614
	θ $(\times 10^{-3})$	Present	1.8268063	1.7159678
		Ref. [21]	1.9820400	1.8348800
8 Plies $(90°, 0°)_4$	Point of origin p $(\times 10^{-1})$	Present	7.3690617	7.8554361
		Ref. [21]	6.8940005	7.4512986
	θ $(\times 10^{-3})$	Present	1.8587842	1.7438284
		Ref. [21]	1.9863800	1.8379600
10 Plies $(0°, 90°)_5$	Point of origin p $(\times 10^{-1})$	Present	7.5022391	7.9760989
	θ $(\times 10^{-3})$	Present	1.8258282	1.7174763
10 Plies $(90°, 0°)_5$	Point of origin p $(\times 10^{-1})$	Present	7.3991511	7.8740275
	θ $(\times 10^{-3})$	Present	1.8512348	1.7397156

Tables 5.2 and 5.3 listed the first two instability regions of a two-layered cross-ply $(90°/0°)$

laminate subjected to various magnitudes of tensile and compressive loadings respectively. The

results illustrate that the instability regions shifted to the higher excitation frequencies once the

magnitude of tensile axial loading is increased from $F_s = 0.1N_{cr}$ to $F_s = 0.3N_{cr}$ Hence it can

be expected that by increasing the tensile axial load the shell's stiffness is also increased. Although the results in Table 3 indicate that the inverse trend can be seen in the case of compressive loading, in compressive loading conditions increasing the absolute magnitude of compressive loads from $F_s = -0.1N_{cr}$ to $F_s = -0.3N_{cr}$ causes the instability region to shift to lower excitation frequencies. This can be expected again since by increasing the magnitude of axial compressive loads the shell's stiffness is reduced. Also it can be observed from these tables that the width of instability regions are increased once the absolute value of magnitude of axial loads are increased for both tensile and compressive loading conditions. All these outcomes again are in an excellent conformance with those reported by Ng et al. [23] and also in terms of the accuracy of the results there are good agreements between these two studies.

Table 5.2 The first two unstable regions of an antisymmetric cross-ply laminated cylindrical shells having aspect ratios of $L/R = 2$ and $R/h = 200$ subjected to various tensile loading

Load			1st Mode $(m,n) = (1,6)$	2nd Mode $(m,n) = (1,5)$
$F_s = 0.1N_{cr}$	Point of origin p ($\times 10^{-1}$)	Present	6.3547085	6.3959595
		Ref. [62]	5.6544179	5.9596621
	θ ($\times 10^{-3}$)	Present	2.1550190	2.1411435
		Ref. [62]	2.4095530	2.2971360
$F_s = 0.2N_{cr}$	Point of origin p ($\times 10^{-1}$)	Present	6.3977001	6.4386756
		Ref. [62]	5.7026828	6.0054732
	θ ($\times 10^{-3}$)	Present	4.2775352	4.2504033
		Ref. [62]	4.7959232	4.5549685
$F_s = 0.3N_{cr}$	Point of origin p ($\times 10^{-1}$)	Present	6.4404047	6.4811102
		Ref. [62]	5.7505425	6.0509375
	θ ($\times 10^{-3}$)	Present	6.3686202	6.3288172
		Ref. [62]	7.1268993	6.7749563

Table 5.3 The first two unstable regions of an antisymmetric cross-ply laminated cylindrical shells having aspect ratios of $L/R = 2$ and $R/h = 200$ subjected to various compressive loading

Load			1st Mode $(m,n) = (1,6)$	2nd Mode $(m,n) = (1,5)$
$F_s = -0.1N_{cr}$	Point of origin p ($\times 10^{-1}$)	Present	6.2678408	6.3096597
		Ref. [62]	5.5566307	5.8669669
	θ ($\times 10^{-3}$)	Present	2.1886489	2.1741179
		Ref. [62]	2.4634550	2.3333558
$F_s = -0.2N_{cr}$	Point of origin p ($\times 10^{-1}$)	Present	6.2239523	6.2660642
		Ref. [62]	5.5070860	5.8200656
	θ ($\times 10^{-3}$)	Present	4.4121140	4.3823579
		Ref. [62]	4.9655192	4.6995054
$F_s = -0.3N_{cr}$	Point of origin p ($\times 10^{-1}$)	Present	6.1797521	6.2221631
		Ref. [62]	5.4570915	5.7727834
	θ ($\times 10^{-3}$)	Present	6.6716455	6.6259279
		Ref. [62]	7.5075589	7.0994407

To investigate the effects of geometric non-linearity on the dynamic instability of cross-ply laminated composite cylindrical shells the results are plotted in Figures 5.4-5.10 and listed in Tables 5.4-5.11.

In the analysis of dynamic stability of shells, there exist simultaneously the stable and unstable solutions. Figure 5.4 displays the both stable and unstable solutions of amplitude-frequency of steady-state vibrations for a two-layered $(90^o/0^o)$ laminated cylindrical shell subjected to tensile load of $F_s = 0.1N_{cr}$ and $F_d = 0.3F_s$. The graphs show the fundamental (first) mode i.e. mode (1, 6) having aspect ratios of $L/R = 2$ and $R/h = 200$. It is a key feature of the non-linear response that the amplitude-frequency curves are sloping toward the axis of increasing frequencies [1].
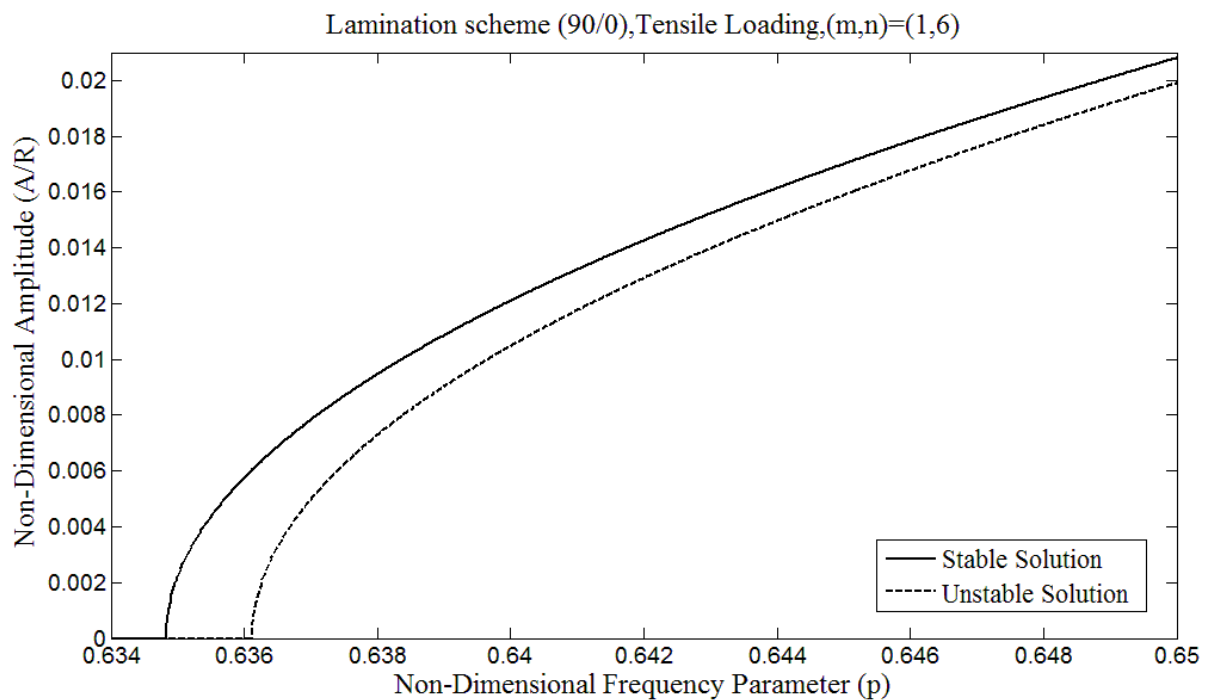
Figure 5.4 The stable and unstable solution amplitude of steady-state vibrations of the first transverse mode, mode (1, 6) of a two- layered $(\boldsymbol{90^o/0^o})$ cross-ply laminated cylindrical shell having aspect ratios of $\boldsymbol{L/R = 2}$ and $\boldsymbol{R/h = 200}$ subjected to tensile loading of $\boldsymbol{F_s = 0.1N_{cr}}$ and $\boldsymbol{F_d = 0.3F_s}$

The width of the region bounded by stable and unstable solutions of amplitude-frequency curves refers to the possibility of a parametric resonance i.e. closer these two stable and unstable amplitude curves to each other the more possibility of parametric resonance occurring.

175

Therefore if this region width is large, the dynamic stability of such a shell system is said to be good [1, 18].

Here and in following figures, tables and discussions the first two amplitude-frequency curves i.e. from left to right of the frequency's axis refer to the first two modes. Figures 5.5 and 6 show the variation of stable-solutions amplitude of steady-state vibrations corresponding to the circumferential wave numbers $m = 1$, $n = 1,2,3,4,5,6,7,8$ for a two-layered and ten-layered $(90^o/0^o / ...)$cross-ply laminated cylindrical shell with aspect ratios of $L/R = 2$ and $R/h = 200$ subjected to tensile loading of $F_s = 0.1N_{cr}$ and $F_d = 0.3F_s$.

As it can be observed from Fig.5 the sequences of the transverse modes from left to right of frequency's axis for two-layered laminated shell are as $(1, 6)$, $(1, 5)$, $(1, 7)$, $(1, 4)$, $(1, 8)$, $(1, 3)$, $(1, 2)$ and $(1, 1)$ while from Fig. 5.6 these sequences for ten-layered shell are as $(1, 5)$, $(1,4)$, $(1, 6)$, $(1, 7)$, $(1, 3)$, $(1, 8)$, $(1, 2)$ and $(1, 1)$. Hence the sequence of the vibration modes for the same geometric and loading conditions are affected by the number of the layers. So in the results in the Tables 5.1-5.6 the first two modes of the two-layered shell are mode $(1, 6)$ and mode$(1, 5)$, respectively and the first two modes of four-, six-, eight- and ten-layered laminated composite shells are mode $(1, 5)$ and mode $(1, 4)$, respectively.

Fig. 5.7 shows the influence of the lamination scheme on the fundamental mode of stable-solution amplitude-frequency of steady-state vibrations for antisymmetric cross-ply laminated cylindrical shells subjected to tensile loading of $F_s = 0.1N_{cr}$ and $F_d = 0.3F_s$. It is observed that the first mode amplitude of steady-state vibrations shifts to the right along the frequency axis where having higher frequencies of excitation as the number of layers are increased. This is probably due to the bending-extension coupling of lamination which is reduced by increasing the number of the plies in antisymmetric cross-ply laminates. This shifting to the right of the frequency axis of the steady-state amplitude (reducing the amplitude at a certain excitation frequency) is reduced once the number of layers is doubled and appears to converge at a certain
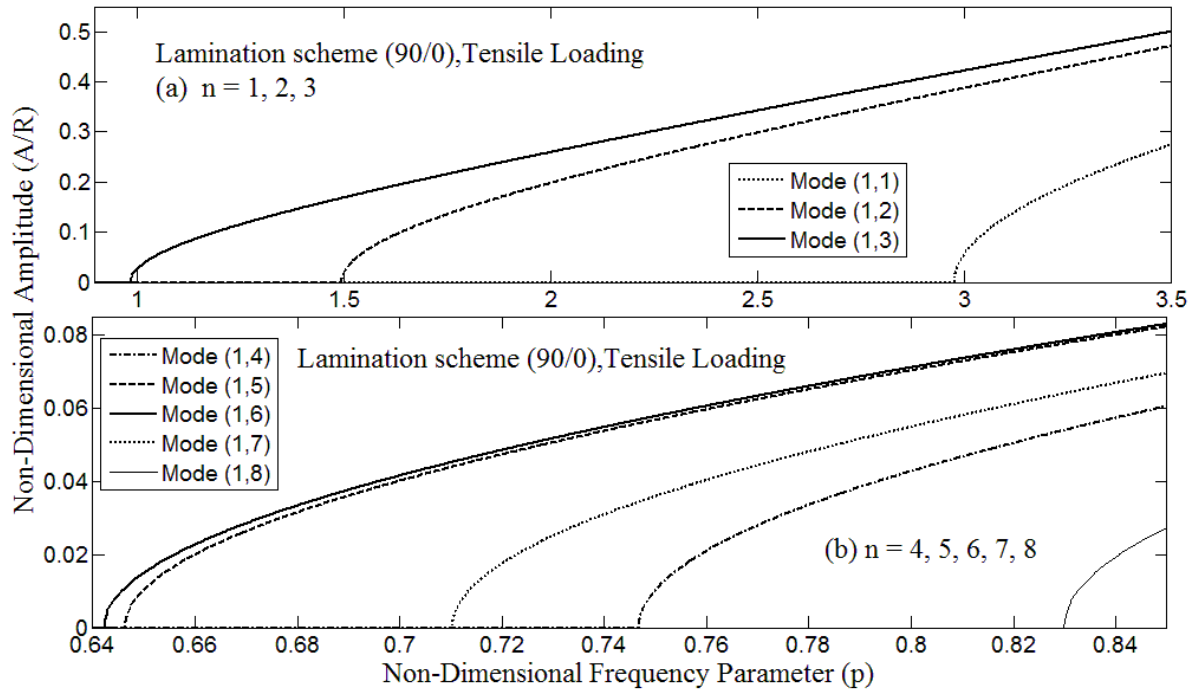
Figure 5.5 Variation of stable-solution amplitude of steady-state vibrations corresponding to the circumferential wave numbers $m = 1$, $n = 1, 2, 3, 4, 5, 6, 7, 8$ for a two-layered ($90^o/0^o$)cross-ply laminated cylindrical shell having aspect ratios of $L/R = 2$ and $R/h = 200$ subjected to tensile loading of $F_s = 0.1 N_{cr}$ and $F_d = 0.3 F_s$
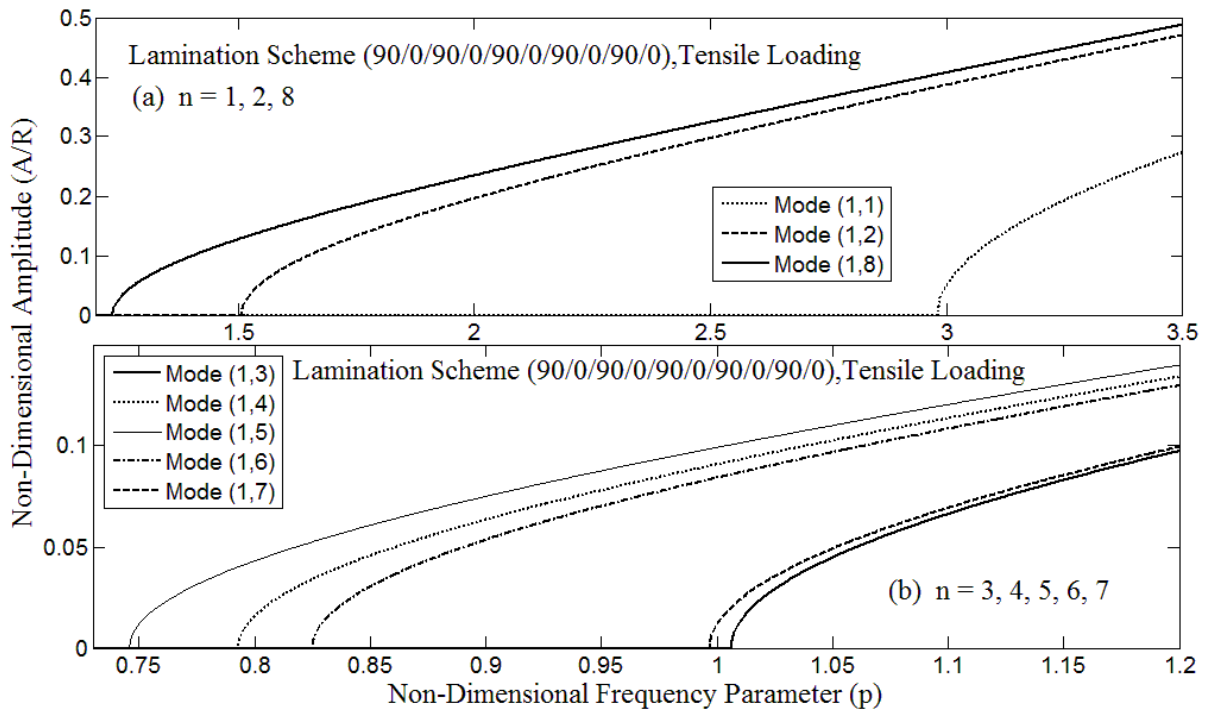
Figure 5.6 Variation of stable-solution amplitude of steady-state vibrations corresponding to the circumferential wave numbers $m = 1$, $n = 1, 2, 3, 4, 5, 6, 7, 8$ for a ten-layered ($90^o/0^o/90^o/ ...$) cross-ply laminated cylindrical shell having aspect ratios of $L/R = 2$ and $R/h = 200$ subjected to tensile loading of $F_s = 0.1 N_{cr}$ and $F_d = 0.3 F_s$

177
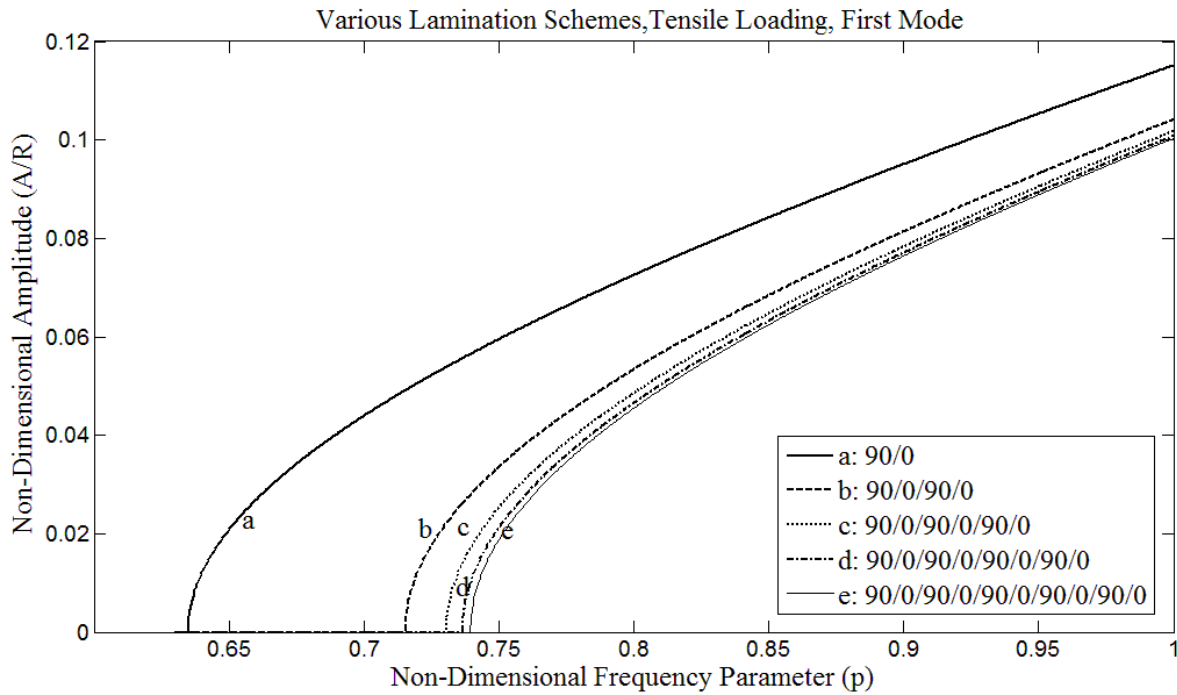
Figure 5.7 The stable-solution amplitude of steady-state vibrations of the first mode corresponding to various lamination schemes for the antisymmetric cross-ply laminated cylindrical shell having aspect ratios of $L/R = 2$ and $R/h = 200$ subjected to tensile loading of $F_s = 0.1N_{cr}$ and $F_d = 0.3F_s$

value as can be observed from this figure the amplitudes of eight- and ten-layered laminates almost coincide with each other.

Tables 5.4-5.9 also present a detailed study considering again the effects of variation of the lamination scheme on the first two modes, both stable and unstable solutions amplitude of steady-state vibrations of antisymmetric cross-ply laminated cylindrical shells. Tables 5.4-5.6 present the result for tensile load, $F_s = 0.1N_{cr}$, $F_s = 0.3N_{cr}$ and $F_s = 0.5N_{cr}$ respectively and the corresponding results for compressive loads, $F_s = -0.1N_{cr}$, $F_s = -0.3N_{cr}$ and $F_s = -0.5N_{cr}$ are tabulated in Tables 5.7-5.9 respectively. For the comparison studies the results are normalized using the same non-dimensional excitation frequency parameter $p = 1$. All the discussions and corresponding observations that were mentioned in the previous paragraph about Fig. 5.7 are also observed from these tables and hence are valid. In addition it is also observed that for the studied antisymmetric cylindrical shell, the shell with stacking sequence of $(0^o/90^o/0^o ...)$ generally have slightly lower amplitude of steady-state vibrations both in stable and unstable solutions in comparison with the laminations having the stacking sequence

178

of $(90^o/0^o/90^o\ldots)$ so it can be concluded that $(0^o/90^o/0^o\ldots)$ laminate shows more

rigidity.

Table 5.4 The stable and unstable solution amplitudes corresponding to first two modes of steady-state vibrations for an antisymmetric cross-ply laminated cylindrical shell having aspect ratios of $L/R = 2$ and $R/h = 200$ subjected to tensile loading of $F_s = 0.1 N_{cr}$ and $F_d = 0.3 F_s$ under the excitation with non-dimensional frequency parameter $p = 1$

Lamination scheme	Non-Dimensional Amplitude (A/R)	1st Mode	2nd Mode
2 Plies $(0°, 90°)$	Stable-Solutions $(\times 10^{-2})$	10.78910398	10.69022499
	Unstable-Solutions $(\times 10^{-2})$	10.7721744	10.67313857
2 Plies $(90°, 0°)$	Stable-Solutions $(\times 10^{-2})$	11.51062486	11.45980633
	Unstable-Solutions $(\times 10^{-2})$	11.49475799	11.443869
4 Plies $(0°, 90°)_2$	Stable-Solutions $(\times 10^{-2})$	9.99371264	8.949960089
	Unstable-Solutions $(\times 10^{-2})$	9.975433268	8.929544341
4 Plies $(90°, 0°)_2$	Stable-Solutions $(\times 10^{-2})$	10.41140806	9.438122574
	Unstable-Solutions $(\times 10^{-2})$	10.3938633	9.418765008
6 Plies $(0°, 90°)_3$	Stable-Solutions $(\times 10^{-2})$	9.891296312	8.964490851
	Unstable-Solutions $(\times 10^{-2})$	9.872827319	8.944108271
6 Plies $(90°, 0°)_3$	Stable-Solutions $(\times 10^{-2})$	10.17446934	9.292273366
	Unstable-Solutions $(\times 10^{-2})$	10.15651529	9.272611329
8 Plies $(0°, 90°)_4$	Stable-Solutions $(\times 10^{-2})$	9.866003675	8.982071823
	Unstable-Solutions $(\times 10^{-2})$	9.847487246	8.961729229
8 Plies $(90°, 0°)_4$	Stable-Solutions $(\times 10^{-2})$	10.07966226	9.228531861
	Unstable-Solutions $(\times 10^{-2})$	10.06153903	9.208733727
10 Plies $(0°, 90°)_5$	Stable-Solutions $(\times 10^{-2})$	9.859215961	8.995901351
	Unstable-Solutions $(\times 10^{-2})$	9.84068676	8.975590101
10 Plies $(90°, 0°)_5$	Stable-Solutions $(\times 10^{-2})$	10.03062259	9.193301364
	Unstable-Solutions $(\times 10^{-2})$	10.0124106	9.173427196

Table 5.5 The stable and unstable solution amplitudes corresponding to first two modes of steady-state vibrations for an antisymmetric cross-ply laminated cylindrical shell having aspect ratios of $L/R = 2$ and $R/h = 200$ subjected to tensile loading of $F_s = 0.3 N_{cr}$ and $F_d = 0.3 F_s$ under the excitation with non-dimensional frequency parameter $p = 1$

Lamination scheme	Non-Dimensional Amplitude (A/R)	1st Mode	2nd Mode
2 Plies $(0°, 90°)$	Stable-Solutions $(\times 10^{-2})$	10.69281527	10.59303753
	Unstable-Solutions $(\times 10^{-2})$	10.64148618	10.54122259
2 Plies $(90°, 0°)$	Stable-Solutions $(\times 10^{-2})$	11.42042112	11.36919939
	Unstable-Solutions $(\times 10^{-2})$	11.37237654	11.32093744
4 Plies $(0°, 90°)_2$	Stable-Solutions $(\times 10^{-2})$	9.88968281	8.833647001
	Unstable-Solutions $(\times 10^{-2})$	9.834162685	8.771445091
4 Plies $(90°, 0°)_2$	Stable-Solutions $(\times 10^{-2})$	10.31159306	9.327898557
	Unstable-Solutions $(\times 10^{-2})$	10.25835665	9.269014032
6 Plies $(0°, 90°)_3$	Stable-Solutions $(\times 10^{-2})$	9.786177828	8.848368774
	Unstable-Solutions $(\times 10^{-2})$	9.730067118	8.786271086
6 Plies $(90°, 0°)_3$	Stable-Solutions $(\times 10^{-2})$	10.07230659	9.180298365
	Unstable-Solutions $(\times 10^{-2})$	10.01779865	9.120460937
8 Plies $(0°, 90°)_4$	Stable-Solutions $(\times 10^{-2})$	9.760612802	8.866180011
	Unstable-Solutions $(\times 10^{-2})$	9.704354275	8.80420795
8 Plies $(90°, 0°)_4$	Stable-Solutions $(\times 10^{-2})$	9.976528703	9.115773915
	Unstable-Solutions $(\times 10^{-2})$	9.921494574	9.055510129
10 Plies $(0°, 90°)_5$	Stable-Solutions $(\times 10^{-2})$	9.753751745	8.880190024
	Unstable-Solutions $(\times 10^{-2})$	9.697453416	8.818316421
10 Plies $(90°, 0°)_5$	Stable-Solutions $(\times 10^{-2})$	9.926979564	9.080105931
	Unstable-Solutions $(\times 10^{-2})$	9.871669205	9.019603836

Table 5.6 The stable and unstable solution amplitudes corresponding to first two modes of steady-state vibrations for an antisymmetric cross-ply laminated cylindrical shell having aspect ratios of $L/R = 2$ and $R/h = 200$ subjected to tensile loading of $F_s = 0.5N_{cr}$ and $F_d = 0.3F_s$ under the excitation with non-dimensional frequency parameter $p = 1$

Lamination scheme	Non-Dimensional Amplitude (A/R)	1st Mode	2nd Mode
2 Plies $(0°, 90°)$	Stable-Solutions $(\times 10^{-2})$	10.59565157	10.49495011
	Unstable-Solutions $(\times 10^{-2})$	10.50917289	10.40763472
2 Plies $(90°, 0°)$	Stable-Solutions $(\times 10^{-2})$	11.3294992	11.27786454
	Unstable-Solutions $(\times 10^{-2})$	11.2486637	11.19665626
4 Plies $(0°, 90°)_2$	Stable-Solutions $(\times 10^{-2})$	9.784546992	8.715781841
	Unstable-Solutions $(\times 10^{-2})$	9.690832914	8.610443416
4 Plies $(90°, 0°)_2$	Stable-Solutions $(\times 10^{-2})$	10.24054967	9.24930255
	Unstable-Solutions $(\times 10^{-2})$	10.09093631	9.08337688
6 Plies $(0°, 90°)_3$	Stable-Solutions $(\times 10^{-2})$	9.679917884	8.730702361
	Unstable-Solutions $(\times 10^{-2})$	9.585180904	8.625546154
6 Plies $(90°, 0°)_3$	Stable-Solutions $(\times 10^{-2})$	9.969096941	9.066940599
	Unstable-Solutions $(\times 10^{-2})$	9.877134025	8.965728891
8 Plies $(0°, 90°)_4$	Stable-Solutions $(\times 10^{-2})$	9.654071474	8.748753154
	Unstable-Solutions $(\times 10^{-2})$	9.559078342	8.643816545
8 Plies $(90°, 0°)_4$	Stable-Solutions $(\times 10^{-2})$	9.872317798	9.001603625
	Unstable-Solutions $(\times 10^{-2})$	9.779444843	8.8996489
10 Plies $(0°, 90°)_5$	Stable-Solutions $(\times 10^{-2})$	9.647134645	8.762950908
	Unstable-Solutions $(\times 10^{-2})$	9.552072529	8.658186378
10 Plies $(90°, 0°)_5$	Stable-Solutions $(\times 10^{-2})$	9.822242973	8.965481442
	Unstable-Solutions $(\times 10^{-2})$	9.72889201	8.863111204

Table 5.7 The stable and unstable solution amplitudes corresponding to first two modes of steady-state vibrations for an antisymmetric cross-ply laminated cylindrical shell having aspect ratios of $L/R = 2$ and $R/h = 200$ subjected to compressive loading of $F_s = -0.1N_{cr}$ and $F_d = 0.3F_s$ under the excitation with non-dimensional frequency parameter $p = 1$

Lamination scheme	Non-Dimensional Amplitude (A/R)	1st Mode	2nd Mode
2 Plies $(0°, 90°)$	Stable-Solutions $(\times 10^{-2})$	10.901296	10.8034439
	Unstable-Solutions $(\times 10^{-2})$	10.88454092	10.78653682
2 Plies $(90°, 0°)$	Stable-Solutions $(\times 10^{-2})$	11.61585014	11.56549397
	Unstable-Solutions $(\times 10^{-2})$	11.6001272	11.54970248
4 Plies $(0°, 90°)_2$	Stable-Solutions $(\times 10^{-2})$	10.11473094	9.084892695
	Unstable-Solutions $(\times 10^{-2})$	10.09667067	9.064780848
4 Plies $(90°, 0°)_2$	Stable-Solutions $(\times 10^{-2})$	10.52762592	9.566172036
	Unstable-Solutions $(\times 10^{-2})$	10.51027516	9.547074105
6 Plies $(0°, 90°)_3$	Stable-Solutions $(\times 10^{-2})$	10.01355244	9.099207983
	Unstable-Solutions $(\times 10^{-2})$	9.995309349	9.079127847
6 Plies $(90°, 0°)_3$	Stable-Solutions $(\times 10^{-2})$	10.29336272	9.422305132
	Unstable-Solutions $(\times 10^{-2})$	10.27561641	9.402915003
8 Plies $(0°, 90°)_4$	Stable-Solutions $(\times 10^{-2})$	9.988569377	9.11652916
	Unstable-Solutions $(\times 10^{-2})$	9.970280575	9.09648726
8 Plies $(90°, 0°)_4$	Stable-Solutions $(\times 10^{-2})$	10.19966082	9.359449236
	Unstable-Solutions $(\times 10^{-2})$	10.19966082	9.339928616
10 Plies $(0°, 90°)_5$	Stable-Solutions $(\times 10^{-2})$	9.981865009	9.130155027
	Unstable-Solutions $(\times 10^{-2})$	9.963563901	9.110143103
10 Plies $(90°, 0°)_5$	Stable-Solutions $(\times 10^{-2})$	10.15120088	9.324713383
	Unstable-Solutions $(\times 10^{-2})$	10.1332056	9.305119893

Table 5.8 The stable and unstable solution amplitudes corresponding to first two modes of steady-state vibrations for an antisymmetric cross-ply laminated cylindrical shell having aspect ratios of $L/R = 2$ and $R/h = 200$ subjected to compressive loading of $F_s = -0.3N_{cr}$ and $F_d = 0.3F_s$ under the excitation with non-dimensional frequency parameter $p = 1$

Lamination scheme	Non-Dimensional Amplitude (A/R)	1st Mode	2nd Mode
2 Plies $(0°, 90°)$	Stable-Solutions $(\times 10^{-2})$	11.028906	10.93219617
	Unstable-Solutions $(\times 10^{-2})$	10.97914829	10.88199627
2 Plies $(90°, 0°)$	Stable-Solutions $(\times 10^{-2})$	11.73569289	11.68585315
	Unstable-Solutions $(\times 10^{-2})$	11.68894423	11.63890431
4 Plies $(0°, 90°)_2$	Stable-Solutions $(\times 10^{-2})$	10.25213613	9.23762894
	Unstable-Solutions $(\times 10^{-2})$	10.19858935	9.178165289
4 Plies $(90°, 0°)_2$	Stable-Solutions $(\times 10^{-2})$	10.65971015	9.711341853
	Unstable-Solutions $(\times 10^{-2})$	10.60822088	9.654796229
6 Plies $(0°, 90°)_3$	Stable-Solutions $(\times 10^{-2})$	10.1523271	9.2517079
	Unstable-Solutions $(\times 10^{-2})$	10.0982511	9.192335324
6 Plies $(90°, 0°)_3$	Stable-Solutions $(\times 10^{-2})$	10.42841451	9.56965763
	Unstable-Solutions $(\times 10^{-2})$	10.3757775	9.512269803
8 Plies $(0°, 90°)_4$	Stable-Solutions $(\times 10^{-2})$	10.12768638	9.268744094
	Unstable-Solutions $(\times 10^{-2})$	10.0734781	9.209481349
8 Plies $(90°, 0°)_4$	Stable-Solutions $(\times 10^{-2})$	10.33593702	9.507775931
	Unstable-Solutions $(\times 10^{-2})$	10.28282664	9.450012317
10 Plies $(0°, 90°)_5$	Stable-Solutions $(\times 10^{-2})$	10.12107416	9.282146517
	Unstable-Solutions $(\times 10^{-2})$	10.06683028	9.222969891
10 Plies $(90°, 0°)_5$	Stable-Solutions $(\times 10^{-2})$	10.28811899	9.473583948
	Unstable-Solutions $(\times 10^{-2})$	10.23476048	9.415610573

Table 5.9 The stable and unstable solution amplitudes corresponding to first two modes of steady-state vibrations for an antisymmetric cross-ply laminated cylindrical shell having aspect ratios of $L/R = 2$ and $R/h = 200$ subjected to compressive loading of $F_s = -0.5N_{cr}$ and $F_d = 0.3F_s$ under the excitation with non-dimensional frequency parameter $p = 1$

Lamination scheme	Non-Dimensional Amplitude (A/R)	1st Mode	2nd Mode
2 Plies $(0°, 90°)$	Stable-Solutions $(\times 10^{-2})$	11.15505628	11.05944964
	Unstable-Solutions $(\times 10^{-2})$	11.07294737	10.97662558
2 Plies $(90°, 0°)$	Stable-Solutions $(\times 10^{-2})$	11.85432414	11.80498526
	Unstable-Solutions $(\times 10^{-2})$	11.77709147	11.72742767
4 Plies $(0°, 90°)_2$	Stable-Solutions $(\times 10^{-2})$	10.38772393	9.38788057
	Unstable-Solutions $(\times 10^{-2})$	10.29949955	9.290166001
4 Plies $(90°, 0°)_2$	Stable-Solutions $(\times 10^{-2})$	10.81833195	9.885193279
	Unstable-Solutions $(\times 10^{-2})$	10.67681807	9.73011737
6 Plies $(0°, 90°)_3$	Stable-Solutions $(\times 10^{-2})$	10.28923023	9.401734533
	Unstable-Solutions $(\times 10^{-2})$	10.20015399	9.304165462
6 Plies $(90°, 0°)_3$	Stable-Solutions $(\times 10^{-2})$	10.56173955	9.714775361
	Unstable-Solutions $(\times 10^{-2})$	10.47498091	9.620381647
8 Plies $(0°, 90°)_4$	Stable-Solutions $(\times 10^{-2})$	10.26491814	9.418499363
	Unstable-Solutions $(\times 10^{-2})$	10.17562908	9.32110578
8 Plies $(90°, 0°)_4$	Stable-Solutions $(\times 10^{-2})$	10.47043969	9.653823922
	Unstable-Solutions $(\times 10^{-2})$	10.38291818	9.55882833
10 Plies $(0°, 90°)_5$	Stable-Solutions $(\times 10^{-2})$	10.25839439	9.431688986
	Unstable-Solutions $(\times 10^{-2})$	10.16904804	9.334433022
10 Plies $(90°, 0°)_5$	Stable-Solutions $(\times 10^{-2})$	10.42323872	9.620151037
	Unstable-Solutions $(\times 10^{-2})$	10.33531752	9.524819615

Comparing the results in the Tables 5.4-5.6 indicate that by increasing the magnitude of tensile axial loading from $F_s = 0.1N_{cr}$ to $F_s = 0.5N_{cr}$ both the stable and unstable solutions of amplitudes decrease which means that the corresponding excitation frequency that causes instability shifts to the right of frequency axis having higher frequencies. Hence it can be expected that by increasing the tensile axial load the shell stiffness is also increased. The inverse trend can be seen in the case of compressive loading. For the compressive loading the results have been listed in Tables 5.7-5.9. The shells have higher stable and unstable amplitudes as the magnitude of axial compressive loading is increased from $F_s = -0.1N_{cr}$ to $F_s = -0.5N_{cr}$ meaning that by increasing the magnitude of axial compressive loading the corresponding excitation frequency that causes instability shifts to the left of frequency axis having lower frequencies. This was expected since by increasing the magnitude of axial compressive loading the shell stiffness reduces.

To comparatively study the effect of symmetry in the lamination schemes of the above studied cylindrical shells the numerical results for both the stable and unstable solutions amplitude of steady-state vibrations were determined and are listed in Tables 5.10 and 5.11 for the tensile and compressive axial loads respectively. A graphical presentation of Table 5.10 has also been provided in Fig. 5.8. The first and second modes in these two tables refer to the modes (1,5) and (1,4) respectively which shows no change in terms of circumferential wave numbers in comparison with antisymmetric laminates. All the above discussions about Table 5.6, Table 5.9 and Fig. 5.5 remain valid about Table 5.10, Table 5.11 and Fig. 5.8 respectively. It can also be observed from these two tables (Tables 5.10 and 5.11) and Fig. 5.8 that by increasing the number of plies in symmetric laminate the amplitude of steady-state vibration converges to a certain value where the non-dimensional amplitude vs non-dimensional frequency curves of symmetric laminates having twenty, twenty-four and twenty-eight plies almost coincide with each other.
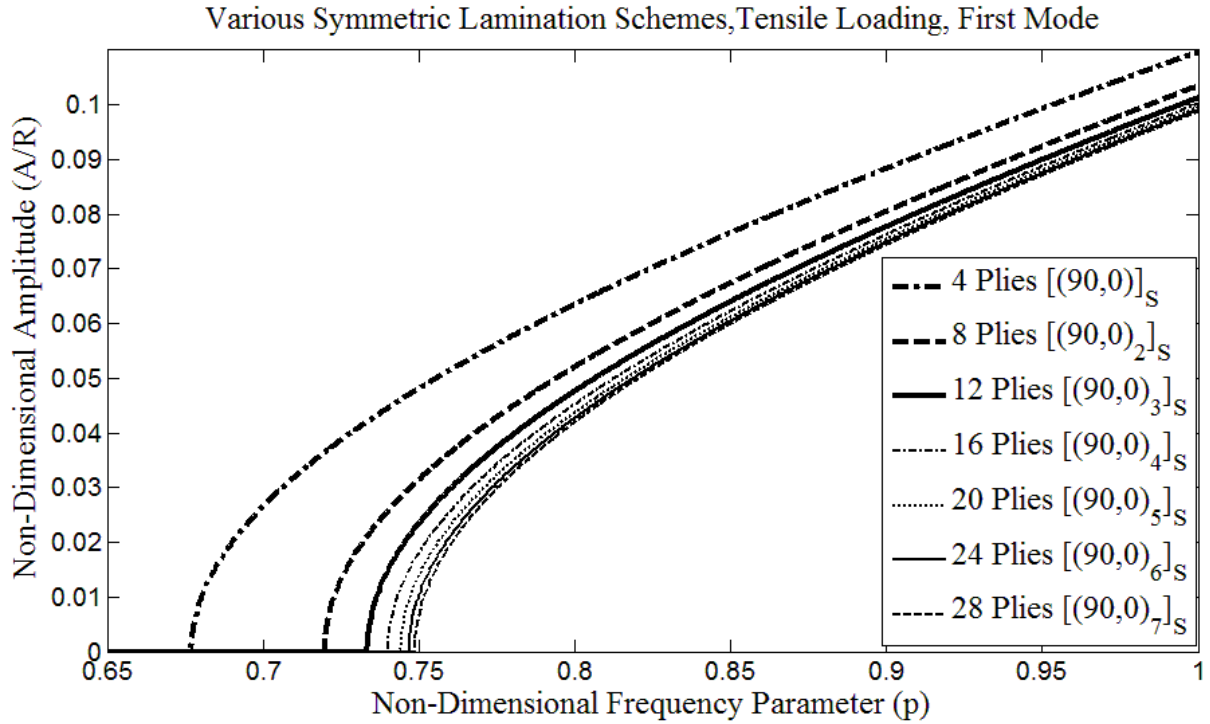
Figure 5.8 The stable-solution amplitude of steady-state vibrations of the first mode corresponding to various lamination schemes for the symmetric cross-ply laminated cylindrical shell having aspect ratios of $L/R = 2$ and $R/h = 200$ subjected to tensile loading of $F_s = 0.5N_{cr}$ and $F_d = 0.3F_s$

Another comparison of the results for symmetric laminates in Tables 5.10 and 5.11 with corresponding results for antisymmetric laminates in Tables 5.6 and 5.9 reveals that at the same non-dimensional frequency parameter (p) for both tensile and compressive loading conditions, symmetric laminates having stacking sequence of $[(90°, 0°)_n]_S$ have higher amplitude than antisymmetric $(90°/0°/\dots)$ laminate even though this trend is inverse for the case of lamination schemes of symmetric $[(0°, 90°)_n]_S$ and antisymmetric $(0°/90°/\dots)$ laminates. This behavior is in good agreement with that reported by Najafov et. al [22] but for non-linear free vibration of truncated orthotropic thin laminated conical shells.

Figure 5.9 displays the effects of variation of the length-to-radius ratio L/R on the stable-solution amplitude of steady-state vibrations for the eight-layered $(90°/0°/90°/\dots)$ cross-ply laminated cylindrical shell having thickness ratio $R/h = 100$ subjected to the axial tensile loading of $F_s = 0.5N_{cr}$ and $F_d = 0.3F_s$. As expected at the specific excitation frequency the shell having higher aspect ratio L/R has a larger amplitude or in other words the corresponding

183

excitation frequency that causes instability shifts to the left of frequency axis corresponding to lower frequencies, once the aspect ratio L/R is increased. This is due to the fact that increasing the length of the shell makes the shell to be less stiff.

Table 5.10 The stable and unstable solution amplitudes corresponding to first two modes of steady-state vibrations for a symmetric cross-ply laminated cylindrical shell having aspect ratios of $L/R = 2$ and $R/h = 200$ subjected to tensile loading of $F_s = 0.5N_{cr}$ and $F_d = 0.3F_s$ under the excitation with non-dimensional frequency parameter $p = 1$

Lamination scheme	Non-Dimensional Amplitude (A/R)	1st Mode	2nd Mode
4 Plies $[(0°, 90°)]_S$	Stable-Solutions ($\times 10^{-2}$)	8.287918645	8.205471326
	Unstable-Solutions ($\times 10^{-2}$)	8.177070269	8.093493832
4 Plies $[(90°, 0°)]_S$	Stable-Solutions ($\times 10^{-2}$)	10.96460814	9.36844586
	Unstable-Solutions ($\times 10^{-2}$)	10.88106219	9.270526445
8 Plies $[(0°, 90°)_2]_S$	Stable-Solutions ($\times 10^{-2}$)	8.975131066	8.570830826
	Unstable-Solutions ($\times 10^{-2}$)	8.872872161	8.463688545
8 Plies $[(90°, 0°)_2]_S$	Stable-Solutions ($\times 10^{-2}$)	10.34405209	9.11033656
	Unstable-Solutions ($\times 10^{-2}$)	10.25545203	9.009612365
12 Plies $[(0°, 90°)_3]_S$	Stable-Solutions ($\times 10^{-2}$)	9.217413791	8.663081991
	Unstable-Solutions ($\times 10^{-2}$)	9.117872543	8.557094852
12 Plies $[(90°, 0°)_3]_S$	Stable-Solutions ($\times 10^{-2}$)	10.12875482	9.022659459
	Unstable-Solutions ($\times 10^{-2}$)	10.03825468	8.920945378
16 Plies $[(0°, 90°)_4]_S$	Stable-Solutions ($\times 10^{-2}$)	9.336197655	8.708841131
	Unstable-Solutions ($\times 10^{-2}$)	9.237936424	8.603417727
16 Plies $[(90°, 0°)_4]_S$	Stable-Solutions ($\times 10^{-2}$)	10.01937147	8.978499844
	Unstable-Solutions ($\times 10^{-2}$)	9.927874262	8.876279748
20 Plies $[(0°, 90°)_5]_S$	Stable-Solutions ($\times 10^{-2}$)	9.406748027	8.736181569
	Unstable-Solutions ($\times 10^{-2}$)	9.309231503	8.631092117
20 Plies $[(90°, 0°)_5]_S$	Stable-Solutions ($\times 10^{-2}$)	9.953164463	8.951899513
	Unstable-Solutions ($\times 10^{-2}$)	9.953164463	8.849372159
24 Plies $[(0°, 90°)_6]_S$	Stable-Solutions ($\times 10^{-2}$)	9.453489108	8.754361091
	Unstable-Solutions ($\times 10^{-2}$)	9.356459749	8.649492519
24 Plies $[(90°, 0°)_6]_S$	Stable-Solutions ($\times 10^{-2}$)	9.9087807	8.934121959
	Unstable-Solutions ($\times 10^{-2}$)	9.816252732	8.831388221
28 Plies $[(0°, 90°)_7]_S$	Stable-Solutions ($\times 10^{-2}$)	9.486734599	8.767323385
	Unstable-Solutions ($\times 10^{-2}$)	9.39004878	8.662611734
28 Plies $[(90°, 0°)_7]_S$	Stable-Solutions ($\times 10^{-2}$)	9.876955904	8.921402018
	Unstable-Solutions ($\times 10^{-2}$)	9.876955904	8.818520096

It is also observed from the Figure 5.9 that by increasing the length, the circumferential wave numbers corresponding to the first two modes approach successively to lower values. The first two modes at $L/R = 1$ are modes $(1, 5)$ and $(1, 4)$, for $L/R = 5$ they are modes $(1, 4)$ and $(1, 3)$, and for $L/R = 10$ they are modes $(1, 3)$ and $(1, 2)$ respectively.

Table 5.11 The stable and unstable solution amplitudes corresponding to first two modes of steady-state vibrations for a symmetric cross-ply laminated cylindrical shell having aspect ratios of $L/R = 2$ and $R/h = 200$ subjected to compressive loading of $F_s = -0.5N_{cr}$ and $F_d = 0.3F_s$ under the excitation with non-dimensional frequency parameter $p = 1$.

Lamination scheme	Non-Dimensional Amplitude (A/R)	1st Mode	2nd Mode
4 Plies $[(0°, 90°)]_S$	Stable-Solutions ($\times 10^{-2}$)	8.992054491	8.916120691
	Unstable-Solutions ($\times 10^{-2}$)	8.889990252	8.813177118
4 Plies $[(90°, 0°)]_S$	Stable-Solutions ($\times 10^{-2}$)	11.50608883	9.996760792
	Unstable-Solutions ($\times 10^{-2}$)	11.42650265	9.905054723
8 Plies $[(0°, 90°)_2]_S$	Stable-Solutions ($\times 10^{-2}$)	9.629144622	9.253463652
	Unstable-Solutions ($\times 10^{-2}$)	9.53390313	9.154314408
8 Plies $[(90°, 0°)_2]_S$	Stable-Solutions ($\times 10^{-2}$)	10.91635755	9.755289885
	Unstable-Solutions ($\times 10^{-2}$)	10.83243947	9.661292019
12 Plies $[(0°, 90°)_3]_S$	Stable-Solutions ($\times 10^{-2}$)	9.855362271	9.338974145
	Unstable-Solutions ($\times 10^{-2}$)	9.762328012	9.240742438
12 Plies $[(90°, 0°)_3]_S$	Stable-Solutions ($\times 10^{-2}$)	10.71256845	9.673460199
	Unstable-Solutions ($\times 10^{-2}$)	10.62704124	9.57865935
16 Plies $[(0°, 90°)_4]_S$	Stable-Solutions ($\times 10^{-2}$)	9.966545798	9.381437116
	Unstable-Solutions ($\times 10^{-2}$)	9.874559123	9.283654726
16 Plies $[(90°, 0°)_4]_S$	Stable-Solutions ($\times 10^{-2}$)	10.60920606	9.632284669
	Unstable-Solutions ($\times 10^{-2}$)	10.52283877	9.537074534
20 Plies $[(0°, 90°)_5]_S$	Stable-Solutions ($\times 10^{-2}$)	10.0326645	9.406822892
	Unstable-Solutions ($\times 10^{-2}$)	9.941289638	9.309307151
20 Plies $[(90°, 0°)_5]_S$	Stable-Solutions ($\times 10^{-2}$)	10.54670239	9.607494647
	Unstable-Solutions ($\times 10^{-2}$)	10.45981903	9.512036381
24 Plies $[(0°, 90°)_6]_S$	Stable-Solutions ($\times 10^{-2}$)	10.07650261	9.423708751
	Unstable-Solutions ($\times 10^{-2}$)	9.985528906	9.326369569
24 Plies $[(90°, 0°)_6]_S$	Stable-Solutions ($\times 10^{-2}$)	10.50482667	9.590932368
	Unstable-Solutions ($\times 10^{-2}$)	10.41759407	9.495307599
28 Plies $[(0°, 90°)_7]_S$	Stable-Solutions ($\times 10^{-2}$)	10.10769914	9.435751578
	Unstable-Solutions ($\times 10^{-2}$)	10.01700876	9.338537924
28 Plies $[(90°, 0°)_7]_S$	Stable-Solutions ($\times 10^{-2}$)	10.47481295	9.579084636
	Unstable-Solutions ($\times 10^{-2}$)	10.3873283	9.483340402

The effect of the thickness ratio R/h on the stable-solution amplitude of steady-state vibrations for the eight-layered $(90°/0°/90°/...)$ cross-ply laminated cylindrical shell with length ratio $L/R = 2$ subjected to axial compressive loading of $F_s = -0.3N_{cr}$ and $F_d = 0.3F_s$ is presented in Figure 5.10. Here the first two modes are modes $(1, 5)$ and $(1, 4)$ respectively. It shows that by increasing the thickness ratio R/h, at any specific frequency, the amplitude of steady-state vibrations is also increased or in other words the corresponding frequency of excitation that causes instability shifts to the left of frequency axis having lower frequencies, by increasing the thickness ratio R/h. This is again due to the fact that decreasing the thickness of the shell makes the shell to be less stiff.
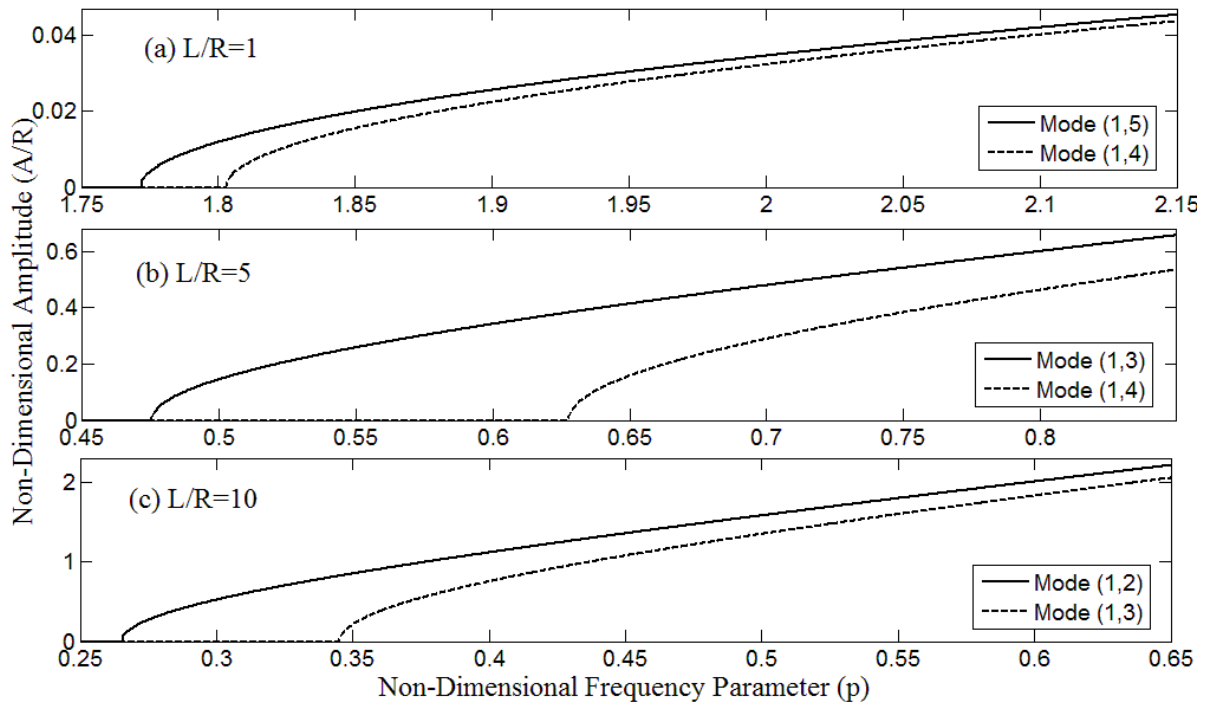
Figure 5.9 Variation of the first two stable-solution amplitudes of steady-state vibrations with shell length of an eight-layered ($90^°/0^°/90^°/\dots$) antisymmetric cross-ply laminated cylindrical shell having thickness
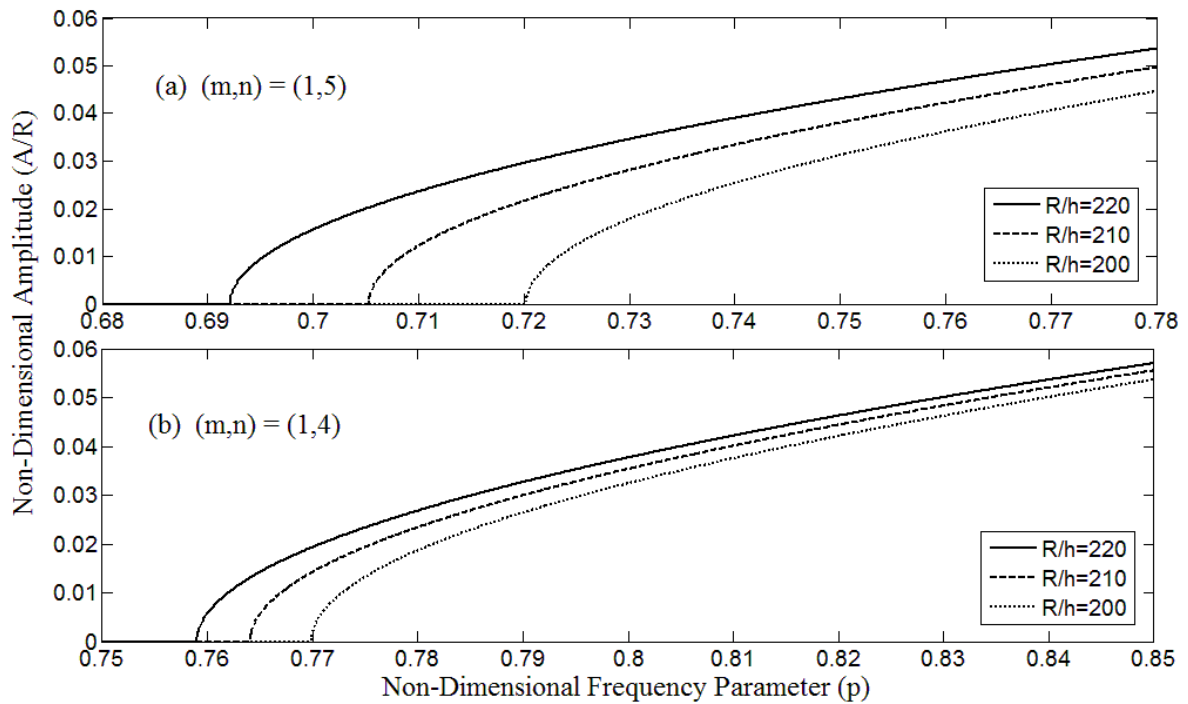
Figure 5.10 Variation of the first two stable-solution amplitudes of steady-state vibrations with shell thickness of an eight-layered ($90^°/0^°/90^°/\dots$) antisymmetric cross-ply laminated cylindrical shell having length ratio $L/R = 2$ subjected to compressive loading of $F_s = -0.3N_{cr}$ and $F_d = 0.3F_s$

5.7   Conclusions

In the present work, the non-linear dynamic stability of both symmetric and antisymmetric cross-ply laminated composite cylindrical shells under combined static and periodic axial loading has been studied. Donnell's shallow-shell equations of motion with von Karman-type of non-linearity were solved by employing Galerkin's technique. By applying Bolotin's method to the governing system of non-linear Mathieu-Hill equations the amplitudes of both stable and unstable solutions were obtained for steady-state vibrations. It is confirmed that the both instability regions and amplitudes of stable and unstable solutions are significantly influenced by the lamination schemes including symmetry, antisymmetry and the number and sequence of the plies, the magnitude and direction of the axial periodic loads, different aspect ratios of the shell including length-to-radius and thickness-to-radius ratios, and circumferential wave numbers. So for any particular application specific configurations of laminate should be considered in the design of composite cylindrical shells. A comparative study of the present work with those available in literature shows a very good agreement However, as the results of the present study reveal, the linear analysis carried out in available literature can only provide the information about the instability region and unable to predict the vibration amplitudes in these regions. The non-linear analysis developed in the present work can determine such vibration amplitude. The present work has shown that there is vibration with steady-state amplitude in the instability region which approaches almost constant amplitude when the excitation frequencies are increased. Hence, for more perfect and complete studies of dynamic instability of laminates, the non-linear analysis is required to determine both the stable and unstable vibration amplitudes in addition to instability regions. Where the occurrence of dynamic instability is inevitable, in order to have a control on vibration amplitudes in the unstable regions the non-linear analysis is required. By adjusting the corresponding effective

parameters as explained in the present work, steady-state vibrations with allowable amplitudes based on the design criteria can be achieved in the dynamically-unstable regions.

The major outcomes of the present study are summarized as follow:

- The sequence of the vibration modes are affected by the number of the layers and aspect ratios.

- For both symmetric and antisymmetric laminated cylindrical shells, amplitude of steady-state vibrations are decreased, corresponding dynamically-unstable regions shift to the right along the frequency axis having higher frequencies of excitation, and the widths of the instability regions are decreased when the number of plies are increased. Convergence is also achieved at a specific number of the plies in each case.

- Increasing the magnitude of compressive axial load causes increasing amplitude of steady-state vibrations, shifting dynamically-unstable regions to the left along the frequency axis, and increasing albeit very slowly the widths of instability regions.

- Increasing the magnitude of tensile axial loads results in decreasing the amplitude of steady-state vibrations, shifting dynamically-unstable regions to the right along the frequency axis, and increasing albeit very slowly the widths of instability regions.

- The shell having higher aspect ratio L/R has a larger amplitude of steady-state vibrations.

- By increasing the thickness ratio R/h, the amplitude of steady-state vibrations is also increased.

The present work can be used as a bench mark study in future studies on dynamic instability of composite shells.

CHAPTER 6

Contribution, conclusions, and future work

6.1 Major Contributions

This research dissertation presents a comprehensive study and investigation on non-linear dynamic instability of uniform and internally-thickness-tapered laminated composite plates and uniform composite cylindrical shells. The major contribution of this dissertation research is that the non-linear von Karman strains associated with large deflections are considered not only to predict the dynamically-unstable regions but also to determine both the stable and stable- and unstable-solutions of steady-state vibrations in these regions for these uniform laminated composite plates, internally-thickness-tapered laminated composite flat plates, internally-thickness-tapered laminated composite cylindrical panels, and uniform laminated composite cylindrical shells.

The displacement-based approximate analytical solutions considering the non-linear von Karman strains associated with large out-of-plane deflections in the modeling and in formulations of the dynamic instability problems that are generated in this dissertation for the internally-thickness-tapered laminated composite plates and cylindrical panels form the novelty of this Ph.D. research work. These approximate analytical solutions of dynamic instability, allow engineers and designers of composite structures to specify the dynamically-unstable regions of composite plates/shells, to avoid applying unreliable periodic axial loads that cause these composite structures to fall into these dynamically-unstable regions. However, for whatever reason in practice, these composite plates/shells may be subjected to larger periodic axial loads or have higher excitation frequencies than reliable periodic axial loads so as to fall into these dynamically-unstable regions. The parametric studies were carried out in

this dissertation provide an additional design criterion to engineers and designers of composite plates and shells, to design more efficient composite plates/shells so as to have lower amplitudes of steady-state vibrations in these dynamically-unstable regions in such a practical case. The two in-plane displacements were determined from the two in-plane force-equilibrium equations of motion. Then the in-plane force-resultants were obtained from the in-plane displacements and further by applying the boundary conditions. Substituting the moment resultants which are in terms of the out-of-plane displacement function and the computed in-plane force-resultants together in the moment-equilibrium equation of motion, then applying the general Galerkin method to this equation to satisfy spatial dependence in the partial differential equation of motion, a set of non-linear Mathieu-Hill equations were obtained. Then Bolotin's method is applied to these non-linear Mathieu-Hill equations to determine the dynamically-unstable regions, and also the stable- and unstable-solutions amplitudes of the steady-state vibrations in these dynamically-unstable regions.

Here in this dissertation research work a comprehensive parametric study on non-linear dynamic instability of these simply supported cross-ply laminated composite uniform plates, flat and cylindrical internally-thickness-tapered plates and uniform cylindrical shells is conducted in order to understand the effects of various parameters on the dynamic instability regions and steady-state vibrations amplitudes in these regions to provide a basis and guidelines in the design of these four composite structures for better dynamic stability. These parametric studies are on the effects of the orthotropy in the laminated composite uniform plates, number of layers for symmetric and antisymmetric uniform cross-ply laminated composite plates and cylindrical shells, different taper configurations and taper angles in both flat tapered plates and tapered cylindrical panels, magnitudes of both tensile and compressive axial loads in the uniform and tapered plates and uniform cylindrical shells, aspect ratios of the loaded-to-unloaded width of the uniform plates, flat and cylindrical thickness-tapered plates, and length-

190

to-radius of the cylindrical shells, length-to-average-thickness ratios of the flat plates and cylindrical panels and radius-to-thickness ratio of the cylindrical shells, and curvature of the tapered cylindrical panels i.e. radius-to-side ratio on the instability regions and the parametric resonance particularly the steady-state vibrations amplitudes of all these four composite structures.

6.2 Major Conclusions

The major conclusions extracted from the present dissertation research which is on the non-linear dynamic instability of uniform and internally-thickness-tapered cross-ply laminated composite plates and uniform cross-ply laminated composite cylindrical shells are summarized as follow:

- When the number of plies is increased in both symmetric and antisymmetric uniform laminated plates and uniform cylindrical shells, the dynamically-unstable regions occur at higher excitation frequencies, the instability regions become smaller and consequently, the amplitudes of steady-state vibrations are decreased. However at a specific number of plies in each case these dynamically-unstable regions and the amplitudes of steady-state vibrations are converged i.e. increasing the number of plies above ten layers in antisymmetric or twenty layers in symmetric uniform laminated plates and uniform cylindrical shells doesn't have any significant effect in these instability regions and the corresponding amplitudes of steady-state vibrations in these regions.

- Both dynamically-unstable regions and corresponding amplitudes of the steady-state vibrations are significantly influenced by taper configurations. The results show that configuration C is the most stable flat thickness-tapered plates and cylindrical thickness-tapered panels under parametric excitation among all the thickness-tapered configurations i.e. configurations A, B, C and D, and also the uniform-

thickness laminate having the thickness equal in value to the average thickness of the corresponding thickness-tapered cylindrical panel. Overall, tapering the flat plates /cylindrical panels makes the panel's stiffness to be increased although its total weight might be decreased due to the existence of resin pockets. In physical meaning, increasing stiffness and decreasing mass make the natural frequency of the system, here the laminated composite flat thickness-tapered plates and cylindrical thickness-tapered panels, to be increased. Hence, higher stiffness of the thickness-tapered cylindrical panel results in the shifting of the dynamically-unstable regions toward higher frequencies and consequently decreasing both stable- and unstable-solutions amplitudes of the steady-state vibrations. However, almost the same widths of instability regions as that of flat thickness-tapered plates and cylindrical thickness-tapered panels having its thickness as the average thickness of the tapered plate are obtained, although reducing the total weight of the thickness-tapered structure causes the rate of increase of the amplitudes of the steady-state vibrations to be increased. Hence in comparison to the uniform flat plate and uniform cylindrical panel, although the flat thickness-tapered plate and cylindrical thickness-tapered panel with configuration C has the amplitude of steady-state vibrations lower than that of the uniform laminate in the initial stages of the excitation, by increasing the excitation frequencies this trend is changed; influenced by the lower total weight of the flat thickness-tapered plate and cylindrical thickness-tapered panel (configuration C) at the higher level of the excitation frequencies, the first mode steady-state vibration amplitude is very slightly increased from the first mode steady-state vibration amplitude of the uniform flat plate and uniform cylindrical panel.

192

- The taper angle is the other most important parameter in the design of the thickness-tapered flat plate and thickness-tapered cylindrical panel which, as observed from the results obtained, makes the flat plate/cylindrical panel stiffer. The higher the taper angle is, the higher the excitation frequencies corresponding to the dynamically-unstable regions are, and consequently, the lower is the amplitude of the steady-state vibrations. Also, the widths of dynamically-unstable regions decrease very slightly for higher values of taper angles. The variation of dynamic instability response of thickness-tapered flat plate and thickness-tapered cylindrical panel from that of the uniform one is very smooth for smaller taper angles of less than 0.3° but the rates of the deviations are high for increasing values of taper angle above 0.5°.

- Increasing the amplitude of the tensile in-plane harmonically pulsating load results in the shifting of the instability regions to higher frequencies along the frequency axis, and consequently decreasing the amplitudes of the steady-state vibrations and also decreasing very slightly the widths of the dynamically-unstable regions. However, increasing the amplitude of the compressive in-plane load results in the shifting of the instability regions to lower frequencies along the frequency axis, and consequently increasing the amplitudes of the steady-state vibrations and also increasing the widths of the dynamically-unstable regions. These outcomes can be expected because increasing the tensile in-plane load makes the plate/shell to be stiffer that physically means they have a higher natural frequency, and contrarily increasing the compressive in-plane load results in decreasing the plate's/shell's stiffness that physically means they have a lower natural frequency.

- With a decrease in width, i.e. overall decrease in aspect ratio of width over length, uniform plate stiffness, flat thickness-tapered plate stiffness and cylindrical

thickness-tapered panel stiffness are increased as well such that as mentioned before it means to make the natural frequency of these composite structures to be increased, hence the dynamically-unstable regions occur at higher frequencies of excitation, and consequently the amplitudes of steady-state vibrations are decreased and further, the widths of instability regions are also increased. It is also noticed that the increase in the widths of instability regions is more influenced by the compressive loading than the tensile loading. However, the points of origins of dynamically-unstable regions are more influenced by the tensile loading than the compressive loading. The uniform laminated composite cylindrical shell having a higher aspect ratio L/R has a larger amplitude of steady-state vibrations too.

- In the internally-thickness-tapered laminated composite flat plates and cylindrical panels with decreasing the length-to-average-thickness ratio which is achieved by increasing the number of plies, in the laminated composite uniform plates with decreasing the length-to-thickness ratio, and in the uniform laminated composite cylindrical shells with decreasing the radius-to-thickness ratio, the dynamically-unstable regions occur at higher excitation frequencies, and consequently the amplitudes of steady-state vibrations are decreased and also the widths of dynamically-unstable regions are increased. An increase in the widths of instability regions is more influenced by the compressive loading than the tensile loading. However, the points of origins of dynamically-unstable regions are more influenced by the tensile loading than the compressive loading. These outcomes are due to the fact that increasing the thickness of the plate/shell makes the plate/shell stiffer and consequently, the natural frequencies of those structures are increased.

- Thickness-tapered cylindrical panels with higher values of curvature are dynamically more stable. Subjected to either the tensile or the compressive loadings,

decreasing the curvature or increasing the overall radius-to-width ratio of the laminated tapered cylindrical panel, makes the dynamically-unstable regions occur at lower frequencies of excitation, the widths of instability regions are increased, and consequently, the amplitudes of steady-state vibrations are increased. These changes are very fast for the radius-to-width ratio between 1 to 3, are moderate thereafter until 5 and are very slow until 10 and thereafter it appears to be converged at a certain value. The dynamic instability's parameters are too close to each other for the radius-to-width ratio equal to 10 to ∞ (flat plate).

The thickness-tapered flat plates and thickness-tapered cylindrical panels, through increasing the stiffness and at the same time decreasing the weight, cause more complicated structural behavior as exhibited by their vibration response and dynamic instability characteristics, in comparison to the uniform plates and uniform cylindrical panels, respectively. All of the parametric study results indicate that the thickness-tapered cylindrical panels with higher values of curvature (lower values of radius-to-width ratio) having configuration C are more stable and have better vibrational behavior in comparison to any other thickness-tapered configurations (A, B or D) and even in comparison to the uniform cylindrical panels having the thickness as the average-thickness of the corresponding thickness-tapered cylindrical panels having configuration C. The present work can be used as a benchmark study in future studies on the dynamic instability of laminated composite plates and shells either uniform or internally-thickness-tapered ones. The approximate analytical solution method proposed in this Ph.D. research work is limited to the dynamic instability which is the loadings are harmonic in-plane loadings and it is not capable of the other insatiability analysis of the plates and shells such as buckling and post-buckling analysis. This research work and the proposed solution is limited to the simply supported boundary conditions, and the in-plane inertia forces in the equation of motions have been neglected. The damping term wasn't considered in the

formulation too. Considering other boundary conditions,   in-plane inertia forces to increase the accuracy, the damping terms in the solution and corresponding damping effects in the results are addressed in the future works. The other limitation of this approximate analytical solution for the laminated composite internally-thickness-tapered flat plates and cylindrical panels is those extensional stiffnesses terms were replaced by their average values in the formulation. Without this assumption solving the two in-plane force-equilibrium equations of motion are impossible mathematically with the analytical method so this simplification was applied in the solution method in this study.

6.3   Recommendation for the future works

In this dissertation, the non-linear dynamic instability of uniform and internally-thickness-tapered cross-ply laminated composite plates and uniform cross-ply laminated composite cylindrical shells were studied based on the analytical approach. All these uniform and internally-thickness-tapered cross-ply laminated composite plates and uniform cross-ply laminated composite cylindrical shells are considered to be under simply supported boundary conditions. In internally-thickness-tapered cross-ply laminated composite plates either the flat plates or the cylindrical panels since the gradients of variations of extensional stiffnesses from the thickest to the thinnest sides of the thickness-tapered plate are too small in comparison to the corresponding variations of bending stiffnesses, the extensional stiffnesses terms were replaced by their average values. Without this assumption solving the two in-plane force-equilibrium equations of motion are impossible mathematically with the analytical method so this simplification was applied in the solution method in this study. Hence, this study can be continued in future studies on these following recommendations:

➢ Non-linear dynamic instability analysis of damped uniform-thickness and damped internally-thickness-tapered laminated composite plates and cylindrical shells subjected to periodic in-plane loads

196

- ➢ Non-linear dynamic instability analysis of uniform-thickness and internally-thickness-tapered laminated composite plates and cylindrical shells with cut-outs subjected to periodic in-plane loads

- ➢ Non-linear dynamic instability analysis of uniform-thickness and internally-thickness-tapered laminated composite stiffened plates subjected to periodic in-plane load

- ➢ Effect of boundary conditions on the non-linear dynamic instability of uniform-thickness and internally-thickness-tapered laminated composite plates and cylindrical shells subjected to non-uniform periodic in-plane loads

- ➢ Non-linear dynamic instability analysis of uniform-thickness and internally-thickness-tapered composite plates and cylindrical shells with piezoelectric layers subjected to periodic in-plane load

References

[1] Bolotin, V. V.;, The dynamic stability of elastic systems, San Francisco: Holden-Day, 1964.

[2] Darabi, M.; Darvizeh, M.; Darvizeh, A.;, "Non-linear analysis of dynamic stability for functionally graded cylindrical shells under periodic axial loading," *Composite Structures,* vol. 83, pp. 201-211, 2008.

[3] Argento, A.; Scott, R. A.;, "Dynamic instability of layered anisotropic circular cylindrical shells, part I: Theoretical development,," *Sound and Vibration,* vol. 162, no. no. 2, pp. 311-322, 1993.

[4] Evan-Iwanowsky, R. M.;, "On the parametric response of structures(Parametric response of structures with periodic loads).," *Applied Mechanics Reviews,* vol. 18, pp. 699-702, 1965.

[5] Sahu, S. K.; Datta, P. K.;, "Research advances in the dynamic stability behavior of plates and shells: 1987–2005—part I: conservative systems," *Sahu, S. K., and P. K. Datta. "Research advances in the dynamic stability behavior of plateApplied mechanics reviews,* vol. 60, no. 2, pp. 65-75, 2007.

[6] Srinivasan, R. S.; Chellapandi, P.;, "Dynamic stability of rectangular laminated composite plates," *Computers & Structures,* vol. 24, no. 2, pp. 233-238, 1986.

[7] Bert, C. W.; Birman, V.;, "Dynamic instability of shear deformable antisymmetric angle-ply plates," *Solids and Structures,* vol. 23, no. 7, pp. 1053-1061, 1987.

[8] Birman, V.;, "Dynamic stability of unsymmetrically laminated rectangular plates," *Mechanics research Communications,* vol. 12, no. 2, pp. 81-86, 1985.

[9] Moorthy, J.; Reddy, J. N.; Plaut, R. H.;, "Parametric instability of laminated composite plates with transverse shear deformation," *Solids and Structures,* vol. 26, no. 7, pp. 801-811, 1990.

[10] Patel, B. P.; Ganapathi, M.; Prasad, K. R.; Balamurugan, V.;, "Dynamic instability of layered anisotropic composite plates on elastic foundation," *Engineering Structures,* vol. 21, pp. 988-995, 1999.

[11] Ramachandra, L. S.; Panda, S. K.;, "Dynamic instability of composite plates subjected to non-uniform in-plane loads," *Sound and Vibration,* vol. 331, pp. 53-65, 2012.

[12] Popov, A. A.;, "Parametric resonance in cylindrical shells: a case study in the nonlinear vibration of structural shells," *Engineering Structures,* vol. 25, pp. 789-799, 2003.

[13] Alijani, Farbod; Amabili, Marco;, "Non-linear vibrations of shells: Aliterature review from 2003 to 2013," *Non-linear Mechanics,* vol. 58, pp. 233-257, 2014.

[14] Librescu, L.; Thangjitham, S.;, "Parametric instability of laminated composite shear-deformable flat panels sunbjected to in-plane edge loads," *Non-linear Mechanics,* vol. 25, no. 2-3, pp. 263-273, 1990.

[15] Ganapathi, M.; Patel, B. P.; Boisse, P.; Touratier, M.;, "Non-linear dynamic stability characteristics of elastic plates subjected to periodic in-plane load," *Non-linear Mechanics,* vol. 35, pp. 467- 480, 2000.

[16] Amabili, Marco;, Nonlinear vibrations and stability of shells and plates, New York, NY, USA: Cambridge University Press, 2008.

[17] Fung, Y. C.;, Foundation of Solid Mechanics, Englewood Cliffs, NJ, USA: Prentice-Hall, 1965.

[18] Cheng-ti, Z.; Lie-dong, W.;, "Nonlinear theory of dynamic stability for laminated composite cylindrical shells," *Applied Mathematics and Mechanics,* vol. 22, no. 1, pp. 53-62, 2001.

[19] Ostiguy, G. L.; Evan-Iwanowski, R. M.;, "Influence of the aspect ratio on dynamic stability and nonlinear response of rectangular plates," *Mechanical Design,* vol. 104, pp. 417-425, 1982.

[20] Timoshenko, S. P.; Gere, J. M.;, Theory of elasticity, New York: Mc Graw-Hill, 1961.

[21] Ng, T. Y.; Lam, K. Y.; Reddy, J. N.;, "Dynamic stability of cross-ply laminated composite cylindrical shells," *Int. J. Mechanical Science,* vol. 40, no. 8, pp. 805-823, 1998.

[22] Najafov, A. M.; Sofiyev, A. H.; Hui, D.; Kadiglu, F.; Dorofeyskaya, N. V.; Huang, H.;, "Non-linear dynamic analysis of symmetric and antisymmetric cross-ply laminated orthotropic thin shells," *Mechanica,* vol. 49, pp. 413-427, 2014.

[23] Lam, K. Y.; Ng, T. Y.;, "Dynamic stability analysis of laminated composite cylindrical shells subjected to conservative periodic axial loads," *Composite Part B,* vol. 29B, pp. 769-785, 1998.

[24] He, K.; Hoa, S. V.; Ganesan, R.;, "The study of tapered laminated composite structures: a review," *Composite Science and Technology,* vol. 60, pp. 2643-2657, 2000.

[25] Ganesan, Rajamohan; Zabihollah, Abolghasem;, "Vibration analysis of tapered composite beams using a higher-order finite element. part I: Formulation," *Composite Structures,* vol. 77, pp. 306-318, 2005.

[26] Ganesan, Rajamohan; Zabihollah, Abolghasem;, "Vibration analysis of tapered composite beams using a higher-order finite element. Part II: parametric study," *Composite Structures,* vol. 77, pp. 319-330, 2007.

[27] Steeves, Craig A.; Fleck, Norman A.;, "Compressive strength of composite laminates with terminated internal plies," *Composite Part A: Applied Science and manufacturing,* vol. 36, pp. 798-805, 2005.

[28] Ganesan, Rajamohan; Liu, Dai Ying;, "Progressive failure and post-buckling response of tapered composite plates under uni-axial compression," *Composite Structures,* vol. 82, pp. 159-176, 2008.

[29] Ganesan, Rajamohan; Akhlaque-E-Rasul, Shaikh;, "Compressive response of tapered composite shells," *Composite Structures,* vol. 93, pp. 2153-2162, 2011.

[30] Akhlaque-E-Rasul, Shaikh; Ganesan, Rajamohan, "Non-linear buckling analysis of tapered curved composite plates based on a simplified methodology," *Composites: Part B,* vol. 43, pp. 797-804, 2012.

[31] Akhlaque-E-Rasul, Shaikh; Ganesan, Rajamohan;, "Compressive response of tapered curved composite plates based on a nin-node composite shell elemnt," *Composite Structures,* vol. 96, pp. 8-16, 2013.

[32] Darabi, Mehdi; Ganesan, Rajamohan;, "Non-linear dynamic instability analysis of laminated composite cylindrical shells subjected to periodic axial loads," *Composite Structures,* vol. 147, pp. 168-184, 2016.

[33] Kim, W.; Argento, A.; Scott, R. A.;, "Forced Vibration and dynamic stabilit of a rotating tapered composite Timoshenko shaft: Bending motions in end-millig operation," *Sound and Vibration,* vol. 246, no. 4, pp. 583-600, 2001.

[34] Liu, Weiguang; Ganesan, Rajamohan, "Dynamic instability analysis of tapered composite plates using Ritz and finite element methods," Concordia University, Montreal, 2005.

[35] Hyer, Michael W.;, Stress analysis of fiber-reinforced composite materials., Lancaster: DEStech Publications, Inc, 2009.

[36] Sahu, S. K.; Datta, P. K.;, "Research advances in the dynamic stability behavior of plates and shells: 1987-2005- Part I: Conservative Systems," *Applied Mechanics Reviews,* vol. 60, pp. 65-75, 2007.

[37] R. M. Ewan-Iwanowski, "On the Parametric Response of Structures," *Applied Mechanics Review,* vol. 18, no. 9, pp. 699-702, 1965.

[38] Ng, T. Y.; Lam, K. Y.; Reddy, J. N.;, "Dynamic stability of cylindrical panels with transverse shear e}ects," *Solids and Structures,* vol. 36, pp. 3483-3496, 1999.

[39] Ganapathi, M.; Varadan, T. K.; Balamurugan, V.;, "Dynamic instability of laminated composite curved panels using finite element method," *Computeres & Structures,* vol. 53, no. 2, pp. 335-342, 1994.

[40] Sahu, S. K.; Datta, P. K.;, "Dynamic stability of laminated composite curved panels with cutouts," *Journal of Engineering Mechanics,* vol. 129, no. 11, pp. 1245-1253, 2003.

[41] Liew, K. M.; Lee, Y. Y.; Ng, T. Y.; Zhao, X.;, "Dynamic stability analysis of composite laminated cylindrical panels via the mesh-free kp-Ritz method," *International Journal of Mechanical Sciences,* vol. 49, pp. 1156-1165, 2007.

[42] Whitney, J. M.;, Structural analysis of laminated anisotropic plates, Lancaster, Pennsylvania: Technomic Publishing Company, 1987.

[43] Darabi, M.; Ganesan, R.;, "Nonlinear dynamic instability analysis of laminated composite thin plates subjected to periodic in-plane loads," *Nonlinear Dynamics,* pp. DOI 10.1007/s11071-017-3863-9, 2017.

[44] Jones, R. M.;, Mechanics of composite materials, Philadelphia: Taylor & Francis, 1999.

[45] Argento, A.; Scott, R. A.;, "Dynamic instability of layered Anisotropic circular cylindrical shells- Part II: Numerical results," *Sound and Vibration,* vol. 162, pp. 323-332, 1993.

[46] A. Argento, "Dynamic instability of a composite circular cylindrical shell subjected to combined axial and torsional loading," *Composite Materials,* vol. 27, pp. 1722-1738, 1993.

[47] Ng, T. Y.; Lam, K. Y.; Reddy, J. N.;, "Dynamic stability of cylindrical panels with transverse shear effects," *Solids and Structures,* vol. 36, pp. 3483-3496, 1999.

[48] Ng, T. Y.; Lam, K. Y.;, "Parametric resonance of a rotationg cylindrical shell subjevted to periodic axial loads," *Sound and Vibration,* vol. 214, no. 3, pp. 513-529, 1998.

[49] Ng, T. Y.; Lam, K. Y.;, "Dynamic stability analysis of cross-ply laminated cylindrical shells using different thin shell theories," *Acta Mechanica,* vol. 134, pp. 147-167, 1999.

[50] Liew, K. M.; Hu, Y. G.; Zhao, X.; Ng., T. Y., "Dynamic stability analysis of composite laminated cylindrical shells via the mesh-free kp-Ritz method," *computer methods in applied mechanics and engineering,* vol. 196, pp. 147-160, 2006.

[51] Fazilati, J.; Ovesy, H. R.;, "dynamic instability analysis of composite laminated thin-walled structures using two versions of FSM," *Composite Structures,* vol. 92, no. 9, pp. 2060-2065, 2010.

[52] Ovesy, H. R.; Fazilati, J.;, "Parametric instability analysis of laminated composite curved shells subjected to non-uniform in-plane load," *Composite Structures,* vol. 108, pp. 449-455, 2014.

[53] Fazilati, J.; Ovesy, H. R.;, "Finite strip dynamic instability analysis of perforated cylindrical shell panels," *Composite Structures,* vol. 94, no. 3, pp. 1259-1264, 2012.

[54] Fazilati, J.; Ovesy, H. R.;, "Parametric instability of laminated longitudinally stiffened curved panels with cutout using higher order FSM," *Composite Structures,* vol. 95, pp. 691-696, 2013.

[55] Hui, D.; Du, I.;, "Initial postbuckling behavior of imperfect, antisymmetric cross-ply cylindrical-shelss under torsion," *Applied Mechanics,* vol. 54, pp. 174-180, 1987.

[56] Xu, C. S.; Xian, Z. Q.; Chia, C. Y.;, "Nonlinear theory and vibration analysis of laminated truncated thick conical shells," *Non-Linear Mechanics,* vol. 16, pp. 139-154, 1995.

[57] Liu, R. H.; Li, J.;, "Nonlinear vibration of shallow conical sandwich shells," *Non-Linear Mechanics,* vol. 16, pp. 139-154, 1995.

[58] Lakis, A. A.; Selmane, A.; Toledano, A.;, "Nonlinear free vibration analysis of laminated orthotropic cylindrical shells," *Mechanical Science,* vol. 40, pp. 27-49, 1998.

[59] Gonçalves, P. B.; Del, P. Z.;, "Nonlinear oscilations and stability of parametrically excited cylindrical shells," *Mechanica,* vol. 37, pp. 569-597, 2002.

[60] Qatu, M. S.; Sullivan, R. W.; Wang, W.;, "Recent research advances on dynamic analysis of composite shells:2000-2009," *Composite Structures,* vol. 93, pp. 14-31, 93.

Appendix

$$M_{mn} = -16\,\pi\,a^4\,A22\,\rho_t\,A11\left(A22\,A66\,a^4\,n^4 + n^2\left(A11\,A22 - A12\left(A12 + 2\,A66\right)\right)m^2\,b^2\,a^2\right.$$
$$\left. + A11\,A66\,b^4\,m^4\right)m\,b^4$$

$$(A.1)$$

$$Q_{mn} = 16\,A11\,A22\,a^2\,m^3\left(A22\,A66\,a^4\,n^4 + n^2\left(A11\,A22 - A12\left(A12 + 2\,A66\right)\right)m^2\,b^2\,a^2\right.$$
$$\left. + A11\,A66\,b^4\,m^4\right)\pi^3\,b^4$$

$$(A.2)$$

$$\eta_{mn} = -\left(A11\,b^4\,m^4 + A22\,a^4\,n^4\right)\pi^5\,m\left(A11\,A22 - A12^2\right)\left(A22\,A66\,a^4\,n^4 + n^2\left(A11\,A22\right.\right.$$
$$\left.\left. - A12\left(A12 + 2\,A66\right)\right)m^2\,b^2\,a^2 + A11\,A66\,b^4\,m^4\right)$$

$$(A.3)$$

$$K_{mn} = 16\,m\,A22\,A11\,\pi^5\left(b^8\,A66\left(-A11\,D11 + B11^2\right)m^8 + \left(D11\,A12^2 + \left(2\,D11\,A66\right.\right.\right.$$
$$\left. - 2\,B11\left(B12 + B66\right)\right)A12 + \left(-D11\,A22 + \left(-2\,D12 - 4\,D66\right)A66 + \left(B12\right.\right.$$
$$\left.\left. + 2\,B66\right)^2\right)A11 + B11^2\,A22\right)a^2\,n^2\,b^6\,m^6 + 2\,a^4\,n^4\,b^4\left(\left(D12 + 2\,D66\right)A12^2 + \left(\left(2\,D12\right.\right.\right.$$
$$\left. + 4\,D66\right)A66 - B22\,B11 - B12^2 - 4\,B66\,B12 - 4\,B66^2\right)A12 + \left(\left(-2\,D66 - D12\right)A22\right.$$
$$\left. - \frac{1}{2}\,D22\,A66 + B22\left(B12 + 2\,B66\right)\right)A11 + \left(-\frac{1}{2}\,D11\,A66 + B11\left(B12\right.\right.$$
$$\left.\left. + 2\,B66\right)\right)A22 - B11\,B22\,A66\right)m^4 + \left(D22\,A12^2 + \left(2\,D22\,A66 - 2\,B22\left(B12\right.\right.\right.$$
$$\left. + 2\,B66\right)\right)A12 + \left(-A22\,D22 + B22^2\right)A11 + A22\left(\left(-2\,D12 - 4\,D66\right)A66 + \left(B12\right.\right.$$
$$\left.\left.\left. + 2\,B66\right)^2\right)\right)a^6\,n^6\,b^2\,m^2 + a^8\,n^8\,A66\left(-A22\,D22 + B22^2\right)\right)$$

$$(A.4)$$

$$T_\theta =$$

$$\begin{bmatrix} (\cos\theta)^2 & (\sin\theta)^2 & 0 & 0 & 0 & -2\sin\theta\cos\theta \\ (\sin\theta)^2 & (\cos\theta)^2 & 0 & 0 & 0 & 2\sin\theta\cos\theta \\ 0 & 0 & 1 & 0 & 0 & 0 \\ 0 & 0 & 0 & \cos\theta & \sin\theta & 0 \\ 0 & 0 & 0 & -\sin\theta & \cos\theta & 0 \\ \sin\theta\cos\theta & -\sin\theta\cos\theta & 0 & 0 & 0 & (\cos\theta)^2 - (\sin\theta)^2 \end{bmatrix}\dots$$

$$\dots\dots\dots\dots\dots\dots\dots\dots\dots\dots\dots\dots\dots\dots\dots\dots\dots\dots\dots\dots\dots\dots\dots\dots\dots(A.5)$$

$$T_\Psi =$$

$$\begin{bmatrix} (\cos\Psi)^2 & 0 & (\sin\Psi)^2 & 0 & 2\sin\Psi\cos\Psi & 0 \\ 0 & 1 & 0 & 0 & 0 & 0 \\ (\sin\Psi)^2 & 0 & (\cos\Psi)^2 & 0 & -2\sin\Psi\cos\Psi & 0 \\ 0 & 0 & 0 & \cos\Psi & 0 & -\sin\Psi \\ -\sin\Psi\cos\Psi & 0 & \sin\Psi\cos\Psi & 0 & (\cos\Psi)^2 - (\sin\Psi)^2 & 0 \\ 0 & 0 & 0 & \sin\Psi & 0 & \cos\Psi \end{bmatrix}$$

$$(A.6)$$

Table A.1 Variation of the both extension- and bending-stiffness ratios of the left (thick) side to the right (thin) side of symmetric cross-ply laminated thickness-tapered cylindrical panel having configuration C with the taper ratio (N_L/N_R).

Stiffness ratios	40-34 Plies	40-28 Plies	40-22 Plies	40-16 Plies	40-10 Plies
$(A_{11})_L/(A_{11})_R$	1.12	1.42	1.68	2.49	3.40
$(A_{12})_L/(A_{12})_R$	1.16	1.41	1.80	2.47	3.98
$(A_{22})_L/(A_{22})_R$	1.13	1.30	1.80	2.28	4.41
$(A_{66})_L/(A_{66})_R$	1.14	1.39	1.77	2.43	3.89
$(D_{11})_L/(D_{11})_R$	1.61	2.84	5.73	14.31	54.23
$(D_{12})_L/(D_{12})_R$	1.63	2.92	6.01	15.66	64.50
$(D_{22})_L/(D_{22})_R$	1.65	3.00	6.37	17.45	80.53
$(D_{66})_L/(D_{66})_R$	1.63	2.92	6.01	15.62	64.00

Figure A.1 Variation of the both extension- and bending-stiffness ratios of the left (thick) side to the right (thin) side of symmetric cross-ply laminated thickness-tapered cylindrical panel having configuration C with the taper ratio (N_L/N_R).

$$M_{mn} = 16A_{66}(A_{11} - A_{12})R^4\rho_t A_{22}(A_{11} + A_{12})(R^4 A_{22}A_{66}\lambda_m^4 + (A_{11}^2 - A_{12}^2 -$$

$$2A_{12}A_{66})R^2n^2\lambda_m^2 + n^4 A_{22}A_{66}) \tag{A.7}$$

$$Q_{mn} = -16A_{66}R^4(R^4 A_{22}A_{66}\lambda_m^4 + (A_{11}^2 - A_{12}^2 - 2A_{12}A_{66})R^2n^2\lambda_m^2 +$$

$$n^4 A_{22}A_{66})\lambda_m^2 A_{22}(A_{11} - A_{12})(A_{11} + A_{12}) \tag{A.8}$$

$$\eta_{mn} = A_{66}R^4(R^4 A_{22}A_{66}\lambda_m^4 + (A_{11}^2 - A_{12}^2 - 2A_{12}A_{66})R^2n^2\lambda_m^2 + n^4 A_{22}A_{66})\lambda_m^4(A_{11} -$$

$$A_{12})^2(A_{11} + A_{12})^2 \tag{A.9}$$

$$K_{mn} = 16A_{22}((R^8((-A_{22}D_{11} + B_{22}^2)A_{12}^2 + A_{22}B_{12}(B_{11} - B_{22})A_{12} + A_{22}A_{11}^2 D_{11} -$$

$$A_{22}^2 B_{11}^2)\lambda_m^8 - 2R^6((A_{11} - A_{12})(A_{11} + A_{12})(A_{12}B_{22} - A_{22}B_{12})R + (-D_{11}A_{12}^3 + ((D_{22} +$$

$$2D_{66})A_{22} + B_{12}(B_{11} - B_{22}))A_{12}^2 + (-(B_{11} - B_{12})(B_{11} - 2B_{22} + B_{12})A_{22} + D_{11}A_{11}^2)A_{12} -$$

$$A_{22}((2B_{11}B_{12} - B_{11}B_{22} - B_{12}^2)A_{22} + A_{11}^2(D_{22} + 2D_{66})))n^2)\lambda_m^6 + ((A_{11} - A_{12})^2(A_{11} +$$

$$A_{12})^2 R^2 - 4n^2(A_{11} - A_{12})(A_{11} + A_{12})(A_{12}B_{12} - A_{22}B_{11})R + (2((2D_{22} + 4D_{66})A_{12}^3 +$$

$$(-A_{22}D_{11} + 2B_{12}^2 - 4B_{12}B_{22} + B_{22}^2)A_{12}^2 + ((2B_{12}^2 + (-3B_{11} - B_{22})B_{12} + 2B_{11}B_{22})A_{22} -$$

$$2A_{11}^2(D_{22} + 2D_{66}))A_{12} + A_{22}A_{11}^2 D_{11} + A_{22}^2 B_{11}^2))n^4)R^4\lambda_m^4 - 2R^2((A_{11} - A_{12})(A_{11} +$$

$$A_{12})(A_{12}B_{22} - A_{22}B_{12})R + (-D_{11}A_{12}^3 + ((D_{22} + 2D_{66})A_{22} + B_{12}(B_{11} - B_{22}))A_{12}^2 +$$

$$(-(B_{11} - B_{12})(B_{11} - 2B_{22} + B_{12})A_{22} + D_{11}A_{11}^2)A_{12} - A_{22}((2B_{11}B_{12} - B_{11}B_{22} -$$

$$B_{12}^2)A_{22} + A_{11}^2(D_{22} + 2D_{66})))n^2)n^4\lambda_m^2 + ((-A_{22}D_{11} + B_{22}^2)A_{12}^2 + A_{22}B_{12}(B_{11} -$$

$$B_{22})A_{12} + A_{22}A_{11}^2 D_{11} - A_{22}^2 B_{11}^2)n^8)A_{66}^2 - 4R^2\lambda_m^2(A_{11} - A_{12})n^2(A_{11} + A_{12})(((1/$$

$$4)D_{11}A_{12}^2 - (1/4)B_{12}(B_{11} + B_{22})A_{12} + (B_{66}^2 + (1/4)B_{11}^2 + (1/4)B_{12}^2)A_{22} - (1/$$

$$4)D_{11}A_{11}^2)R^4\lambda_m^4 - 2R^2((-(1/4)D_{22} - (1/2)D_{66})A_{12}^2 + (B_{66}^2 + (1/2)B_{12}B_{22})A_{12} + (-(1/$$

$$4)B_{11}B_{22} - (1/4)B_{12}^2)A_{22} + (1/4)A_{11}^2(D_{22} + 2D_{66}))n^2\lambda_m^2 + ((1/4)D_{11}A_{12}^2 - (1/$$

$$4)B_{12}(B_{11} + B_{22})A_{12} + (B_{66}^2 + (1/4)B_{11}^2 + (1/4)B_{12}^2)A_{22} - (1/4)D_{11}A_{11}^2)n^4)A_{66} -$$

$$8R^4 B_{66}^2 \lambda_m^4 n^4(A_{11} - A_{12})^2(A_{11} + A_{12})^2 \tag{A.10}$$